UNIVERSITAT DE BARCELONA

Advancing antileishmanial treatments through innovative nanotechnology *in vitro* approaches and characterization of novel therapeutic compounds

Lucía Román Álamo

UNIVERSITAT DE BARCELONA

FACULTAT DE FARMÀCIA I CIÈNCIES DE L'ALIMENTACIÓ

Advancing antileishmanial treatments through innovative nanotechnology *in vitro* approaches and characterization of novel therapeutic compounds

Lucía Román Álamo

2024

UNIVERSITAT DE BARCELONA

FACULTAT DE FARMÀCIA I CIÈNCIES DE L'ALIMENTACIÓ

PROGRAMA DE DOCTORAT DE BIOTECNOLOGIA

Advancing antileishmanial treatments through innovative nanotechnology *in vitro* approaches and characterization of novel therapeutic compounds

Lucía Román Álamo

2024

UNIVERSITAT DE BARCELONA

IBEC

Institute for Bioengineering of Catalonia

ISGlobal

Institut de Salut Global Barcelona

Universitat de Barcelona - Institut de Bioengenyeria de Catalunya (IBEC) - Institut de Salut Global de Barcelona (ISGlobal)

Projecte finançat per Fundació La Marató de TV3, Ref. 201811 (X.F.-B.)

Memòria presentada per Lucía Román Álamo per optar al títol de doctora per la universitat de Barcelona

Director: Xavier Fernàndez Busquets

Co-directora: Yunuen Ávalos Padilla

Tutora: Josefa Badía Palací

A mis padres y mi hermano,

Abstract

Leishmaniasis is a vector-borne disease, caused by the parasite *Leishmania* spp. and transmitted by sand flies of the genus *Phlebotomus* or *Lutzomyia.* There are over 12 million people infected worldwide and around one million new cases each year, which represents a significant global health challenge. Actually, leishmaniasis is the second deadliest parasitic disease in the world after malaria, but it is still considered a neglected tropical disease.

The current treatment options of leishmaniasis face challenges, such as long regimens, drug resistance, side effects, issues related to the parenteral administration, limited availability in endemic regions, and high costs. Thus, there is an urgent need to develop new safer treatments with a better patient compliance and more effective than the actual antileishmanial drugs. In this work, three strategies are proposed to overcome some of the challenges mentioned above.

Firstly, nanotechnology was applied with the aim of developing nanoformulations to encapsulate high amounts of pentamidine (one of the antileishmanial drugs currently used for clinical purposes) and, using heparin and chondroitin sulfate as targeting elements, to direct the nanoformulations to the free parasite or to macrophages infected with the parasite. Such specific delivery allowed for (i) increasing the targeting to macrophages when liposomes were coated with either heparin or CS, (ii) significantly reducing the IC_{50} of the drug on *L. infantum* and *L. pifanoi* promastigotes when liposomes were coated with heparin or chondroitin sulfate, (iii) significantly reducing the cytotoxicity on human umbilical endothelial cells, and (iv) obtaining a higher deposition of the nebulized liposomal preparations in the deeper stages of a human lung airway simulator when compared to free pentamidine.

The second approach was focused in the search for new drugs with a different mechanism of action than the current antileishmanial drugs. In here, different compounds which interfere with protein aggregation showed some extent of antileishmanial activity. In particular, the bis(styrylpyridinium) salt YAT2150 had a better activity against *L. infantum* than most of the currently used drugs for the clinical treatment of leishmaniasis, including pentamidine, miltefosine and

paromomycin. In relation to the mode of action of YAT2150, a reduction in the overall protein aggregation in a culture of *L. infantum* promastigotes was observed, according to Thioflavin T analysis. This finding aligns with the proposed mode of action of YAT2150 in *P. falciparum* determined in a previous study. The encapsulation of YAT2150 in liposomes or immunoliposomes functionalized with an antibody against LPG, significantly increased the selectivity index of the drug above 100. Therefore, the activity of YAT2150 against both *Leishmania* and *Plasmodium* represents a promising opportunity for the treatment of co-infections with these parasites.

The third strategy was spurred by the urgent need to develop ligands that specifically recognise the parasite, and that could be used, e.g., for the functionalization of drug delivery systems or as diagnostic tools. Aptamers emerge as a cost-efficient and more stable alternative to antibodies, rendering them a valuable approach to diagnose tropical parasitic diseases, including leishmaniasis, particularly in endemic regions. Leishmanolysin, or GP63, is the major surface protein present in *Leishmania* promastigotes and constitutes one of its main virulence factors, playing a role in the adhesion of the parasite to the macrophage and in the survival of amastigotes. DNA aptamers were developed against a *L. infantum* mature form of GP63 (*Li*GP63m), using the systematic evolution of ligands by exponential enrichment (SELEX) method. After 7 SELEX cycles, 5 out of 20 individual aptamer sequences were selected, based on dot blot analysis confirming the specific recognition of recombinant *Li*GP63m and flow cytometry analysis where these five aptamers targeted more than 75% of promastigotes. The aptamers showed a high affinity for endogenous *Li*GP63 within a promastigote lysate, with a binding affinity in the µM range, according to an Aptamer Linked Immobilized Sorbent Assay (ALISA). In conclusion, the aptamers discussed here hold promise for interventions against leishmaniasis as potential diagnostic tools and as targeting molecules for drug delivery nanocarriers.

Resum

La leishmaniosi és una malaltia transmesa per vectors, causada pel paràsit *Leishmania* spp. i transmesa per mosques de sorra del gènere *Phlebotomus* o *Lutzomyia*. Hi ha més de 12 milions de persones infectades a tot el món i al voltant d'un milió de casos nous cada any, cosa que representa un desafiament significatiu per a la salut global. Actualment, la leishmaniosi és la segona malaltia parasitària més mortal del món després de la malària, però encara es considera una malaltia tropical desatesa.

Les opcions de tractament actuals de la leishmaniosi s'enfronten a diversos reptes, com ara règims llargs, resistència als medicaments, efectes secundaris, problemes relacionats amb l'administració parenteral, disponibilitat limitada a les regions endèmiques i costos elevats. Per tant, hi ha una necessitat urgent de desenvolupar nous tractaments més segurs, amb una millor complaença dels pacients i més eficaços que els actuals fàrmacs antileishmanials. En aquest treball es proposen tres estratègies per superar alguns dels desafiaments esmentats anteriorment.

En primer lloc, es va aplicar la nanotecnologia amb l'objectiu de desenvolupar nanoformulacions per encapsular grans quantitats de pentamidina (un dels fàrmacs antileishmanials actualment utilitzats per a finalitats clíniques) i, utilitzant heparina i sulfat de condroïtina com a elements d'orientació, dirigir les nanoformulacions cap al paràsit lliure o als macròfags infectats amb el paràsit. Aquesta distribució específica va permetre (i) augmentar l'orientació cap als macròfags quan els liposomes estaven recoberts amb heparina o CS, (ii) reduir significativament l'IC50 del fàrmac en promastigots de *L. infantum* i *L. pifanoi* quan els liposomes estaven recoberts amb heparina o sulfat de condroïtina, (iii) reduir significativament la citotoxicitat en cèl·lules endotelials umbilicals humanes, i (iv) obtenir una major deposició de les preparacions liposomals nebulitzades en les etapes més profundes d'un simulador de vies respiratòries humanes en comparació amb la pentamidina lliure.

El segon enfocament es va centrar en la recerca de nous fàrmacs amb un mecanisme d'acció diferent dels actuals fàrmacs antileishmanials. Aquí, diferents compostos que interfereixen amb l'agregació de proteïnes van mostrar una certa activitat antileishmanial. En particular, la sal bis(stiripiridinium) YAT2150 va tenir

una millor activitat contra *L. infantum* que la majoria dels fàrmacs actualment utilitzats per al tractament clínic de la leishmaniosi, incloent pentamidina, miltefosina i paromomicina. En relació amb el mode d'acció de YAT2150, es va observar una reducció de l'agregació global de proteïnes en un cultiu de promastigots de *L. infantum*, segons l'anàlisi de tioflavina T. Aquesta troballa s'alinea amb el mode d'acció proposat de YAT2150 en *P. falciparum* determinat en un estudi anterior. L'encapsulació de YAT2150 en liposomes o immunoliposomes funcionalitzats amb un anticòs contra LPG va augmentar significativament l'índex de selectivitat del fàrmac per sobre de 100. Per tant, l'activitat de YAT2150 contra *Leishmania* i *Plasmodium* representa una oportunitat prometedora per al tractament de coinfeccions amb aquests paràsits.

La tercera estratègia va sorgir de la necessitat urgent de desenvolupar lligands que reconeguin específicament el paràsit, i que puguin ser utilitzats, per exemple, per a la funcionalització de sistemes d'alliberament de fàrmacs o com a eines de diagnòstic. Els aptàmers emergeixen com una alternativa més rendible i estable als anticossos, convertint-los en un enfocament valuós per diagnosticar malalties parasitàries tropicals, incloent la leishmaniosi, especialment en regions endèmiques. La leishmanolisina, o GP63, és la principal proteïna de superfície present en els promastigots de *Leishmania* i constitueix un dels seus principals factors de virulència, jugant un paper en l'adhesió del paràsit als macròfags i en la supervivència dels amastigots. Es van desenvolupar aptàmers d'ADN contra una forma madura de GP63 de *L. infantum* (LiGP63m), utilitzant el mètode de selecció sistemàtica de lligands per l'enriquiment exponencial (SELEX). Després de 7 cicles de SELEX, es van seleccionar 5 de les 20 seqüències d'aptàmers individuals, basant-se en l'anàlisi de dot blot que confirmava el reconeixement específic de LiGP63m recombinant i l'anàlisi de citometria de flux, on aquests cinc aptàmers van apuntar a més del 75% dels promastigots. Els aptàmers van mostrar una alta afinitat per LiGP63 endogen dins d'un lisat de promastigots, amb una afinitat de vinculació en el rang µM, segons un assaig d'aptàmer lligat a sorbent immobilitzat (ALISA). En conclusió, els aptàmers aquí discutits tenen un gran potencial per a intervencions contra la leishmaniosi com a eines de diagnòstic potencials i com a molècules d'orientació per a nanotransportadors d'alliberament de fàrmacs.

Funding

The work presented in this thesis was funded by different grants. Firstly, we are very thankful to Fundació La Marató de TV3 for their financial support to the project entitled *Coated liposome nanocomplexes as drug delivery systems for treatment of leishmaniasis* (Ref. 201811-32). We also acknowledge the Generalitat de Catalunya, Spain (AGAUR: 2017-SGR-908 and 2021-SGR-00635) and the Ministerio de Ciencia e Innovación/Agencia Estatal de Investigación (MCIN/AEI/10.13039/501100011033) for the grant PID2021-128325OB-I00.

Index

Abbreviations

A	Adenine
AmB	Amphotericin B
ATP	Adenosine triphosphate
CC_{50}	Cytotoxicity concentration 50%
CDK12	Cyclin-dependent kinase 12
CL	Cutaneous leishmaniasis
DALYs	Disability-adjusted life years
DDS	Drug delivery systems
DNA	Deoxyribonucleic acid
DNDi	Drugs for Neglected Diseases initiative
ELISA	Enzyme-Linked ImmunoSorbent Assay
FDA	Food and Drug Administration
GAG	Glycosaminoglycans
Gal	Galactose
GO	Gene ontology
HBPs	Heparin-binding proteins
IC_{50}	Half maximal inhibitory concentration
IDP	Intrinsically disordered proteins
IDR	Intrinsically disordered regions
IM	Intramuscularly
IV	Intravenously
kDa	Kilodalton
KMP-11	Kinetoplastid membrane protein 11
LAMP	Loop-mediated isothermal amplification
LDC	Lipid drug conjugates
***Li*H2A**	*L. infantum* histone H2A
***Li*H3**	*L. infantum* histone H3
***Li*PABP**	*L. infantum* poly(A)-binding protein
***Li*KMP-11**	*L. infantum* KMP-11
LPG	Lipophosphoglycan
MA	Meglumine antimoniate
Man	Mannose
MCL	Mucocutaneous leishmaniasis

mRNA	Messenger RNA
N	Asparagine
NPs	Nanoparticles
NTD	Neglected tropical disease
PCR	Polymerase chain reaction
PEG	Polyethylene glycol
PKDL	Post-kala-azar dermal leishmaniasis
PLAAC	Prion-like amino acid composition
PLGA	Poly (lactide-co-glycolide)
PMM	Paromomycin
PMN	Polymorphonuclear neutrophil granulocytes
PrD	Prion domains
PrLDs	Prion-like domains
PrP	Prion protein
PSG	Promastigote secretory gel
PV	Parasitophorous vacuole
Q	Glutamine
RDT	Rapid diagnostic tests
RNA	Ribonucleic acid
rRNA	Ribosomal ribonucleic acid
SELEX	Systematic evolution of ligands by exponential enrichment
SI	Selectivity index
SLN	Solid lipid nanoparticles
ssDNA	single-stranded DNA
T	Thymine
VL	Visceral leishmaniasis
WHO	World Health Organization

Introduction

1. Leishmaniases relevance

The leishmaniases are a group of poverty-related parasitic diseases caused by protozoan parasites from the *Leishmania* genus. More than 20 of these protozoa pathogenically infect humans and other vertebrates, like dogs. These diseases are transmitted by different species of female sand flies that belong to the genus *Phlebotomus*, in Africa, Asia and Europe (Old World), or the genus *Lutzomyia,* in America (New World) (Brindha et al., 2021; Burza et al., 2018; WHO, 2023b).

There are mainly three different forms of the disease called visceral leishmaniasis (VL), which can be fatal if left untreated. The most frequent type of leishmaniasis is cutaneous leishmaniasis (CL), which typically results in skin lesions and mucocutaneous leishmaniasis (MCL) produces severe mutilations of the nose, palate and face (WHO, 2023b).

1.1 *Leishmania* parasite

The causative agent of leishmaniasis is a parasitic protozoan of the genus *Leishmania*, order *Trypanosomatida*, class *Kinetoplastea*.

Leishmania-like species were identified in two extinct and fossilized sand flies dating back from 100-20 million years ago (Steverding, 2017). Mitochondrial DNA from *L. donovani* was found in 4 mummies from Egypt and 9 mummies from Nubia (the actual Sudan) dating back 4000 years (Zink et al., 2006). Thousands of years later, upon his arrival in America, Pizarro noted symptoms resembling MCL, observing individuals with severe damage in their noses and lips (Steverding, 2017). However, it was not until 1903 when William Leishman (1865-1926) discovered this parasite. He reported the finding of “small oval bodies” from the spleen of a dead soldier in Dum Dum, India. He published the data, termed the illness “Dum-dum fever”, and thought that was a type of trypanosomiasis. Charles Donovan (1863-1951), a physiology professor, observed the same small oval bodies in splenic samples from Indian patients with splenomegaly and fever but was convinced that they were not trypanosomes. It was Ronald Ross (1857-1932), who was awarded the Nobel Prize in Physiology or Medicine in 1902 for his discovery of the vector of malaria (Nobel Prize Outreach, 2024), in charge of investigate kala-azar in India, who finally proposed the name *Leishmania* for the new genus and *Leishmania donovani* for the specie observed by Leishman and Donovan (Ross, 1903). The different

Leishmania species were later identified and described. *L. infantum* was named by Charles Jules Henry Nicolle (1866-1936) after he discovered it in Tunisian children, from there its name 'infantum' (Steverding, 2017).

1.1.1 *Leishmania* classification

Within the genus *Leishmania*, there are two main subgenera: *L. (Leishmania)* and *L. (Viannia)*. Both of these subgroups infect mammals, while a third subgroup, called *L.* (*Sauroleishmania),* exclusively infects reptiles (Figure 1). This classification is based on the specific regions of colonization within the sand fly gut. Parasites from the subgenus *Viannia* are restricted to the New World, and consequently, their vectors are exclusively *Lutzomyia* species (P. A. Bates, 2007).

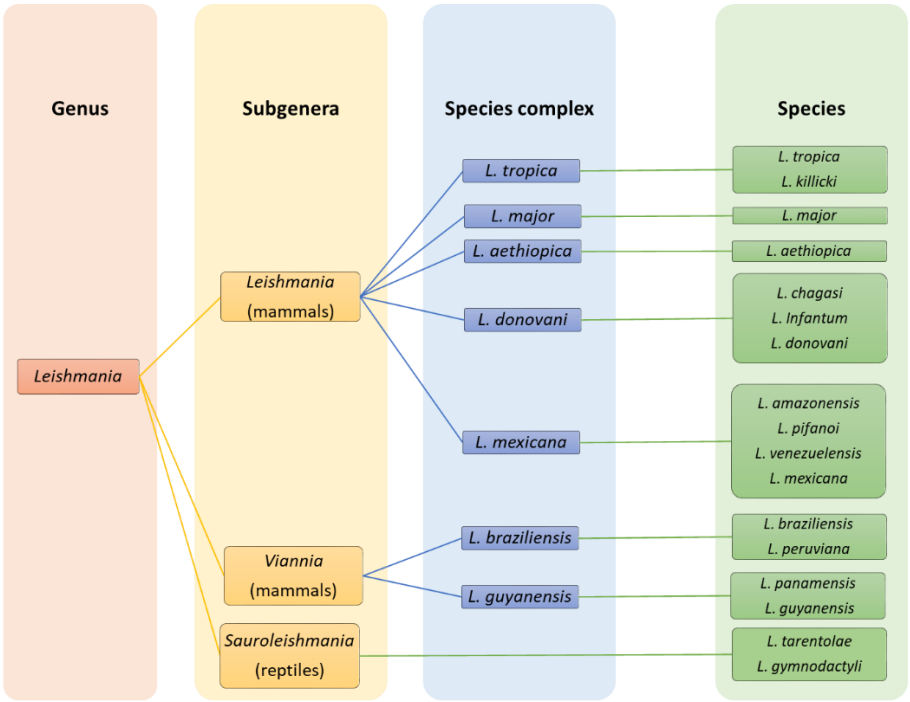

Figure 1. Classification of *Leishmania*, outlining the three subgenera. Parasites belonging to the subgenera *Leishmania* and *Viannia* infect mammals, while *Sauroleishmania* infects reptiles as their vertebrate hosts (P. A. Bates, 2007; Real et al., 2013).

1.1.2 Life cycle

Leishmania parasites have two morphological forms, namely amastigotes and promastigotes. These forms are found in mammalian and sand fly hosts, respectively (P. Bates & Rogers, 2004). During blood meals, female sand flies transmit promastigotes through bites (Figure 2). Subsequently, some promastigotes enter the bloodstream where they are phagocytized by macrophages and other mononuclear phagocytic cells. Inside them, promastigotes transform into the intracellular stage, amastigotes, (CDC, 2017). Amastigotes multiply and escape from cells via a poorly understood mechanism. Subsequently, they infect new phagocytic cells, primarily macrophages, as well as non-phagocytic cells like fibroblasts, recognized as host cells in latent leishmaniasis (McConville et al., 2007). Sandflies ingest infected cells during blood meals, and this cycle repeats. Amastigotes transform into promastigotes inside the sandflies' gut, specifically in the hindgut for the *Viannia* subgenus and in the midgut for the *Leishmania s*ubgenus, before migrating to the proboscis (CDC, 2017).

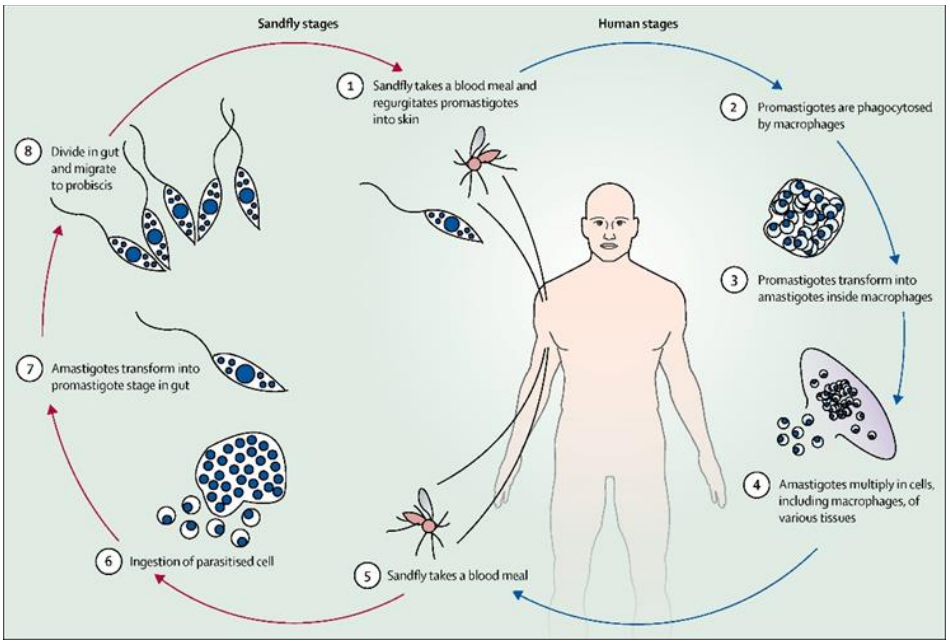

Figure 2. Life cycle of the *Leishmania* parasite in both human and sand fly host. Reproduced from (Burza et al., 2018) by permission of Elsevier.

Promastigote step

After the sand fly ingestion of amastigotes-containing cells, amastigotes undergo differentiation into promastigotes. Temperature and pH play pivotal roles in the transformation from amastigote to promastigote morphology (Figure 3a). Within the promastigote stage, five distinct cell types exist, distinguished by variations in the length of the cell body and flagellum, as well as their position within the sand fly's body (Figure 3b). They are procyclic promastigotes that will transform into nectomonad promastigotes, which further differentiate into leptomonad promastigotes. These will then differentiate into either metacyclic promastigotes, which represent the mammalian infective form transmitted during the sand fly's subsequent blood meal, or haptomonad promastigotes (Sunter & Gull, 2017). In 2018, a new *Leishmania* developmental form called retroleptomonads was identified in the sand fly stage (Serafim et al., 2018), highlighting that *Leishmania* life cycle is complex and may not be fully understood yet.

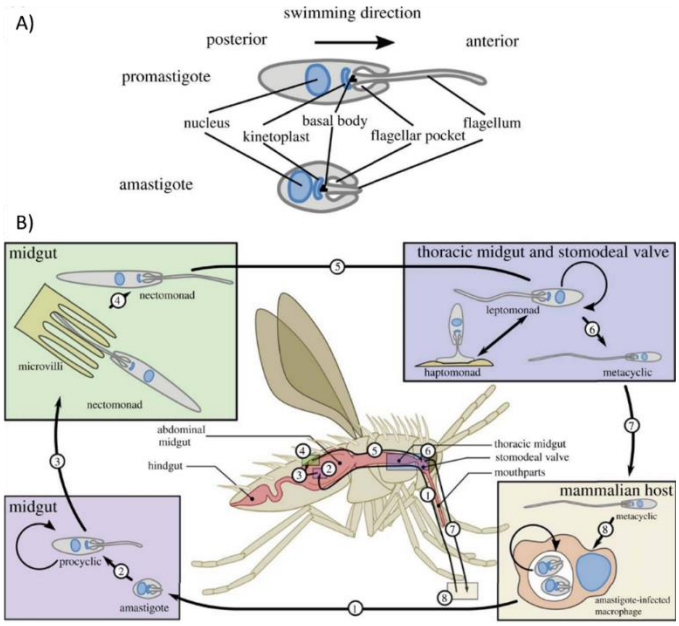

Figure 3. Morphology of *Leishmania* parasite and life cycle of the promastigote step. A) *Leishmania* promastigote and amastigote morphology. B) Life cycle of the *Leishmania* parasite focused on the promastigote step. A circular arrow denotes proliferative stages. Reproduced from (Sunter & Gull, 2017) under the terms of the Creative Commons Attribution License (http://creativecommons.org/licenses/by/4.0/).

Variables influencing the promastigote stage

Previously viewed as a mere carrier of *Leishmania* parasites between hosts, a phlebotomine sand fly is now recognized to play a crucial role in *Leishmania* development and transmission success, as revealed by seminal studies (Serafim et al., 2021). During the infection, there are some factors to consider:

1. **The sand fly gut microbiota**: Antibiotic-induced microbiota elimination impedes *L. infantum* multiplication in *Lutzomyia longipalpis*, which means that specific microbial content in the sand fly midgut may be crucial for the survival and differentiation of *L. infantum* parasites, although the underlying biochemical mechanisms remain unclear (Kelly et al., 2017).
2. **The number of blood meals that the sand fly takes**: Research suggest that sand flies taking multiple uninfected blood meals after acquiring *Leishmania* enhance infection (Serafim et al., 2018).
3. **Promastigote secretory gel (PSG):** PSG is produced by leptomonads and is crucial to induce a 'blocked fly,' causing infected sand flies to regurgitate parasites into the skin before a second blood meal. This enables the transmission of metacyclic parasites to the animal or person along with the PSG (P. A. Bates, 2018) (P. A. Bates, 2007).
4. **Sand fly saliva**: It possesses potent vasodilatory and antihaemostatic properties that exacerbates CL (P. A. Bates, 2007).

Amastigote step

Once a *Leishmania*-infected sand fly takes a blood meal, the sand fly bite introduces the flagellated, nondividing metacyclic promastigotes into the skin of the mammalian host. The bite produces a skin damage where the macrophages and polymorphonuclear neutrophil granulocytes (PMN) will be attracted (De Menezes et al., 2016). Macrophages phagocytose metacyclic promastigotes, either directly or after passing through the wave of PMN rapidly recruited to the sand fly bite site. PMN constitute the initial defence against infection, by phagocytosing the pathogen and releasing mediators that modify the extracellular environment. They also attract inflammatory cells (Lagasse & Weissman, 1994) and macrophages via monocyte-attracting chemotactic factors like the chemokine MIP-1β (van Zandbergen et al., 2004). PMN act like 'Trojan horses' when they are infected and are phagocytosed by macrophages. *Leishmania* survives within PMN *in vivo*, and it

is suggested that is due to the inhibition of oxidative burst induction, as observed *in vitro.* *Leishmania* infected PMN became apoptotic, therefore present phosphatidylserine in the outer cell membrane, recognised as a 'eat me' signal by macrophages. *Leishmania* inside PMN cannot replicate and remains as promastigote stage (Laskay et al., 2003).

Promastigotes directly internalized by macrophages undergo differentiation within the phagolysosome, transforming into small, aflagellated amastigotes. Amastigotes represent a replicative stage characterized by periodic escape from the host cell, followed by rapid reinfection of other phagocytes such as macrophages or dendritic cells, as well as certain non-phagocytic cell types like fibroblasts. In those cells, the parasite will remain in latent infections that may persist throughout the host's lifetime (McConville et al., 2007) (Bogdan et al., 2000).

Various factors influence the interaction between the parasite and the host cell. One very important factor is the *Leishmania* species, which will result in differences in the parasitophorous vacuole (PV). For the *L. donovani* complex (*L. donovani, L. infanum* and *L. chagasi*), there is a tight-fitting PV that serves as an insulating barrier for individual parasites, ensuring a more intimate environment and the descent cells will segregate into their respectives PVs. In contrast, a significantly larger communal PV contains multiple parasites in species belonging to the *L. mexicana* complex (*L. mexicana, L. amazonensis and L. pifanoi*), with a shared and expansive space. PV differences highlight varied intracellular strategies and pathogenesis among *Leishmania* species (Kima, 2007). The nutritional requirements and metabolism of *Leishmania* amastigotes are very complex and highly dependent on the host cell environment they inhabit. They acquire essential nutrients, cations and carbon sources through both endocytic pathways and direct uptake from the macrophage cytosol. Moreover, amastigotes are capable of internalizing large macromolecules such as proteins, carbohydrates, deoxyribonucleic acid (DNA), and ribonucleic acid (RNA) through endocytosis (McConville et al., 2007). For a more detailed understanding, the forthcoming review delineates the metabolic pathways requisite for *Leishmania* amastigotes (McConville et al., 2007).

1.1.3 Epidemiology

By 2022, 99 out of 200 countries or territories reporting to the World Health Organization (WHO) were endemic for both VLs and CLs, while 9 were endemic for

VLs only and 19 for CLs only (WHO, 2024) (Figure 4). Within all those regions, Brazil, east Africa and India were the most affected by VL. Central Asia, America, the Middle East and the Mediterranean basin, registered the 95% of the CL cases and 90% of MCL took place in Bolivia, Brazil, Ethiopia and Peru (WHO, 2023b).

Nowadays, leishmaniasis is a neglected tropical disease (NTD), despite there are over 12 million people infected worldwide and the annual incidence is approximately 600,000 to 1 million cases of CL and from 50,000 to 90,000 new cases of VL (WHO, 2023b). Moreover, leishmaniasis is the second deadliest parasitic disease after malaria (eBioMedicine, 2023a)

The disease burden of NTDs is usually measured in disability-adjusted life years (DALYs). According to the systematic analysis conducted for the Global Burden of Disease Study 2017 (Kyu et al., 2018) leishmaniasis was responsible for 774,000 DALYs in 2017, with VL contributing 66% of the overall burden of leishmaniasis. A total of 62 million DALYs were attributed to NTD(Kyu et al., 2018)

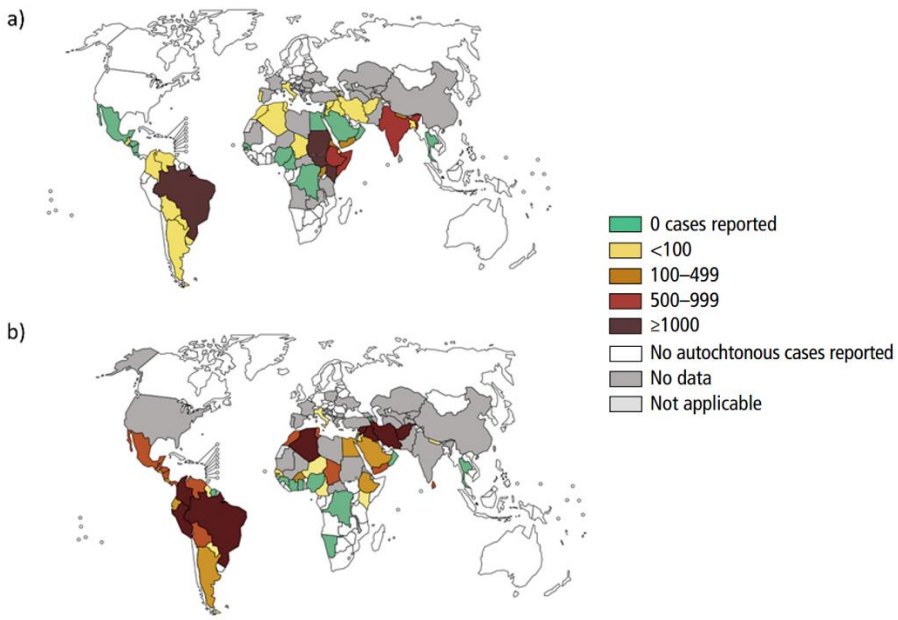

Figure 4. Global map depicting the worldwide distribution of visceral (a) and cutaneous (b) leishmaniasis. Adapted from (WHO, 2023b).

In the WHO European Region, the specie causing VL is *L. infantum*. This specie is also responsible of some CL but is genetically different from the one causing VL. Also, *L. tropica* and *L. major* cause CL in the WHO European Region (WHO Regional Office for Europe, 2017).

In the south of Europe, leishmaniasis is hypoendemic and mainly caused by *Leishmania infantum* where dogs are the main reservoir (Gil-Prieto et al., 2011). In Spain, the vectors of *L. infantum* are *Phlebotomus perniciosus* and *P. ariasi*, and the dog is the main animal reservoir (WHO Regional Office for Europe, 2017)

In Spain, leishmaniasis became a notifiable disease in 2015. Since then, between 2016 and 2018, a total of 1,172 cases of leishmaniasis were reported. This number remained consistent from 2019 to 2021, with a total of 1,074 reported cases, of which 1,041 were autochthonous. The regions with the highest incidence rates, in descending order, were the Balearic Islands, Valencian Community and Murcia (Figure 5). Among the reported cases, 48.6% were classified as VL, 49.5% as CL and MCL represented only 1.9% of the cases. Hospitalization was necessary for 49.6% of the cases, with 92.2% attributed to VL and the rest to CL and MCL (Fernández Martínez, 2023).

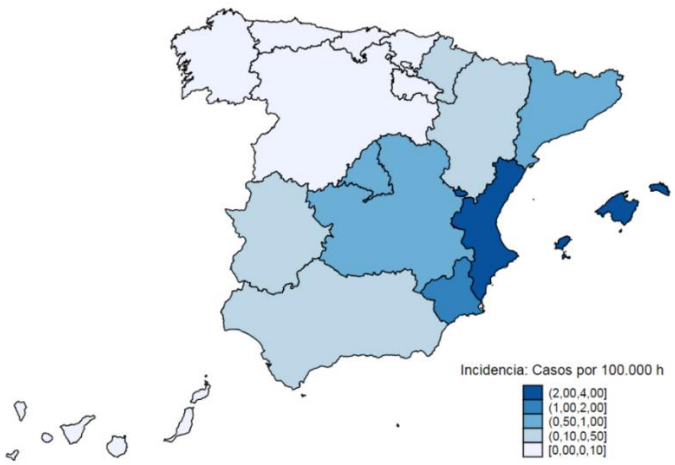

Figure 5. Incidence rate of leishmaniasis by Autonomous Community in Spain. Period 2019-2021. Adapted from (Fernández Martínez, 2023).

1.2 Leishmaniasis clinical manifestations

As reviewed in (Arenas et al., 2017; WHO, 2023a; WHO, 2010), there are different clinical manifestations of leishmaniasis depending on the species of *Leishmania* (Table 1) and the host genetic factors that will define the effectiveness of the host immune response. In summary:

- The most severe clinical form of the disease is VL, also called kala-azar. It is slowly progressive and is characterized by intermittent episodes of fever, hepatosplenomegaly, anaemia, lymphadenopathy, pallor, leukopenia, night sweats, weakness, asthenia, thrombocytopenia and weight loss. If not treated, VL will be fatal in more than 95% of cases. In the later stages, frequent intercurrent infections, such as pneumonia, dysentery, and tuberculosis along with multisystem failure and hemorrhage resulting from thrombocytopenia will contribute to mortality.
- In some cases, 6 months to one or more years after VL has apparently been cured, post-kala-azar dermal leishmaniasis (PKDL) appears as a rash with macular, papular, or nodular characteristics, typically affecting the face, upper arms, and trunk.
- The most prevalent form of leishmaniasis is CL, typically healing spontaneously but resulting in skin lesions on body areas exposed to insect bites, such as the ears, nose, lips, and legs. Although the ulcers produced are usually painless, they may endure for a time ranging from 3 months up to 20 years, potentially leading to disability or stigmatization.
- Mucocutaneous leishmaniasis (MCL) is characterized by very destructive lesions in nose and other sites as pharynx, larynx, palate and esophagus. MCL can go unnoticed in the initial phases. However, it does not heal spontaneously, and last stages might result in gross mutilations of the nose, palate, and face. In the worst scenario, if MCL affects the nasal cavity it can cause death. MCL is rarely observed in the Old World.
- Diffuse cutaneous leishmaniasis is characterized by widely disseminated cutaneous macules since there is a deficiency in the cellular immune response to parasite antigens. This form of the disease generally does not respond to treatment, so there are some cases where the disease has been evolving up to 20 years. Generally, it does not heal spontaneously.

- Leishmaniasis recidivans represents a rare complication of CL with a prolonged duration that can extend over several years. If left untreated, this condition may result in destruction and disfigurement.

Table 1. Subgenus, tropism, and localization of *Leishmania* species infecting humans. Adapted from (WHO, 2010).

	Subgenera			
	L. (Leishmania)		*L. (Viannia)*	
	Mainly viscerotropic	Mainly dermotropic	Mainly dermotropic	Mainly mucotropic
Found in Old World	*L. donovani* *L. infantum*	*L. major* *L. tropica* *L. killicki*[a] *L. aethiopica* *L. infantum*		
Found in New World	*L. infantum*	*L. infantum* *L. mexicana* *L. pifanoi*[a] *L. venezuelensis* *L. garnhami*[a] *L. amazonensis*	*L. braziliensis* *L. guyanensis* *L. panamensis* *L. shawi* *L. naiffi* *L. lainsoni* *L. lindenbergi* *L. peruviana* *L. colombiensis*[b]	*L. braziliensis* *L. panamensis*

[a]: Species status is under discussion

[b]: Taxonomic position is under discussion

1.3 Leishmaniasis diagnosis

Leishmaniasis diagnosis is based on the detection of *Leishmania* parasites or DNA in the tissues affected. There is not a validated rapid diagnostic test (RDT) for detecting *Leishmania* antigens in cases of leishmaniasis. The Roadmap for Neglected Tropical Diseases 2021-2030 by the WHO, outlines key priorities for the diagnosis of VL (WHO, 2020). In general, the number of parasites in the blood during a trypanosomatid infection is low, making them undetectable by polymerase chain reaction (PCR) or loop-mediated isothermal amplification (LAMP) in this sample (Martín et al., 2013).

1.3.1 VL

The diagnostic tools for VL vary depending on the country and the level of the health system (Table 2). The gold standard technique is considered the detection of amastigotes in a splenic aspirate by light microscope examination. The drawback of the splenic aspiration is its association with haemorrhage (1 case per 1000 procedures). Amastigotes can be detected in other tissues such as bone marrow or lymph nodes, but their sensitivity decreases (96% in the spleen, 69.5% in bone marrow and 59% in lymph node). Moreover, all those procedures are quite invasive (van Griensven & Diro, 2019; WHO, 2010).

Techniques for the detection of antibodies such as serological tests can be used as diagnostic tool (Enzyme-Linked ImmunoSorbent Assay (ELISA), immunofluorescence, Western blot or direct agglutination test). However, active and quiescent infection cannot be reliably differentiated and sensitivity is low (Burza et al., 2018; van Griensven & Diro, 2019).

RDTs based on the rK39 or rK28 antigen detect the presence of antibodies against *Leishmania.* They offer different sensitivity depending on the geographical region and can only serve as a supplementary tool alongside the clinical context (splenomegaly, hepatomegaly, loss of weight, fever) or other techniques (Burza et al., 2018).

Antigen detection tests applied to non-invasively obtained fluids, such as urine, are promising techniques. In 2001, a new antigen detection latex agglutination test (KATex, Kalon Biological, Ltd., Guildford, UK) was able to detect a low molecular weight carbohydrate antigen from *Leishmania* in pre-boiled urine. This test is simple to use and cheap. However, its sensitivity must be improved (WHO, 2010) (Attar et al., 2001). This test revealed that urine can be a good biological sample for further assays, in fact, it has been determined the potential of rK28 ELISA for the detection of antibodies in urine of VL patients with a sensitivity similar to the detection in serum (Ghosh et al., 2016). Saliva does not seem as effective as urine for the diagnosis of VL (Vaish et al., 2012).

Molecular techniques, such as PCR, are sensitive, but they are not routinely used in the field. To overcome that, a reverse transcriptase LAMP assay has been developed as a point-of-care diagnostic tool able to detect all *Leishmania* species in one test with basic equipment (Adams et al., 2010).

Table 2. Diagnostic techniques for VL in highly endemic areas, depending on the health system level. Adapted from (WHO, 2010).

Level of health system	Diagnostic tests
Primary health care centre	- rK39 RDT
District hospital	- rK39 RDT - Microscopy on bone marrow, spleen or lymph node aspiration
Tertiary care (referral hospital)	- Serological test: rK39 RDT, agglutination test… - Microscopy on bone marrow, spleen or lymph node aspiration - Culture or PCR

The leishmanin skin test or Montenegro test is based on a T cell inflammatory reaction when the soluble part of a promastigote lysate, called leishmanin antigen, is injected intradermally into the forearm of individuals. It has been widely used in epidemiological studies to detect exposure and immunity to *Leishmania*, and as complementary diagnostic tool for CL in endemic regions of South America. However, nowadays it is no longer used due to the absence of leishmanin obtained under good manufacturing practice conditions (Carstens-Kass et al., 2021).

1.3.2 CL and MCL

The gold standard technique for CL diagnosis involves the observation of amastigotes from the lesion. The samples taken from the lesion include biopsies of the lesion border, needle aspirates from the active lesion border, and dermal scrapings (de Vries et al., 2015). In MCL, the parasite load at the lesion site is generally low, making molecular methods for detecting parasite DNA the most sensitive option. Serological tests have limited use in MCL or CL infection, as they cannot distinguish between active and past infections, and the humoral response in CL is poor (WHO, 2010).

There is one RDT for CL approved by the Food and Drug Administration (FDA) called CL Detect™ Rapid Test (InBios International Inc.). The antigen recognized by

the test is the peroxidoxin. This antigen is expressed in both promastigotes and amastigotes. According to the manufacturer, its specificity varies from 84% to 96% depending on the endemicity of the region, according to the manufacturer InBios International, Inc. However, in some regions, such as Sri Lanka, this test may not be useful, since one study showed that the sensitivity of the CL RDT, compared to the PCR, was only 36% in detecting CL caused by *L. donovani* (De Silva et al., 2017). Another FDA-approved diagnostic real-time PCR test relies on detecting the 16S ribosomal RNA (rRNA) gene to identify *Leishmania* infections. Known as SMART Leish (Cepheid EUA, Sunnyvale, CA, USA and WRAIR, Silver Spring, MD, USA), it is exclusively authorized in Department of Defense laboratories (Gow et al., 2022)

There are some more detection kits in progress, such as VIASURE *Leishmania* Real Time PCR Detection Kit (CerTest Biotec, S.L., Zaragoza, Spain), which detects the 18S rRNA gene and it is indicated for the diagnosis of VL and CL from skin biopsy, blood and bone-marrow aspirate samples, according to the manufacturer.

1.3.3 PKDL

The diagnosis of this clinical form of leishmaniasis is complicated; its symptoms are hypopigmented macules in immunocompetent patients and papulo-nodules in immunocompromised individuals distributed all over the body. On one hand, the detection of amastigotes is not always easy, being more difficult in the macular than in the nodular lesions. Serological tests are useful for excluding alternative illnesses such as leprosy, but they cannot differentiate between a present PKDL and a previous VL. They are also more sensitive in India than in Africa. PCR is not always available in the field. To address these challenges, the WHO developed an algorithm for PKDL diagnosis and treatment (WHO, 2012) (Kumar et al., 2020).

1.4 Leishmaniasis control and elimination

The prevention and control of the spread of leishmaniasis depend on implementing measures for vector and animal reservoir control. These measures include the application of repellents, insecticide-treated nets, and antiparasitic agents like collars and pipettes. Furthermore, the vaccination of dogs is crucial in this preventive approach, whenever feasible. Additionally, minimizing exposure to the vector, early diagnosis, and appropriate management of cases, both in humans

and domestic animals, are essential components of preventive strategies. In addition, effective behavioural change interventions are essential for community mobilization and education (WHO, 2023b). The ultimate goal of prevention and control measures is disease elimination. To date, the primary initiative for VL elimination is the regional kala-azar elimination initiative. It was launched collaboratively, in 2005, by Bangladesh, India, and Nepal trying to address the significant burden of the disease they collectively represented (70% of the global cases between 2004 and 2008). Bhutan and Thailand joined the initiative in 2014 (WHO, 2023a). Bangladesh successfully achieved elimination in 2017, which means < 1 VL case per 10000 population annually, and has maintained this elimination status since. India and Nepal significantly decreased the number of cases since the beginning of the initiative (Figure 6). This framework had three clear strategic interventions with specific plans within them (Figure 7). The last update of this framework was in 2022 (WHO, 2022).

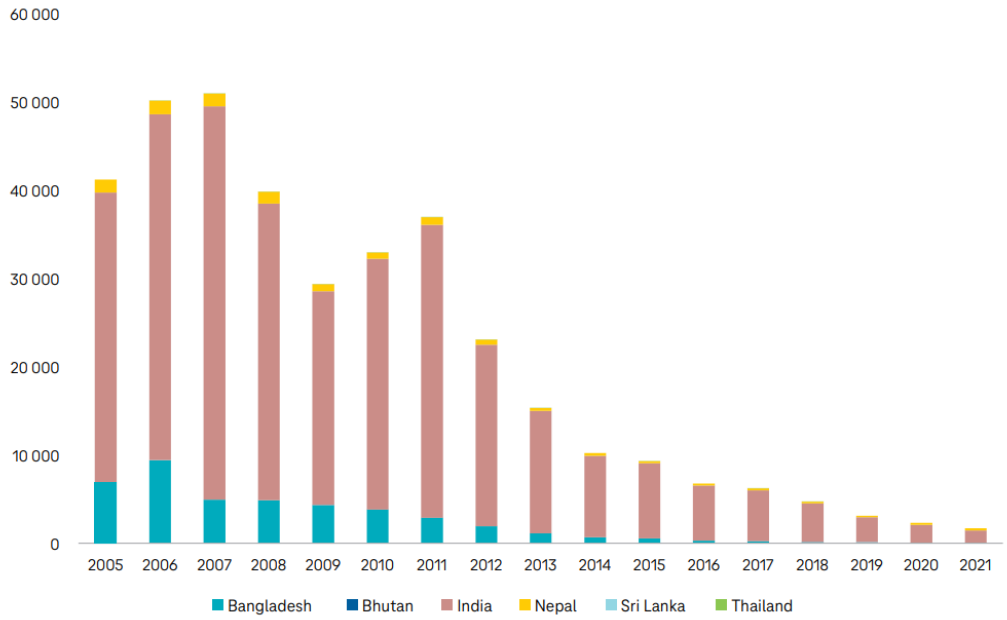

Figure 6. The number of new VL cases reported in the South-East Asia Region, 2005–2021. Reproduced from (WHO, 2022) with its permission and under the licence: CC BY-NC-SA 3.0 IGO.

In the described elimination initiative, humans have been considered the only *L. donovani* reservoir in the South-East Asia Region (WHO, 2022). VL produced by *L. donovani* or CL caused by *L. tropica* are usually considered anthroponotic leishmaniases, because humans are the reservoir hosts. In contrast, *L. infantum* has a zoonotic cycle where dogs are the principal reservoir hosts. The control of reservoir hosts with treatment and vaccination it is a vital element in strategies aimed at controlling zoonotic visceral and CL. Firstly, it is necessary to determine the distribution and prevalence of the infection in dogs and infected dogs should be eliminated or treated; allopurinol is widely used in the Mediterranean region (World Health Organization, 2010). Currently, there are no vaccines or chemoprophylaxis available for humans, but there are for dogs (Aronson et al., 2017). The initial vaccine for canine leishmaniasis was called Canileish®, was approved in 2011 and it is administered in three doses. Currently LetiFend® is the exclusive vaccine available in Europe. It comprises five distinct antigens derived from the four proteins most immunogenic in *L. infantum*, forming a recombinant chimeric protein known as Protein Q (Fernández Cotrina et al., 2018). The primary vaccination involves a single injection, followed by annual booster shots. The vaccine demonstrates an efficacy of 72% (LeishVet, 2024). Also, the prevention of sand fly bites is crucial in stopping the spread of *L. infantum* (Montoya et al., 2020).

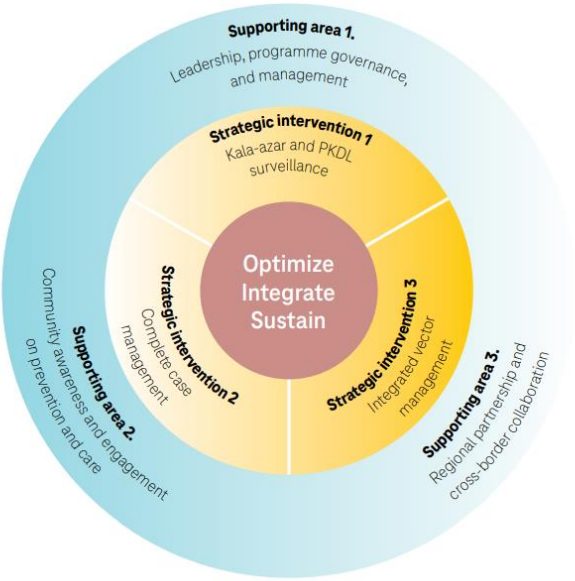

Figure 7. Strategic aim, interventions and supporting areas to achieve the goal of the regional strategy of accelerating and sustaining elimination of kala-azar in the South-East Asia region, 2022–2026. Reproduced from (WHO, 2022) with its permission under the licence: CC BY-NC-SA 3.0 IGO.

1.5 Leishmaniasis treatment

The drugs currently employed in the treatment of human leishmaniasis are the pentavalent antimonials, amphotericin B (AmB), L-AmB, pentamidine isethionate, miltefosine, and paromomycin (PMM). Subsequently, a detailed discussion regarding these medications will be presented (Table 3) along with their chemical structures (Figure 8). The current chemotherapy varies depending on the leishmaniasis clinical form. Nevertheless, there are some challenges that must be overcome, such as drug resistance, concerns about toxicity, issues linked to parenteral administration, availability, and the elevated costs of specific formulations (Ghorbani & Farhoudi, 2017; Olías-molero et al., 2021; Sundar & Singh, 2018b). Indeed, the 2020 Roadmap for Neglected Tropical Diseases 2021-2030 of the WHO aims to eliminate Chagas disease and leishmaniasis as public health issues. The development of new, patient-friendly, safe, and effective therapeutic breakthroughs is crucial for successfully reaching this goal (WHO, 2020).

Treatment guidelines vary among regions, due to differences in the efficacy of treatments across them (eBioMedicine, 2023b). For instance, in India, miltefosine exhibited cure rates above 90%, where VL is caused by *L. donovani*¸ while in Brazil, where *L. infantum* is the cause of VL, cure rates ranged from 43 to 67% (eBioMedicine, 2023b). This variation is thought to result from the natural resistance of *L. infantum* to miltefosine, which is associated with the absence of the 3' nucleotidase/nuclease genes NUC1 and NUC2. These genes are part of the miltefosine susceptibility locus (Carnielli et al., 2022). Another challenge is the treatment of certain forms of the disease, such as recurrent leishmaniasis in some immunosuppressed individuals due to the absence of a proper treatment protocol (Piccica et al., 2021).

Table 3. Currently employed antileishmanial drugs for VL, CL, MCL and/or PKDL indicated with (X). IV: Intravenously; IM: intramuscularly.

	Pentavalent antimonials	**Pentamidine**	**AmB / L-AmB**	**Miltefosine**	**PMM**
VL	X	X	X	X	X
CL	X	X		X	X
MCL	X	X		X	
PKDL	X		X		
Introduction Year	1937–1945	1973	1959/1997	2002	2006
Mechanism of action	Trypanothione reductase inhibition, key enzyme for the reduction of the oxidative stress produced during *Leishmania* infection	Not clear. Interaction with kinetoplast DNA, inhibition of RNA polymerase and mithocondrial topoisomerase II	Binding to cell membrane sterols, impaired cell membrane permeability	Not clear. Lipid interaction, inhibition of cytochrome c oxidase (decreasing ATP levels)	Not clear. Alteration of membrane fluidity and mithocondrial membrane potential, binding to 30S ribosomal subunit
Described resistance	Yes	Yes	Laboratory strains	Laboratory strains	Laboratory strains
Route of administration	IM or IV	IM or IV	IV	Orally	IM
Doses (for VL in WHO European Region)	20 mg Sb^{5+}/kg/day	4 mg/kg/day	3-5 mg/kg/day (AmB-L)	2.5 mg/kg/day	15-20 mg/kg/day
Time (for VL in WHO European Region)	28-30 days	15-20 days	3-10 days (AmB-L)	28 days	21-28 days
Reference	(Capela et al., 2019; Olías-molero et al.,	(Olías-molero et al., 2021; Capela et al., 2019; WHO	(Olías-molero et al., 2021; FDA, 2008; Capela et	(FDA, 2014; Olías-molero et al., 2021; Capela et	(Olías-molero et al., 2021; Sundar & Chakravarty,

	2021; WHO Regional Office for Europe, 2017)	Regional Office for Europe, 2017)	al., 2019; WHO Regional Office for Europe, 2017)	al., 2019; WHO Regional Office for Europe, 2017)	2008; Capela et al., 2019; WHO Regional Office for Europe, 2017)

1.5.1 Pentavalent antimonials

In 1913, Gaspar Vianna was the first to use organic antimonials for the treatment of CL (Haldar et al., 2011). For over 70 years, two pentavalent antimonials, sodium stibogluconate (under the brand name Pentostam®) and meglumine antimoniate (MA) (under the brand name Glucantime®) (Figure 8) have been the first choice for treatment of VL, CL and MCL consisting of 28-30 days of painful treatment and producing well-known side effects, such as cardiac arrhythmias, tachycardia, myalgia… (Sundar & Singh, 2018a). Pentavalent antimonials continue to demonstrate high efficacy in treating VL caused by *L. donovani*. However, in the WHO European region, where *L. infantum* is the causative agent of VL, these antimonials are currently considered the secondary option and they are also used as systemic treatment for CL. The primary choice for VL in this region is L-AmB (WHO Regional Office for Europe, 2017). It is noteworthy, however, that over the past 25 years, the emergence of widespread resistance (Table 3) has resulted in failure rates exceeding 60% in the treatment of VL caused by *L. donovani* in Bihar state (India), which accounts for more than 90% of the VL cases in India (Perry et al., 2013). This underscores the evolving challenges in managing VL and emphasizes the need for ongoing research and alternative therapeutic strategies (Capela et al., 2019; WHO Regional Office for Europe, 2017).

Pentavalent antimonials act as prodrugs and become activated upon the reduction of Sb (V) to Sb (III). The Sb (III) species are responsible for inducing apoptosis in *Leishmania*. Importantly, this reduction process is stage-specific, occurring exclusively in amastigotes. In fact, an inhibition of Sb (V) activation and a reduction in the uptake of the active form Sb (III) by amastigotes has been noted in the context of *in vivo* antimonial resistance (Capela et al., 2019).

1.5.2 Pentamidine isethionate

Pentamidine is an aromatic diamidine (Figure 8) formulated as isethionate (FDA, 2019). Pentamidine isethionate administered intravenously or intramuscularly started to be used in 1980. However, due to high toxicity and cost,

AmB and its lipid formulation started to be widely employed to treat VL (Sundar & Singh, 2018). In the WHO region of the Americas, pentamidine stands as one of the therapeutic options for leishmaniasis treatment. Additionally, it is advised for patients with diffuse cutaneous leishmaniasis (Pan American Health Organization (PAHO), 2022) and it is considered a first-line treatment for CL caused by *Leishmania guyanensis* and *Leishmania panamensis* (PAHO, 2018). In the WHO European region, pentamidine is a treatment option for the imported diffuse CL produced by *L. aethiopica* and a secondary prophylaxis in VL and Human Immunodeficiency Virus-coinfected patients (WHO Regional Office for Europe, 2017). It is recommended to be administered only at the second level of care due to the potential acute events such as hypoglycemia or hypotension (Pan American Health Organization (PAHO), 2022).

One of the major drawbacks of pentamidine are its side effects. However, in a systematic review (Piccica et al., 2021) it was reported that most of its side effects were related to the administration route, the high dose needed for VL and the baseline health condition of patients. The cure rate was like other first-option antileishmanial drugs in both CL and VL. One of the major advantages of pentamidine is its low price and its availability in some places, such as Italy, while other drugs are more complicated to acquire. Therefore, it is still an option when the first-line drugs fail or cannot be used for some reason (Piccica et al., 2021). In this sense, targeted delivery and/or changing the administration route would help to improve pentamidine delivery. Actually, pentamidine already exist in an oral inhalation solution under the name of Nebupent to treat *Pneumocystis carinii* and *Pneumocystis jiroveci* pneumonia, in the market since 1989 (FDA, 2010). Another formulation of pentamidine, available in the market under the name Pentam 300, has been available since 1984 for treating pneumonia caused by *Pneumocystis carinii*, administered via parenteral (FDA, 2001). Both pentamidine compounds are considered orphan drugs.

1.5.3 AmB and L-AmB

AmB is a macrocyclic polyene (Figure 8) antifungal antibiotic produced by *Streptomyces nodosus* (FDA, 2008). AmB has been widely employed as a deoxycholate suspension (Fungizome®) for the treatment of VL after the failure and emergence of resistance against antimonials and pentamidine (Sundar & Singh,

2018b). Despite its efficacy, it presented side effects including fever, rigor, nephrotoxicity, and even myocarditis, necessitating hospital-based treatment (WHO, 2010). These drawbacks are reduced in its liposomal formulation (L-AmB), approved on 1997 as a safe and effective drug product for the treatment of VL under the name Ambisome® (Gilead, Foster City, CA, USA) (FDA, 1997). Although this compound was accepted more than 20 years ago, it is still being used, as there are no better options to treat leishmaniasis. In fact, L-AmB is the only FDA-approved for the treatment of VL (Aronson et al., 2017). However, high costs limit its use in most endemic countries. For example, according to guidelines of Somalia and South Sudan from 2012 (Somali Federal Government Ministry of Health and WHO, 2012), L-AmB, although it is the safest antileishmanial drug, it is the first line treatment in VL only in a few cases: for pregnancy, severe patients and HIV co-infected patients. Moreover, Ambisome® requires cold chain, something that in some countries is a significant problem (Somali Federal Government Ministry of Health and WHO, 2012). In an effort to address the high cost, additional L-AmB formulations have been developed, including Fungisome®, which has been commercially available in India as a safe and effective therapy for VL since 2003, with a lower price (Wijnant et al., 2018).

1.5.4 Miltefosine

Miltefosine, an alkyl phospholipid (hexadecylphosphocholine) (Figure 8), was originally formulated as an oral anticancer medication; however, it has also demonstrated antileishmanial activity (WHO, 2010). Miltefosine under the brand name Impavido® is recommended for VL caused by *L. donovani*, CL caused by *L. braziliensis, L. guyanensis,* and *L. panamensis* and MCL caused by *L. braziliensis* (FDA, 2014). It is, so far, the only oral FDA-approved drug against *Leishmania* (Aronson et al., 2017). Miltefosine has teratogenic potential and should not be taken by pregnant women. Additionally, common side effects may include gastrointestinal issues, such as nausea, vomiting, or diarrhea (Pijpers et al., 2019; WHO, 2010).

1.5.5 PMM

PMM an aminoglycoside antibiotic (Figure 8) is typically administered intramuscularly; however, it can be administered topically for CL (WHO, 2010). Injectable PMM is commercialized in India and available in East Africa, but not in countries of the WHO European Region. In combination with antimonials, it has

been shown to be very effective in East Africa (WHO Regional Office for Europe, 2017). Currently recommended in the WHO American region for monotherapy in patients with CL caused by *L. panamensis*, *L. braziliensis*, and *L. mexicana*, PMM is administered as a cream. Unfortunately, this alternative is currently commercially unavailable for purchase (Pan American Health Organization (PAHO), 2022). In general, PMM is well-tolerated and does not manifest numerous adverse effects and has a low cost (Capela et al., 2019)

The combination of PMM and sodium stibogluconate is cheaper than sodium stibogluconate in monotherapy and the treatment duration is reduced from 30 to 17 days. It is recommended in East Africa. Additionally, this treatment mitigates the risk of cardiotoxicity linked to sodium stibogluconate (DNDi, 2011). The combination of miltefosine and PMM proved to be as effective as sodium stibogluconate and PMM, requiring one less daily injection and a 3-day shorter treatment duration of 14 days. This patient-friendly regimen is significant, given that the majority of the population affected by VL are children (Musa et al., 2023).

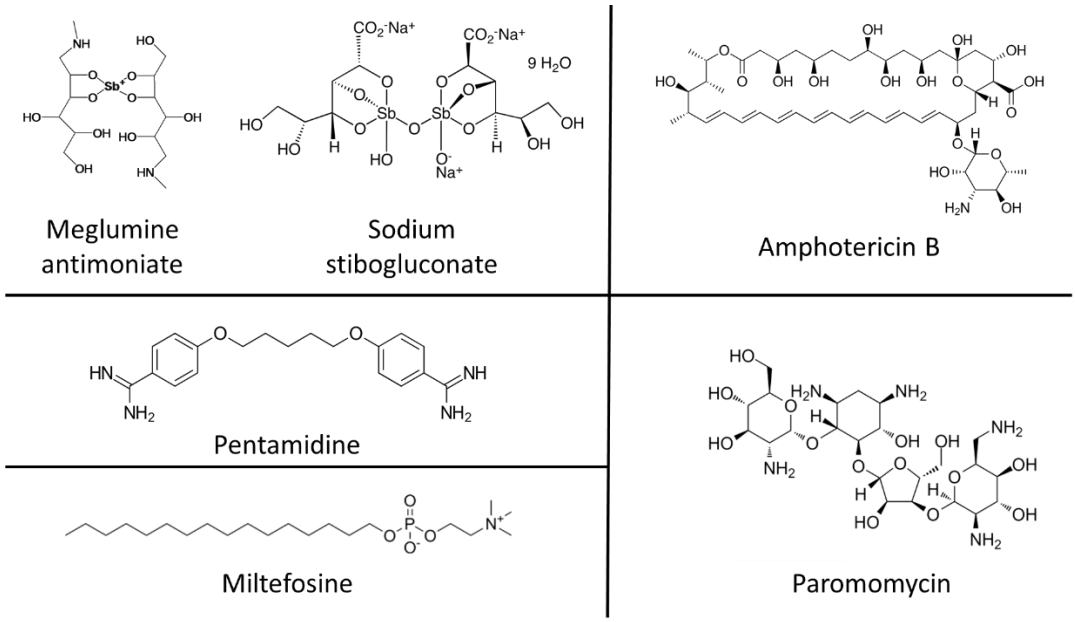

Figure 8. Chemical structures of the currently employed antileishmanial drugs described in Table 3.

2. Drug discovery for leishmaniasis

In summary, none of the current drugs is ideal. Moreover, they do not eliminate the parasites completely in all the cases. This underscores the urgent necessity for the development of newer therapeutic options more effective and user-friendly (WHO, 2020).

For the discovery of new compounds, high throughput screening has become the classical approach. Within this method, two strategies can be adopted: target-based or a whole phenotypic assay. In the context of anti-leishmanial drugs, and anti-kinetoplastid drugs in general, the preferred strategy is the whole phenotypic assay (Roquero et al., 2019), where it is not necessary to know the target. The high throughput screening comprises assays to evaluate the efficacy of a drug against *Leishmania* promastigotes and intracellular amastigotes, as well as assays to determine the cytotoxicity in human cells (Figure 9). Several concepts are crucial for clarity:

- **Half-maximal inhibitory concentration (IC_{50}):** This measures the efficacy of a drug against *Leishmania.* It refers to the concentration capable of inhibiting 50% of the growth of *Leishmania* promastigotes or amastigotes.
- **Cytotoxicity concentration 50% (CC_{50}):** This determines the concentration that induces unspecific cytotoxicity in 50% of host's cells.
- **Selectivity index (SI):** SI determines the therapeutic window of a compound against *Leishmania*. The SI is defined as the ratio between CC_{50} and IC_{50} ($SI=CC_{50}/IC_{50}$). A higher SI indicates a safer compound.

A compound with a SI value greater than 1 is considered more selective against *Leishmania* (Koutsoni et al., 2019). However, the accepted criteria for VL drug discovery include a SI>100 and an IC_{50} <10 µM (Katsuno et al., 2015).

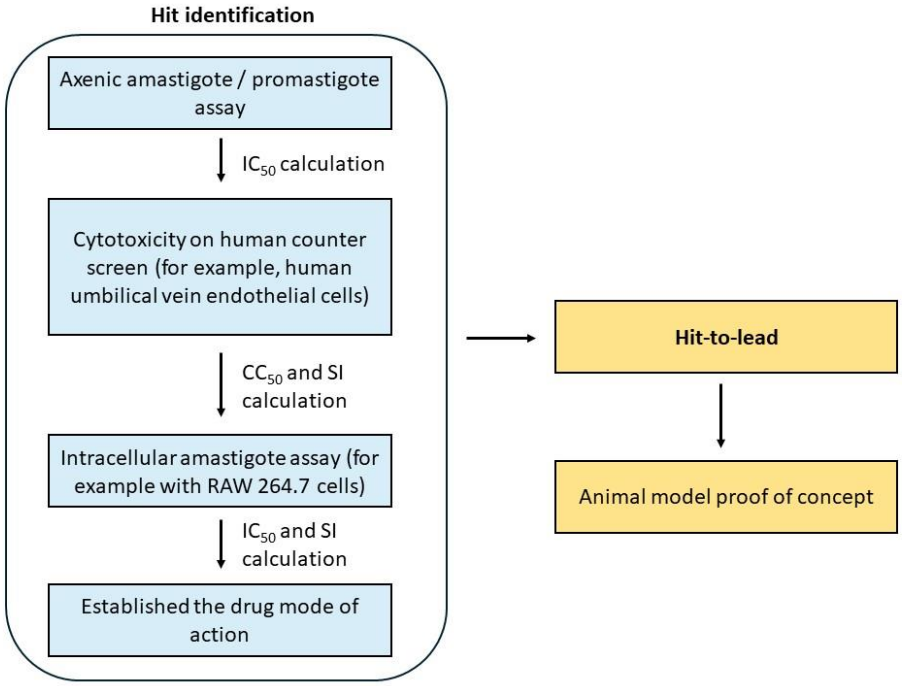

Figure 1. Screening cascade for the selection of new antileishmanial drugs according to a whole cell phenotypic assay. IC_{50}: inhibitory concentration 50%; CC_{50}: cytotoxic concentration 50%; SI: Selectivity index (SI). Adapted from (Katsuno et al., 2015).

2.1 Drugs currently in clinical trials for leishmaniasis

Aligned with the objective of discovering new drugs, the Drugs for Neglected Diseases initiative (DNDi) aims to provide safer, shorter, more effective, and readily accessible antileishmanial treatments through two distinct strategies (DNDi, 2020):

1. Short-term strategies involve improving existing treatments with known tools.
2. Long-term strategy developing a new generation of orally administered treatments. To accomplish this goal, they established the NTD Drug Discovery Booster in 2015. This initiative is an international consortium of pharmaceutical companies collaborating to identify new potential treatments for NTDs.

Indeed, some emerging treatments for leishmaniasis that are already in clinical trials are a result from the DNDi consortium (Table 4).

Table 4. Drugs in clinical trials for the treatment of leishmaniasis.

Drug name	Chemical class	What for?	Clinical phase	Mechanism of action	Ref.
LXE408	Triazolopyrimidine	VL	Phase II	Inhibition of kinetoplastid proteasome	(DNDi, 2022; Nagle et al., 2020)
DNDI-6148	Benzoxaborole	VL	Phase I: good tolerability	Inhibition of *Leishmania* cleavage and polyadenylation specificity factor (CPSF3) endonuclease	(DNDi, 2018; Mowbray et al., 2021)
DNDI-0690	Nitroimidazole	VL and CL	Phase I: favourable safety profile	Formation of toxic intermediates when activated by the nitroreductase enzyme NTR2	(Alves et al., 2018; DNDi, 2021a; Van Bocxlaer et al., 2021)
GSK3494245/ DDD1305143 (GSK245)	Imidazopyrimidine	VL	Phase I: adverse event stopped the trial	Proteasome inhibition	(eBioMedicine, 2023b; Wyllie et al., 2019)
DNDi-6899/ GSK899/DDD 853651	Pyrazolopyrimidine	VL	Phase I: ongoing	CRK-12 kinase inhibition	(Pinheiro & de Souza, 2022)
DNDI-5561	Amino-pyrazole	VL	Phase I: unfavourable safety results	Not elucidated yet	(Alves et al., 2018; Pinheiro & de Souza, 2022)
DNDI 6174	Benzoxaborole	VL and CL	Phase I: in 2025	Cytochrome bc_1 inhibitor	(Braillard et al., 2023; DNDi, 2024)
DNDI-2319/ CpG-D35	CpG oligonucleotide	CL and PKDL	Phase I: well tolerated and safe	Modulation of the host immune response	(DNDi, 2021b; Pinheiro & de Souza, 2022)

2.2 Novel *Leishmania* targets

The factors determining the leishmaniasis clinical form are linked to the host's immune response and the specific *Leishmania* species causing the infection (Arenas et al., 2017). However, only a few genes are species-specific, and these may be the key to why different forms of the disease are generated. On the other hand, *Leishmania*-specific factors should be explored as pan-*Leishmania* drug targets or vaccine candidates (Peacock et al., 2007). In this section, some novel *Leishmania* targets are going to be explored.

2.2.1 Nucleoside analogues and the purine salvage pathway

Leishmania lacks the ability to synthesize purine nucleotides *de novo* and relies on the host cell's purine salvage system for their acquisition. For this reason, nucleoside transporters are vital to facilitate the transport of nucleosides to the parasite. The targeting of those transporters or of enzymes involved in the purine salvage pathway can be explored as potential drug targets. Allopurinol is a purine analogue used to treat canine leishmaniasis, but due to its pharmacokinetic properties its use is not recommended in humans (Brindha et al., 2021). An analogue of purine, known as azathioprine, showed a SI higher than 30 for amastigotes from *L. infantum* and *L. donovani.* In *Leishmania* pyrimidine biosynthesis can occur through the pyrimidine salvage pathway and, unlike purine biosynthesis, also via *de novo* synthesis. As seen with purine analogues, a pyrimidine analogue, 5-fluorouracil, also exhibited activity against amastigotes of *L. infantum* and *L. donovani,* maintaining a high SI (Azzouz & Lawton, 2017).

2.2.2 Kinetoplastid proteasome inhibition

LXE408 (Table 4) is an oral candidate in phase II human clinical trials that showed good tolerability in phase I (DNDi, 2022). It is the optimized product from the previous GNF6702 (Khare et al., 2016), which had too low solubility for an effective absorption through oral administration (Nagle et al., 2020). In *T. cruzi,* GNF6702 resulted in an accumulation of ubiquitylated proteins (Khare et al., 2016). The two mentioned compounds and GSK3494245 (Table 4), which progressed to phase I human clinical trials, primarily act by inhibiting of the chymotrypsin-like activity catalysed by the β5 *L. donovani* proteasome subunit (Nagle et al., 2020; Wyllie et al., 2019).

2.2.3 Mitochondria inhibitors

A single mitochondrion is present in trypanosomatid parasites occupying about 12% of the cell volume and displaying structural and functional differences from mammalian mitochondria. The differences present in the *Leishmania* spp. electron transport chain are present in complex I, complex II, complex III and complex IV (Fidalgo & Gille, 2011; Ortiz et al., 2016). Specifically, the amino acid sequence of cytochrome b within the complex III, showed variations in putative ubiquitin interactions sites (Fidalgo & Gille, 2011; Ortiz et al., 2016). The new drug DNDI-6174 (Table 4) interacts with the Qi active site from complex III (Wall et al., 2020). In addition, in complex IV, the protein Ldp27, which is abundantly expressed in metacyclic promastigotes and amastigotes, may serve as a promising target. Ldp27-deficient parasites were unable to proliferate within macrophages likely due to an observed reduction of ATP production attributable to the absence of Ldp27 (Dey et al., 2010). The pentamidine mechanism of action is not clear, but it is related to a disruption in the mitochondrial membrane potential, caused by an imbalance of the intracellular Ca^{2+} levels. In addition, it is known to interact with the kinetoplast DNA (Table 3) (Fidalgo & Gille, 2011).

2.2.4 Cyclin-dependent kinase 12 (CDK12)

CDK12 is the target of pyrazolopyrimidines, such as DNDi-6899 (Table 4), which is already in phase I human clinical trials (Pinheiro & de Souza, 2022; Wyllie et al., 2018). In mammalian cells, more than 20 cyclin-dependent kinases have been identified. Some, such as Cyclin-dependent kinase 1, are involved in the regulation of the cell cycle, and their activity varies throughout it (Satyanarayana & Kaldis, 2009). Although the physiological function of CDK12 in *Leishmania* is still unknown (Wyllie et al., 2018), its gene is essential for *L. donovani* and *L. mexicana* promastigotes and the protein exists in a complex with the cyclin 9 (Broni et al., 2021).

2.2.5 Protein aggregation and *Leishmania*

The two stages of *Leishmania* life cycle, involving the human host and the sand fly vector, expose the parasite to significant environmental changes. This requires a coordinated cellular response involving a precise control of gene expression, protein synthesis, folding and degradation. In certain *Leishmania* species, a lack of correlation between protein abundance and mRNA levels has been

described (De Pablos et al., 2016), indicating that the gene expression control occurs at post-transcriptional and post-translational levels (Karamysheva et al., 2020), underscoring the high importance of proper protein homeostasis.

2.2.5.1 Protein folding process

The primary structure of a protein is determined by its linear sequence of amino acids. The link between the amino acid carboxyl and amino groups through a peptidic bond and the stabilization of the structure through hydrogen bonds conform the secondary structure. The two main secondary structures are α-helices and β-sheets (Sanvictores & Farci, 2022). The interaction among the amino acid R-groups from α-helices, β-sheets and unstructured regions form the tertiary structure. Some proteins may show also a quaternary structure when composed of multiple subunits (Floudas et al., 2006).

The native protein state typically represents the most thermodynamically stable structure under physiological conditions, which corresponds with the lowest-energy conformation (Dobson, 2003). However, Cyrus Levinthal illustrated that for a protein to explore all possible conformations until reaching the most stable one, it would require more time than the age of the universe. This phenomenon is known as Levinthal's paradox (Cyrus Levinthal, 1696). Currently, there is a consensus that protein folding is governed by an energy landscape (Figure 10). In this landscape, regions that achieve correct folding have low energy, while unfolded regions continue to search for the optimal conformations (Raskatov & Teplow, 2017). Those conformations require the coordination of numerous weak interactions, including hydrophobic forces, which play a crucial role by isolating the nonpolar amino acid residues from the aqueous environment, which drives the folding of the protein into its native three-dimensional structure (Kim et al., 2013).

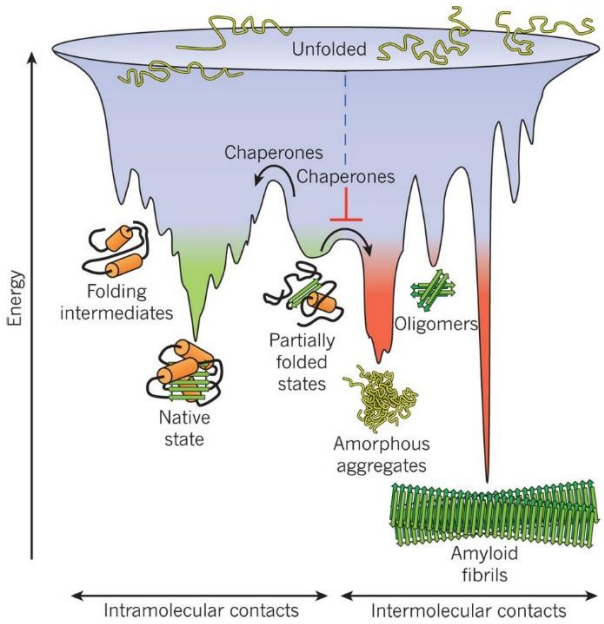

Figure 10. Protein folding and aggregation scheme illustrating the funnel-shaped free-energy landscape, showing the generation of low-energy structures through folding or aggregation. Reproduced from (Kim et al., 2013) with permission from Springer Nature.

2.2.5.2 *Protein misfolding and aggregation*

Elevated hydrophobicity and a low net charge are two factors observed to promote protein aggregation in partially folded or misfolded states. This occurs due to the exposure of the hydrophobic residues, usually buried in the native state, to the solvent. Aggregation may result in the formation of amorphous aggregates or amyloid-like fibrils, characterized by a low energy and entropy (Figure 10). While many proteins can adopt these aggregation states *in vitro*, their formation *in vivo* is strictly limited by chaperone machinery (Chiti & Dobson, 2006; Hartl et al., 2011; Kim et al., 2013). Not only partially folded, misfolded or intrinsically disordered proteins have the ability to form aggregates, but globular proteins can also undergo aggregation, and be implicated in protein folding diseases such as Alzheimer's or Parkinson's disease (Hartl et al., 2011). Various factors, such as fluctuations in pH, high temperature, concentration of proteins, salts and solvents are known to destabilize the free energy of a native protein. These conditions can promote the transition to an aggregated precursor, ultimately resulting in the formation of mature aggregates (Figure 10) (Chiti & Dobson, 2009)

Protein aggregates vary from highly structured cross-β amyloid fibrils to less ordered amorphous aggregates, with oligomeric and protofibrillar forms in between. Despite considerable efforts, accurately predicting the final structure of a specific protein within particular environment remains challenging (Santos et al., 2020). Aggregation propensity is dictated by the protein primary sequence. Within this sequence, certain short amino acid sequences, known as aggregation hot spots, can inhibit or promote the conversion of the entire globular protein into amyloid fibrils. These hot spots are typically characterized by high hydrophobicity and low net charge (Ventura et al., 2004). For example, low complexity regions enriched in glutamine/asparagine (Q/N) repeats show a high propensity to self-aggregate in amyloid fibrils (Tartaglia et al., 2005). Several aggregation predictive algorithms have been developed as an initial screening tool to identify aggregative regions. Some examples are AGGRESCAN (Conchillo-Solé et al., 2007), Aggrescan3D (Santos et al., 2020), PrionW (Zambrano et al., 2015), PLAAC (prion-like amino acid composition) (Lancaster et al., 2014) and Waltz (Maurer-Stroh et al., 2010).

2.2.5.3 Intrinsically disordered regions

The conventional structure-function paradigm is founded on the notion that a protein sequence, determines its structure, which designates the protein function (Van Der Lee et al., 2014). However, nowadays this paradigm is questioned. Structural similarities may lead to different functions, while varied structures can share functions. Point mutations can range from neutral to disrupting crucial protein features, such as the disruption of a disulphide bond network (Laskowski & Thornton, 2008; Sinha & Nussinov, 2001). Moreover, a significant proportion of an organism's proteome consists of polypeptide segments unlikely to form a precise three-dimensional structure. Nonetheless, these segments are functional (Forman-Kay & Mittag, 2013) and called intrinsically disordered regions (IDRs). A protein can consist entirely of intrinsically disordered regions (IDRs), which do not adopt a tertiary structure. These proteins are known as intrinsically disordered proteins (IDPs). In contrast, proteins that lack IDRs are called structured proteins. However, most eukaryotic proteins comprise structured and disordered regions (Dunker et al., 2013). For years, IDRs were seen as passive segments connecting structural domains in proteins. However, it is now known that functional regions either can be structured or disordered (Van Der Lee et al., 2014).

2.2.5.4 Prions and prion-like proteins

Prions possess the ability to become infectious proteins in a specific misfolded conformation, transitioning from a native, soluble state to a self-replicating and self-propagating toxic form (amyloid state). The self-propagation occurs between and within individuals (Kraus et al., 2013). In humans, the prion protein (PrP) can form prions that contribute to the devastating neurodegenerative Creutzfeldt-Jakob disease. In contrast, prions in yeast are usually benign and may even confer advantages under stress conditions (Kraus et al., 2013; March et al., 2016). Prion domains (PrDs) in yeast are low complexity regions rich in polar, uncharged amino acids such as glutamine, asparagine, tyrosine, serine and glycine. This specific amino acid composition determines prionogenesis (March et al., 2016). IDRs with a similar composition to PrDs in eukaryotic cells are called prion-like domains (PrLDs).

Prion-like proteins are known for their tendency to aggregate, mediated by their PrLDs, which can trigger amyloid formation from a soluble and properly folded protein (Batlle et al., 2017). However, PrLDs can also induce other types of phenomena such as liquid-liquid phase separation, which may contribute to the formation of membraneless organelles and condensates (Batlle et al., 2020).

2.2.5.5 Amyloids

Amyloid fibrils are insoluble structures where β-strands assemble into highly organized β-sheets oriented perpendicular to the fibril axis (Monsellier & Chiti, 2007). β-sheets are packed and stabilized through hydrogen bonds, van der Waals and hydrophobic interactions (Salvatella, 2013) (Figure 11A). This characteristic structure has the capacity to bind dyes such as Thioflavin T or Congo red (Chiti & Dobson, 2017).

The amyloid fibril formation is well established and involves two nucleation steps and one elongation step (Figure 11B). During the first nucleation, monomers associate to form a nucleus. In the elongation step, this nucleus recruits more monomers until the formation of the fibril, which may later undergo fragmentation or branching. Then, these new fibrils can recruit additional monomers, in a process known as second nucleation. Preformed fibrils can significantly increase the aggregation rate by bypassing the first nucleation step (Salvatella, 2013).

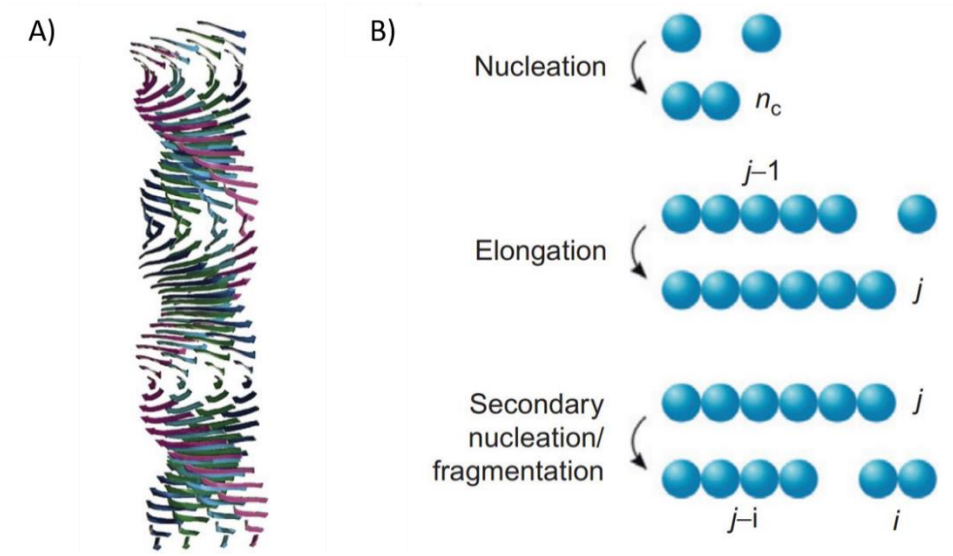

Figure 11. Amyloid fibril structure and formation schemes. A) Schematic representation of an amyloid fibril illustrating the alignment of the β-strands in relation to the fibrillar axis. B) Scheme of the amyloid fibril formation. Adapted from (Salvatella, 2013).

Amyloid fibril formation is observed in both mammalian and fungal prion phenomena (March et al., 2016). This process is associated with several pathologies such as Alzheimer's disease, Parkinson's disease or type II diabetes, where toxicity can occur due to the formation of soluble cytotoxic oligomers and/or fibrils and the absence of properly functioning polypeptides (Chiti & Dobson, 2017). In contrast, there are amyloids with physiological roles, known as functional amyloids (Santos et al., 2020), such as those implicated in the release of hormones from secretory granules (Maji et al., 2009).

2.2.5.6 Protein aggregation in protozoan parasites

The malaria-causing parasite *Plasmodium falciparum* stands out due to its genome composition, which is highly biased towards adenine (A) and thymine (T) content, reaching an AT content of 80.6%. In *P. falciparum* uracil (U)T-codons are preferentially translated into asparagines (N), leading to around 30% of the parasites proteome consisting of long sequences rich in N. As previously mentioned, Glutamine (Q)/N repeats show a high propensity to form amyloid fibrils, as confirmed by the PLAAC algorithm, which predicts that 9.4% of protein sequences

in *P. falciparum* are prion-like (Pallarès et al., 2018). In contrast, in humans ca. 1.2% of the proteins contain PrLDs, according to PLAAC (March et al., 2016).

Although, the prion-like propensity calculated by PLAAC is much lower in humans compared to *P. falciparum*, what remains similar are the functions of the prion-like proteins according to gene ontology (GO) analysis. In *P. falciparum* ca. 33% of its prion-like proteins are related to DNA/RNA-binding (Pallarès et al., 2018). The same profile was observed for the human genome, where 30% of prion-like proteins were RNA-binding and 33% DNA-binding (March et al., 2016). RNA-binding proteins have been described to be related with protein aggregation. As examples of this, the high presence of low-complexity IDRs in RNA-binding domains leads to a phase transition involving the formation of a highly dynamic hydrogel state (Van Der Lee et al., 2014). Certain RNA-binding proteins, such as fused in sarcoma protein, are implicated in neurological diseases, with specific RNA recognition motifs within them being potentially able to form amyloids in nature (S. Agrawal et al., 2019). Generally, RNA binding seems to be associated with PrLD-containing proteins across different organisms (Iglesias et al., 2015). The percentages of IDPs in the *Leishmania* species: *L. braziliensis, L. major, L. infantum, L. mexicana and L. tarentolae* is approximately 70% and in *Trypanosoma cruzi* and *T. brucei,* 55%. Among these IDPs, the term 'binding' is the most common in the GO molecular function, consistent with the previously mentioned findings (Ruy et al., 2014).

In *Plasmodium falciparum*, it was possible to stain intracellular aggregates in all the stages of the parasite with ProteoStat®, a commercial dye able to detect aggregated proteins, and to isolate peptides from *P. falciparum* proteins able to form amorphous aggregates or amyloid fibrils *in vitro* (Biosca et al., 2020). Then, it was described that protein aggregation likely plays a functional role in the parasite, and its presumed inhibition by the main component of ProteoStat, a compound called YAT2150, reduced the parasite viability with an IC_{50} of 90 nM. Moreover, YAT2150 compound stains the parasite in all its stages, emerging as a promising theragnostic agent (Bouzón-Arnáiz et al., 2022). In this thesis, a similar approach will be explored in *L. infantum.*

3. Nanotechnology and nanomedicine

The discovery and development of new drugs to address the limitations of current leishmaniasis treatments is a process that can take over 12 years and require high costs. A more rapid and cost-effective strategy involves optimizing existing drug

formulations. Within this approach, one of the most promising tools is the utilization of nanotechnology-based drug delivery systems (De Almeida et al., 2017).

The application of nanotechnology to the medical field is termed nanomedicine. It employs nanomaterials that will have a specific effect based on their characteristic compositions and structures (Figure 12) (De Almeida et al., 2017; Wagner et al., 2006).

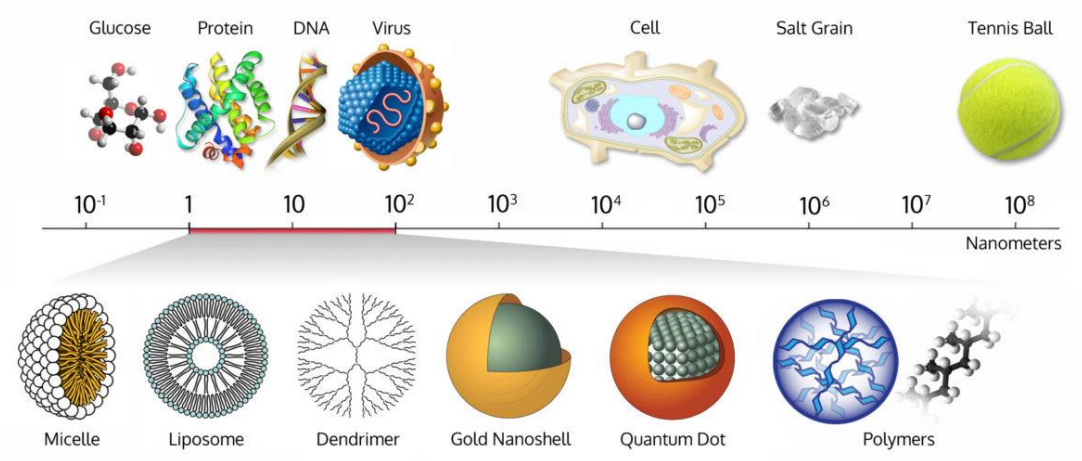

Figure 12. Scale with the size range of different structures. Nanoscale is highlighted in red. Reproduced form *https://www.wichlab.com/*.

2.3 Nanotechnology for drug delivery of antileishmanial drugs

In order to improve the performance of antileishmanial drugs using nanotechnology, it is necessary to understand that one of the challenges involved is reaching the hidden location of amastigotes inside the macrophage's phagolysosomes (De Almeida et al., 2017). In recent years, there have been significant advancements in nanotechnology and drug delivery systems (DDS). Various DDS specifically target macrophages and minimize toxic effects in the host's cells (Maza Vega et al., 2023). DDS for treating leishmaniasis should ideally be suitable for oral administration, possess low immunogenicity and toxicity, reduce treatment duration by enhancing pharmacokinetic or pharmacodynamic profiles, facilitate the delivery of drug combinations, remain economically affordable for endemic countries and selectively target the parasite for maximum efficacy with minimal toxicity (Date et al., 2007).

Various types of nanoparticles (NPs) are being explored for their potential in treating leishmaniasis:

2.3.1 *Polymeric NPs*

Polymeric NPs are solid colloidal particles with a size below 1 µm. Two types of polymeric NPs can be defined according to their morphology: nanocapsules and nanospheres. Nanocapsules have an oily core wherein the drug will be dissolved, encapsulated within a shell made of polymers. Nanospheres are made of a polymeric matrix, where the drug may be retained in the inner part or absorbed on the surface. Polymers can increase the biocompatibility and control the release of the drug, and can be synthetic such as poly (lactide-co-glycolide) (PLGA) or natural such as gelatin, albumin, chitosan, and alginate (de Souza et al., 2018; Zielinska et al., 2020).

In 1991, Gaspar et al. (Gaspar et al., 1992) showed that polyisohexylcyanoacrylate NPs loaded with primaquine had an IC_{50} 21-fold higher compared to free primaquine when tested against *L. donovani* amastigotes (Gaspar et al., 1992). Since then, several drugs have been encapsulated in polymeric NPs, with AmB being the most relevant for leishmaniasis to address the challenge of increasing its low solubility and reducing its nephrotoxicity (Van De Ven et al., 2012).

PLGA is an FDA-approved biodegradable polymer, frequently employed in long-acting formulations. Its wide use is exemplified by the FDA's approval of more than 20 PLGA-based drug products to date, with the first such approval in January 1989 (Wang et al., 2021). PLGA NPs loaded with AmB have proved to be more effective than the free drug in: (i) reducing the lesion area of CL in *L. major*-infected BALB/c mice (Abu Ammar et al., 2019), (ii) showing greater efficacy against intracellular *L. infantum* amastigotes and extracellular *L. infantum* promastigotes (Van De Ven et al., 2012), (iii) reducing the IC_{50} of the drug in *L. donovani* extracellular promastigotes and the number of intracellular amastigotes in the spleen of infected female hamsters (Kumar et al., 2015).

2.3.2 *Metallic and metal oxide NPs*

Metals and metal oxide NPs are known to have antimicrobial activity (Nafari et al., 2020). Metal oxides manifest distinct structural forms as a result of the reaction between a metallic element and an oxygen under varying conditions.

Significantly, metal oxides in the nanoscale range have demonstrated varied applications in different fields, including biomedicine (Alhalili, 2023). It is important to note that sodium stibogluconate and MA are derived from the heavy metal antimony and they remain among the most widely used antileishmanial drugs. This exemplifies the potential use of metal-based drugs to treat leishmaniasis (Navarro et al., 2010).

Silver (Ag)-NPs showed antileishmanial effect on both *L. tropica* promastigotes and amastigotes, with enhanced effectiveness observed when parasites were subjected to a combination of Ag-NPs and UV light exposure (Allahverdiyev et al., 2011). Hybrid NPs, consisting of TiO_2 and Ag, reduced the viability in both *L. tropica* and *L. infantum* promastigotes and amastigotes. Amastigotes were more sensitive to the NPs compared to promastigotes, possibly due to the activation of macrophages, leading to the release of antileishmanial molecules, such as nitric oxide (Allahverdiyev et al., 2013).

Selenium NPs also showed inhibitory effects on the growth of both *L. major* promastigotes and amastigotes, and additionally, reduced the diameter of the lesions in a CL animal model of *L. major*-infected BALB/c mice (Beheshti et al., 2013). ZnO NPs can decrease the amastigote/macrophage ratio and the viability percentage of promastigotes in a concentration-dependent manner (Delavari et al., 2014).

2.3.3 *Lipid NPs*

Lipid NPs can be categorized into two main types: lipid drug conjugates (LDC) and solid lipid NPs (SLN). SLNs, ranging in size from 1 to 1000 nm, are compact nanocarriers composed of biocompatible lipids capable of encapsulating both hydrophilic and hydrophobic drugs. To enhance the delivery of hydrophilic drugs, LDC play a crucial role by converting the hydrophilic drug into a lipophilic drug conjugate or prodrug (Date et al., 2007). PMM encapsulated into SLN showed a higher reduction in the parasite burden in *L. major*-infected BALB/c compared to the free drug. Moreover, both PMM-SLN and SLN alone were found to be safe in the mouse model (Heidari-Kharaji et al., 2016).

2.3.4 *Liposome NPs*

Liposomes were firstly described by Alec Bangham in 1964 (Bangham & Horne, 1964). In the 1970s, liposomes were introduced as carriers for drug delivery (Lasic,

1998). They are spherical particles with varying numbers of lipid bilayers surrounding an aqueous core (Figure 13). Depending on the number of bilayers and the size, liposomes can be divided as follows: small unilamellar vesicles, size range 20-100 nm; large unilamellar vesicles, size range >100 nm; multilamellar vesicles, size >500 nm; and multivesicular vesicles, size>1000 nm. Liposomes have the capacity to encapsulate molecules within the aqueous lumen or in the lipophilic membrane, providing both hydrophobic and hydrophilic characteristics. They are widely used as nanocarriers due to their biodegradability, biocompatibility, low inherent toxicity and immunogenicity (Nsairat et al., 2022). Moreover, liposomes accumulate in the mononuclear phagocyte system, primarily in the liver and spleen, when administered *in vivo*. This is a useful characteristic when targeting microorganisms residing within these cells, such as *Leishmania* (A. K. Agrawal & Gupta, 2000).

Among nanocarriers, liposomes stand out as the most widely studied structures (Nafari et al., 2020). This is evident in the existence of liposomes encapsulating the main antileishmanial drugs, employed for passive or active targeting of macrophages or the *Leishmania* parasite itself. Several examples of passive and active targeting will be discussed in the following sections.

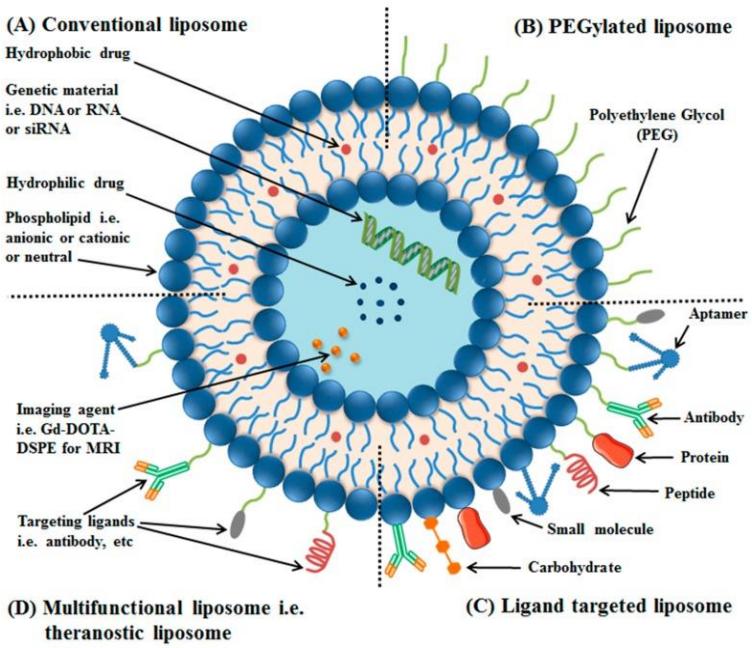

Figure 13. Schematic representation of a liposome. Conventional liposomes (A) encapsulate hydrophilic substances in the lumen and hydrophobic compounds in the membrane. Modification options include stealth liposomes with polymers like PEG (B), those with targeting ligands (C), and multifunctional liposomes, exemplified by theragnostic liposomes (D), capable of both diagnosis and treatment, especially in solid tumors. Reproduced from (Riaz et al., 2018) under the terms of the Creative Commons Attribution License (http://creativecommons.org/licenses/by/4.0/).

2.3.4.1 Passive targeting

Passive targeting is accomplished through the utilization of conventional liposomes or long-circulating liposomes, usually coated with the hydrophilic polymer polyethylene glycol (PEG) (Torchilin, 2005). PEG-modification helps enhancing liposomal solubility, increasing the circulation time, preventing liposomal aggregation, which is associated with toxicity issues, as well as avoiding opsonization and phagocytosis (Hussain et al., 2019). MA-loaded liposomes including PEG showed more efficacy in reducing the parasite burden in liver and spleen from *L. infantum*-infected BALB/c mice when compared to free MA. Inflammation and damage in the hepatic tissue was also decreased when MA was encapsulated (Azevedo et al., 2014). More examples of passive targeting with the main antileishmanial drugs are presented below:

- **Pentavalent antimonials:** MA-loaded liposomes had a SI higher than free MA for intracellular *L. major* amastigotes. Neither free MA nor MA-loaded NPs were effective on *L. major* promastigotes, as it would be expected since the reduction of Sb (V) to Sb (III) is stage-specific of amastigotes (Treiger Borborema et al., 2011).
- **PMM:** Liposomes loaded with PMM showed lower IC_{50} values than the free drug against both *L. major* promastigotes and *L. major* intracellular amastigotes. In *in vivo* studies conducted with BALB/c mice, a 12-week topical application of PMM-loaded liposomes resulted in complete cure without any observed relapse and no parasite load was detected in the spleen (Jaafari et al., 2009).
- **AmB:** The case of liposomes encapsulating AmB is the most successful, as previously mentioned. There are at least two commercialized AmB liposomes

for the treatment of VL: Ambisome (FDA, 2008) and Fungisome (Wijnant et al., 2018).

- **Miltefosine and pentamidine isethionate:** There is limited research on encapsulating pentamidine or miltefosine into liposomes. Zahra Kavian et al. developed miltefosine-loaded liposomes for topical application. These formulations successfully reduced the lesion size in *L*. *major*-infected BALB/c mice, along with a decrease in the parasite burden at the lesion site and in the spleen (Kavian et al., 2019). Liposomes containing pentamidine enhanced the therapeutic efficacy of the drug against *L. donovani*-infected golden hamsters compared to pentamidine alone. Furthermore, this enhancement was more pronounced when liposomes were grafted with the sugar mannose (Man) (Banerjee et al., 1996a). The addition of this molecule actively targeted macrophages. In the next section, additional molecules used for active targeting will be discussed.

2.3.4.2 Active targeting

Active targeting is promoted by the functionalization of liposomes with specific ligands such as antibodies, aptamers or small molecules (Figure 13) (Riaz et al., 2018).

2.3.4.2.1 Functionalization with antibodies

The process of linking antibodies to liposomes results in the formation of immunoliposomes. Both antibody fragments and whole antibodies are viable options for this conjugation. A main technique employed for this coupling involves the introduction of a sulfhydryl group to the antibody, followed by its attachment to a reactive group on the liposome, such as maleimide (Figure 14) (Riaz et al., 2018). Using this method, an anti-glycophorin A antibody, which targets a major glycoprotein in the erythrocyte membrane, was conjugated to a liposomal maleimide group, thereby forming immunoliposomes specifically engineered for malaria therapy. At equivalent concentrations of pyronanidine and atovaquone, encapsulation in immunoliposomes resulted in a 50% inhibition of *Plasmodium falciparum* growth, whereas no significant inhibition effect was observed when administered in their free form (Biosca et al., 2019). Furthermore, Moles et al. (2015) demonstrated that immunoliposomes conjugated with the anti-glycophorin

A antibody had a significantly enhanced effect on parasite viability compared to free chloroquine. The viability of *P. falciparum* was completely arrested at a concentration of 50 nM, whereas free chloroquine exhibited no significant effect at 200 nM. Furthermore, this was extrapolated to an *in vivo* test in *P. falciparum*-infected mice, where free chloroquine was observed to be at most 40-fold less efficient in clearing *P. falciparum* than the chloroquine-immunoliposome formulation (Moles et al., 2015).

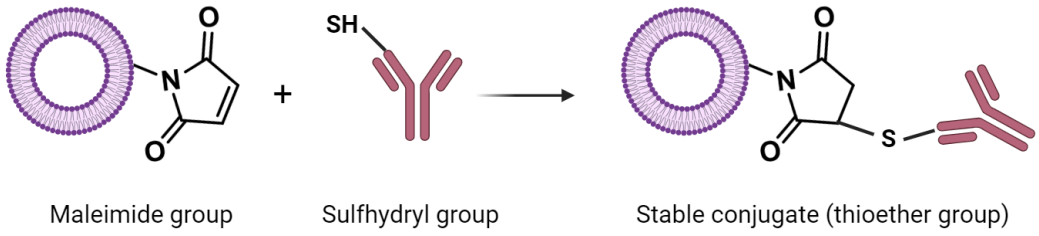

Figure 14. Reaction scheme of the conjugation of a maleimide group to a sulfhydryl group. Created with BioRender.com.

In *Leishmania,* immunoliposomes loaded with doxorubicin, an antitumoral drug, showed reduced toxicity and enhanced antileishmanial activity against *L. donovani* amastigotes, when compared to both the free drug and liposomes loaded with doxorubicin. These immunoliposomes were specifically conjugated with a fragment of an antibody targeting a 51-kilodalton (kDa) protein specific to the parasite (Mukherjee et al., 2004). The coupling method employed in this study involved the covalent binding of the F(ab')2 fragment to phosphatidylethanolamine, as detailed in previous literature (Heath et al., 1981).

Antibodies are widely used for active targeting, but they present some drawbacks, such as their relatively high production cost (Li, Xu, Yan, Li, Yazd, Li, Huang, Heng Cui, et al., 2021). To address this, less expensive molecules have also been used for active targeting like glycoconjugates, glycosaminoglycans and aptamers.

2.3.4.2.2 Functionalization with glycoconjugates

Glycoconjugates play key roles in different aspects of *Leishmania* biology, with lipophosphoglycan (LPG) standing out as the predominant glycoconjugate on

the surface of *Leishmania* promastigotes. LPG facilitates the adhesion of *Leishmania* promastigotes to the midgut of the sand fly vector through its Man or galactose (Gal) residues (Figure 15). Besides, in the human host, serum mannan-binding protein binds the Man residues in the LPG, thereby facilitating the attachment of the parasite to the macrophage (DOI: 10.1016/s0925-4439(99)00065-4). C-reactive protein is synthesized in the liver, and its concentration increases in response to inflammatory stimuli, making it a major acute phase protein. It binds to the Gal(β1,4)Man(α1-PO4) repeating units of *L. donovani* LPG (Figure), serving as an opsonin, thus promoting phagocytosis (Culley et al., 1996).

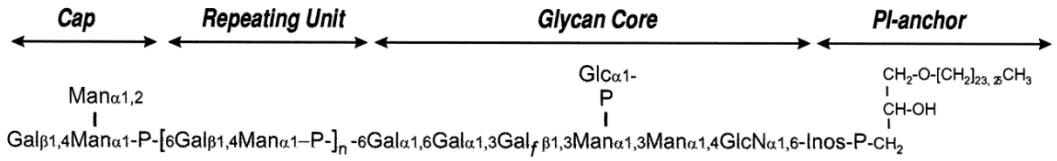

Figure 15. LPG structure of *L. donovani.* Gal_f, galactofuranose; P, phosphate. Reproduced from (Descoteaux & Turco, 1999).

Moreover, the macrophage Man receptor has affinity for carbohydrate moieties. Functioning as a pattern recognition receptor, it has the capacity to identify various pathogen surfaces, including those of *Leishmania* (Cummings, 2022). In light of the above, coating liposomes with glycoconjugates seems a promising strategy for the targeted delivery against *Leishmania* infection. AmB encapsulated in Man-grafted liposomes resulting in an increased drug accumulation in the spleen and liver compared to the free drug, representing a promising avenue for the treatment of VL (Rathore et al., 2011). As another example, Man-coated liposomes containing pentamidine enhanced the therapeutic efficacy of the drug against *L. donovani*-infected golden hamsters compared to pentamidine alone (Banerjee et al., 1996b).

2.3.4.2.3 Functionalization with glycosaminoglycans

Glycosaminoglycans (GAGs) are negatively charged polysaccharide compounds constituted of repeating disaccharide units, which are ubiquitous in mammalian tissues. The four main groups of GAGs, categorized by their core

disaccharide units, are heparin/heparan sulfate, chondroitin sulfate/dermatan sulfate, keratan sulfate, and hyaluronic acid (Casale & Crane, 2023).

The *Leishmania* life cycle depends on the ability of the molecules from the surface of the parasite to recognize both mammalian mononuclear phagocytic cells and sand fly gut components. In this sense, GAG receptors on the surface of *Leishmania* seem to be important for the binding to the sand fly gut epithelium (Azevedo-Pereira et al., 2007) and to the macrophage (Figure 16), where the binding of heparin may stimulate phagocytosis (Butcher et al., 1992). Specifically, heparin-binding proteins (HBPs) found in the *Leishmania* parasite interact with carbohydrates present in molecules like heparin, with an affinity that, in some cases, falls within the micromolar range (Martins et al., 2018). The location of HBPs varies among *Leishmania* species (Merida-De-Barros et al., 2018), with presence observed either in the plasma membrane of promastigotes (Martins et al., 2015) or/and in the flagella and flagellar pocket (De Castro Côrtes et al., 2012). Chondroitin sulfate is known for its ability to activate macrophages through CD44 and toll-like receptor 2. It is documented to enhance phagocytosis in RAW 264.7 cells in a dose-dependent manner and elevate nitric oxide levels (F. Wu et al., 2018). Therefore, the functionalization of liposomes with heparin or chondroitin sulfate will target the parasite and/or the macrophage. Heparin has been used as a ligand for functionalizing liposomes to actively target other parasites, such as *P. falciparum* (Lantero, Aláez-Versón, et al., 2020).

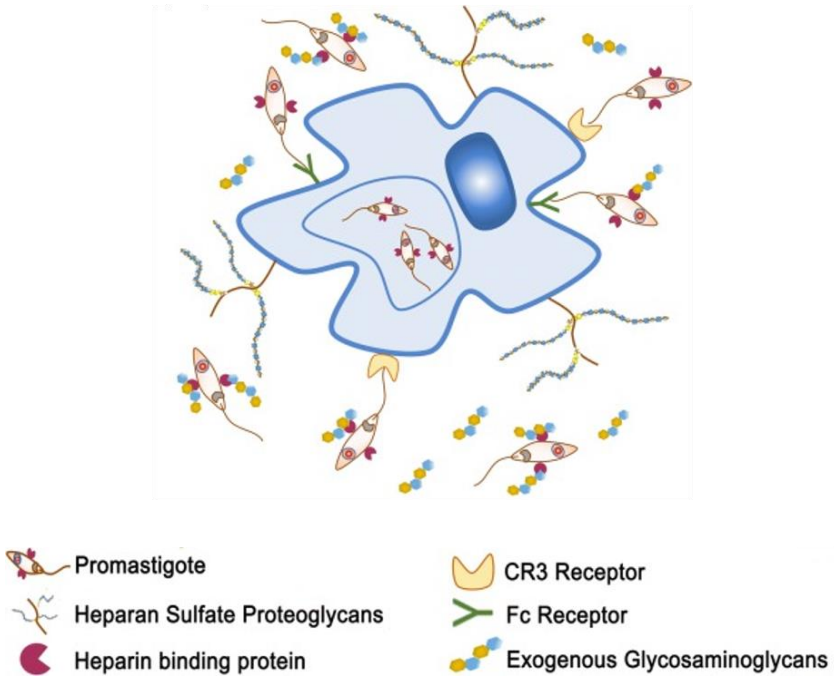

Figure 16. Glycosaminoglycans interaction with *Leishmania* promastigotes and macrophage. Reproduced from (Merida-De-Barros et al., 2018) under the terms of the Creative Commons Attribution License (http://creativecommons.org/licenses/by/4.0/).

2.3.4.2.4 Functionalization with aptamers

Monoclonal antibodies and aptamers utilized as pharmaceutical agents exemplify a modern manifestation of the "magic bullet" concept (Strebhardt & Ullrich, 2008), targeting specific molecular entities with precision. Aptamers are single-stranded RNA or DNA oligonucleotides, typically comprising fewer than 100 nucleotides. They possess the capability to adopt distinctive three-dimensional structures, enabling precise interactions with target molecules characterized by high affinity and specificity. This capacity for specific molecular recognition makes aptamers comparable to monoclonal antibodies but offering some additional advantages (Lakhin et al., 2013; Ospina-Villa et al., 2018). These advantages include small size (5-15 kDa) compared to antibodies (150-1000 kDa), allowing for better tissue penetration. Aptamers are nonimmunogenic, stable at room temperature, efficiently cleared from the bloodstream, and can be prepared against multiple target molecules. Their animal-free production reduces production time, making it cost-effective, scalable and promotes ethical practices by reducing animal suffering

in research. Additionally, aptamers are easily modifiable to address some of their limitations, such as susceptibility to nuclease degradation or low bioavailability. As a result, aptamers represent an attractive tool in biomedical research for diagnostic and therapeutic applications (Cao et al., 2009; Li, Xu, Yan, Li, Yazd, Li, Huang, Cui, et al., 2021; Nagar et al., 2021)

For active targeting, similar to antibodies, the coupling between aptamers and liposomes can occur through various processes (Alshaer et al., 2015; Riaz et al., 2018). Aptamer-liposomes loaded with cisplatin were capable of targeting specific cells and reducing their viability, with no observed targeting or cell death in the control cells. Addtionally, in this study, complementary DNAs were employed as inhibitors of the aptamer to regulate its activity when necessary, potentially reducing adverse effects (Cao et al., 2009). Apart from their role in functionalizing liposomes, aptamers serve as valuable diagnostic and therapeutic tools owing to their exceptional ability to target molecules with high affinity (Ospina-Villa et al., 2018).

The FDA approved the first RNA aptamer under the name of MACUGEN® (pegaptanib sodium injection) in 2004 as a vascular endothelial growth factor antagonist for the treatment of age-related macular degeneration in humans (FDA, 2004).

Aptamer selection process

The selection of specific aptamers capable of recognizing particular ligands is achieved through the systematic evolution of ligands by exponential enrichment (SELEX) from a randomized pool of oligonucleotides (Ellington & Szostak, 1990), first described in 1990 (Ellington & Szostak, 1990). In this method, a large initial library of oligonucleotides, ranging from 10^{13} to 10^{15} different sequences, is initially mixed with the target of interest. Each oligonucleotide consists of a random sequence of approximately 30-40 nucleotides flanked by two conserved PCR primer-binding sites. The different sequences within the pool interact with the target molecule with high specificity and affinity (Figure 17B). Following this, the sequences are amplified by PCR and single-stranded sequences are isolated and subjected to repeated incubation with the target molecule for multiple such cycles, until a few sequences with high specificity are obtained. Aptamers with low or non-binding ability are in this way progressively removed from the pool. A negative control is also added to

eliminate the presence of sequences showing affinity towards non-target molecules. This iterative process serves to enrich the pool of aptamers with high specificity and affinity towards the molecule of interest (Ospina-Villa et al., 2018; Sefah et al., 2010; Stoltenburg et al., 2007).

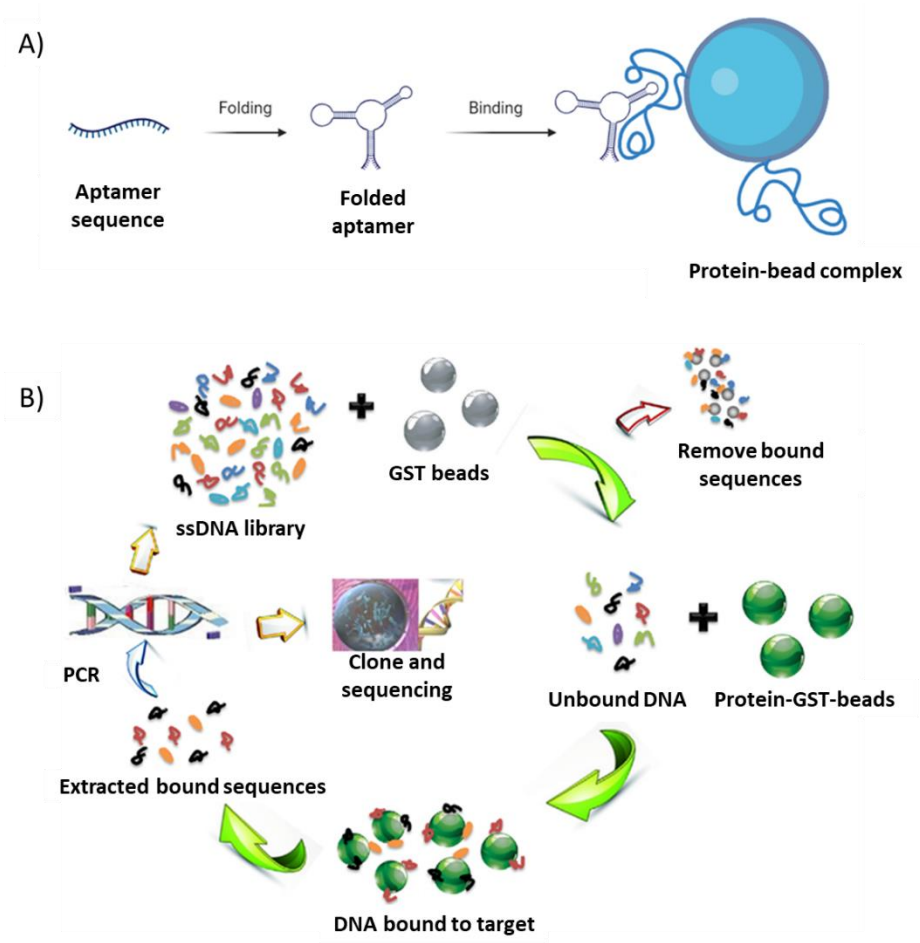

Figure 17. Bead-based SELEX diagram. A) Scheme of aptamer folding and its subsequent binding to the target molecule, in this case a protein-bead complex. Created with BioRender.com. B) Bead-based SELEX scheme starting from a ssDNA library. Adapted from (J. Wu et al., 2012) under the terms of the Creative Commons Attribution License (http://creativecommons.org/licenses/by/4.0/).

Aptamers have been developed against a broad spectrum of molecules, including whole cell protozoa (Bruno et al., 2014; Lantero, et al., 2020), bacteria (Afrasiabi et al., 2020), small molecules, such as metal ions (Rajendran & Ellington,

2008), or specific purified and/or recombinant proteins (Figure 17A) (Frezza et al., 2020; Roca et al., 2022). The SELEX method has been optimized and customized for various molecular targets to enhance the enrichment in selected sequences and the elimination of non-binding counterparts. Among these methods, the bead-based SELEX (Figure 17B) is particularly significant for this thesis. This approach relies on the co-expression of a protein along with glutathione-S-transferase (GST) to enable the binding of GST to Sepharose Glutathione-beads. The resulting protein-GST-bead complex functions as the positive control, while the negative control involves GST-beads aimed at eliminating sequences capable of binding to either GST or to the surface of the bead (J. Wu et al., 2012).

Aptamers in *Leishmania*

As previously mentioned, diagnostic and therapeutic tools available for *Leishmania* are very limited, leaving considerable room for improvement. The ideal diagnostic tool would be a RDT capable of detecting an antigen from the parasite.

In accordance with the above, the group led by Gonzalez has developed various aptamers targeting *L. infantum* proteins, with a proposed diagnostic application. The initial single-stranded DNA (ssDNA) aptamers, developed in 2002, targeted the kinetoplastid membrane protein 11 (KMP-11), an 11 kDa protein mainly found in the flagellum and flagellar pocket, and believed to be involved in parasite mobility (M. Moreno et al., 2003). Using the ssDNA aptamer population that specifically binds *Leishmania infantum* KMP-11 (*Li*KMP-11), the same group developed an aptamer-based sensor able to detect 2.27 µM of *Li*KMP-11 (M. Moreno et al., 2011).

Gonzalez's group also produced aptamers against nuclear proteins. Although histones are typically highly conserved proteins. Trypanosomatida present some variations between species, mainly in the C- and N- terminal regions. These differences were used to generate aptamers that specifically recognize *L. infantum* histones H2A (*Li*H2A) and H3 (*Li*H3) (Iborra et al., 2004). From the aptamer pools that specifically recognized *Li*H2A and *Li*H3 (Ramos et al., 2007, 2010), two individual aptamers for each protein were selected (AptLiH2A#1, AptLiH2A#2 and ApLiH3#4, ApLiH3#10), showing a dissociation constant (concentration of ligand required to reach half-maximal binding) in the nM range. These two aptamers were proposed as a tool for the purification of *Li*H2A and *Li*H3, respectively, as they were capable

of purifying the protein from *L. infantum* and *E. coli* cell lysates. However, one limitation of the study was that the amount of protein recognized corresponded to 7500 parasites for *Li*H2A (Martín et al., 2013) and 6000 for the *Li*H3 (Frezza et al., 2020), which is higher than what is desirable for a diagnostic test. In a subsequent study, this number was reduced to 2500 parasites with three aptamers named ApPABP#3, ApPABP#7 and ApPABP#11. These aptamers were developed against the *L. infantum* poly(A)-binding protein (*Li*PABP). *Li*PABP interacts with the 3´ end poly(A) tail of mRNAs and plays a crucial role in the translation process. Using an aptamer or antibody to bind *Li*PABP and thereby inhibit its interaction with the poly(A) tail could offer a promising therapeutic approach (Guerra-Pérez et al., 2015).

Bruno et al. (2014) selected aptamers through whole cell-SELEX using *L. major* promastigotes as the target. With the selected aptamers a fluorescent enzyme-linked DNA aptamer-magnetic bead sandwich assay was developed. This assay had the capability to detect soluble proteins extracted from *L. major* promastigotes in less than an hour, offering sensitive detection (Bruno et al., 2014).

GP63 as targeting molecule for the development of aptamers

The *Leishmania* glycoprotein GP63, also called leishmanolysin, is a promising candidate for the development of aptamers, and its potential will be discussed in this section.

Since GP63 was discovered in 1980, it has been widely studied (Isnard et al., 2012). In *L. infantum*, GP63 is encoded by five genes located on chromosome 10 (LINJ_10_0490, LINJ_10_0500, LINJ_10_0510, LINJ_10_0520, LINJ_10_0530), two in chromosome 28 (LINJ_28_0610, LINJ_28_0600) and another related gene on the chromosome 31 (LINJ_31_2040) (NCBI, n.d.). GP63 in promastigotes is the most abundant surface protein (Schlagenhauf et al., 1998). However, in amastigotes, GP63 is downregulated, while still playing important roles in amastigote survival by modulating the response of the host cell (Olivier et al., 2005).

GP63 synthesis occurs in the endoplasmic reticulum, where a small fraction of it remains (around 1.5%) with most of the protein being exported to the parasite surface (around 75%). The remaining portion is either exported via vesicles or anchored to the membrane through a GPI anchor (Isnard et al., 2012).

GP63 functions

GP63 has multiple functions in the parasite (Figure 18), among which (i) adhesion to macrophages (Brittingham et al., 1999), (ii) the creation of an environment favourable for *Leishmania* by cleaving numerous host proteins and protecting the parasite from antimicrobials peptides (Gurjar et al., 2022), (iii) the suppression of an efficient immune response (Devsani et al., 2023), and (iv) complement inactivation (Brittingham et al., 1995).

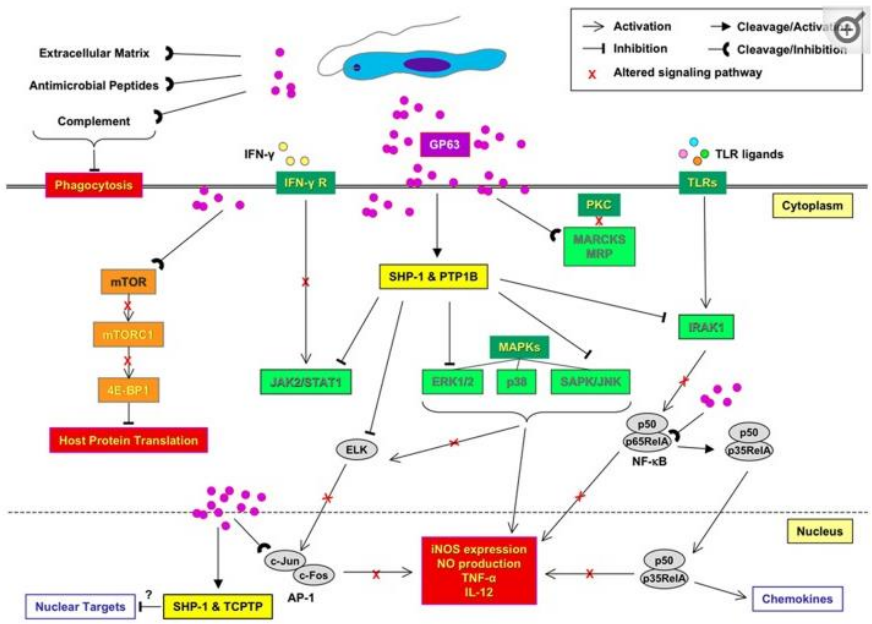

Figure 18. GP63 effect on macrophage signalling pathways and the innate immune response. Reproduced from (Isnard et al., 2012) under the terms of the Creative Commons Attribution License (http://creativecommons.org/licenses/by/4.0/).

GP63 inhibitors

Different GP63 inhibitors have been studied and, although none of them have reached preclinical studies, there are some interesting results with the following inhibitors: Glycoside 2 (IC_{50} 1.13 µM in *L. donovani* promastigotes, (Chakrabarti et al., 2022)), benzimidazole compounds (IC_{50} value of 0.62–0.92 µg/mL in *L. major* promastigotes, (Shaukat et al., 2013)) and 4-({bis[(pyridine-2-il)methil]amino}methil)-7-hydroxy2H-1-benzopyran-2 (L1) (IC_{50} value of 1.24 µM in *L. amazonensis* promastigotes, (C. J. G. Moreno et al., 2022)).

Based on the explanations provided in this section, GP63 is a promising target for aptamer generation in *Leishmania*. In fact, while exploring GP63 proteolytic activity to degrade certain proteins, such as casein, Diouani et al. (2019) developed gold NPs conjugated with casein. These casein- NPs interacted with GP63, enabling the detection of *Leishmania* parasites down to 0.55 parasites/mL (Diouani et al., 2019). However, casein can interact with multiple molecules beyond GP63. Developing specific aptamers against GP63 could address this issue while maintaining the focus on the target molecule.

Objectives

Objective 1

To develop innovative vesicular nanoformulations of low toxicity able to stably incorporate high amounts of pentamidine and target them to *Leishmania* parasites to increase the selectivity index.

Objective 2

To characterize the activity of the aggregated protein dye YAT2150 on *L. infantum* viability.

Objective 3

To develop DNA aptamers against the mature form of the GP63 protein of *L. infantum* with potential use for diagnostic, prophylactic and/or therapeutic approaches.

Results

Article 1: *In Vitro* evaluation of aerosol therapy with pentamidine-loaded liposomes coated with chondroitin sulfate or heparin for the treatment of leishmaniasis

Auhors: Lucía Román-Álamo, Mohamad Allaw, Yunuen Avalos-Padilla, Maria Letizia Manca, Maria Manconi, Federica Fulgheri, Jorge Fernández-Lajo, Luis Rivas, José Antonio Vázquez, José Esteban Peris, Xavier Roca-Geronès, Srisupaph Poonlaphdecha, Maria Magdalena Alcover, Roser Fisa, Cristina Riera, Xavier Fernàndez-Busquets

Journal: *Pharmaceutics*

Publication date: 6th April 2023

DOI: https://doi.org/10.3390/pharmaceutics15041163

Journal Impact factor: 4.9

General summary: The study titled "In Vitro Evaluation of Aerosol Therapy with Pentamidine-Loaded Liposomes Coated with Chondroitin Sulfate or Heparin for the Treatment of Leishmaniasis," published in *Pharmaceutics*, investigates the potential of using aerosolized liposomal formulations of pentamidine to improve the treatment of leishmaniasis. The research demonstrates that pentamidine-loaded liposomes coated with chondroitin sulfate or heparin significantly improve the drug targeting to macrophages, with uptake rates increasing approximately twofold compared to non-coated liposomes. These liposomal formulations show enhanced activity against both amastigote and promastigote forms of *Leishmania infantum* and *Leishmania pifanoi* while reducing cytotoxicity to human cells. The nebulization studies using the Next Generation Impactor revealed a promising, patient-friendly approach to treating leishmaniasis, potentially improving drug bioavailability and reducing adverse effects, thereby facilitating self-administration.

pharmaceutics

MDPI

Article

In Vitro Evaluation of Aerosol Therapy with Pentamidine-Loaded Liposomes Coated with Chondroitin Sulfate or Heparin for the Treatment of Leishmaniasis

Lucía Román-Álamo [1,2,3], Mohamad Allaw [4], Yunuen Avalos-Padilla [1,2,3], Maria Letizia Manca [4], Maria Manconi [4], Federica Fulgheri [4], Jorge Fernández-Lajo [5], Luis Rivas [5], José Antonio Vázquez [6], José Esteban Peris [7], Xavier Roca-Geronès [8], Srisupaph Poonlaphdecha [8], Maria Magdalena Alcover [8], Roser Fisa [8], Cristina Riera [8] and Xavier Fernàndez-Busquets [1,2,3,*]

1 Barcelona Institute for Global Health (ISGlobal), Hospital Clínic-Universitat de Barcelona, Rosselló 149-153, 08036 Barcelona, Spain
2 Nanomalaria Group, Institute for Bioengineering of Catalonia (IBEC), The Barcelona Institute of Science and Technology, Baldiri Reixac 10-12, 08028 Barcelona, Spain
3 Nanoscience and Nanotechnology Institute (IN2UB), University of Barcelona, Martí i Franquès 1, 08028 Barcelona, Spain
4 Department of Life and Environmental Sciences, University of Cagliari, University Campus, S.P. Monserrato-Sestu Km 0.700, 09042 Monserrato, Italy
5 Centro de Investigaciones Biológicas Margarita Salas, Consejo Superior de Investigaciones Científicas (CSIC), Ramiro de Maeztu 9, 28040 Madrid, Spain
6 Group of Recycling and Valorization of Waste Materials (REVAL), Marine Research Institute (IIM-CSIC), Eduardo Cabello 6, 36208 Vigo, Spain
7 Department of Pharmacy and Pharmaceutical Technology, University of Valencia, 46100 Burjassot, Spain
8 Section of Parasitology, Department of Biology, Health and Environment, Faculty of Pharmacy and Food Science, University of Barcelona, Av. Joan XXIII 27-31, 08028 Barcelona, Spain
* Correspondence: xfernandez@ibecbarcelona.eu; Tel.: +34-93-227-5400 (ext. 4581)

Citation: Román-Álamo, L.; Allaw, M.; Avalos-Padilla, Y.; Manca, M.L.; Manconi, M.; Fulgheri, F.; Fernández-Lajo, J.; Rivas, L.; Vázquez, J.A.; Peris, J.E.; et al. In Vitro Evaluation of Aerosol Therapy with Pentamidine-Loaded Liposomes Coated with Chondroitin Sulfate or Heparin for the Treatment of Leishmaniasis. *Pharmaceutics* **2023**, *15*, 1163. https://doi.org/10.3390/pharmaceutics15041163

Academic Editor: Thierry Vandamme

Received: 28 February 2023
Revised: 30 March 2023
Accepted: 2 April 2023
Published: 6 April 2023

Abstract: The second-line antileishmanial compound pentamidine is administered intramuscularly or, preferably, by intravenous infusion, with its use limited by severe adverse effects, including diabetes, severe hypoglycemia, myocarditis and renal toxicity. We sought to test the potential of phospholipid vesicles to improve the patient compliance and efficacy of this drug for the treatment of leishmaniasis by means of aerosol therapy. The targeting to macrophages of pentamidine-loaded liposomes coated with chondroitin sulfate or heparin increased about twofold (up to ca. 90%) relative to noncoated liposomes. The encapsulation of pentamidine in liposomes ameliorated its activity on the amastigote and promastigote forms of *Leishmania infantum* and *Leishmania pifanoi*, and it significantly reduced cytotoxicity on human umbilical endothelial cells, for which the concentration inhibiting 50% of cell viability was 144.2 ± 12.7 μM for pentamidine-containing heparin-coated liposomes vs. 59.3 ± 4.9 μM for free pentamidine. The deposition of liposome dispersions after nebulization was evaluated with the Next Generation Impactor, which mimics human airways. Approximately 53% of total initial pentamidine in solution reached the deeper stages of the impactor, with a median aerodynamic diameter of ~2.8 μm, supporting a partial deposition on the lung alveoli. Upon loading pentamidine in phospholipid vesicles, its deposition in the deeper stages significantly increased up to ~68%, and the median aerodynamic diameter decreased to a range between 1.4 and 1.8 μm, suggesting a better aptitude to reach the deeper lung airways in higher amounts. In all, nebulization of liposome-encapsulated pentamidine improved the bioavailability of this neglected drug by a patient-friendly delivery route amenable to self-administration, paving the way for the treatment of leishmaniasis and other infections where pentamidine is active.

Keywords: *Leishmania infantum*; *Leishmania pifanoi*; leishmaniasis; pentamidine; liposomes; drug encapsulation; aerosol therapy

1. Introduction

Leishmania is a kinetoplastid protozoan responsible for leishmaniasis, a vector-borne disease transmitted to vertebrates through the bite of infected female sandflies [1]. This parasite has a digenic life cycle consisting of the flagellated promastigote, dwelling in the gut of the sandfly, which once transmitted into the vertebrate host invades macrophages, where it transforms into the amastigote form that reproduces inside a parasitophorous vacuole [2], the pathological form in vertebrates. Leishmaniasis ranks among the most important tropical neglected diseases, with a wide geographical distribution and an important impact on global health and economic concerns involving humans, domestic animals and wildlife of endemic areas [3]. From clinical criteria, leishmaniasis is classified under three major groups: cutaneous (CL), mucocutaneous (MCL) or visceral (VL). An annual incidence of 600,000 to 1 million cases for CL and 50,000 to 90,000 for VL has been estimated, mostly affecting populations from low- and middle-income countries [4]; about 95% of CL cases occur in the Americas, the Mediterranean basin, the Middle East and Central Asia [5]. In addition to thermo- and cryotherapy and photodynamic therapy for nondiffuse forms of CL [6], chemotherapy is nowadays the only available treatment for leishmaniasis [7,8], but only four drugs are under current clinical use and they are threatened by rising resistance and, for some of them, important side effects and unaffordable cost.

For over 70 years, pentavalent antimonials (i.e., sodium stibogluconate and meglumine antimoniate) have been the first choice in therapy for leishmaniasis, and they still remain so in New World MCL and VL [9]. Although their use for VL is under progressive decline due to severe side effects and rising resistance emergence, even in untreated patients in the Indian subcontinent [10,11], local intralesional pentavalent antimonial injections are the recommended treatment for CL [12], despite being painful and not always effective [13]. The polyene amphotericin B (AmB) has been widely employed as a deoxycholate suspension for VL. Nevertheless, the frequently associated nephrotoxicity has limited its clinical use, a drawback absent in its liposomal formulations (L-AmB) [14]. AmBisome® (Gilead, Foster City, CA, USA), a liposome suspension administered through slow intravenous infusion, is the most used formulation of L-AmB for VL treatment [15–17]. Miltefosine (hexadecylphosphocholine), so far the only oral drug against *Leishmania*, has evolved to a first-line medicine since its introduction 20 years ago [18]. However, it is potentially teratogenic and should not be taken by women of child-bearing age without contraception treatment [19]. Paromomycin (aminosidine) is an aminoglycoside antibiotic usually administered intramuscularly to treat VL and CL, with mild pain at the injection site and the ototoxicity associated to aminoglycosides as its most common adverse effects [20]. It is also used as a local treatment in nondiffuse CL as an ointment on the ulcers [12]. Systemic drugs, especially AmB-loaded liposomes, are also used to treat mucocutaneous, diffuse cutaneous and post-kala-azar dermal leishmaniases, but the treatment options are still unsatisfactory [21]. Combination therapies offer an interesting alternative to monotherapy, since most combinations allow to reduce the effective drug dose, cost and time of treatment, in addition to improving the parasitological control of *Leishmania* [22].

Nowadays, pentamidine (Figure 1), formulated as isethionate, is mostly used as a second-line drug, once failure of or relapse after first-line drugs occurs [23,24], but also extensively employed as a first choice for MCL treatment in many South American regions endemic for this form and for CL caused by *Leishmania guyanensis* and *Leishmania panamensis* (reviewed in [25]). Its use in canine leishmaniasis was also reported [26,27], as well as its role as a component within combination therapies [7,28,29]. The clinical use of pentamidine as leishmanicidal drug has undergone multiple ups and downs, following the effectiveness and availability of other alternative treatments, and has been stalled by its occasional but sometimes irreversible side effects, such as diabetes mellitus, severe hypoglycemia, shock, myocarditis and renal toxicity [30]. Due to its two basic amidine groups, pentamidine isethionate is poorly absorbed in the gastrointestinal tract after oral intake. Thus, for clinical purposes, it is usually administered parenterally, which provides a rapid absorption from

the moment of injection and ensures a constant plasma concentration during the first 24 h [31].

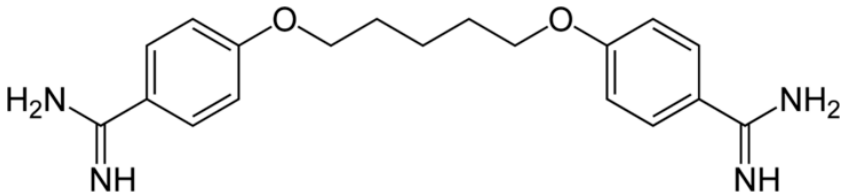

Figure 1. Chemical structure of pentamidine (1,5-bis(4-amidinophenoxy)pentane).

To overcome the aforementioned drawbacks of the current chemotherapy against leishmaniasis, it is urgent to develop alternative and innovative treatments, with a special focus on self-administering therapies, drug combinations and different intake routes, achieved through new nanotechnological delivery systems [30,32,33]. The encapsulation of pentamidine has been carried out in several nanodevices such as niosomes coated with chitosan glutamate [34], which is an example of a smart system capable of crossing the blood–brain barrier upon nasal administration, chitosan nanoparticles enriched with mucin as a system for the local treatment of CL [35], or cerium-doped nanoparticles specifically designed for the treatment of VL, thanks to the presence of a polycationic branched polyethylenimine polymer [36]. The delivery of drugs by oral aerosols is more patient-friendly than parenteral administration and profits from the large surface of lung alveoli for adsorption. If a systemic level of pentamidine by aerosol route similar to that obtained by its parenteral administration could be achieved, avoidance of patient hospitalization might be possible [37,38]. The systemic distribution of pentamidine after aerosolization may be ameliorated by its loading into nanocarriers specifically tailored to be effectively nebulized and capable of reaching the deeper airways [39,40]. Particles ranging from 1 to 5 μm are inhalable, but differences in aerosol characteristics can modulate their regional distribution [41]. A decrease in the size of the aerosolized particles down to 1 or 2 μm improves their deposition within alveolar regions, which are the most favorable sites for systemic absorption of drugs and macrophage uptake [42,43]. Liposomes are ideal carriers for lung administration, and several studies confirmed their promising advantages, as they increase the lung bioavailability of delivered drugs due to a reduction in their clearance rate and an improvement of their uptake by macrophages [44]. Indeed, liposomes undergo passive targeting to macrophages, which represents a useful property, especially in the case of parasites that reside within the endocytic pathway compartments of those cells, such as *Leishmania* [45]. To improve macrophage targeting, liposomes can be easily functionalized with specific ligands, such as glycosaminoglycan molecules like chondroitin sulfate (CS) or heparin. Sugar-grafted liposomes encapsulating pentamidine have been shown to increase the therapeutic efficacy of the drug against experimental leishmaniasis in vivo [46]. CS can bind surface molecules such as CD44 or TLR2 and activate macrophages [47], whereas heparin has been described to bind certain parasites such as *Plasmodium falciparum* [48] and *Leishmania chagasi* [49]. Glycosaminoglycan-binding receptors in *Leishmania* include heparin-binding proteins (HBP), and it has been observed that promastigotes incubated with heparin before macrophage infection reached a higher infection rate, suggesting that heparin could play a role in the interaction between HBPs and macrophages [50].

Under these premises, the aim of the present work was to develop an innovative delivery system of low toxicity by loading pentamidine in liposomes coated with CS or heparin specifically tailored for lung administration. The main physicochemical characteristics (mean diameter, surface charge and stability on storage) and technological properties (encapsulation efficiency, aerodynamic behavior and drug release) of different pentamidine-containing nanoformulations have been evaluated along with their toxicity in an endothelial cell line. Finally, the ability of encapsulated pentamidine to inhibit the

growth of *Leishmania infantum* and *Leishmania pifanoi* promastigotes and amastigotes was determined and compared with the free drug in solution.

2. Materials and Methods

2.1. Materials

Enriched soy phosphatidylcholine (Phospholipon® 90G, P90G) was kindly supplied by AVG S.r.l. (Garbagnate Milanese, Milan, Italy). CS extracted from rabbitfish (*Chimaera montrosa*) cartilages was kindly supplied by the Group of Recycling and Valorisation of Waste Materials (REVAL) from the Marine Research Institute (IIM-CSIC, Vigo, Spain) and was produced following the protocol reported in [51]. Pentamidine isethionate, heparin and all other chemicals and solvents of analytical grade were purchased from Sigma-Aldrich (Milan, Italy), unless otherwise indicated. Reagents and plastic labware for cell culture were purchased from Life Technologies Europe (Monza, Italy).

2.2. Liposome Preparation and Pentamidine Quantification

To prepare the vesicles (Table 1), P90G (60 mg/mL), with or without pentamidine isethionate (5 mg/mL), was weighed in a glass vial and hydrated with water to a final volume of 1 mL for plain liposomes and 0.9 mL for CS- and heparin-coated liposomes (CS- and heparin-liposomes, respectively). The resulting dispersion was sonicated 2 times (5 cycles, 5 sec on and 2 sec off and 13 μm of probe amplitude) using a high-intensity ultrasonic disintegrator (Soniprep 150, MSE Crowley, London, UK). To prepare CS and heparin liposomes, 100 μL of a water solution of CS (5 mg/mL) or heparin (10 mg/mL) was added dropwise to liposome dispersions. After ultracentrifugation (150,000× *g*, 4 °C, 1 h) and three washes with phosphate-buffered saline, pH 7.4 (PBS), the amount of CS and heparin attached to liposomes was quantified in triplicate assays with the colorimetric Alcian blue assay [52]. Rhodamine-labeled liposomes were prepared as described above, but with a molar lipid formulation P90G:1,2-dipalmitoyl-*sn*-glycero-3-phosphoethanolamine-N-(lissamine rhodamine B sulfonyl) 99.75:0.25. The liposome dispersions were sterilized by filtration through a 0.22 μm filter (VWR, Radnor, PA, USA) under manual pressure.

Table 1. Composition of liposomes encapsulating pentamidine.

Formulation	P90G (mg/mL)	Pentamidine (mg/mL)	CS (mg/mL)	Heparin (mg/mL)
Pentamidine-liposomes	60.0	5.0	-	-
Pentamidine-CS-liposomes	60.0	5.0	0.5	-
Pentamidine-heparin-liposomes	60.0	5.0	-	1.0

The quantification of pentamidine was carried out by ultraperformance liquid chromatography (UPLC, ACQUITY H-class Plus system, Waters Corporation, Milan, Italy) using a chromatograph equipped with a UV photodiode array detector and a C18 reverse-phase column (Waters Corporation, 1.7 μm, 2.1 mm × 50 mm) at 25 °C. The composition of the mobile phase was methanol:acetonitrile:solution A (25:10:65% volume). Solution A was an aqueous solution of triethylamine and H_3PO_4 (both 0.5% w/vol), adjusted at pH 3.3 with HCl. Flow rate was 200 μL/min for 10 min, and pentamidine, with a retention time of 5.7 min, was detected at 270 nm. A calibration curve was built using pentamidine at different concentrations (0.2, 0.1, 0.05, 0.025 and 0.0125 mg/mL).

2.3. Characterization of Liposomes

The average diameter and polydispersity index of liposomes were measured by dynamic light scattering in a Zetasizer Ultra equipment (Malvern Instruments, Worcestershire, UK). Samples were backscattered by a helium–neon laser (633 nm) at an angle of 173° and a constant temperature of 25 °C. Zeta potential was estimated using the Zetasizer Ultra mixed-mode measurement phase analysis light scattering (M3-PALS) configuration, which

measures particle electrophoretic mobility. Before the measurements, samples were diluted 1/100 with water. The liposome dispersions were separated from the unencapsulated drug by dialysis. Each sample (1 mL) was loaded into Spectra/Por® polycarbonate tubing (12–14 kDa cut-off, 3 nm pore size; Spectrum Laboratories Inc., Breda, The Netherlands) and dialyzed against water (2 L) at room temperature for 2 h. The pentamidine content was measured by UPLC as reported above after disruption of liposomes with methanol (1:100 dilution). Encapsulation efficiency (EE) was calculated as the percentage of pentamidine recovered after dialysis relative to the amount initially present. The stability of liposome dispersions prior to dialysis was evaluated after their storage at 4 °C for up to 6 months by measuring their mean diameter, polydispersity index and zeta potential at scheduled times.

For cryogenic transmission electron microscopy (cryo-TEM) analysis, 1.5 µL of sample diluted tenfold in water was applied on the carbon surface of a glow-discharged Lacey Carbon 300 mesh copper grid (Ted Pella, Inc., Redding, CA, USA). The sample was kept at 100% humidity inside the chamber of a Vitrobot Mark III (FEI Company, Eindhoven, The Netherlands). The excess of liquid was automatically blotted with filter paper, followed by cryo-immobilization by plunge freezing in liquefied ethane. The plunge-frozen sample was transferred to a Tecnai F20 electron microscope (FEI Company) in the Cryomicroscopy Unit from the Scientific and Technological Centers from the *Universitat de Barcelona* using a cryo-holder (Gatan, Pleasanton, CA, USA). The sample was examined in cryogenic conditions at 200 kV and using low-dose imaging conditions. Images were recorded with a 4096 × 4096 pixel CCD Eagle camera (FEI Company).

2.4. Drug Release Analysis

The amount of pentamidine released from the liposomes was measured using a dissolution tester equipped with 6 stations (DT 720 Series-ERWEKA, distributed by EMME 3 SRL, Milan, Italy), using as reference a pentamidine water solution. Pentamidine formulations (1 mL) were transferred into Spectra/Por® dialysis tubes that were placed in the baskets of the dissolution tester containing 1 L of PBS and left under constant stirring at 37 °C, replacing the buffer at different time points (0.25, 0.5, 1, 2, 4, 8, 24, 36 and 96 h). At each time point, 50 µL samples were withdrawn, diluted with 950 µL of methanol:water (1:1), and analyzed for drug quantification. The fraction of released pentamidine was calculated according to the following formula:

$$\text{Pentamidine release}(\%) = \frac{\text{released pentamidine}}{\text{initial pentamidine}} \times 100$$

2.5. Nebulization of Formulations for the Determination of Aerodynamic Behavior

The in vitro deposition of vesicle dispersions was evaluated using the Next Generation Impactor (Eur. Ph 7.2, Copley Scientific Ltd., Nottingham, UK) and the PARI SX® air jet nebulizer connected to a PARI BOY SX® compressor (PARI GmbH, Starnberg, Germany) [53]. Dispersions (2 mL) were placed in the jet nebulizer and aerosolized to dryness directly into the throat of the impactor. At the end of the experiment, the sample deposited into the different stages of the impactor was recovered with methanol, and drug content was quantified by UPLC as reported above. Deposition performances were evaluated calculating the total mass output (TMO), fine particle dose (FPD) and fine particle fraction (FPF). Mass median aerodynamic diameter (MMAD) and geometric standard deviation values were calculated, avoiding the inclusion of the mass deposited in the induction port [54]. The cumulative amount of particles with a diameter smaller than the stated size of each stage was plotted as a percentage of recovered drug versus the cut-off diameter, and the MMAD of the particles was extrapolated from the graph.

2.6. Promastigote Growth Inhibition Assay

L. infantum promastigotes (strain MHOM/ES/2016/CATB101, isolated from a patient with cutaneous and visceral leishmaniasis [55]), were maintained at 26 °C in Schneider's insect medium, supplemented with 20% heat-inactivated fetal bovine serum (FBS), 25 µg/mL gentamycin and 1% sterile human urine, pH 6.7 (complete Schneider). Ten 1:2 serial dilutions in complete Schneider of pentamidine (starting from 100 µM), either free or loaded in liposomes, were performed in 96-well microtiter plates (Corning®, St. Louis, MO, USA), to which was added 100 µL/well of a suspension of 2×10^6 *L. infantum* promastigotes/mL at their logarithmic growth phase (200 µL/well final volume). After 48 h of incubation at 26 °C, 0.0125% resazurin sodium salt (Sigma-Aldrich Corporation, St. Louis, MO, USA) was added, and plates were incubated for 24 h in the same conditions. Afterwards, resorufin fluorescence (λex/em: 535/590 nm) was measured in a Synergy™ HTX Multi-Mode microplate reader (Thermo Electron Corporation, Waltham, MA, USA).

L. pifanoi promastigotes of the MHOM/VE/60/Ltrod line were grown at 26 °C in Roswell Park Memorial Institute 1640 medium (RPMI) supplemented with 10% heat-inactivated FBS plus 2 mM L-glutamine. For cytotoxicity assays, parasites were harvested at late exponential phase of growth and resuspended at 2×10^6 cells/mL in the same medium devoid of phenol red. Parasites were incubated for 72 h with the corresponding test samples disposed in six 1:2 serial dilutions (starting from 25 µM pentamidine). Cytotoxicity was evaluated by the inhibition of MTT (3-(4,5-dimethyl-2-thiazolyl)-2,5-diphenyl-2*H*-tetrazolium bromide) reduction (0.5 mg/mL final concentration) by measuring the reduced formazan, after its solubilization with 0.1% SDS, at 595 nm in a Bio-Rad microplate reader.

For both species, the concentration inhibiting 50% of parasite growth (IC_{50}) was determined by nonlinear regression analysis with GraphPad Prism 8.0 (GraphPad Software, La Jolla, CA, USA). Experiments were performed in triplicate.

2.7. Amastigote Growth Inhibition Assay

Two complementary methods, microscopic observation and a fluorescence-based technique, were used to evaluate the effect of pentamidine-loaded liposomes on *L. infantum* amastigotes. For preliminary microscopic analysis, 300 µL of murine RAW 264.7 macrophages (Abelson murine leukaemia virus-induced tumour cell line) was seeded (5×10^4 cells/mL) in 8-well chamber slides (ibidi GmbH, Gräfelfing, Germany) and grown in RPMI supplemented with 10% FBS and 1% penicillin–streptomycin (complete RPMI) at 37 °C in the presence of 5% CO_2 for 24 h, when >90% of macrophages were adhered in each well. Afterwards, infection was allowed to proceed for 24 h. For that, a late stationary phase *L. infantum* promastigote suspension (5×10^5 promastigotes/mL in complete RPMI) was added to each well. Nonphagocytosed parasites were removed by washing, seven 1:2 serial dilutions of pentamidine-loaded liposomes or free drug (starting from 100 µM) were added and macrophages were incubated in the same conditions for an additional 48 h. Then, cells were washed, fixed with 100% methanol and stained with 10% Giemsa for 7 min. IC_{50} was determined by microscopic counting of infected macrophages in a total of at least 300 macrophages per well [56] in triplicate.

To better quantify the preliminary microscopic results, a fluorescence-based approach was used, following a parasite rescue and transformation assay protocol [57] and the resazurin method described above. RAW 264.7 cells were seeded at 10^5 cells/mL in 96-well microtiter plates and incubated for 24 h at 37 °C in the presence of 5% CO_2 in order to allow cell adherence. Then, infection was carried out adding *L. infantum* promastigotes at 10^6 parasites/mL in complete RPMI (1:10 macrophage:parasite ratio). After a further 24 h incubation in the same conditions, nonphagocytosed parasites were removed by washing, and eight 1:2 serial dilutions of drug in solution or loaded in liposomes (starting from 100 µM) were added to each well, and the plates were incubated for another 48 h. Then, cells were washed with FBS-free Schneider's medium and treated with 40 µL of Schneider's medium supplemented with 0.05% SDS in order to induce cell lysis. After 40 s, SDS was

quenched with 160 µL/well of complete Schneider, plates were incubated for 72 h at 26 °C, and parasite proliferation and the resulting IC_{50} were determined by the resazurin method as described above.

The axenic *L. pifanoi* amastigote line MHOM/VE/60/Ltrod, which affords the study of the amastigote form of this species without interference of the macrophage, was maintained at 32 °C in M199 medium supplemented with 20% heat-inactivated FBS, 0.01% hemin, 0.5% trypticase, 0.25% D-glucose, and 2 mM L-glutamine, pH 6.5. Axenic amastigotes (2×10^6 cells/mL) were incubated with the corresponding test samples (six 1:2 serial dilutions, 25 µM being the highest pentamidine concentration) for 72 h in 96-well plates (200 µL/well). Afterwards, the medium was removed by washing the parasites twice with 1 mL Hank's medium supplemented with 10 mM D-glucose. Then, MTT reduction by axenic amastigotes was carried out by resuspending them into 100 µL of the same medium containing 0.5 mg/mL of MTT, followed by incubation at 32 °C for 2 h. The formed formazan was evaluated as for promastigotes of the same species, as described above, thus avoiding the autofluorescence and scattering problems that might be encountered with the resazurin method at high concentrations. IC_{50} was calculated with GraphPad Prism 8.0 fitting the data with a nonlinear regression analysis. Experiments were performed in triplicate.

2.8. Cytotoxicity Assay

Human umbilical vein endothelial cells (HUVECs) were maintained in M199 supplemented with 10% FBS and 1% penicillin–streptomycin at 37 °C in the presence of 5% CO_2 and seeded in 96-well plates at a density of 5×10^4 cells/mL. After allowing cell adherence for 24 h, the medium was removed, and eight 1:2 serial dilutions of pentamidine in solution or loaded in liposomes (starting from 500 µM) was added in M199 supplemented with 1% penicillin–streptomycin, and cultures were incubated in the same conditions for 24 h. Then, the medium in each well was replaced with 100 µL of M199 containing 1% penicillin–streptomycin and 10 µL of 4-[3-(4-iodophenyl)-2-(4-nitrophenyl)-2*H*-5-tetrazolio]-1,3-benzene disulfonate labeling reagent (WST-1, Roche, Basel, Switzerland). Plates were incubated for 4 h, and absorbance was measured at 440 nm in a Synergy™ HTX Multi-Mode microplate reader. The concentration inhibiting 50% of cell viability (CC_{50}) was determined by linear regression analysis calculated with GraphPad Prism 8.0. Experiments were performed in triplicate.

2.9. Confocal Fluorescence Microscopy

RAW 264.7 macrophages were seeded (50,000 cells/mL) in an 8-well chamber slide system (ibidi GmbH) and allowed to adhere overnight. Then, they were incubated with pentamidine-containing, rhodamine-labeled liposomes (55 µM P90G) for 3 h in RPMI. After three RPMI washes, cells were stained for 30 min with 2 µg/mL of the DNA dye Hoechst 33342 and rinsed with RPMI. Fluorescence microscopy analysis was conducted in a Leica TCS SP5 confocal microscope (Leica Camera, Mannheim, Germany). Hoechst 33342 was excited with a 405 nm diode laser and rhodamine with a 561 nm diode-pumped solid-state laser. Fluorescence emissions were collected in the 416–464 and 575–661 nm ranges, respectively.

2.10. Flow Cytometry Analysis

A total of 1.5×10^5 RAW 264.7 cells/mL was seeded in T-25 flasks (SPL, Pochon, Kyonggi-do, Republic of Korea) and left overnight to allow their adhesion. Pentamidine-containing, rhodamine-labeled liposomes (165 µM P90G) were then added to each flask and incubated for 3 h with the cells before treating with 2 µg/mL Hoechst 33342 for 30 min. Cells were detached with 0.25% trypsin–EDTA (Sigma-Aldrich Corporation) and the trypsin reaction was stopped by adding 10 volumes of prewarmed RPMI, followed by 3× washes with PBS. The uptake of labeled liposomes was analyzed with a five-laser LSRFortessa flow cytometer (BD Biosciences, San Jose, CA, USA) in the

20-parameter standard configuration. Lasers used for the excitation of Hoechst 33342 and rhodamine were, respectively, 350 and 561 nm, and emissions were collected with 450/50 BP and 570LP-582/15 BP nm bandpass filters. A total of 20,000 events were recorded for each sample.

2.11. Statistical Data Analysis

The results are expressed as mean values ± standard deviations, unless otherwise indicated. Statistically significant differences were determined using the one-way analysis of variance and Student's *t* test. The minimum significance level chosen was $p < 0.05$.

3. Results

3.1. Liposome Characterization

Empty liposomes, uncoated or coated with CS or heparin, had diameters between 80 and 90 nm and a polydispersity index between 0.30 and 0.36 (Table 2). The encapsulation of pentamidine did not significantly change their mean diameter but led to a slight decrease in the polydispersity index to below 0.30.

Table 2. Mean diameter (MD), polydispersity index (PDI), zeta potential (ZP), and pentamidine encapsulation efficiency (EE) of liposomes. Mean values ± standard deviations are reported ($n = 6$).

Formulations	MD (nm)	PDI	ZP (mV)	EE (%)
Plain liposomes	85 ± 5	0.302 ± 0.002	−9 ± 4	–
CS-liposomes	79 ± 6	0.361 ± 0.006 *	−14 ± 5 **	–
Heparin-liposomes	81 ± 6	0.351 ± 0.004 *	−13 ± 6 **	–
Pentamidine-liposomes	81 ± 3	0.274 ± 0.001	+34 ± 3 ***	47 ± 4
Pentamidine-CS-liposomes	82 ± 4	0.282 ± 0.003	+34 ± 5 ***	48 ± 5
Pentamidine-heparin-liposomes	84 ± 4	0.285 ± 0.002	+35 ± 5 ***	46 ± 6

*: $p \leq 0.05$; **: $p \leq 0.01$; ***: $p \leq 0.001$ (relative to plain liposomes).

The functionalization of empty liposomes with CS and heparin led to a significant decrease in zeta potential, consistent with the coating of liposomes with the negatively charged glycosaminoglycan polymers. On the contrary, pentamidine-containing liposomes had a large positive zeta potential, indicative of the presence in their formulation of the drug, whose two amidine groups impart a strong cationic character. The positive surface charge may be connected with the location of part of the drug on the vesicle surface, especially the positively charged groups. The zeta potential of liposomes encapsulating pentamidine was not significantly affected by CS or heparin addition. The amount of CS and heparin in pentamidine-containing liposomes (60 mg lipid/mL) was, respectively, 0.33 ± 0.04 and 0.36 ± 0.07 mg/mL, as determined by the Alcian blue assay. The encapsulation efficiency of pentamidine was ca. 47%, without statistical differences among the three formulations ($p > 0.05$).

One month after their preparation, pentamidine-containing liposomes were visualized by cryo-TEM to study their morphological characteristics (Figure 2). Cryo-TEM images revealed the presence of mostly spherical unilamellar liposomes with a mean size range below 100 nm, in agreement with dynamic light scattering data.

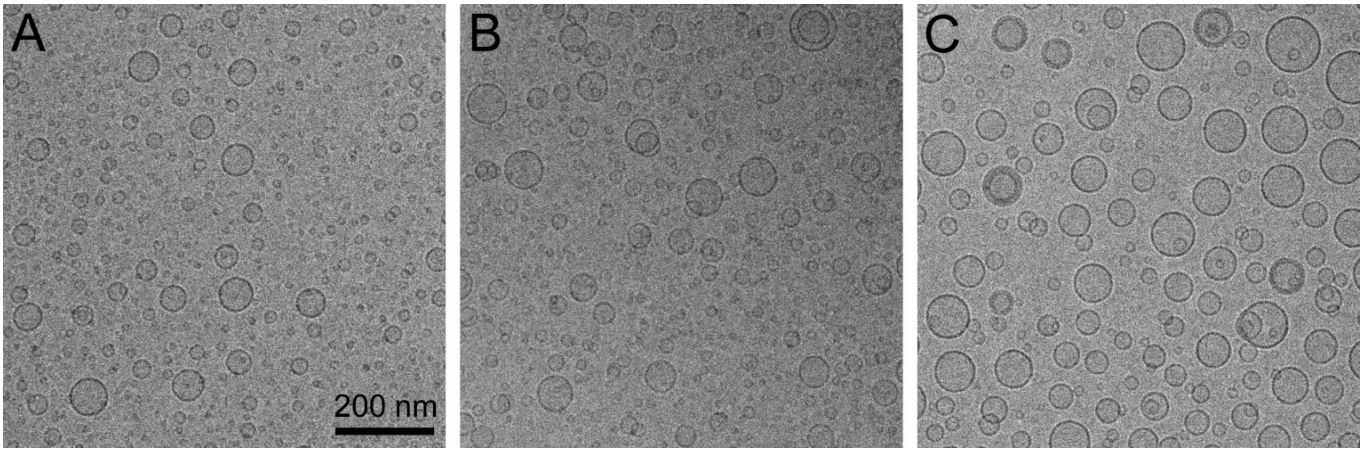

Figure 2. Cryo-TEM images of pentamidine-encapsulating (**A**) plain liposomes, (**B**) CS-liposomes and (**C**) heparin-liposomes, one month after their preparation.

The physicochemical characteristics of undiluted pentamidine-encapsulating liposome suspensions (containing 60 mg/mL P90G) were evaluated by measuring their mean diameter, polydispersity index and zeta potential at the time of preparation and after 2, 4 and 6 months of storage at 4 °C (Figure 3). While the mean diameter of pentamidine-liposomes did not change significantly, the size of pentamidine-containing CS- and heparin-liposomes underwent a significant increase of 6 nm to 120 and up to 500 nm, respectively. The polydispersity index reached values between 0.4 and 0.5 after 4 months for pentamidine- and pentamidine-CS-liposomes, while in pentamidine-heparin-liposomes, it increased above 0.3 only after 6 months. The zeta potential of pentamidine- and pentamidine-CS-liposomes significantly decreased after 4 months, and after 6 months, it reached ~9 mV for all three formulations. This behavior can be due to aggregation and fusion phenomena that may modify the organization of vesicles and also induce the release of the drug or its redistribution in the final system, thus changing the electrical properties of liposome surfaces. Accordingly, for subsequent experiments, all the formulations were used within the first two months after preparation.

The release in PBS of pentamidine from liposomes uncoated and coated with CS or heparin was measured and compared with the free drug in solution using a membrane dialysis approach (Figure 4). Free pentamidine quickly crossed the dialysis membrane, with around 50% of it found in the receptor medium after 30 min and ca. 90% after 2 h, supporting the suitability of this method to evaluate drug release. In contrast, encapsulated pentamidine crossed the dialysis bag at a significantly slower pace, regardless of the used formulation: pentamidine-containing liposomes, either nonmodified or coated with CS or heparin, released ca. 50%, 75% and 90% of drug after 2, 8 and 40 h, respectively, reaching a complete release at 72 h. Because dialysis quickly removes extraliposomal pentamidine, the encapsulated drug exits the liposome to maintain equilibrium, illustrating the contrast between long-term stability of concentrated drug-loaded liposomes and relatively fast content release upon their dilution in aqueous medium.

3.2. Cell Targeting of Liposomes

Targeting to and uptake into RAW 264.7 macrophages of pentamidine-loaded, rhodamine-labeled liposomes was analyzed by flow cytometry and confocal fluorescence microscopy, respectively. After three hours of incubation, pentamidine-liposomes were targeted to ca. 40% of macrophages according to flow cytometry data (Figures 5 and S1), whereas this fraction increased to ca. 90% and 85% for pentamidine-CS- and pentamidine-heparin-liposomes, respectively. At this time, the rhodamine label of the formulations was observed inside the macrophages by fluorescence confocal microscopy (Figure 6). The qualitative microscope images actually showed liposome-derived fluorescence in most

macrophages for all three formulations. This indicated that the displacement observed for all the cell population in quantitative flow cytometry plots of liposome-containing samples reflected the presence of liposomes in virtually all macrophages, although in some of them their fluorescence was too low to displace them beyond the threshold set by the cell-only sample.

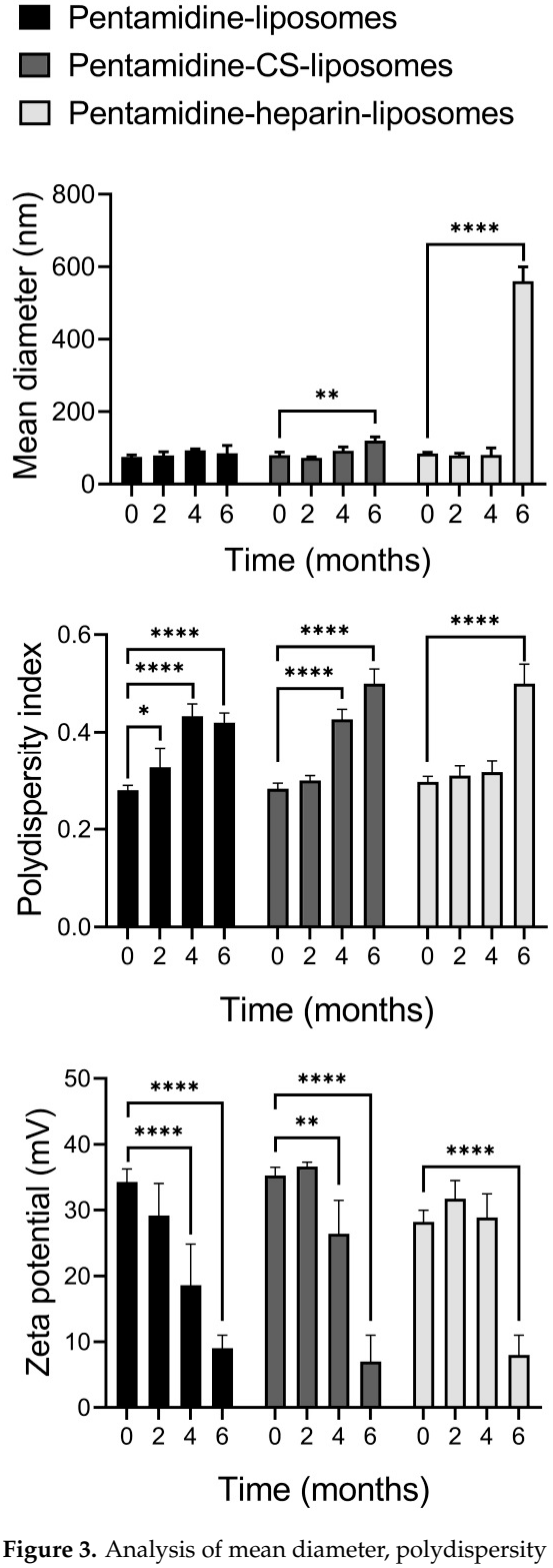

Figure 3. Analysis of mean diameter, polydispersity index and zeta potential of pentamidine-loaded liposomes during 6 months of storage at 4 °C. Mean values ± standard deviations (error bars) are reported ($n = 3$). *: $p \leq 0.05$; **: $p \leq 0.01$; ****: $p \leq 0.0001$.

Figure 3. Analysis of mean diameter, polydispersity index and zeta potential of pentamidine-loaded liposomes during 6 months of storage at 4 °C. Mean values ± standard deviations (error bars) are reported ($n = 3$). *: $p \leq 0.05$; **: $p \leq 0.01$; ****: $p \leq 0.0001$.

The release in PBS of pentamidine from liposomes uncoated and coated with CS o heparin was measured and compared with the free drug in solution using a membran

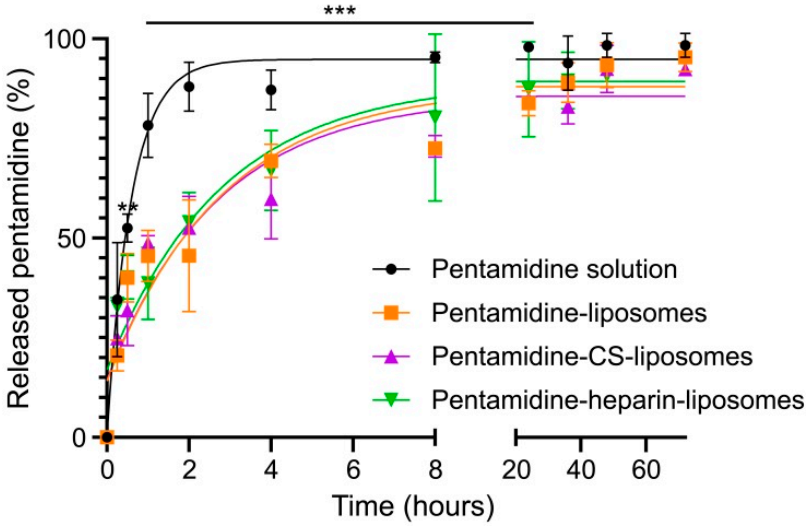

Figure 4. Amount of pentamidine (%) released from dialysis bags along 72 h of incubation in PBS. Mean values ± standard deviations (error bars) are reported (n = 3). **: $p \leq 0.01$; ***: $p \leq 0.001$ (relative to free pentamidine solution).

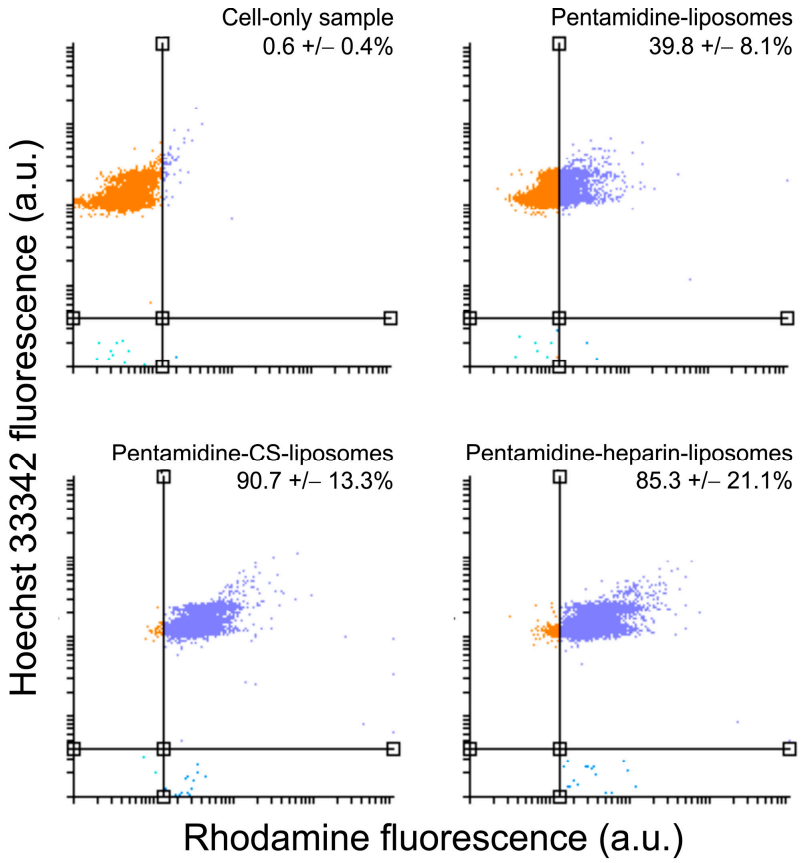

Figure 5. Flow cytometry analysis of liposome targeting to RAW 264.7 macrophages after 3 h of incubation. The vertical line indicates the threshold set to separate rhodamine-free cells (orange dots) from rhodamine-stained cells (purple dots). a.u.: arbitrary units. Mean values ± standard deviations are indicated (n = 3).

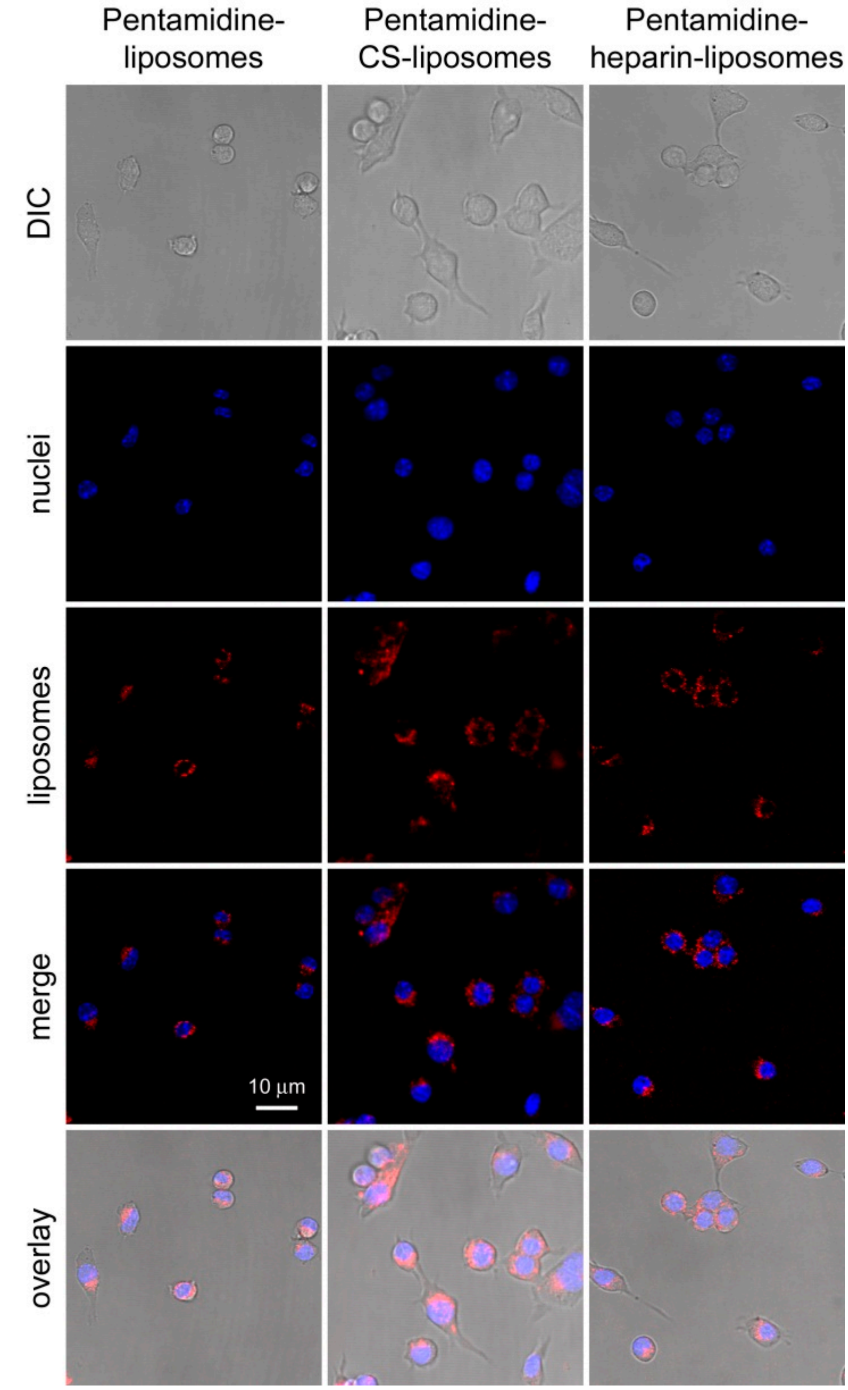

Figure 6. Confocal fluorescence microscopy analysis of pentamidine-loaded liposome uptake in RAW 264.7 macrophages after 3 h of incubation. DIC: differential interference contrast. Nuclei were stained with Hoechst 33342 and liposomes with rhodamine. Merge: fluorescence channels; overlay: superposition of merge and DIC images.

3.3. *In Vitro Activity of Nanoformulations in Leishmania Promastigotes and Amastigotes*

The activity of the different formulations was assayed in *L. infantum* and *L. pifanoi*, the commonly causative agents of VL and New World CL, respectively. The IC_{50} for pentamidine on *Leishmania* promastigotes was found to decrease when the drug was encapsulated in liposomes compared with its free form in solution. In the case of *L. infantum*, this decrease was significant for all pentamidine-containing liposomes, while in *L. pifanoi*, only when pentamidine-liposomes were coated with CS or heparin (Table 3). All three liposomal

formulations of pentamidine had a higher activity against amastigote forms than the free drug, although with modest effectiveness (Tables 3 and S1). The CC_{50} values were always significantly higher for liposome-encapsulated pentamidine, resulting in an improved selectivity index (SI, CC_{50}/IC_{50}) for all three liposomal formulations relative to the drug in solution (Table 3). The observed accumulation of the liposomes inside macrophages (Figure 6) was consistent with the increased activity on amastigotes of pentamidine-loaded liposomes relative to the free drug. The CC_{50} (HUVECs) and IC_{50} (*L. infantum* promastigotes) of pentamidine-free plain liposomes and liposomes coated with CS or heparin was above the maximum tested concentrations (500 μM and 100 μM, respectively).

Table 3. IC_{50}, CC_{50} and selectivity index (SI, CC_{50}/IC_{50}) for pentamidine in solution or loaded in liposomes. Mean values ± standard deviations are reported (n = 3).

		L. infantum			***L. pifanoi***		
	CC_{50} HUVECs (μM)	**IC_{50} Promastigotes (μM)**	**IC_{50} Amastigotes [1] (μM)**	**SI [2]**	**IC_{50} Promastigotes (μM)**	**IC_{50} Axenic Amastigotes (μM)**	**SI [2]**
Pentamidine solution	59.3 ± 4.9	25.8 ± 2.2	3.5 ± 0.9	17.2	7.9 ± 3.7	10.7 ± 3.8	5.5
Pentamidine-liposomes	112.0 ± 12.0 ***	11.3 ± 1.7 ***	2.6 ± 0.4	42.9	3.5 ± 1.0	8.3 ± 0.5	13.6
Pentamidine-CS-liposomes	83.4 ± 9.3 *	18.7 ± 3.7 *	2.5 ± 0.4	33.6	2.0 ± 0.4 *	10.2 ± 1.2	8.2
Pentamidine-heparin-liposomes	144.2 ± 12.7 ****	19.7 ± 1.5 *	3.3 ± 0.8	43.3	2.4 ± 0.4 *	9.9 ± 0.7	14.5

[1] Data obtained with the fluorescence method. The data obtained with the microscopy method are presented in Supplementary Table S1. [2] In amastigotes. *: $p \leq 0.05$; ***: $p \leq 0.001$; ****: $p \leq 0.0001$ (relative to pentamidine solution).

3.4. Nebulization of Nanoformulations and Aerodynamic Behavior

Several studies indicate that aerosolized liposomes could enhance pulmonary and hepatic delivery and accumulation of entrapped drugs, while minimizing systemic exposure and toxicity [37,58,59]. The deposition of liposome dispersions after nebulization was evaluated using the Next Generation Impactor, which mimics the human airways [60] (Table 4). The nebulization of free pentamidine in solution led to a drug deposition in the deeper stages of the impactor of around 53% and 4 mg (fine particle fraction and dose, respectively), and the median aerodynamic diameter was ~2.8 μm, endorsing only a partial deposition on the lung alveoli. In contrast, nebulization of the dispersions of encapsulated pentamidine increased the fine particle fraction and dose up to ~68% and 5 mg, respectively. The significant increase for encapsulated pentamidine observed in the fine particle fraction (particle percentage with aerodynamic diameter below 5 μm) suggests that liposomes will reach alveoli in a more efficient way than the free drug. Supporting this, the median aerodynamic diameter decreased to between 1.4 and 1.8 μm when pentamidine was encapsulated, indicating a better ability to reach the deeper airways of the respiratory tree in higher amounts, although no statistical differences were found among the three liposome formulations. Taking into account the low mass median aerodynamic diameter of pentamidine encapsulated in liposomes (plain or coated with CS and heparin), these systems seem to be suitable for the treatment of leishmaniasis by aerosol administration.

Table 4. Total mass output (TMO), fine particle dose (FPD), fine particle fraction (FPF) and mass median aerodynamic diameter (MMAD) ± geometric standard deviation (GSD) measured for nebulized pentamidine, free in solution or encapsulated in liposomes. Mean values ± standard deviations are reported for TMO, FPD and FPF (n = 3).

	TMO (%)	FPD (mg)	FPF (%)	MMAD (μm) ± GSD
Pentamidine solution	72 ± 6	4.0.± 3.0	53 ± 4	2.8 ± 2.0
Pentamidine-liposomes	74 ± 7	5.0 ± 0.5	70 ± 3 ***	1.7 ± 1.4
Pentamidine-CS-liposomes	82 ± 12	5.0 ± 2.0	68 ± 4 **	1.8 ± 1.5
Pentamidine-heparin-liposomes	84 ± 3 *	5.0 ± 2.0	65 ± 11 *	1.4 ± 1.3

*: $p \leq 0.05$; **: $p \leq 0.01$; ***: $p \leq 0.001$ (relative to pentamidine solution).

4. Discussion

Current conventional therapies used against leishmaniasis are beset with high toxicity, limited efficacy and high associated cost [61]. Nanotechnology has been implemented in recent years as a promising approach to enhance antileishmanial activity while reducing side effects due to toxicity of the drug [44,62,63].

The location of amastigotes inside macrophage phagolysosomes is responsible for an impaired accession of therapeutic drugs by diffusion across successive membrane barriers, rendering them poorly selective, or forcing their administration in repeated and high doses by parenteral routes [64,65]. These facts contribute to the high toxicity and, in most cases, to the limited efficacy of current conventional medications used against clinical forms of leishmaniasis [66–68]. However, the parasitophorous vacuole has selective, yet intense, traffic, with different endosomal compartments. This might render it accessible to drugs vehiculated in nanosystems, profiting from their massive endocytosis routing, and thus endorsing these nanotechnological systems as capable of providing innovative useful tools for future antileishmanial therapies [69]. Among the different nanodelivery systems, liposomes, when administered in vivo by a variety of routes, rapidly accumulate in the mononuclear phagocyte system, a phenomenon profusely used to target drugs for the treatment of intravacuolar parasites that reside in macrophages, such as *Leishmania* [45], as evidenced in the literature [70–77]. Liposomes can be functionalized with polyethyleneglycol covalently attached to phospholipid heads for increased circulation times [78], specific ligands for preferential in vivo delivery to specific cells or organs enriched in the respective receptors or antigens [79], or polymers providing protection from the external environment and increasing mucoadhesion, resulting in an improved residence time of the system (and drug) at the site of action [80]. Because liposome-encapsulated pentamidine will enter the macrophage by endocytosis, and not through receptor-mediated uptake, this will reduce the likelihood of resistance evolution, as it has been shown for African trypanosomiasis, where pentamidine delivered in chitosan nanoparticles bypassed drug resistance mechanisms in the parasite associated to cell surface receptors [81].

The delivery of drugs encapsulated in small liposomes (<100 nm) has been reported to be more efficient than in larger ones, especially when administered in the lungs, likely because of their greater uptake by macrophages [82]. We determined that uncoated liposomes and liposomes coated with chondroitin sulfate or heparin were small in size, homogeneously dispersed and stable up to at least two months of storage at 4 °C. Upon dilution through dialysis, pentamidine release from all three liposome formulations was almost complete (90%) after 40 h, a timeframe that must be taken into account when designing future administration methods and regimens. The current route of pentamidine delivery is intramuscular or intravenous with a regimen of 3 to 20 doses spaced every two or three days depending on the clinical status of the patient [83]. This method is very painful and can lead to side effects associated with the parenteral route, such as muscular aseptic abscess after intramuscular injection [25]. In the present

study, nebulization was explored as a harmless route of administration, which would maximize pentamidine deposition in lung alveoli by tailoring liposomes small in size and capable of resisting the harsh conditions that occur during the nebulization process, thus leading to droplets sized between 1 and 2 μm [42,43]. In vitro lung deposition studies underlined the ability of vesicles to deliver pentamidine up to the deeper stages of the impactor in significantly higher amounts than the free compound. However, some nebulized drug may not reach the deeper airways, since a small portion of larger droplets can be produced by the nebulizer, which will interact with the upper part of the respiratory tree where are mainly located the parasites responsible for MCL, the most difficult form of the disease to treat [9]. The nebulization of pentamidine-loaded liposomes is an undemanding methodology and a patient-friendly strategy for the treatment of leishmaniasis, and it is less aggressive than intravenous, intramuscular or subcutaneous administration [84]. The pulmonary delivery of pentamidine can target the drug to *Leishmania* parasites via uptake by the macrophages, reducing toxic systemic effects and limiting the emergence of resistance in the pathogen. If the drug is retained by alveolar macrophages, these cells will behave as a repository for a sustained release of the drug. Alternatively, if the nanocarriers undergo transcytosis and become systemic, they will be available for further uptake by other macrophages. The findings reported here can be especially relevant for the treatment of mucosal leishmaniasis, which damages the upper respiratory tract. As pentamidine is also used for other infections, such as pneumonia produced by *Pneumocystis carinii*, a serious condition that affects people with a weak immune system [85], the spectra of infectious diseases to which nebulization of pentamidine could be applied is not restricted to leishmaniasis.

Although the coating of liposomes with CS or heparin resulted in an enhanced macrophage uptake, this did not translate to a significantly improved IC_{50} for encapsulated pentamidine. It is likely that the relatively fast drug release after its dilution in the cell culture medium, with ca. 50% of it having left the liposomes after 2 h according to PBS dialysis, tends to mask the potential benefits of targeted drug delivery after the 48 h incubation of in vitro growth inhibition assays. Eventual in vivo assays, where the blood residence times will be shortened, might reveal a better performance of the liposomal formulations relative to the free drug. Such targeting to macrophages, underlain by the reported internalization of glycosaminoglycan-coated liposomes through receptor-mediated uptake [47,50], may make them more efficient than uncoated liposomes when tested in vivo. Interestingly, other works documented the induction of an anti-inflammatory status in heparin-treated macrophages [86], which may contribute to reducing the executor function of these cells in synergy with the direct effect of the drug on the parasite, pointing to heparin-coated, pentamidine-containing liposomes as an optimal combination for the treatment of leishmaniasis. Future pharmacokinetics analysis and animal experimentation in preparation for clinical trials should provide valuable information regarding the potential of the nanoformulations developed here to be part of new antileishmanial therapies.

5. Conclusions

Given the high toxicity of currently available drugs against leishmaniasis, we undertook a study to ameliorate their therapeutic prospects, using pentamidine as a model compound. The encapsulation of pentamidine in liposomes coated with chondroitin sulfate or heparin provided (i) lower cytotoxicity, (ii) better targeting to macrophages, (iii) a significantly increased efficacy against *L. infantum* and *L. pifanoi* promastigotes and (iv) a higher deposition of the nebulized liposomal preparations in the deeper stages of a human lung airway simulator. Together, these four improvements represent a promising step forward in the formulation of antileishmanial drugs for their optimized administration.

Supplementary Materials: The following supporting information can be downloaded at: https://www.mdpi.com/article/10.3390/pharmaceutics15041163/s1, Supplementary Figure S1: One-way analysis of variance to determine statistically significant differences between the different samples of the flow cytometry data in Figure 5; Supplementary Table S1: Comparison of the IC_{50} of pentamidine in *L. infantum* amastigotes calculated with the microscopy and fluorescence methods.

Author Contributions: Conceptualization, M.M., C.R. and X.F.-B.; data curation, L.R.-Á.; formal analysis, L.R.-Á., M.L.M., M.M., L.R., C.R. and X.F.-B.; funding acquisition, M.M., L.R., C.R. and X.F.-B.; investigation, L.R.-Á., M.A., Y.A.-P., M.L.M., F.F., J.F.-L., L.R., J.A.V., J.E.P., X.R.-G., S.P., M.M.A. and R.F.; methodology, M.M., C.R. and X.F.-B.; project administration, X.F.-B.; Resources, M.M., L.R., C.R. and X.F.-B.; supervision, M.M., L.R., C.R. and X.F.-B.; visualization, L.R.-Á. and M.A.; writing—original draft, L.R.-Á., M.M. and X.F.-B.; writing—review and editing, L.R.-Á., M.A., Y.A.-P., M.L.M., M.M., F.F., J.F.-L., L.R., J.A.V., J.E.P., X.R.-G., S.P., R.F., C.R. and X.F.-B. All authors have read and agreed to the published version of the manuscript.

Funding: This work was funded by *Fundació La Marató de TV3* (Ref. 201811) and supported by the *Generalitat de Catalunya*, Spain (http://agaur.gencat.cat/, accessed on 20 February 2023), grant numbers 2017-SGR-908 and 2021-SGR-00635. L.R. was supported by MCIN *Subdirección General de Redes y Centros de Investigación Cooperativa*-FEDER RD16/0027/0010 and CSIC PIE 201620E038.

Institutional Review Board Statement: The study was conducted in accordance with the Declaration of Helsinki and approved by the Clinical Research Ethics Committee from the *Hospital Clínic de Barcelona* (www.clinicbarcelona.org/ceim, accessed on 20 February 2023; Reg. HCB/2018/1223, 23 January 2019).

Informed Consent Statement: Not applicable.

Data Availability Statement: All the data supporting the reported results can be found in the main article and in the Supplementary Materials files.

Acknowledgments: ISGlobal and IBEC are members of the CERCA Programme, *Generalitat de Catalunya*. We acknowledge support from the Spanish Ministry of Science, Innovation, and Universities through the "*Centro de Excelencia Severo Ochoa 2019–2023*" Program (CEX2018-000806-S). This research is part of ISGlobal's Program on the Molecular Mechanisms of Malaria, partially supported by the *Fundación Ramón Areces*.

Conflicts of Interest: The funders had no role in the design of the study; in the collection, analyses, or interpretation of data; in the writing of the manuscript, or in the decision to publish the results.

References

1. Bates, P.A. Transmission of *Leishmania* metacyclic promastigotes by phlebotomine sand flies. *Int. J. Parasitol.* **2007**, *37*, 1097–1106. [CrossRef] [PubMed]
2. Mougneau, E.; Bihl, F.; Glaichenhaus, N. Cell biology and immunology of *Leishmania*. *Immunol. Rev.* **2011**, *240*, 286–296. [CrossRef] [PubMed]
3. Oryan, A.; Akbari, M. Worldwide risk factors in leishmaniasis. *Asian Pac. J. Trop. Med.* **2016**, *9*, 925–932. [CrossRef] [PubMed]
4. Burza, S.; Croft, S.L.; Boelaert, M. Leishmaniasis. *Lancet* **2018**, *392*, 951–970. [CrossRef]
5. World Health Organization. World Health Organization Leishmaniasis Factsheet. 2023. Available online: https://www.who.int/news-room/fact-sheets/detail/leishmaniasis (accessed on 20 February 2023).
6. Ameen, M. Cutaneous and mucocutaneous leishmaniasis: Emerging therapies and progress in disease management. *Expert Opin. Pharmacother.* **2010**, *11*, 557–569. [CrossRef]
7. Sundar, S.; Singh, A. Chemotherapeutics of visceral leishmaniasis: Present and future developments. *Parasitology* **2018**, *145*, 481–489. [CrossRef]
8. Nico, D.; Conde, L.; Palatnik de Sousa, C.B. Classical and modern drug treatments for leishmaniasis. In *Antiprotozoal Drug Development and Delivery*; Vermelho, A.B., Supuran, C.T., Eds.; Springer: Berlin/Heidelberg, Germany, 2021; Volume 39, pp. 1–21.
9. Pinart, M.; Rueda, J.R.; Romero, G.A.; Pinzón-Flórez, C.E.; Osorio-Arango, K.; Silveira Maia-Elkhoury, A.N.; Reveiz, L.; Elias, V.M.; Tweed, J.A. Interventions for American cutaneous and mucocutaneous leishmaniasis. *Cochrane Database Syst. Rev.* **2020**, *8*, CD004834.

10. Dumetz, F.; Cuypers, B.; Imamura, H.; Zander, D.; D'Haenens, E.; Maes, I.; Domagalska, M.A.; Clos, J.; Dujardin, J.C.; De Muylder, G. Molecular preadaptation to antimony resistance in *Leishmania donovani* on the Indian subcontinent. *mSphere* **2018**, *3*, e00548-17. [CrossRef]
11. Ponte-Sucre, A.; Gamarro, F.; Dujardin, J.C.; Barrett, M.P.; López-Vélez, R.; García-Hernández, R.; Pountain, A.W.; Mwenechanya, R.; Papadopoulou, B. Drug resistance and treatment failure in leishmaniasis: A 21st century challenge. *PLoS Negl. Trop. Dis.* **2017**, *11*, e0006052. [CrossRef]
12. Azim, M.; Khan, S.A.; Ullah, S.; Ullah, S.; Anjum, S.I. Therapeutic advances in the topical treatment of cutaneous leishmaniasis: A review. *PLoS Negl. Trop. Dis.* **2021**, *15*, e0009099. [CrossRef]
13. Soto, J.; Rojas, E.; Guzman, M.; Verduguez, A.; Nena, W.; Maldonado, M.; Cruz, M.; Gracia, L.; Villarroel, D.; Alavi, I.; et al. Intralesional antimony for single lesions of bolivian cutaneous leishmaniasis. *Clin. Infect. Dis.* **2013**, *56*, 1255–1260. [CrossRef]
14. Amato, V.S.; Rabello, A.; Rotondo-Silva, A.; Kono, A.; Maldonado, T.P.; Alves, I.C.; Floeter-Winter, L.M.; Neto, V.A.; Shikanai-Yasuda, M.A. Successful treatment of cutaneous leishmaniasis with lipid formulations of amphotericin B in two immunocompromised patients. *Acta Trop.* **2004**, *92*, 127–132. [CrossRef]
15. Chakravarty, J.; Sundar, S. Current and emerging medications for the treatment of leishmaniasis. *Expert Opin. Pharmacother.* **2019**, *20*, 1251–1265. [CrossRef]
16. Mosimann, V.; Neumayr, A.; Paris, D.H.; Blum, J. Liposomal amphotericin B treatment of Old World cutaneous and mucosal leishmaniasis: A literature review. *Acta Trop.* **2018**, *182*, 246–250. [CrossRef]
17. Kumari, S.; Kumar, V.; Tiwari, R.K.; Ravidas, V.; Pandey, K.; Kumar, A. Amphotericin B: A drug of choice for visceral leishmaniasis. *Acta Trop.* **2022**, *235*, 106661. [CrossRef]
18. Davies, C.R.; Kaye, P.; Croft, S.L.; Sundar, S. Leishmaniasis: New approaches to disease control. *Br. Med. J.* **2003**, *326*, 377–382. [CrossRef]
19. Dorlo, T.P.; Balasegaram, M.; Beijnen, J.H.; de Vries, P.J. Miltefosine: A review of its pharmacology and therapeutic efficacy in the treatment of leishmaniasis. *J. Antimicrob. Chemother.* **2012**, *67*, 2576–2597. [CrossRef]
20. Matos, A.P.S.; Viçosa, A.L.; Ré, M.I.; Ricci-Júnior, E.; Holandino, C. A review of current treatments strategies based on paromomycin for leishmaniasis. *J. Drug Deliv. Sci. Technol.* **2020**, *57*, 101664. [CrossRef]
21. Guery, R.; Henry, B.; Martin-Blondel, G.; Rouzaud, C.; Cordoliani, F.; Harms, G.; Gangneux, J.P.; Foulet, F.; Bourrat, E.; Baccard, M.; et al. Liposomal amphotericin B in travelers with cutaneous and muco-cutaneous leishmaniasis: Not a panacea. *PLoS Negl. Trop. Dis.* **2017**, *11*, e0006094. [CrossRef]
22. Bastos, D.S.S.; Silva, A.C.; Novaes, R.D.; Souza, A.C.F.; Santos, E.C.; Gonçalves, R.V.; Marques-Da-Silva, E.A. Could combination chemotherapy be more effective than monotherapy in the treatment of visceral leishmaniasis? A systematic review of preclinical evidence. *Parasitology* **2022**, *149*, 751–764. [CrossRef]
23. Chechi, F.; Corsi, P.; Bartolozzi, D.; Gaiera, G.; Bartoloni, A.; Zammarchi, L. Case report: Intravenous pentamidine rescue treatment for active chronic visceral leishmaniasis in an HIV-1 infected patient. *Am. J. Trop. Med. Hyg.* **2021**, *106*, 639–642. [CrossRef] [PubMed]
24. Soto, J.A.; Berman, J.D. Miltefosine treatment of cutaneous leishmaniasis. *Clin. Infect. Dis.* **2021**, *73*, e2463–e2464. [CrossRef] [PubMed]
25. Piccica, M.; Lagi, F.; Bartoloni, A.; Zammarchi, L. Efficacy and safety of pentamidine isethionate for tegumentary and visceral human leishmaniasis: A systematic review. *J. Travel Med.* **2021**, *28*, taab065. [CrossRef] [PubMed]
26. Noli, C.; Auxilia, S.T. Treatment of canine Old World visceral leishmaniasis: A systematic review. *Vet. Dermatol.* **2005**, *16*, 213–232. [CrossRef] [PubMed]
27. Olías-Molero, A.I.; Fontán-Matilla, E.; Cuquerella, M.; Alunda, J.M. Scientometric analysis of chemotherapy of canine leishmaniasis (2000–2020). *Parasit. Vectors* **2021**, *14*, 36. [CrossRef]
28. Basile, G.; Cristofaro, G.; Locatello, L.G.; Vellere, I.; Piccica, M.; Bresci, S.; Maggiore, G.; Gallo, O.; Novelli, A.; Di Muccio, T.; et al. Refractory mucocutaneous leishmaniasis resolved with combination treatment based on intravenous pentamidine, oral azole, aerosolized liposomal amphotericin B, and intralesional meglumine antimoniate. *Int. J. Infect. Dis.* **2020**, *97*, 204–207. [CrossRef]
29. Vechi, H.T.; Vasconcelos de Sousa, A.S.; Alves da Cunha, M.; Shaw, J.J.; Luz, K.G. Case report: Combination therapy with liposomal amphotericin B, N-methyl meglumine antimoniate, and pentamidine isethionate for disseminated visceral leishmaniasis in a splenectomized adult patient. *Am. J. Trop. Med. Hyg.* **2020**, *102*, 268–273. [CrossRef]
30. Roatt, B.M.; de Oliveira Cardoso, J.M.; De Brito, R.C.F.; Coura-Vital, W.; de Oliveira Aguiar-Soares, R.D.; Reis, A.B. Recent advances and new strategies on leishmaniasis treatment. *Appl. Microbiol. Biotechnol.* **2020**, *104*, 8965–8977. [CrossRef]
31. Valle, I.V.; Machado, M.E.; Araújo, C.D.C.B.; da Cunha-Junior, E.F.; da Silva Pacheco, J.; Torres-Santos, E.C.; da Silva, L.C.R.P.; Cabral, L.M.; do Carmo, F.A.; Sathler, P.C. Oral pentamidine-loaded poly(d,l-lactic-co-glycolic) acid nanoparticles: An alternative approach for leishmaniasis treatment. *Nanotechnology* **2019**, *30*, 455102. [CrossRef]
32. Tuon, F.F.; Dantas, L.R.; de Souza, R.M.; Ribeiro, V.S.T.; Amato, V.S. Liposomal drug delivery systems for the treatment of leishmaniasis. *Parasitol. Res.* **2022**, *121*, 3073–3082. [CrossRef]

33. Assolini, J.P.; Carloto, A.C.M.; da Silva Bortoleti, B.T.; Gonçalves, M.D.; Tomiotto Pellissier, F.; Feuser, P.E.; Cordeiro, A.P.; Hermes de Araújo, P.H.; Sayer, C.; Miranda Sapla, M.M.; et al. Nanomedicine in leishmaniasis: A promising tool for diagnosis, treatment and prevention of disease—An update overview. *Eur. J. Pharmacol.* **2022**, *923*, 174934. [CrossRef]
34. Rinaldi, F.; Hanieh, P.N.; Chan, L.K.N.; Angeloni, L.; Passeri, D.; Rossi, M.; Wang, J.T.; Imbriano, A.; Carafa, M.; Marianecci, C. Chitosan glutamate-coated niosomes: A proposal for nose-to-brain delivery. *Pharmaceutics* **2018**, *10*, 38. [CrossRef]
35. Khan, M.M.; Zaidi, S.S.; Siyal, F.J.; Khan, S.U.; Ishrat, G.; Batool, S.; Mustapha, O.; Khan, S.; ud Din, F. Statistical optimization of co-loaded rifampicin and pentamidine polymeric nanoparticles for the treatment of cutaneous leishmaniasis. *J. Drug Deliv. Sci. Technol.* **2023**, *79*, 104005. [CrossRef]
36. Kannan, S.; Harel, Y.; Israel, L.L.; Lellouche, E.; Varvak, A.; Tsubery, M.N.; Lellouche, J.P.; Michaeli, S. Novel nanocarrier platform for effective treatment of visceral leishmaniasis. *Bioconjug. Chem.* **2021**, *32*, 2327–2341. [CrossRef]
37. Vyas, S.P.; Kannan, M.E.; Jain, S.; Mishra, V.; Singh, P. Design of liposomal aerosols for improved delivery of rifampicin to alveolar macrophages. *Int. J. Pharm.* **2004**, *269*, 37–49. [CrossRef]
38. Rudokas, M.; Najlah, M.; Alhnan, M.A.; Elhissi, A. Liposome delivery systems for inhalation: A critical review highlighting formulation issues and anticancer applications. *Med. Princ. Pract.* **2016**, *25* (Suppl. 2), 60–72. [CrossRef]
39. Sakagami, M. In vivo, in vitro and ex vivo models to assess pulmonary absorption and disposition of inhaled therapeutics for systemic delivery. *Adv. Drug Deliv. Rev.* **2006**, *58*, 1030–1060. [CrossRef]
40. Manca, M.L.; Manconi, M.; Valenti, D.; Lai, F.; Loy, G.; Matricardi, P.; Fadda, A.M. Liposomes coated with chitosan-xanthan gum (chitosomes) as potential carriers for pulmonary delivery of rifampicin. *J. Pharm. Sci.* **2012**, *101*, 566–575. [CrossRef]
41. Derendorf, H.; Hochhaus, G.; Möllmann, H. Evaluation of pulmonary absorption using pharmacokinetic methods. *J. Aerosol Med.* **2001**, *14* (Suppl. 1), S9–S17. [CrossRef]
42. Rubin, B.K. Air and soul: The science and application of aerosol therapy. *Respir. Care* **2010**, *55*, 911–921.
43. Patton, J.S. Mechanisms of macromolecule absorption by the lungs. *Adv. Drug Deliv. Rev.* **1996**, *19*, 3–36. [CrossRef]
44. Prasanna, P.; Kumar, P.; Kumar, S.; Rajana, V.K.; Kant, V.; Prasad, S.R.; Mohan, U.; Ravichandiran, V.; Mandal, D. Current status of nanoscale drug delivery and the future of nano-vaccine development for leishmaniasis—A review. *Biomed. Pharmacother.* **2021**, *141*, 111920. [CrossRef] [PubMed]
45. Agrawal, A.K.; Gupta, C.M. Tuftsin-bearing liposomes in treatment of macrophage-based infections. *Adv. Drug Deliv. Rev.* **2000**, *41*, 135–146. [CrossRef] [PubMed]
46. Banerjee, G.; Nandi, G.; Mahato, S.B.; Pakrashi, A.; Basu, M.K. Drug delivery system: Targeting of pentamidines to specific sites using sugar grafted liposomes. *J. Antimicrob. Chemother.* **1996**, *38*, 145–150. [CrossRef]
47. Wu, F.; Zhou, C.; Zhou, D.; Ou, S.; Liu, Z.; Huang, H. Immune-enhancing activities of chondroitin sulfate in murine macrophage RAW 264.7 cells. *Carbohydr. Polym.* **2018**, *198*, 611–619. [CrossRef]
48. Mulloy, B.; Hogwood, J.; Gray, E.; Lever, R.; Page, C.P. Pharmacology of heparin and related drugs. *Pharmacol. Rev.* **2015**, *68*, 76–141. [CrossRef]
49. Martins, T.V.F.; de Carvalho, T.V.; de Oliveira, C.V.M.; de Paula, S.O.; Cardoso, S.A.; de Oliveira, L.L.; Marques-da-Silva, E.d.A. *Leishmania chagasi* heparin-binding protein: Cell localization and participation in *L. chagasi* infection. *Mol. Biochem. Parasitol.* **2015**, *204*, 34–43. [CrossRef]
50. Merida-de-Barros, D.A.; Chaves, S.P.; Belmiro, C.L.R.; Wanderley, J.L.M. Leishmaniasis and glycosaminoglycans: A future therapeutic strategy? *Parasit. Vectors* **2018**, *11*, 536. [CrossRef]
51. Vázquez, J.A.; Fraguas, J.; Novoa-Carballal, R.; Reis, R.L.; Pérez-Martín, R.I.; Valcarcel, J. Optimal isolation and characterisation of chondroitin sulfate from rabbit fish (*Chimaera monstrosa*). *Carbohydr. Polym.* **2019**, *210*, 302–313. [CrossRef]
52. Frazier, S.B.; Roodhouse, K.A.; Hourcade, D.E.; Zhang, L. The quantification of glycosaminoglycans: A comparison of HPLC, carbazole, and Alcian blue methods. *Open Glycosci.* **2008**, *1*, 31–39. [CrossRef]
53. Manca, M.L.; Valenti, D.; Sales, O.D.; Nacher, A.; Fadda, A.M.; Manconi, M. Fabrication of polyelectrolyte multilayered vesicles as inhalable dry powder for lung administration of rifampicin. *Int. J. Pharm.* **2014**, *472*, 102–109. [CrossRef]
54. Manconi, M.; Manca, M.L.; Valenti, D.; Escribano, E.; Hillaireau, H.; Fadda, A.M.; Fattal, E. Chitosan and hyaluronan coated liposomes for pulmonary administration of curcumin. *Int. J. Pharm.* **2017**, *525*, 203–210. [CrossRef]
55. Martí-Carreras, J.; Carrasco, M.; Gómez-Ponce, M.; Noguera-Julián, M.; Fisa, R.; Riera, C.; Alcover, M.M.; Roura, X.; Ferrer, L.; Francino, O. Identification of *Leishmania infantum* epidemiology, drug resistance and pathogenicity biomarkers with nanopore sequencing. *Microorganisms* **2022**, *10*, 2256. [CrossRef]
56. Noleto Dias, C.; Nunes, T.A.L.; de Sousa, J.M.S.; Costa, L.H.; Rodrigues, R.R.L.; Araújo, A.J.; Marinho Filho, J.D.B.; da Silva, M.V.; Oliveira, M.R.; de Amorim Carvalho, F.A.; et al. Methyl gallate: Selective antileishmanial activity correlates with host-cell directed effects. *Chem. Biol. Interact.* **2020**, *320*, 109026. [CrossRef]
57. Jain, S.K.; Sahu, R.; Walker, L.A.; Tekwani, B.L. A parasite rescue and transformation assay for antileishmanial screening against intracellular *Leishmania donovani* amastigotes in THP1 human acute monocytic leukemia cell line. *J. Vis. Exp.* **2012**, *70*, e4054.
58. Vyas, S.P.; Quraishi, S.; Gupta, S.; Jaganathan, K.S. Aerosolized liposome-based delivery of amphotericin B to alveolar macrophages. *Int. J. Pharm.* **2005**, *296*, 12–25. [CrossRef]

59. Debs, R.J.; Straubinger, R.M.; Brunette, E.N.; Lin, J.M.; Lin, E.J.; Montgomery, A.B.; Friend, D.S.; Papahadjopoulos, D.P. Selective enhancement of pentamidine uptake in the lung by aerosolization and delivery in liposomes. *Am. Rev. Respir. Dis.* **1987**, *135*, 731–737.
60. Nahar, K.; Gupta, N.; Gauvin, R.; Absar, S.; Patel, B.; Gupta, V.; Khademhosseini, A.; Ahsan, F. In vitro, in vivo and ex vivo models for studying particle deposition and drug absorption of inhaled pharmaceuticals. *Eur. J. Pharm. Sci.* **2013**, *49*, 805–818. [CrossRef]
61. Singh, N.; Kumar, M.; Singh, R.K. Leishmaniasis: Current status of available drugs and new potential drug targets. *Asian Pac. J. Trop. Med.* **2012**, *5*, 485–497. [CrossRef]
62. Akbari, M.; Oryan, A.; Hatam, G. Application of nanotechnology in treatment of leishmaniasis: A review. *Acta Trop.* **2017**, *172*, 86–90. [CrossRef]
63. Romero, E.L.; Morilla, M.J. Drug delivery systems against leishmaniasis? Still an open question. *Expert Opin. Drug Deliv.* **2008**, *5*, 805–823. [CrossRef] [PubMed]
64. Murray, H.W.; Berman, J.D.; Davies, C.R.; Saravia, N.G. Advances in leishmaniasis. *Lancet* **2005**, *366*, 1561–1577. [CrossRef] [PubMed]
65. Sundar, S.; Rai, M. Treatment of visceral leishmaniasis. *Expert Opin. Pharmacother.* **2005**, *6*, 2821–2829. [CrossRef] [PubMed]
66. Sundar, S.; Jha, T.K.; Thakur, C.P.; Engel, J.; Sindermann, H.; Fischer, C.; Junge, K.; Bryceson, A.; Berman, J. Oral miltefosine for Indian visceral leishmaniasis. *N. Engl. J. Med.* **2002**, *347*, 1739–1746. [CrossRef]
67. Sundar, S.; Mehta, H.; Suresh, A.V.; Singh, S.P.; Rai, M.; Murray, H.W. Amphotericin B treatment for Indian visceral leishmaniasis: Conventional versus lipid formulations. *Clin. Infect. Dis.* **2004**, *38*, 377–383. [CrossRef]
68. Thakur, C.P.; Narayan, S. A comparative evaluation of amphotericin B and sodium antimony gluconate, as first-line drugs in the treatment of Indian visceral leishmaniasis. *Ann. Trop. Med. Parasitol.* **2004**, *98*, 129–138. [CrossRef]
69. European Science Fundation: ESF. Forward Look on Nanomedicine. 2005. Available online: http://www.nanopharmaceuticals.org/files/nanomedicine.pdf (accessed on 6 October 2022).
70. Ribeiro, R.R.; Moura, E.P.; Pimentel, V.M.; Sampaio, W.M.; Silva, S.M.; Schettini, D.A.; Alves, C.F.; Melo, F.A.; Tafuri, W.L.; Demicheli, C.; et al. Reduced tissue parasitic load and infectivity to sand flies in dogs naturally infected by *Leishmania* (*Leishmania*) *chagasi* following treatment with a liposome formulation of meglumine antimoniate. *Antimicrob. Agents Chemother.* **2008**, *52*, 2564–2572. [CrossRef]
71. Schettini, D.A.; Costa Val, A.P.; Souza, L.F.; Demicheli, C.; Rocha, O.G.; Melo, M.N.; Michalick, M.S.; Frézard, F. Pharmacokinetic and parasitological evaluation of the bone marrow of dogs with visceral leishmaniasis submitted to multiple dose treatment with liposome-encapsulated meglumine antimoniate. *Braz. J. Med. Biol. Res.* **2005**, *38*, 1879–1883. [CrossRef]
72. Tempone, A.G.; Perez, D.; Rath, S.; Vilarinho, A.L.; Mortara, R.A.; de Andrade, H.F., Jr. Targeting *Leishmania (L.) chagasi* amastigotes through macrophage scavenger receptors: The use of drugs entrapped in liposomes containing phosphatidylserine. *J. Antimicrob. Chemother.* **2004**, *54*, 60–68. [CrossRef]
73. Valladares, J.E.; Freixas, J.; Alberola, J.; Franquelo, C.; Cristofol, C.; Arboix, M. Pharmacokinetics of liposome-encapsulated meglumine antimonate after intramuscular and subcutaneous administration in dogs. *Am. J. Trop. Med. Hyg.* **1997**, *57*, 403–406. [CrossRef]
74. Kshirsagar, N.A.; Gokhale, P.C.; Pandya, S.K. Liposomes as drug delivery system in leishmaniasis. *J. Assoc. Physicians India* **1995**, *43*, 46–48.
75. Banerjee, G.; Medda, S.; Basu, M.K. A novel peptide-grafted liposomal delivery system targeted to macrophages. *Antimicrob. Agents Chemother.* **1998**, *42*, 348–351. [CrossRef]
76. Coukell, A.J.; Brogden, R.N. Liposomal amphotericin B. Therapeutic use in the management of fungal infections and visceral leishmaniasis. *Drugs* **1998**, *55*, 585–612. [CrossRef]
77. Alving, C.R. Liposomes as drug carriers in leishmaniasis and malaria. *Parasitol. Today* **1986**, *2*, 101–107. [CrossRef]
78. Blume, G.; Cevc, G. Liposomes for the sustained drug release in vivo. *Biochim. Biophys. Acta* **1990**, *1029*, 91–97. [CrossRef]
79. Turk, M.J.; Waters, D.J.; Low, P.S. Folate-conjugated liposomes preferentially target macrophages associated with ovarian carcinoma. *Cancer Lett.* **2004**, *213*, 165–172. [CrossRef]
80. Catalán-Latorre, A.; Pleguezuelos-Villa, M.; Castangia, I.; Manca, M.L.; Caddeo, C.; Nácher, A.; Díez-Sales, O.; Peris, J.E.; Pons, R.; Escribano-Ferrer, E.; et al. Nutriosomes: Prebiotic delivery systems combining phospholipids, a soluble dextrin and curcumin to counteract intestinal oxidative stress and inflammation. *Nanoscale* **2018**, *10*, 1957–1969. [CrossRef]
81. Unciti-Broceta, J.D.; Arias, J.L.; Maceira, J.; Soriano, M.; Ortiz-González, M.; Hernández-Quero, J.; Muñoz-Torres, M.; de Koning, H.P.; Magez, S.; Garcia-Salcedo, J.A. Specific cell targeting therapy bypasses drug resistance mechanisms in African trypanosomiasis. *PLoS Pathog.* **2015**, *11*, e1004942. [CrossRef]
82. Ahsan, F.; Rivas, I.P.; Khan, M.A.; Torres Suarez, A.I. Targeting to macrophages: Role of physicochemical properties of particulate carriers—Liposomes and microspheres—On the phagocytosis by macrophages. *J. Control. Release* **2002**, *79*, 29–40. [CrossRef]
83. Gradoni, L.; López-Vélez, R.; Mokni, M. *Manual on Case Management and Surveillance of the Leishmaniases in the WHO European Region*; World Health Organization: Geneva, Switzerland, 2017.
84. Andreana, I.; Bincoletto, V.; Milla, P.; Dosio, F.; Stella, B.; Arpicco, S. Nanotechnological approaches for pentamidine delivery. *Drug Deliv. Transl. Res.* **2022**, *12*, 1911–1927. [CrossRef]

85. Awad, W.B.; Asaad, A.; Al-Yasein, N.; Najjar, R. Effectiveness and tolerability of intravenous pentamidine for *Pneumocystis carinii* pneumonia prophylaxis in adult hematopoietic stem cell transplant patients: A retrospective study. *BMC Infect. Dis.* **2020**, *20*, 400. [CrossRef] [PubMed]
86. Abbadi, A.; Loftis, J.; Wang, A.; Yu, M.; Wang, Y.; Shakya, S.; Li, X.; Maytin, E.; Hascall, V. Heparin inhibits proinflammatory and promotes anti-inflammatory macrophage polarization under hyperglycemic stress. *J. Biol. Chem.* **2020**, *295*, 4849–4857. [CrossRef] [PubMed]

Supplementary Materials

In Vitro Evaluation of Aerosol Therapy with Pentamidine-loaded Liposomes Coated with Chondroitin Sulfate or Heparin for the Treatment of Leishmaniasis

Lucía Román-Álamo, Mohamad Allaw, Yunuen Avalos-Padilla, Maria Letizia Manca, Maria Manconi, Federica Fulgheri, Jorge Fernández-Lajo, Luis Rivas, José Antonio Vázquez, José Esteban Peris, Xavier Roca-Geronès, Srisupaph Poonlaphdecha, Maria Magdalena Alcover, Roser Fisa, Cristina Riera, and Xavier Fernàndez-Busquets

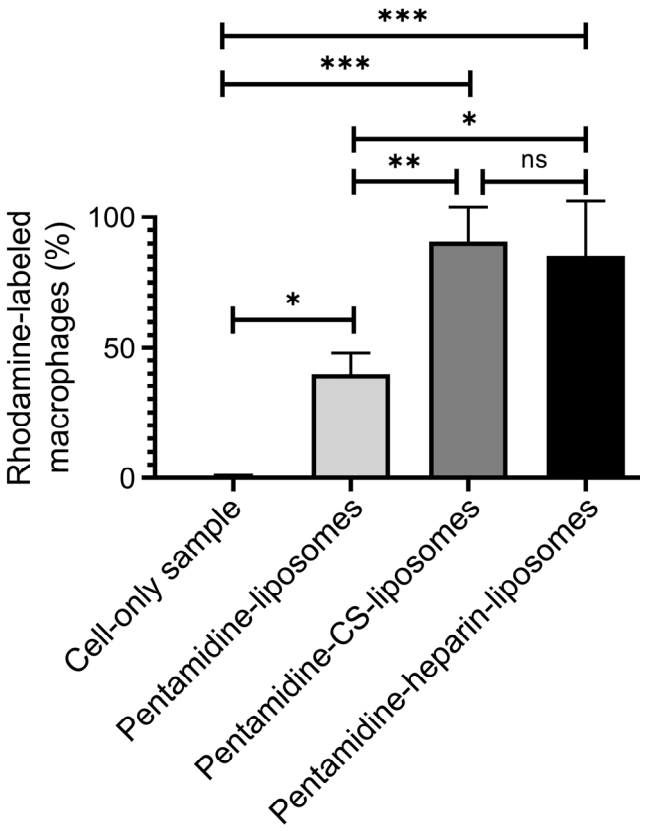

Supplementary Figure S1. One-way analysis of variance to determine statistically significant differences between the different samples of the flow cytometry data in Figure 5. *: $p \leq 0.05$; **: $p \leq 0.01$; ***: $p \leq 0.001$ (relative to the control cell-only sample).

Supplementary Table S1. Comparison of the IC_{50} of pentamidine in *L. infantum* amastigotes calculated with the microscopy and fluorescence methods.

	Pentamidine IC_{50} in *L. infantum* amastigotes (μM)	
	Microscopy method	Fluorescence method
Pentamidine solution	5.6 ± 1.4	3.5 ± 0.9
Pentamidine-liposomes	4.7 ± 2.9	2.6 ± 0.4
Pentamidine-CS-liposomes	3.1 ± 0.6	2.5 ± 0.4
Pentamidine-heparin-liposomes	4.1 ± 0.7	3.3 ± 0.8

Article 2: Effect of the aggregated protein dye YAT2150 on *Leishmania* parasite viability

Authors: Lucía Román-Álamo, Yunuen Avalos-Padilla, Inés Bouzón-Arnáiz, Valentín Iglesias, Jorge Fernández-Lajo, Juan M Monteiro, Luis Rivas, Roser Fisa, Cristina Riera, David Andreu, Carlos Pintado-Grima, Salvador Ventura, Elsa M Arce, Diego Muñoz-Torrero, Xavier Fernàndez-Busquets

Journal: *Antimicrobial agents and chemotherapy*

Publication date: 13th February 2024

DOI: https://doi.org/10.1128/aac.01127-23

Journal Impact factor: 4.1

General summary: The study titled "Effect of the Aggregated Protein Dye YAT2150 on Leishmania Parasite Viability," published in *Antimicrobial Agents and Chemotherapy*, investigates the potential of YAT2150, for treating leishmaniasis. YAT2150 was found to be highly effective against *Leishmania* parasites *in vitro*. The compound mechanism, believed to involve inhibiting protein aggregation within *Leishmania* cells, mirrors its action against the malaria-causing *Plasmodium* parasite. This dual efficacy positions YAT2150 as a promising candidate for addressing co-infections of malaria and leishmaniasis, both major causes of parasitic mortality. The encapsulation of YAT2150 within liposomes enhances its selectivity index and allows targeted delivery through the conjugation of the antibody anti-LPG. The next phase of research involves testing YAT2150 in mouse models of leishmaniasis and malaria co-infection to validate its efficacy and safety *in vivo*. Success in these trials could lead to the development of an innovative, dual-purpose treatment for both malaria and leishmaniasis, addressing a critical need in global health.

AMERICAN SOCIETY FOR MICROBIOLOGY | Antimicrobial Agents and Chemotherapy

Effect of the aggregated protein dye YAT2150 on *Leishmania* parasite viability

Lucía Román-Álamo,[1,2,3] Yunuen Avalos-Padilla,[1,2] Inés Bouzón-Arnáiz,[1,2] Valentín Iglesias,[1,2,4] Jorge Fernández-Lajo,[5] Juan M. Monteiro,[5] Luis Rivas,[5] Roser Fisa,[6] Cristina Riera,[6] David Andreu,[7] Carlos Pintado-Grima,[4] Salvador Ventura,[4] Elsa M. Arce,[8] Diego Muñoz-Torrero,[8] Xavier Fernàndez-Busquets[1,2,9]

AUTHOR AFFILIATIONS See affiliation list on p. 23.

ABSTRACT The problems associated with the drugs currently used to treat leishmaniasis, including resistance, toxicity, and the high cost of some formulations, call for the urgent identification of new therapeutic agents with novel modes of action. The aggregated protein dye YAT2150 has been found to be a potent antileishmanial compound, with a half-maximal inhibitory concentration (IC_{50}) of approximately 0.5 µM against promastigote and amastigote stages of *Leishmania infantum*. The encapsulation in liposomes of YAT2150 significantly improved its *in vitro* IC_{50} to 0.37 and 0.19 µM in promastigotes and amastigotes, respectively, and increased the half-maximal cytotoxic concentration in human umbilical vein endothelial cells to >50 µM. YAT2150 became strongly fluorescent when binding intracellular protein deposits in *Leishmania* cells. This fluorescence pattern aligns with the proposed mode of action of this drug in the malaria parasite *Plasmodium falciparum*, the inhibition of protein aggregation. In *Leishmania major*, YAT2150 rapidly reduced ATP levels, suggesting an alternative antileishmanial mechanism. To the best of our knowledge, this first-in-class compound is the only one described so far having significant activity against both *Plasmodium* and *Leishmania*, thus being a potential drug for the treatment of co-infections of both parasites.

KEYWORDS antileishmanial drugs, *Leishmania*, protein aggregation, YAT2150

Leishmaniasis is a neglected tropical disease caused by protozoan parasites of the *Leishmania* genus, of which more than 20 species can infect humans and other mammals (1). The parasite is transmitted to people through the bite of phlebotomine sandflies, where it is found as extracellular promastigotes, which are eventually phagocytized by macrophages, where they transform into the intracellular amastigote form. Depending on the infecting species and the host immune response, three main clinical manifestations of the disease arise: cutaneous leishmaniasis (CL), mucocutaneous leishmaniasis, and visceral leishmaniasis (VL). Visceral clinical manifestation is the most severe form of the disease and has a ca. 95% mortality rate if untreated. Estimates indicate a global annual incidence of 0.9 to 1.6 million cases of CL and around 90,000 of VL, most of them affecting low-income countries (2). In the European and African Mediterranean regions, *Leishmania infantum* and *Leishmania major* are, respectively, the main species causing a pathological condition. Current treatments for leishmaniasis vary depending on the clinical form but face several challenges, including drug resistance, toxicity concerns, administration as painful injections into the lesions, parenteral delivery, and the high cost of certain formulations (3). The lack of optimal treatment options has prompted the World Health Organization to prioritize the search for new therapeutic targets and drugs as critical for leishmaniasis eradication efforts (4).

Protein misfolding and aggregation are regarded as the molecular bases for numerous human pathologies, ranging from neurodegenerative diseases to cancer and

Editor Audrey Odom John, The Children's Hospital of Philadelphia, Philadelphia, Pennsylvania, USA

Address correspondence to Xavier Fernàndez-Busquets, xfernandez_busquets@ub.edu.

A patent application (priority number: EP21382949.2; application number: PCT/EP2022/079438; application date: 21/10/2022) has been filed to protect some of the results presented in the paper, which includes as inventors IB-A, EMA, DM-T and XF-B. All other authors declare they have no competing interests.

See the funding table on p. 24.

Received 1 September 2023
Accepted 15 January 2024
Published 13 February 2024

type II diabetes (5). In these cases, toxicity arises from either the absence of properly functioning polypeptides or the formation of cytotoxic oligomers and/or fibrils. On the bright side, protein aggregation serves functional purposes in various organisms, e.g., as a rapid mechanism to respond to environmental challenges through stress granule formation (6) or uncovering genetic diversity needed in starvation (7), to facilitate the controlled release of peptidic hormones in secretory granules in a pH-dependent manner (8), or to promote synapse-specific changes that strengthen dendritic spines and contribute to memory consolidation (9). Recently, we described that in the human malaria parasite *Plasmodium falciparum*, protein aggregation presumably plays a functional role and that its inhibition is detrimental to the pathogen (10, 11). Motivated by these findings, we have explored in the current work the therapeutic potential of inhibiting protein aggregation for other parasitic diseases. We evaluated the effect of the aggregated protein dye YAT2150, a potent antiplasmodial drug with a half-maximal inhibitory concentration (IC_{50}) of ca. 90 nM in *in vitro P. falciparum* cultures (11), on the viability of *L. infantum* promastigotes and amastigotes. Malaria and leishmaniasis are the first and second parasitic diseases, respectively, in number of deaths (12), in many cases with overlapping distribution, although the clinical study of co-infection with both pathogens has been mostly neglected (13). A good antileishmanial activity of YAT2150 could postulate it as a drug of choice for the treatment of malaria and leishmaniasis co-infections.

RESULTS AND DISCUSSION

Detection of protein aggregation in live *L. infantum* cells

Previous studies demonstrated the effectiveness of the red fluorescent dye ProteoStat to detect intracellular protein aggregates in live cells of the malaria parasite *P. falciparum* (10). However, a straightforward extrapolation of such analysis into *Leishmania* faces stark contrast to the theoretical predictions made for these two protozoa. Aggregation-prone proteomes usually result from genomes with a high proportion of AT bases, which in *P. falciparum* is 80.6% (14), while approximately 37.5% in *L. major* and *L. infantum* (15). Moreover, low-complexity regions, known to promote protein aggregation, constitute 12.2% of the entire genome in the *Leishmania donovani* complex (*L. donovani* and *L. infantum*) (16), while in *P. falciparum*, they represent *ca*. 49% of it (17). Finally, the predicted content in the *L. infantum* proteome of prion-like proteins (directly correlated with aggregation propensity) is merely 0.95% according to the PLAAC algorithm (18), significantly lower than for *P. falciparum* (9.40%) (19). Despite these differences, live *L. infantum* promastigotes and axenic amastigotes were strongly stained with ProteoStat (Fig. 1). The Manders' correlation coefficient with the DNA dye Hoechst 33342 indicated a preferentially non-nuclear localization of the ProteoStat signal. These findings from *in vitro* cultures evidenced protein aggregation as a prevalent phenomenon in *L. infantum*.

Identification of aggregation-prone proteins in *L. infantum* promastigotes

To confirm that the observed ProteoStat staining reflected the presence of intracellular protein aggregates, we proceeded to identify aggregation-prone proteins present in live parasites. With that aim, a homogenate from *L. infantum* promastigotes resisting dissolution in the presence of 0.1% sodium dodecyl sulfate (SDS) was loaded in a polyacrylamide gel electrophoresis (PAGE), and the Coomassie Blue-stained material not entering the separating gel was excised and subjected to liquid chromatography with tandem mass spectrometry analysis (LC-MS/MS) (Fig. 2A and B). A total of 132 *L. infantum* proteins were identified (Table S1), which included a number of membrane proteins that in live cells are protected from aggregation as their hydrophobic stretches are mostly found inside a lipid bilayer. Therefore, proteins annotated as membrane or transmembrane in the UniProt database (20) were removed (Table S1, shadowed in gray), obtaining a group of 92 proteins (Table S1, non-shadowed), whose propensity to aggregate, as expected, was significantly higher than that of the rest of the *Leishmania* proteome (Fig. 2C).

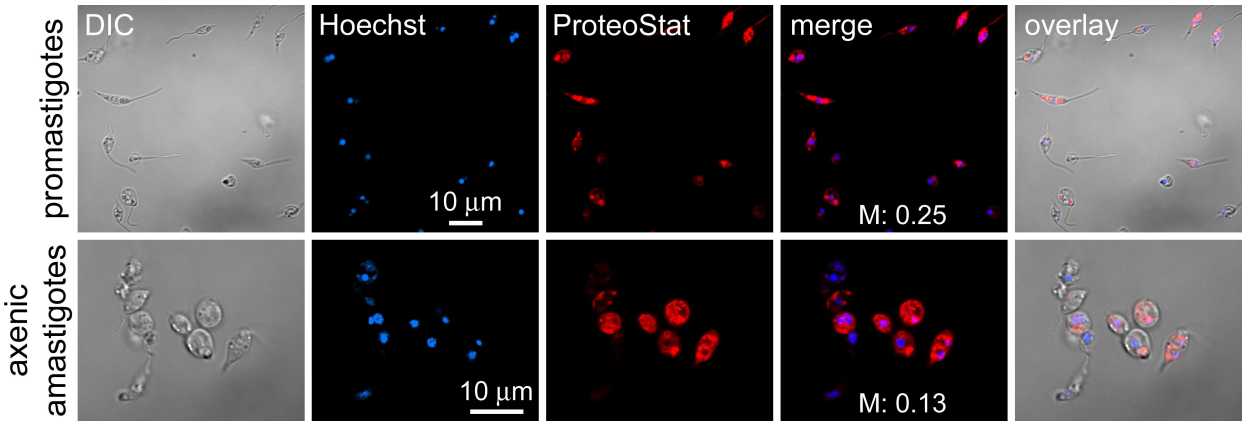

FIG 1 Detection of intracellular protein aggregates in live *L. infantum* promastigotes and axenic amastigotes by confocal fluorescence microscopy using ProteoStat. M, Manders' correlation coefficients indicating the fraction of ProteoStat co-localized with Hoechst 33342; DIC, differential interference contrast image.

To functionally characterize the non-membrane proteins found in 0.1% SDS-resistant aggregates, a Gene Ontology (GO) enrichment analysis was performed (22). The enriched categories (Fig. 2D and Table S2) were mainly related to translation, with the ribosome, small ribosomal subunit and nucleosome as main cellular components, and protein heterodimerization activity, rRNA binding, and structural constituent of ribosome as some of the most represented molecular functions. Ribosomal activity is of singular importance in *Leishmania* since the absence of a regulated transcription by RNA polymerase II leaves the control of gene expression at the translational level (23). Ribosomal proteins often have a high cytoplasmic abundance in concentrations above their solubility limit, existing in a metastable state protected from aggregation by kinetic barriers and assisted by chaperones (24). It is conceivable that changing conditions such as the concentration of molecular components or the disruption of ribosomal complex assembly provoked by internal or external stresses, like changes in temperature, pH, or the presence of drugs, can affect the aggregation state of ribosomal proteins, thereby influencing parasite viability. Several studies have demonstrated a lack of correlation between protein abundance and mRNA levels in certain *Leishmania* species, as regulation predominantly occurs through post-transcriptional and post-translational mechanisms (25). Given this context, it is tempting to speculate that the parasite modulates the abundance of its ribosomal components, to either facilitate or impede their aggregation according to specific physiological requirements.

In vitro characterization of the aggregation of peptides selected from the live *L. infantum* aggregation-prone protein pool

Protein aggregation relies heavily on substantial sequential homology, and even minor mutations influence aggregation reactions (26). As the initial amyloid nucleation step can be expedited when preformed fibrils of the same protein or shorter variants containing the amyloid driver are present (27), highly amyloidogenic peptides found in *L. infantum* proteins with high aggregation propensity may exacerbate protein aggregation in the pathogen. To identify these peptides, proteins resistant to dissolution in 0.1% SDS were analyzed by machine-learning techniques for modeling protein tertiary structure (28) to discern peptides exposed to the solvent in their native state. Two peptides were selected, DNFIFGQ from the β chain of tubulin, a major microtubule component, and AISVFFLEP from the cleavage and polyadenylation specificity factor (CPSF)-like protein, involved in mRNA processing. Notably, both sequences exhibited high amyloidogenic propensity based on the amyloid prediction method WALTZ (29) (Table 1) and solvent exposure according to the AlphaFold structural model (30) (Fig. S1).

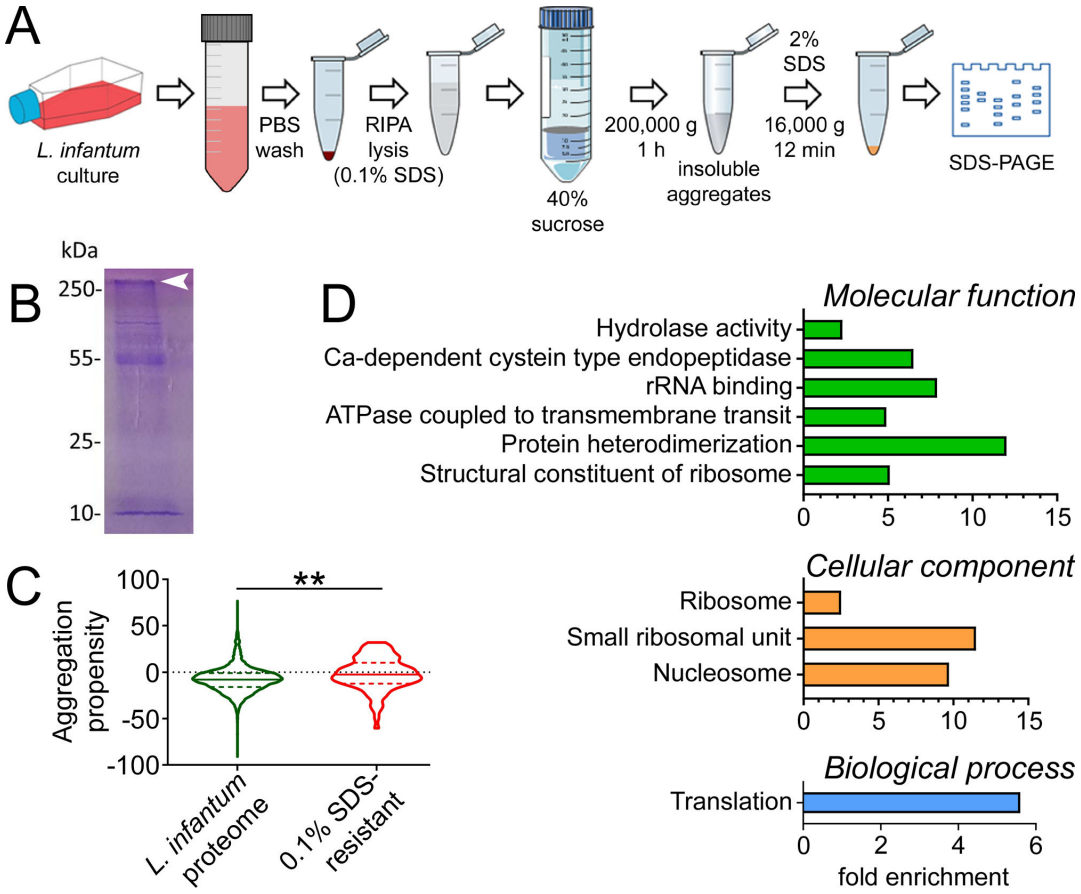

FIG 2 Isolation of *L. infantum* proteins insoluble in 0.1% SDS. (A) Scheme of the process. (B) Coomassie Blue-stained SDS-PAGE fractionation of the 0.1% SDS-resistant sample. The arrowhead indicates the excised region subjected to LC-MS/MS analysis. (C) Aggregation propensity [Aggrescan score (21)] of the *L. infantum* proteins resisting solubilization in 0.1% SDS (excluding membrane proteins) vs. the proteome of the parasite. $^{**}P < 0.005$. (D) GO enrichment analysis of the 92 non-membrane *L. infantum* proteins identified in 0.1% SDS-resistant aggregates, classified according to biological process, cellular component, and molecular function.

The *in vitro* aggregation of peptides DNFIFGQ and AISVFFLEP was confirmed by transmission electron microscopy (TEM) imaging and analysis of thioflavin T (ThT) fluorescence emission, an indicator of amyloid-like aggregation (31) (Fig. 3). Stretches of five or more continuous amino acids from the sequences of both peptides, especially for AISVFFLEP, are found in other *L. infantum* proteins (Table S3), which could contribute to boost their potential aggregative properties in live cells. Nevertheless, treatment for 72 h of *L. infantum* promastigotes with up to 100 µM of either peptide did not significantly affect the viability of this form of the parasite (2% and 0% growth inhibition in the presence of 100 µM DNFIFGQ and AISVFFLEP, respectively), despite both peptides bound and entered promastigotes according to flow cytometry and confocal fluorescence microscopy analysis (Fig. S2). Previous studies have succeeded with targeted aggregation in live plant cells by inducing the endogenous expression of aggregation-prone peptides, obtaining a visible specific phenotype (27). However, similar attempts failed to induce toxicity in *P. falciparum* (11) or human cell lines (32), likely by the difficulty

TABLE 1 Amyloidogenic peptides selected from the aggregation-prone *L. infantum* protein pool non-solubilized by 0.1% SDS

Protein (UniProt accession)	Peptide sequence	WALTZ score
Tubulin β chain (A0A381MS01)	$_{88}$DNFIFGQ$_{94}$	91.97
CPSF (A4I7V5)	$_{663}$AISVFFLEP$_{671}$	94.46

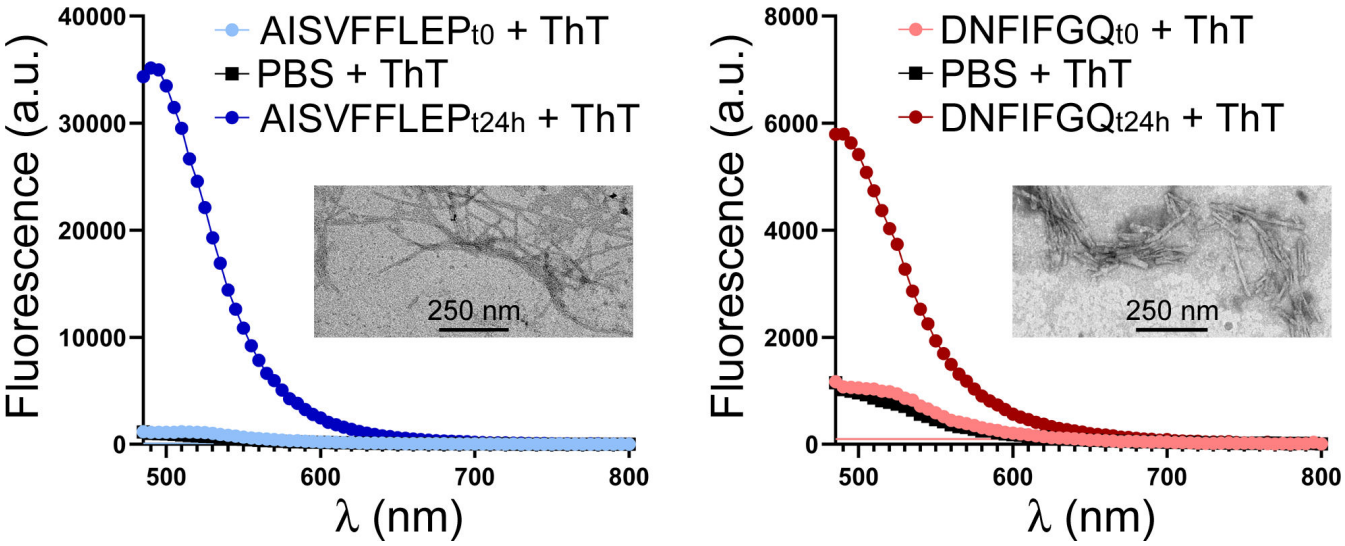

FIG 3 Characterization of the *in vitro* aggregation of peptides AISVFFLEP and DNFIFGQ. Representative TEM images (insets) and ThT fluorescence analyses are shown for 25 µM and 180 µM concentrations of both peptides, respectively. a.u., arbitrary units.

of attaining a critical concentration of seeds necessary to sustain intracellular aggregation of the desired protein, discouraging this approach as a therapeutic alternative in *Leishmania*.

Effect of protein aggregation inhibitors in *L. infantum* cultures

The detection in live *L. infantum* of protein aggregates and the identification in the parasite of proteins containing amyloidogenic peptides mirrored similar phenomena recently observed in *P. falciparum* (10). In the latter pathogen, low concentrations (<100 nM) of certain β-sheet intercalators, which lowered the *in vitro* aggregation of amyloid peptides (33), clearly inhibited its growth (11). When testing the effect on *L. infantum* of some of these small molecules known to interfere with protein aggregation (Fig. 4), they significantly reduced the parasite's viability (Table 2; Fig. S3). One of these compounds, YAT2150, stood out with an *in vitro* IC_{50} of around 0.52 µM against both promastigotes and amastigotes, which was ca. 54-, 20-, and 542-fold lower than that reported in promastigotes for the commonly used antileishmanial agents pentamidine

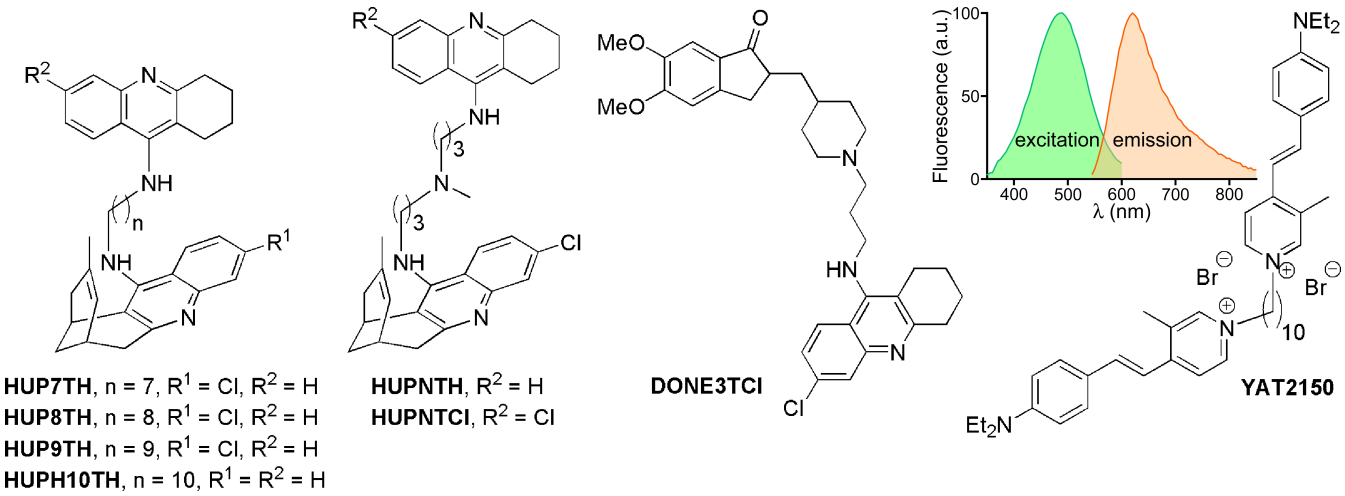

FIG 4 Chemical structures of different compounds which interfere with protein aggregation (33) and inhibit the growth of *P. falciparum* (11). The inset shows the fluorescence excitation/emission spectrum of YAT2150.

TABLE 2 Effect of the compounds from Fig. 4 on the viability of *L. infantum* promastigotes and amastigotes

	IC_{50} promastigotes (μM)	IC_{50} amastigotes (μM)	CC_{50}[a] (μM)	Selectivity index[b] (CC_{50}/IC_{50})
YAT2150	0.52 ± 0.07	0.51 ± 0.11	3.4 ± 0.5	6.6
DONE3TCl	2.09 ± 0.40	0.62 ± 0.08[c]	12.6 ± 2.2	6.0
HUPNTCl	2.03 ± 0.19	1.04 ± 0.21[c]	6.3 ± 0.5	3.1
HUPNTH	2.37 ± 1.40	1.52 ± 0.66[c]	3.4 ± 1.0	1.4
HUP7TH	1.23 ± 0.42	0.92 ± 0.38[c]	7.8 ± 3.4	6.4
HUP8TH	0.99 ± 0.47	1.63 ± 0.34[c]	4.9 ± 1.3	4.9
HUP9TH	0.88 ± 0.29	0.57 ± 0.13[c]	4.9 ± 1.0	5.6
HUPH10TH	0.72 ± 0.11	0.97 ± 0.21[c]	3.4 ± 0.1	4.7

[a]Cytotoxicity assayed in human umbilical vein endothelial cells.
[b]For promastigotes.
[c]$n = 2$.

(34), miltefosine (35), and paromomycin (36), respectively. Amphotericin B has a lower IC_{50} (0.04 μM in promastigotes) (37), but frequently associated nephrotoxicity has limited its clinical use, a drawback absent in its liposomal formulations (38). The half-maximal cytotoxic concentration (CC_{50}) of YAT2150 for human umbilical vein endothelial cells was 3.4 ± 0.5 μM, which resulted in a modest selectivity index (SI: CC_{50}/IC_{50}) of approximately 7.

Leishmania differentiation from promastigotes to amastigotes is induced by acid pH and high temperature (39, 40), two factors which increase protein aggregation (41, 42). The antileishmanial effect of certain peptide aggregation inhibitors on amastigotes might be related to the upsetting of some essential differentiation mechanism in the parasite. In agreement with its proposed activity as a protein aggregation inhibitor in *P. falciparum* (11), at physiologically relevant concentrations below its *in vitro* IC_{50}, YAT2150 reduced in *L. infantum* promastigote cultures the overall aggregation of the parasite's proteins according to ThT analysis (Fig. 5). This result suggested that one of the antileishmanial mechanisms of action of this compound might be related to interfering with the aggregative state of certain proteins in the pathogen. The possibility that such interference hampers particular protein-protein interactions, which might be part of, e.g., essential transcription factor networks whose disruption would compromise parasite viability, remains to be explored in detail.

Physical and pharmacological properties and early safety profiling of YAT2150

To explore the potential of YAT2150 to become a therapeutic agent, its druglikeness has been addressed through a preliminary assessment of physical and drug metabolism and pharmacokinetics (DMPK) properties and of its tolerability (Table 3). The solubility of YAT2150, measured at 37°C in phosphate-buffered saline (PBS) containing 1% dimethyl sulfoxide (DMSO), was found to be 8.5 μM, which indicated a favorable aqueous solubility at a concentration of up to 16-fold higher than its IC_{50}. YAT2150 is moderately lipophilic, with a calculated logP below 5 (clogP = 3.37), i.e., compliant with Lipinski's rule of five (43). Some pharmacokinetic parameters related to intestinal absorption and metabolism were also determined. The intestinal absorption of YAT2150 was assessed using the Caco-2 permeability assay, commonly used to predict the *in vivo* absorption of drugs. The transport across a Caco-2 cell monolayer was determined in both directions, so that not only absorption but also active efflux could be determined. These assays demonstrated a high absorption (>200 nm/s) and moderate efflux (ca. 100 nm/s) for YAT2150, resulting in a favorable efflux ratio of 0.48. The metabolic stability of YAT2150 was determined in human plasma, human microsomes, and human hepatocytes. When incubated at 37°C with human plasma from healthy donors, YAT2150 was perfectly stable after 2 h and 91% of the compound still remained unchanged after 6 h of

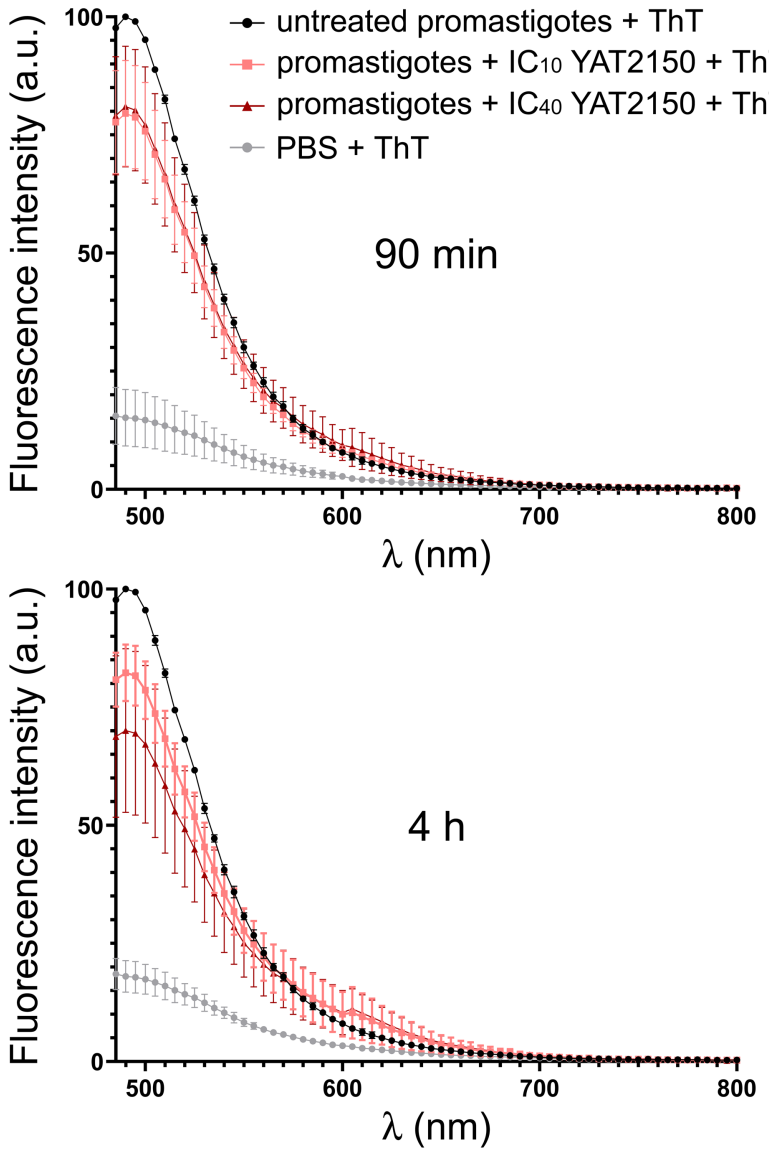

FIG 5 Thioflavin T (ThT) fluorescence of *L. infantum* culture extracts adjusted to have equal protein content, either non-treated or treated with YAT2150 at its *in vitro* IC_{10} (0.15 µM) and IC_{40} (0.3 µM), for 90 min and 4 h ($n = 3$). The arbitrary units (a.u.) of fluorescence intensity are normalized relative to a value of 100 assigned to the untreated promastigotes + ThT sample. Error bars indicate standard deviation.

incubation. YAT2150 showed also a good stability in human microsomes: 55% of the compound remained unchanged after 1 h of incubation at 37°C, displaying a half-life of 80 min and a microsomal intrinsic clearance (CLint) of 10.6 µL/min/mg protein, i.e., below 15 µL/min/mg protein, thereby behaving as a low clearance compound (44). The stability of YAT2150 in human hepatocytes was still higher, with 70% of it remaining unchanged after 2 h of incubation at 37°C, a longer half-life of 277 min and a low intrinsic clearance (2.5 µL/min/10^6 cells). Overall, YAT2150 has quite favorable metabolic stability and should not be eliminated too fast from the organism. With regard to the safety profile, apart from its moderate selectivity index relative to human umbilical vein endothelial cells, the inhibitory effects of YAT2150 on some cytochrome P450 (CYP) isoforms commonly involved in drug metabolism were evaluated. At 10 µM, i.e., a 20-fold higher concentration than its IC_{50} against *L. infantum* promastigotes, YAT2150 inhibited CYP1A2 and CYP2C9 by around 50%, while the inhibition of CYP2C19 and CYP2D6 was two- and threefold less potent, respectively, than its antileishmanial effect. Despite the overall

TABLE 3 DMPK and early safety properties of YAT2150

Physicochemical properties			
Molecular mass	832.85 Da		
Aqueous solubility[a]	8.5 µM		
Lipophilicity (clogP)[b]	3.37		
Pharmacokinetic parameters			
	Intestinal absorption		
	Papp AB (nm/s)	Papp BA (nm/s)	Efflux ratio
Caco-2 permeability[c]	207.6 ± 20.1	100.6 ± 0.4	0.48
	Metabolic stability		
	% remaining[d]	$t_{1/2}$ (min)[e]	CLint[f]
Plasma stability[g]	100.0% after 1 h		
	99.7% after 2 h		
	91.3% after 6 h		
Microsomal stability[g]	54.6% after 1 h	80.5	10.6 µL/min/mg protein
Hepatocyte stability[g]	70.4% after 2 h	277.3	2.5 µL/min/10^6 cells
Safety profiling (CYP inhibition)[h]			
CYP1A2	55% ± 1% inhibition at 10 µM		
CYP2C9	51% ± 4% inhibition at 10 µM		
CYP2C19	IC_{50} = 1.1 µM		
CYP2D6	IC_{50} = 1.7 µM		

[a]Kinetic solubility at 37°C in PBS containing 1% DMSO.
[b]Calculated using Molinspiration.
[c]Transport of compound from A→B (AB) and B→A (BA) in Caco-2 cells incubated at 37°C; apparent permeability (Papp) values in nm/s; efflux ratio = Papp BA/Papp AB.
[d]Percentage unchanged compound after a given incubation time.
[e]Half-life in min.
[f]Intrinsic clearance.
[g]Stability of the compound in human plasma, human microsomes, or human hepatocytes at 37°C.
[h]Inhibition potential of YAT2150 using human recombinant cytochrome P450 enzymes at 37°C.

good DMPK profile, the eventual future pharmacological development of YAT2150 will probably require its optimization through the synthesis of improved derivatives (45), in a similar way as it has been reported for, e.g., DNDI-6148, a preclinical candidate for the treatment of VL (46).

Effect of YAT2150 on *L. major* ATP levels

Due to the experimental availability of promastigotes of a strain of *L. major* (a species associated with cutaneous leishmaniasis) used as a real-time *in vivo* sensor for variation of intracellular ATP levels (47), we tested energy metabolism as a potential target for YAT2150. The extrapolation of the results of this approach to *L. infantum* relies on the relative promiscuity of the interactions underlying the protein aggregation phenomenon and the high homology between *L. infantum* and *L. major* proteomes. A comparative UniProt BLAST analysis between both species of the proteins in Table S1 showed amino acid sequence homology exceeding 90% for most of them, with only 7 out of 132 proteins below 80%.

For the determination of ATP levels, promastigotes expressing a cytoplasmic form of firefly luciferase were used, and, to overcome the poor membrane permeability of luciferin, the membrane-permeable derivative 1-(4,5-dimethoxy-2-nitrophenyl)ethyl ester (DMNPE)-luciferin was employed. Under these conditions, ATP is the limiting substrate for the luminescence reaction in living parasites. Upon exposure to YAT2150, a concentration-dependent reduction in luminescence was observed for concentrations beyond 2 µM (Fig. 6). The disparity between this threshold concentration for YAT2150 and its IC_{50} may likely obey to the higher density of promastigotes required in the ATP experiment, as, presumably, YAT2150 operates via a stoichiometric mechanism to disrupt or prevent the formation of aggregated structures. Furthermore, a rapid response was sought to ensure that the decline in ATP levels represented a primary target rather

than a consequence of overall microorganism deterioration. Currently, it remains unclear whether the decrease of protein aggregation and the drop in ATP are interconnected or independent of each other. In the former hypothesis, it could be postulated that physiological aggregation serves as a protective mechanism against a potentially toxic protein fragment or peptide, which could disrupt the energy metabolism of *Leishmania*. In the latter scenario, the existence of an additional target for YAT2150 might complicate the rational design of new analogs, but, on the other side, it would also hamper the evolution of resistance against this molecule.

Fluorescence microscopy analysis of YAT2150 staining of *L. infantum*

As expected from being the main component of ProteoStat, the fluorescence of YAT2150 was strong in *L. infantum* promastigotes and axenic amastigotes (Fig. S4). YAT2150-stained promastigotes were observed in macrophages that had been incubated in their presence for 24 h (Fig. 7A). However, it could not be unequivocally determined whether these intracellular parasites were amastigotes, recently phagocytosed promastigotes, or intermediate forms. When macrophages exposed to *L. infantum* promastigotes that had been stained with carboxyfluorescein succinimidyl ester (CFSE) were treated for 6 h with YAT2150, sufficient to stain vesicular structures in the cytosol of macrophages, no YAT2150 signal could be observed in the phagolysosomes containing *Leishmania* (Fig. 7B). Although this result might indicate a potential lack of permeability of YAT2150 across phagolysosome membranes, it could also be due to a loss or significant reduction of intracellular protein aggregates in *Leishmania* parasites in phagolysosomes, in a similar way as it has been described in *P. falciparum* following its invasion of red blood cells (10, 11). The presence in *L. infantum* promastigotes of an aggregated protein coat might be a protective barrier for the parasite in the hostile extracellular environment, not required anymore inside the phagolysosome. Another possible function of an aggregated protein structure in promastigotes could be related to interactions with certain macrophage receptors required as part of the phagocytosis mechanism. Overall, YAT2150 might be staining dynamic protein associations that are required in promastigotes but not in intracellular amastigotes, where they would progressively disassemble. In agreement with this hypothesis, it has been established that the surface coat of amastigotes is notably less complex than that of promastigotes (48).

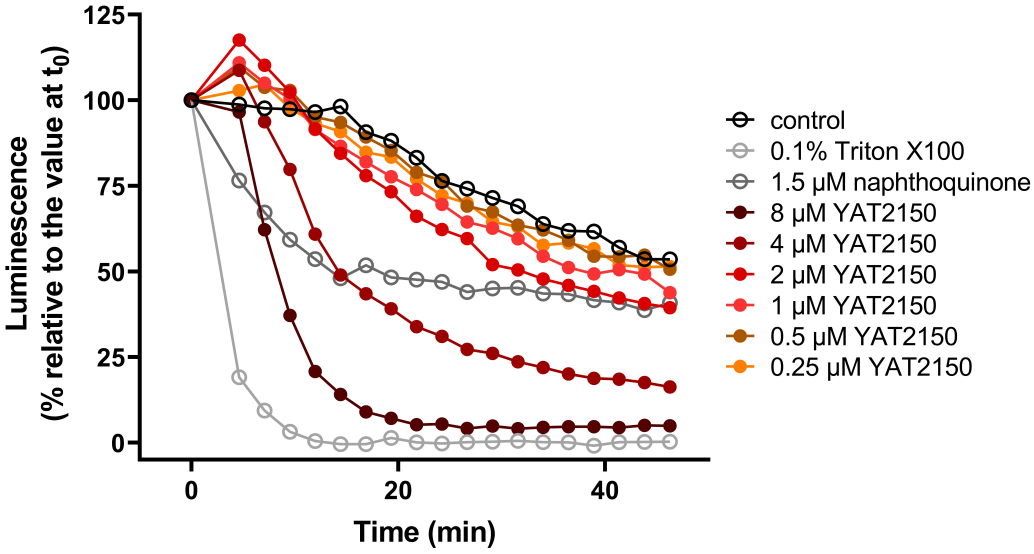

FIG 6 Luciferase assay for the assessment of free intracellular ATP levels in YAT2150-treated *L. major* promastigotes.

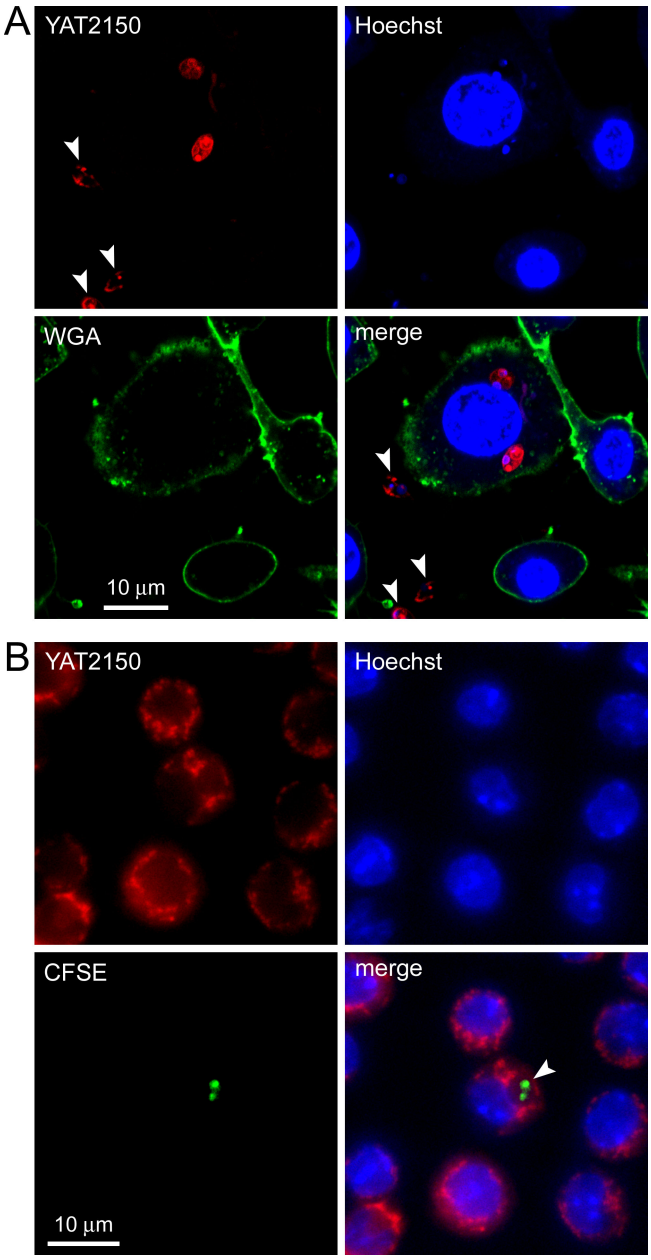

FIG 7 Fluorescence microscopy analysis of YAT2150 staining of *L. infantum* promastigote-exposed RAW 264.7 macrophages. (A) Confocal fluorescence microscopy images of live macrophages incubated for 24 h in the presence of *L. infantum* promastigotes that had been pre-stained for 1 h with 0.38 µM YAT2150. Cell membranes were stained with Oregon Green-conjugated wheat germ agglutinin (WGA). Arrowheads indicate promastigotes outside macrophages. (B) Fluorescence microscopy image of live macrophages exposed to CFSE-stained *L. infantum*. Nuclei were stained for 10 min with 2 µg/mL Hoechst 33342 and protein aggregates for 6 h with 0.38 µM YAT2150. The arrowhead indicates a *Leishmania*-containing phagolysosome.

In vitro activity on *L. infantum* growth of YAT2150 encapsulated in liposomes

In addition to the synthesis of chemical derivatives mentioned above, a second strategy commonly used to improve the selectivity index of drugs is their encapsulation in targeted nanocarriers. Here, to increase the therapeutic window of YAT2150, its incorporation into liposomes was assayed. Targeted delivery offers the potential of reducing drug cytotoxicity through encapsulation (which screens non-specific

interactions) and increasing antiparasitic potency through the local accumulation in or near *Leishmania* cells. Building upon our previous success in enhancing the activity of antimalarials through encapsulation in targeted immunoliposomes (49), a similar approach for YAT2150 was taken. This strategy benefits from the lipophilic properties of YAT2150 to undergo a preferential partition into the lipid bilayer of liposomes, as shown using giant unilamellar vesicles (GUVs) as a membrane model (Fig. 8).

Drug-encapsulating liposomes were prepared with an estimated final concentration of 60 µM YAT2150 (for 10 mM total lipid), corresponding to an encapsulation efficiency of 60%. YAT2150-loaded liposomes showed a growth inhibition activity against *L. infantum* amastigotes and promastigotes higher than that of the free drug (Table 4). As an attempt to increase specificity toward *Leishmania* cells, an antibody raised against lipophosphoglycan (LPG), the major parasite surface glycoconjugate which is present in large numbers in promastigotes and to a lesser extent in amastigote-containing macrophages (50) (Fig. S5), was conjugated to liposomes (Fig. S6). However, the incorporation of anti-LPG antibodies to liposomes did not improve drug activity in amastigotes and did it only marginally in promastigotes, suggesting that LPG might not be an adequate antigen for targeted drug delivery approaches against *Leishmania*. The unspecific cytotoxicity of liposome-encapsulated YAT2150 decreased to a CC_{50} > 50 µM, thus increasing the SI of this drug formulation to above 100. Encapsulation of YAT2150 might offer the additional benefit of minimizing its interaction with cell membranes, thus contributing to reduce its presumably high biodistribution, which would be an important issue regarding an eventual future pharmaceutical development.

As expected, confocal fluorescence microscopy analysis of live *L. infantum* cells treated with YAT2150 encapsulated in liposomes (Fig. S7) and anti-LPG immunoliposomes (Fig. 9) showed the drug's fluorescence associated to promastigotes (Fig. 9A) and in parasite-treated macrophages (Fig. 9B). However, in this case, YAT2150 fluorescence could be occasionally observed co-localizing with the parasite inside phagolysosomes (Fig. 9C), perhaps reflecting an improved entry facilitated by liposome encapsulation.

Conclusions

Treatment of *L. infantum* cultures with peptide aggregation inhibitors showed a significant *in vitro* antileishmanial effect. In particular, the compound YAT2150 had a better *in vitro* activity against *L. infantum* (IC_{50} of ca. 0.5 µM for both amastigote and promastigote forms) than some drugs currently used for the clinical treatment of leishmaniasis, such as miltefosine, pentamidine, and paromomycin. Encapsulation in liposomes of YAT2150 significantly improved the *in vitro* antileishmanial activity relative to the free drug and reduced its unspecific cytotoxicity, which led to a SI > 100 and therefore to good perspectives regarding preclinical assays of this compound or of its eventual future derivatives having less toxicity and/or higher antiparasitic activity. The antileishmanial mode of action of YAT2150 might be multipronged, with protein aggregation and ATP biosynthesis as potential cellular targets. The properties of YAT2150

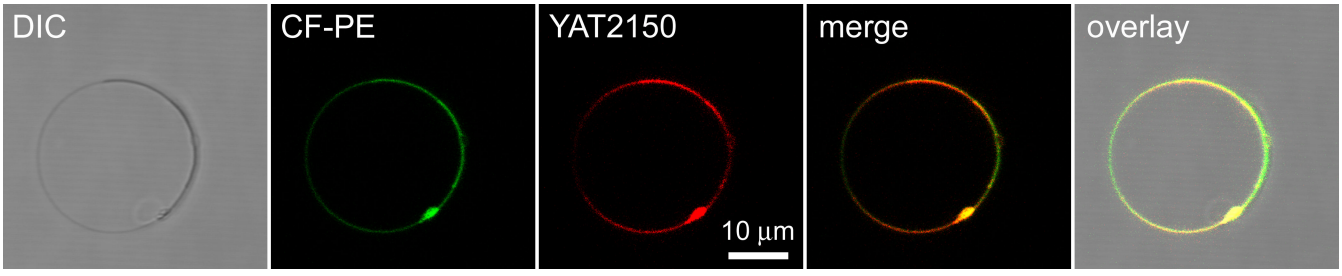

FIG 8 Confocal fluorescence microscopy analysis of the encapsulation of 2.5 µM YAT2150 in GUVs (10 mM total lipid concentration; see Materials and Methods for GUV lipid composition). To stain the lipid bilayer, the lipid carboxyfluorescein-phosphatidylethanolamine (CF-PE) was included in the GUV formulation. DIC, differential interference contrast image.

TABLE 4 Determination of diameter, polydispersity index, IC_{50} in *L. infantum* promastigotes and amastigotes, and CC_{50} of YAT2150 encapsulated in liposomes and in immunoliposomes functionalized with antibodies against LPG

	Diameter (nm)	Polydispersity index	IC_{50} promastigotes (μM)	IC_{50} amastigotes (μM)	CC_{50} (μM)	SI
YAT2150 in solution	–	–	0.52 ± 0.07	0.51 ± 0.11	3.4 ± 0.5	6.6
YAT2150-liposomes	154.7 ± 1.8	0.113 ± 0.025	0.37 ± 0.01[a]	0.19 ± 0.02[b]	>50	>100
YAT2150-immunoliposomes	155.3 ± 0.9	0.130 ± 0.009	0.34 ± 0.02[b]	0.35 ± 0.08	>50	>100

[a]$P < 0.05$.
[b]$P < 0.005$.

that postulate it as an excellent drug candidate against *Plasmodium* and *Leishmania* hold promise for its use in the treatment of co-infections of both pathogens.

MATERIALS AND METHODS

Reagents

Except where otherwise indicated, reagents were purchased from Sigma-Aldrich Corporation (St. Louis, MO, US), and reactions were performed at room temperature (22°C–24°C). The tested compounds were synthesized as previously described (11, 51–53).

Data acquisition and bioinformatics analysis

The reference *L. infantum* proteome (JPCM5, proteome ID UP000008153) was downloaded from UniProt [release 2022_01 (20)]. The subcellular location of *L. infantum* proteins was extracted from UniProt annotations and manually cured. Transmembrane annotated proteins were analyzed with DeepTMHMM v1.0.15, an improved version of TMHMM 2.0 [https://dtu.biolib.com/DeepTMHMM/ (54)], capable of identifying transmembrane beta-barrels. Propensity to protein aggregation was assessed using the Aggrescan prediction method (21), and the Normalized a4vSS for 100 residues (Na4vSS) was acquired as the aggregation reporter. Sequences over 6000 residues were divided into smaller fragments, and the Na4vSS for the whole ensemble was calculated. For the *L. infantum* full proteome, the mean aggregation propensity is displayed. The content in prion-like proteins was assessed with the PLAAC algorithm (18) using the whole proteome for each case as the background probability, and those proteins with at least one window with COREscore > 0 were considered prion-like. Structures for *L. infantum* tubulin β chain (A0A381MS01) and cleavage and polyadenylation specificity factor-like protein (A4I7V5) were obtained from the AlphaFold database (30) version 3 and colored with Pymol. Amyloid prediction was carried out with Waltz (29) in its default "best overall performance" mode. GO enrichment analysis was performed with the functional annotation tool of the Database for Annotation, Visualization and Integrated Discovery knowledge base update v2022q3 (22), where GO terms annotated directly by the source (GO_DIRECT category) were selected and the *L. infantum* JPCM5 data set was chosen as background.

Peptide synthesis

Acetyl-DNFIFGQ-amide and acetyl-AISVFFLEP-amide were synthesized at a 0.1-mmol scale on H-Rink amide-ChemMatrix resin (PCAS BioMatrix Inc., Saint-Jean-sur-Richelieu, QC, Canada) in a Prelude (Gyros Protein Technologies AB, Uppsala, Sweden) synthesizer running Fmoc solid-phase peptide synthesis (SPPS) protocols. After chain assembly, the N-terminus was deprotected and acetylated (acetic anhydride/*N*,*N*-diisopropylethylamine, 1 mmol each, 45 min, dimethylformamide), prior to full deprotection and cleavage with trifluoroacetic acid (TFA)/H_2O/triisopropyl-silane (95:2.5:2.5 vol/vol), 90 min, at room temperature. Peptides were precipitated from the TFA solution by the addition of cold diethyl ether followed by centrifugation (3 × 4800 rpm, 5 min, 4°C), taken up in water, and lyophilized. Crude peptides were checked by analytical reverse-phase high-performance liquid chromatography (RP-HPLC) and liquid chromatography-mass

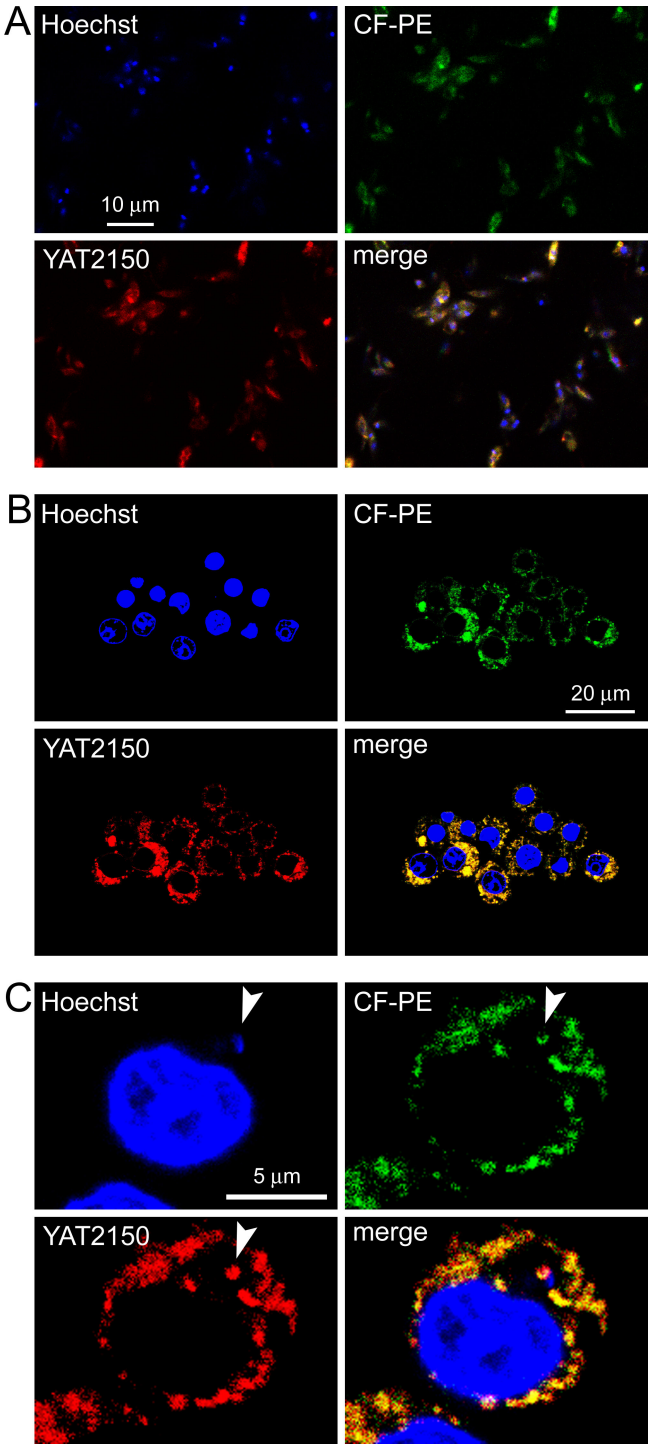

FIG 9 Confocal fluorescence microscopy analysis of the cell targeting of 0.38 µM YAT2150 encapsulated in fluorescein-labeled anti-LPG immunoliposomes. (A) Live *L. infantum* promastigotes were incubated for 1 h with immunoliposomes, stained for 20 min with 4 µg/mL Hoechst 33342 to reveal nuclei, and fixed with 3% paraformaldehyde. (B, C) RAW 264.7 macrophages that had been exposed to *L. infantum* promastigotes were incubated for 3 h with immunoliposomes, stained for 10 min with 2 µg/mL Hoechst 33342, and fixed. The green fluorescence corresponds to CF-PE incorporated in the liposome formulation. The arrowhead indicates a *Leishmania* amastigote inside its phagolysosome.

spectrometry (LC-MS) and purified by preparative RP-HPLC. Analytical RP-HPLC was performed on a LC-20AD instrument (Shimadzu Corporation, Kyoto, Japan) equipped with a Luna C18 column (3 µm, 4.6 mm × 50 mm; Phenomenex, Torrance, CA, US) using linear gradients of solvent B [0.036% TFA in acetonitrile (ACN)] into A (0.045% TFA in H_2O) over 15 min, at a flow rate of 1 mL/min and UV detection at 220 nm. Preparative RP-HPLC was performed on a LC-8 instrument (Shimadzu Corporation) fitted with a Luna C18 column (10 µm, 21.2 mm × 250 mm; Phenomenex), using linear gradients of solvent D (0.1% TFA in ACN) into C (0.1% TFA in H_2O) over 30 min, with a flow rate of 25 mL/min. MS analysis was performed on a LC-MS 2010EV instrument (Shimadzu Corporation) fitted with an XBridge C18 column (3.5 µm, 4.6 mm × 150 mm; Waters, Cerdanyola del Vallès, Spain), eluting with linear gradients of F [0.08% formic acid (FA) in ACN] into E (0.1% FA in H_2O) over 15 min at a 1-mL/min flow rate. Fractions with the expected mass and >95% purity by LC-MS were pooled and lyophilized. Peptide stock solutions were prepared in sterile deionized water and stored at −20°C. Fluorescent versions of the peptides were prepared by coupling 5(6)-carboxyfluorescein to the N-terminus of the peptide resins, as described for acetylation. The fluorescein(Flu)-labeled Flu-DNFIFGQ-amide and Flu-AISVFFLEP-amide were obtained after resin cleavage, preparative RP-HPLC purification, and LC-MS characterization as above.

In vitro peptide aggregation assays

To completely disaggregate the peptides before the assay, around 15 mg of each lyophilized peptide was dissolved in 1 mL of TFA. After thoroughly mixing, TFA was evaporated under a N_2 stream and 0.5 mL of 1,1,1,3,3,3-hexafluoro-2-propanol (HFIP) was added, mixed well, and evaporated as before (repeated twice to fully remove TFA). Then, 2 mL of HFIP was added, 40-nM peptide aliquots were prepared in low-binding Eppendorf tubes (Eppendorf, Hamburg, Germany), and HFIP was evaporated overnight in a desiccator. For aggregation assays, peptide stocks were prepared in PBS at a final concentration of 200 µM peptide and incubated at 37°C under stirring at 1,400 rpm in a ThermoMixer (Eppendorf) for 24 h (t_{24h}). Then, in a 96-well flat-bottom black plate (Greiner Bio-One, Frickenhausen, Germany), the peptide solutions were diluted in PBS and ThT was added to obtain final concentrations of 180 µM peptide and 25 µM ThT. The fluorescence emission of ThT was collected from 460 to 800 nm using an excitation wavelength of 450 nm (Infinite Nano+ multimode microplate reader; Tecan Trading AG, Männedorf, Switzerland). As a non-aggregation control, the ThT fluorescence of a freshly disaggregated 180 µM peptide solution (t_0) was measured.

Transmission electron microscopy

Peptides (25 µM) were incubated in PBS at 37°C for 24 h under orbital stirring at 300 rpm. After 5 min of water bath sonication (FB15053 ultrasonic bath; Thermo Fisher Scientific Inc., Waltham, MA, US), a 5-µL drop of the peptide solution was deposited onto a carbon-coated copper grid (Ted Pella, Redding, CA, US). Next, 5 µL of 2% uranyl acetate was added and left for 5 min before washing it away with H_2O. The resulting samples were observed with a JEM 1010 transmission electron microscope (JEOL Ltd., Tokyo, Japan). Images were acquired using an Orius 832 CCD camera (Gatan Inc., Pleasanton, CA, US).

Encapsulation of YAT2150 in liposomes

Liposomes were prepared by the thin lipid film hydration method (55). Briefly, the lipids 1,2-dioleoyl-*sn*-glycero-3-phosphocholine (DOPC):1,2-distearoyl-*sn*-glycero-3-phosphoethanolamine-*N*-[maleimide(polyethylene glycol)−2000] (DSPE-PEG-Mal):cholesterol (75:5:20 molar ratio) were mixed in chloroform:methanol (2:1 vol/vol) in a glass vial together with 100 µM YAT2150 from a YAT2150 stock solution in DMSO. Organic solvents were removed by evaporation under nitrogen. The thin lipid film formed on the vial walls was hydrated in PBS, in a volume corresponding to a final lipid concentration of 10 mM. Then, three rounds of constant vortexing for 2 min followed by bath

sonication at 35°C for 3 min (FB15053 ultrasonic bath) were performed. Liposomes were extruded through 200 nm polycarbonate membranes (Avanti Polar Lipids Inc., Alabaster, AL, US) using a mini extruder device (Avanti Polar Lipids Inc.). Non-encapsulated YAT2150 was removed by pelleting liposomes by ultracentrifugation (150,000 × *g*, 1 h, 4°C) and replacing the supernatant by PBS, except in the case of cytotoxicity assays, where the pellet was taken up in Medium 199 (M-199) supplemented with 1% penicillin-streptomycin. Fluorescein-labeled liposomes containing a molar ratio of 0.5% CF-PE were prepared as described above, except for a reduced DOPC content of 74.5%. The average diameter and polydispersity index of liposomes were measured after 1:100 sample dilution in PBS, using a Zetasizer NanoZS90 (Malvern Ltd., Malvern, UK). To determine the drug content, liposomes were disrupted by treatment with one volume of 4% SDS, and YAT2150 was quantified by absorbance spectroscopy at a wavelength of 490 nm (Epoch microplate spectrophotometer; BioTek Instruments Inc., Winooski, VT, US). Encapsulation efficiencies are defined as the fraction of YAT2150 in the liposome pool, after ultracentrifugation, relative to the initial amount of drug added to the liposomes. The amount of YAT2150 in the sample is expressed relative to the total lipid concentration of 10 mM, assuming that all the lipids end up in liposomes.

Immunoliposome preparation and characterization

Immunoliposomes were prepared by attaching the anti-lipophosphoglycan (LPG) monoclonal IgM antibody CA7AE (Bio-Rad, Hercules, CA, US) to the maleimide group of DSPE-PEG-Mal following established protocols (49). The *N*-succinimidyl *S*-acetylthioacetate crosslinker (SATA; Thermo Fisher Scientific Inc.) was first coupled to the antibody at a molar ratio of 1:10 (1 mg antibody/mL in 350 µL of PBS) through an incubation step of 30 min at room temperature. Non-reacted SATA was removed by buffer exchange. Thioester groups from SATA-anti-LPG antibody were deacetylated with 0.1 volumes of deacetylation solution (0.5 M hydroxylamine, 25 mM EDTA in PBS) and incubated for 2 h at room temperature. Then, another buffer exchange was performed with PBS containing 10 mM EDTA to remove the remaining deacetylation solution. To 100 µL (10 mM total lipid in PBS) of a suspension of liposomes exposing maleimide groups and carrying YAT2150, were added 55 µL of thiolated SATA-anti-LPG antibody and 45 µL of PBS supplemented with 10 mM EDTA. The resulting sample was incubated for 17 h at room temperature, when unbound SATA-anti-LPG antibody and YAT2150 were removed by ultracentrifugation (150,000 × *g*, 1 h, 4°C) and replaced with PBS containing 10 mM EDTA. The YAT2150 concentration in immunoliposomes was quantified as specified above.

The presence of anti-LPG antibody and YAT2150 in liposomes was assessed by SDS-PAGE. Ten microliters of each sample was mixed with 10 µL of 2× Laemmli sample buffer (0.125 M tris base, 4% SDS, 20% glycerol, 10% 2-mercaptoethanol, and 2 mg/mL bromophenol blue) and heated at 95°C for 5 min. Then, the samples were run in a 12% SDS-PAGE (Mini Protean II System; Bio-Rad), and the gel was stained with silver nitrate following the next steps: fixation (40% ethanol, 10% acetic acid) for 30 min, washing three times with deionized water (Milli-Q system; Millipore Corporation, Burlington, MA, US), staining for 40 min (1 mg/mL silver nitrate, 0.02% formaldehyde), and developing (25 mg/mL Na_2CO_3, 0.01% formaldehyde) until visualization of the protein bands, when 1% acetic acid was used to stop the reaction. Then, the YAT2150 fluorescent signal was detected in a LAS 4000 reader (ImageQuant TL; GE Healthcare, Chicago, IL, US) with the Cy3 filter, and an image of the protein bands was taken by white epi-digitalization.

Gel-assisted formation of giant unilamellar vesicles

GUVs were produced by the gel-assisted method with minor modifications (56). A 5% (wt/wt) polyvinyl alcohol (PVA, 145 kDa; Merck, Darmstadt, Germany) solution was prepared in PBS at 90°C and used to coat a microscope coverslip which was later dried for 30 min in an oven at 50°C. Then, 20 µL of the lipid formulation (10 mM total lipid) DOPC:cholesterol:CF-PE (79.5:20:0.5 molar ratio) was spread over the dried PVA. To evaporate the solvent, the glass slide was placed under vacuum for 30 min at room

temperature. Two coverslips and a Teflon spacer were assembled forming a chamber (2-mL volume) that was filled with PBS. One hour later, GUVs were harvested and YAT2150 was added at a final concentration of 2.5 µM. Fifteen microliters of the resulting GUV suspension was transferred to a 2% bovine serum albumin (BSA)-coated coverslip and observed with a Leica TCS SP5 laser scanning confocal fluorescence microscope (Leica Microsystems, Wetzlar, Germany). Fluorescein and YAT2150 were detected by excitation at 488 and 561 nm and emission collection in ranges 497–543 and 572–657 nm, respectively.

Cytotoxicity assays

Human umbilical vein endothelial cells were maintained in M-199 supplemented with 10% fetal bovine serum (FBS) and 1% penicillin-streptomycin at 37°C, 5% CO_2, and seeded in 96-well plates at a density of 50,000 cells/mL. After allowing cell adherence for 24 h, the medium was removed, and drugs or nanoformulations were added in M-199 supplemented with 1% penicillin-streptomycin. Plates were incubated for 48 h, and then, the medium in each well was replaced by 100 µL of M-199 containing penicillin-streptomycin and 0.00125% resazurin sodium salt (Sigma-Aldrich Corporation). Plates were incubated for 4 h, and resorufin fluorescence emission was measured (λex/em: 535/590 nm) in a Tecan Infinite 200 PRO equipment (Tecan Trading AG).

Solubility screen assay

The stock solutions (10^{-2} M) of the assayed compounds were diluted to decreased molarity, from 300 µM to 0.1 µM, in a 384-well transparent plate (Greiner Bio-One, Madrid, Spain) with DMSO:PBS (1:99 vol/vol). After 2 h of incubation at 37°C, the plate was read in a NEPHELOstar Plus nephelometer (BMG LABTECH GmbH, Ortenberg, Germany) at 635 nm. The results were adjusted to a segmented regression to obtain the maximum concentration at which the compounds were soluble.

Human plasma stability assay

Plates (96-well Polypropylene Deep Well Plate; Corning Inc., Somerville, MA, US) containing 100 µL of 5 µM compounds in human plasma (Seralab, Granollers, Spain), pooled from healthy donors and extracted in citrate tubes, were incubated at 37°C for different times (0, 60, 120, and 360 min). Then, 300 µL ACN was added to precipitate plasma protein, and the plate was centrifuged at 4000 × *g* for 60 min at 4°C. For sample quantification, the resulting supernatant was taken and analyzed by ultra performance liquid chromatography with tandem mass spectrometry (UPLC-MS/MS; ACQUITY Xevo TQD UPLC QSM; Waters) in an ACQUITY BEH C18 column (1.7 µm, 2.1 × 50 mm; Waters). As mobile phase (0.6 mL/min flow rate) was used the following gradient of 0.1% formic acid in water (A) or in ACN (B): 95% A:5% B from 0 to 0.1 min, gradual increase to 100% B from 0.1 to 1 min, maintenance in 100% B from 1 to 2 min, return to 95% A:5% B from 2 to 2.1 min, and maintenance of this ratio from 2.1 to 2.5 min. Compound concentrations were calculated from the MS peak areas.

Human hepatocyte stability assay

A vial of human hepatocytes (100 donor pool HCP100.H15/Lot: 2010012; XenoTech, Kansas City, KS, US) was removed from the liquid nitrogen tank and immersed into a water bath. When only a small ice crystal remained, the cell suspension was transferred to a tube with the preheated suspension medium (OptiThaw hepatocyte medium, K8000; XenoTech). After a brief centrifugation at 100 × *g* for 5 min, hepatocytes were gently resuspended with incubation medium (OptiIncubate hepatocyte medium, K8400; XenoTech) and counted, and viability was determined using trypan blue staining. One-micromolar compounds were incubated at 37°C and 5% CO_2 in the presence of 0.5×10^6 hepatocytes in a 500-µL incubation volume. Aliquots were taken, and reactions

were terminated with ACN at each of the six sampling time points (0, 15, 30, 60, 90, and 120 min). The samples were centrifuged, and the remaining compound was determined by UPLC-MS/MS analysis as above. Intrinsic clearance was calculated from the logarithm of the remaining compound at each of the times evaluated.

Human microsomal stability assay

The following components were added in a 96-well microplate in a final volume of 500 µL 50 mM Na/K phosphate buffer, pH 7.4 (stock solutions are indicated in parentheses, dissolved in the same buffer unless otherwise specified): 1 µM NADP (10 mM), 10 µM glucose 6-phosphate (100 mM), 1 µM glucose 6-phosphate dehydrogenase (40 U/mL, dissolved in 5 mM sodium citrate), 3 µM $MgCl_2$·6 H_2O (30 mM, dissolved in H_2O), 0.8 mg protein/mL of human microsomes (10 mg/mL protein; XenoTech), and 1 µM of test compound (100 µM, dissolved in ACN). Plates were incubated at 37°C and 75 µL samples were taken at 0, 10, 20, 40, and 60 min, to which 75 µL ACN + internal standard (Rolipram) to inactivate the microsomes and 30 µL of 0.5% formic acid in H_2O to improve the chromatographic conditions were added, and kept at 4°C. When all the samples were taken, the plate was centrifuged at 46,000 × *g* for 30 min at 15°C, and UPLC-MS/MS was performed as above, except for the time in 100% B from 1 to 2.5 min, the return to 95% A:5% B from 2.5 to 2.6 min, and the maintenance of this ratio from 2.6 to 3.0 min. Metabolic stability was calculated from the logarithm of the remaining compound at each of the times evaluated.

Cytochrome inhibition activity assay

To screen the inhibition potential of the compounds using recombinant human cytochrome P450 enzymes (CYP1A2, CYP2C9, CYP2C19, and CYP2D6) and probe substrates with fluorescent detection, incubations were conducted in a 200-µL volume in 96-well microtiter plates (Costar #3915; Corning Inc.). Addition of cofactor-buffer mixture (0.2 M KH_2PO_4 buffer, 1.3 mM NADP, 3.3 mM $MgCl_2$, 3.3 mM glucose-6-phosphate, and 0.4 U/mL glucose-6-phosphate dehydrogenase), previously diluted control Supersomes (insect cell control for Supersomes enzymes, baculovirus-insect cell-expressed; Corning Inc.), standard inhibitors (furafylline, tranylcypromine, sulfaphenazole, and quinidine), and test compounds was carried out by a Zephyr liquid handling station (Caliper Life Sciences, Hopkinton, MA, US). The plate was then pre-incubated at 37°C for 5 min, and the reaction was initiated by the addition of pre-warmed enzyme/substrate mix, which contained buffer (KH_2PO_4), cDNA-expressed P450 in insect cell microsomes, substrate (3-cyano-7-ethoxycoumarin for CYP1A2 and CYP2C19, 7-methoxy-4-(trifluoromethyl)coumarin for CYP2C9, and 3-[2-(N,N-diethyl-N-methylammonium)ethyl]-7-methoxy-4-methylcoumarin for CYP2D6) to obtain the final assay concentrations in a reaction volume of 200 µL. Reactions were terminated after a specific time for each cytochrome by the addition of stop solution (ACN:0.5 M tris-HCl, 80:20 vol/vol). Fluorescence in each well was measured using a fluorescence plate reader (EnVision 2104 multilabel plate reader; PerkinElmer, Waltham, MA, US), and percentage of inhibition was calculated.

Caco-2 permeability assay

Caco-2 cells (ATCC under the license of Abcam Inc., doing business as NaviCyte Scientific, Berkeley, CA) cultured to confluency were trypsinized and seeded onto a filter transwell insert (high-throughput screening Transwell 96-well permeable supports; Corning Inc.) at a density of ~10,000 cells/well in Dulbecco's modified Eagle's medium (DMEM). Confluent cells were subcultured at passages 58–62 and grown in a humidified atmosphere of 5% CO_2 at 37°C. Following an overnight attachment period (24 h after seeding), the cell medium was replaced every other day with fresh medium in both the apical and basolateral compartments. The cell monolayers were used for transport studies 21 days post-seeding, when monolayer integrity was checked by measuring the transepithelial

electrical resistance (TEER). If TEER values were ≥500 Ω/cm^2, the medium was removed and the cells were washed twice with pre-warmed (37°C) Hank's Balanced Salt Solution (HBSS). Compound stock solutions were made in DMSO and further diluted in HBSS (1% final DMSO concentration). All compounds, including controls (colchicine, E3S), were tested at a final concentration of 5 to 10 µM. For A → B directional transport, the donor working solution was added to the apical compartment (A) and HBSS as receiver working solution to the basolateral compartment (B). For B → A directional transport, the donor working solution was added to B and HBSS as receiver working solution to A. The cells were incubated at 37°C for 120 min with gentle stirring. At the end of the incubation, samples were taken from both donor and receiver compartments and transferred into 384-well plates, and compound concentrations were determined by UPLC-MS/MS analysis as for the plasma stability assay. After the assay, Lucifer Yellow (LY) was used to further validate the cell monolayer integrity; cells were incubated with 10 µM LY in HBSS for 1 h at 37°C, obtaining apparent permeability (Papp) values for LY of ≤10 nm/s, which confirmed the well-established Caco-2 monolayer.

L. infantum cultures

L. infantum (MHOM/ES/2016/CATB101) promastigotes were maintained at 26°C in complete Schneider's medium (Schneider's insect medium supplemented with 10% FBS, 25 µg/mL gentamycin, 1% penicillin-streptomycin, and 1% sterile human urine, pH 6.7). For growth inhibition assays, promastigotes were used in the logarithmic growth phase, whereas for the infection of macrophages and generation of amastigotes they were used in the stationary phase. Axenic amastigotes were obtained following established protocols (40, 57–59); briefly, 1×10^7 promastigotes/mL in stationary phase were cultured in Schneider's insect medium supplemented with 20% FBS, 25 µg/mL gentamycin, and 3.9 g/L of 2-(*N*-morpholino)ethanesulfonic acid, at pH 5.4 and 37°C. After 48 h, the typical rounded morphology of axenic amastigotes and their flagellum shortening could be observed. This culture was used within a week after its preparation.

Protein aggregation assays in *L. infantum* cultures

Ten milliliters of *L. infantum* promastigote cultures in the logarithmic growth phase at a concentration of 10^7 cells/mL in T-25 flasks (SPL Life Sciences, Pochon, Kyonggi-do, South Korea) was either treated with 0.15 µM or 0.3 µM YAT2150 or left untreated. After 90 min and 4 h of incubation, 1 mL of each culture was washed (3×, 1 mL PBS, 600 × *g*, 3 min) and the parasite-containing pellets were taken up in 100 µL of 4.5 mg/mL NaCl supplemented with 1× cOmplete protease inhibitor cocktail (Roche, Basel, Switzerland) and incubated overnight at 4°C with gentle stirring. After this time, samples were spun down (2,000 × *g*, 10 s) and the protein in each supernatant was quantified with the Pierce BCA protein assay kit (Thermo Electron Corporation, Waltham, MA, US). In a 96-well flat bottom black plate (Greiner Bio-One), 2 µg of protein from each supernatant was diluted in a final volume of 100 µL PBS in duplicates. Protein aggregation was measured by the addition of 25 µM ThT to each well, and after a 15-min incubation with gentle stirring, ThT fluorescence emission intensity was measured as detailed above.

Isolation of aggregation-prone proteins from *L. infantum* cultures

Proteins insoluble in 0.1% SDS were isolated following previously described protocols (60). First, 40 mL of a *L. infantum* preparation containing approximately 10^8 *L. infantum* promastigotes in the logarithmic growth phase was spun down (50 × *g*, 3 min) to remove dead parasites and washed twice with sterile PBS supplemented with one tablet of cOmplete protease inhibitor cocktail in 10 mL. After centrifugation (600 × *g*, 3 min) to pellet the parasites, they were taken up in 300 µL of RIPA buffer (150 mM NaCl, 1% Triton X-100, 0.1% SDS, 2 mM EDTA, 5% glycerol, 50 mM tris-HCl, pH 9.4) supplemented with 1× cOmplete. The solution was homogenized in a bath sonicator (FB15053 ultrasonic bath) for six cycles (pulse: 30 s on, 30 s off) and incubated for 90 min at 4°C. Next, the

lysate was spun (300 × *g*, 2.5 min, 4°C) to remove debris and unbroken cells and the supernatant was carefully loaded on top of 1 mL of 40% sucrose and ultracentrifuged (200,000 × *g*, 1 h) in order to pellet large insoluble aggregates. These were resuspended in 400 µL of lysis buffer (PBS containing 2% SDS, 5 mM DTT, and 2 mM EDTA; supplemented with 1× cOmplete) and incubated at 37°C for 30 min, pipetting up and down every 2 min with siliconized pipette tips. The resulting sample was spun down (16,000 × *g*, 12 min), and the supernatant was recovered and concentrated using an Amicon ultra 0.5 mL centrifugal filter, 3 kDa cutoff (Sigma-Aldrich Corporation). The protein in the concentrated solution was quantified using the Pierce BCA protein assay kit, and 100 µg of protein was loaded in a 12.5% SDS-PAGE stained with Coomassie Brilliant Blue R-250. The material not entering the resolving gel was excised and subjected to liquid chromatography with tandem mass spectrometry (LC-MS/MS) analysis.

LC-MS/MS analysis

Trypsin digestion of proteins in gel slabs was performed in a ProGest automatic digestor (Genomic Solutions Inc., Ann Arbor, MI, US). Each sample was reduced (20 mM DTT in 25 mM NH_4HCO_3, pH 8.0, 60 min, 60°C), alkylated (55 mM iodoacetamide in 50 mM NH_4HCO_3, pH 8.0, 30 min, 25°C, protected from light), and digested for 2 h with 80 ng of porcine trypsin (sequencing-grade modified Trypsin Gold; Promega, Madison, WI, US) in 50 mM NH_4HCO_3, pH 8.0, 37°C. Another aliquot of enzyme was added, and the digestion was allowed to continue overnight under the same conditions. The resulting peptide mixture was extracted from the gel matrix with 5% FA in 50% ACN followed by 100% ACN, cleaned with a C18 tip (PolyLC Inc., Columbia, MD, US) as per manufacturer's protocol, and finally dried in a SpeedVac concentrator and stored at −20°C until LC-MS/MS analysis. To increase peptide amounts, a third digestion with Proteinase K (Sigma-Aldrich Corporation) was performed. To both the extracted tryptic digest and the remaining gel band were added 100 ng Proteinase K in 500 mM NH_4HCO_3, pH 8.0, and after a 15 min digestion the resulting peptides were extracted from the gel as described above, pooled with the remaining in-solution digestion, dried in a SpeedVac concentrator and stored at −20°C until LC-MS/MS analysis.

Mass spectrometry was performed in a NanoAcquity HPLC system (Waters) coupled to an LTQ-OrbitrapVelos mass spectrometer (Thermo Fisher Scientific Inc.). The dried tryptic digests were taken up in 1% FA, and an aliquot was injected into the liquid chromatography system. Peptides were trapped in a Symmetry C18 trap column (5 µm, 180 µm × 20 mm; Waters) and separated in a C18 reverse-phase NanoAcquity UPLC BEH capillary column (130 Å, 1.7 µm, 75 µm × 250 mm; Waters), with a mobile-phase 1% to 40% B gradient in 30 min followed by a 40% to 60% B gradient in 5 min (A: 0.1% FA in water; B: 0.1% FA in ACN) and a flow rate of 250 nL/min. Eluted peptides were ionized in an emitter needle (PicoTip; New Objective Inc., Littleton, MA, US) with an applied spray voltage of 2 KV. A 300–1,600 *m/z* range of peptide masses was analyzed in a data-dependent mode where a full scan MS was acquired in the Orbitrap with a resolution of 60,000 full width at half maximum at 400 *m/z*. Within this range, the 15 most abundant peptides (≥500 counts) were selected from each scan and fragmented in the linear ion trap using collision-induced dissociation (38% normalized collision energy) with He as the collision gas. The scan time settings were as follows: full MS: 250 ms (1 microscan) and MS^n: 120 ms. Generated *.raw data files were collected with Thermo Xcalibur (v. 2.2).

A database was created by merging all protein entries present in the public UniProt database for *L. infantum* (uniprot_Linfantum_taxonomy_5671_cont, v25/3/21) with a small database containing laboratory contaminant proteins. The *.raw data files obtained in the LC-MS/MS analyses were used to search with the SequestHT search engine using Thermo Proteome Discover (v1.4.1.14) against the aforementioned database. Both target and decoy databases were searched to obtain a false discovery rate (FDR) and thus estimate the number of incorrect peptide-spectrum matches that exceeded a given threshold, applying preestablished search parameters [enzyme: trypsin (semi); missed

cleavage: 2; fixed modifications: carbamidomethyl of cysteine; variable modifications: oxidation of methionine and deamination of asparagine and glutamine; and peptide tolerance: 10 ppm and 0.6 Da for MS and MS/MS spectra, respectively]. To improve the sensitivity of the database search, the semi-supervised learning machine Percolator was used in order to discriminate correct from incorrect peptide spectrum matches. The Percolator assigns a *q*-value to each spectrum, which is defined as the minimal FDR at which the identification is deemed correct (0.01, strict; 0.05, relaxed). These *q*-values are estimated using the distribution of scores from decoy database search. Only proteins identified with at least two peptides (FDR ≤ 5%) are reported.

Promastigote growth inhibition assay

In 96-well microtiter plates (Nunclon Delta surface; Thermo Fisher Scientific Inc.), serial dilutions (1:2) of the drugs or peptides were performed, either free or loaded in nanoformulations, in 100 µL of complete Schneider's medium, to which one volume of 2×10^6 logarithmic growth-phase *L. infantum* promastigotes/mL in the same buffer was added. After 48 h, resazurin sodium salt was incorporated at a final concentration of 0.00125% and the plates were incubated at 26°C for another 24 h, when fluorescence from resorufin was measured as described above.

Amastigote growth inhibition assay

Compound activity on amastigotes was determined following the parasite rescue and transformation assay (61). RAW 264.7 macrophages were seeded in 96-well microtiter plates at 10^5 cells/mL of DMEM supplemented with 10% FBS and 1% penicillin-streptomycin (complete DMEM, DMEMc) in a final volume of 200 µL per well. After an overnight incubation (37°C, 5% CO_2) to allow cell adherence, the medium was removed and 10^6 *L. infantum* promastigotes/mL were added (1:10 macrophage:promastigote ratio) in DMEM supplemented with 2% FBS and 1% penicillin-streptomycin (DMEM 2% FBS). After 24 h, parasites not internalized by macrophages were removed by washing (3×, PBS) and dilutions in DMEM 2% FBS of free or liposome-encapsulated compounds were added. After 48 h, the medium was removed, cells were washed three times with PBS, and 40 µL of 0.05% SDS in complete Schneider's medium was added; after 40 s, 160 additional µL/well of complete Schneider's medium was added and plates were incubated at 26°C for another 48 h. Then, resazurin sodium salt was incorporated at a final concentration of 0.00125% and plates were incubated for 24 h more in the same conditions. Afterwards, resorufin fluorescence was measured as above.

Assessment of variation of ATP levels in *L. major*

The process described in reference (62) was followed. Briefly, *L. major* promastigotes (Friendlin strain) were transfected with the pLEXSY-hyg2.1 expression vector (Jena Bioscience, Jena, Germany) containing a cytoplasmic form of firefly luciferase mutated at its C-terminal tripeptide to prevent its import into the glycosome. Promastigotes were grown in Roswell Park Memorial Institute 1640 medium (RPMI) supplemented with 10% FBS, 2 mM L-glutamine, 1,000 U/mL penicillin/streptomycin (Gibco, Billings, MT, US), and 100 µg/mL hygromycin (InvivoGen, San Diego, CA, US) at 26°C. To assess variation in the intracellular concentration of free ATP, parasites were harvested at the late exponential phase of growth. After two washes with Hanks balanced buffer, parasites were resuspended in the same buffer supplemented with 10 mM D-glucose at 2.2×10^7 parasites/mL. After the addition of DMNPE-caged D-luciferin (GoldBio, St. Louis, MO, US) at 50 µM final concentration, the parasite suspension was aliquoted (90 µL/well) into a black 96-microwell plate (Nunc A/S, Roskilde, Denmark), and luminescence readout was monitored in a POLARstar Galaxy microplate reader (BMG LABTECH GmbH) with a luminescence setup. Once the luminescence reached a plateau, 10 µL of a YAT2150 solution at 10× fold its final concentration was added (t_0) and the luminescence value at this point was considered as 100%. DMSO in the parasite suspension was never

above 1%. Controls for membrane permeabilization (0.1% Triton X-100) and inhibition of oxidative phosphorylation (1.5 µM 1,4-naphthoquinone) were used as controls, as well as untreated parasites. Experiments were made in duplicate and repeated at least twice.

Flow cytometry

For the analysis of peptide targeting to promastigotes, 2.5×10^6 promastigotes of the *L. infantum* MHOM/ES/2016/CATB101 strain in the logarithmic growth phase were placed in Eppendorf tubes in a volume of 500 µL of complete Schneider's medium. Disaggregated Flu-AISVFFLEP-amide and Flu-DNFIFGQ-amide were reconstituted with complete Schneider's medium and added to the cells in a final concentration of 50 µM. After overnight incubation, promastigotes were stained for 30 min with 4 µg/mL Hoechst 33342, washed with PBS (3×, 600 × *g*, 3 min), and finally fixed with 3% paraformaldehyde for 20 min. After three more PBS washes, the samples were diluted 1:5 in a final volume of 500 µL PBS in 5 mL polystyrene round-bottom tubes (Corning Inc.) and processed using a 20-parameter standard configuration in a five-laser LSRFortessa flow cytometer (BD Biosciences, San Jose, CA, US). Side- and forward-scatter were used in a logarithmic scale to determine the cell population, acquiring 10,000 events for each sample. Hoechst 33342 and fluorescein were detected by excitation with 350- and 488-nm lasers, and emission was collected with 450/50-BP and 525/50-BP filters, respectively.

For the analysis of YAT2150 targeting, 5×10^6 promastigotes of the *L. infantum* MHOM/ES/2016/CATB101 strain in the logarithmic growth phase and 5×10^6 axenic amastigotes from the same strain in day 5 of growth were placed in Eppendorf tubes with a final volume of 1 mL of complete Schneider's medium. YAT2150 dissolved in DMSO was added in a final concentration of 0.38 µM (final DMSO concentration < 0.1%) along with Hoechst 33342 (4 µg/mL final concentration), incubated for 30 min, and washed (PBS, 300 × *g*, 3 min). Then, parasites were fixed and analyzed by flow cytometry as specified above, substituting fluorescein detection by YAT2150 detection (excitation with a 561-nm laser and emission collection with a 600LP-610/20-BP filter).

For the detection of antibody targeting to promastigotes, 1×10^7 promastigotes of the *L. infantum* MHOM/ES/2016/CATB101 strain in complete Schneider's medium were fixed in an Eppendorf tube for 20 min with 3% paraformaldehyde, washed 3× with PBS, and incubated for 1 h at room temperature with the anti-LPG monoclonal IgM antibody CA7AE diluted 1:500 in PBS containing 0.3% BSA. After three PBS washes, the cells were incubated for 1 h with a secondary goat anti-mouse antibody conjugated to Alexa Fluor 488 (AF488; Invitrogen, Waltham, MA, US) diluted 1:200 in PBS containing 2% BSA. After three final PBS washes, flow cytometry analysis was performed as specified above for peptide targeting with fluorescein, except for the acquisition of 30,000 events.

Fluorescence microscopy

All the samples were visualized in an 8-well chamber slide (ibidi GmbH, Gräfelfing, Germany). For staining with the ProteoStat aggresome detection kit (Enzo Life Sciences Inc., Farmingdale, NY, US), *L. infantum* promastigotes and axenic amastigotes in days 3 and 5 of growth, respectively, were washed twice with PBS. In PBS, a 1:2,000 ProteoStat dye dilution was then added and after 5 min, 4 µg/mL Hoechst 33342 was incorporated and incubated for a further 10 min. The samples were then washed (3×, PBS) and observed with a Leica TCS SP5 laser scanning confocal fluorescence microscope. ProteoStat and Hoechst 33342 were detected by excitation through 561- and 405-nm lasers, respectively. Emission was collected between 590 and 670 nm for ProteoStat and between 415 and 500 nm for Hoechst 33342. The same protocol was followed for YAT2150 staining of promastigotes and axenic amastigotes, substituting ProteoStat by an incubation in 0.38 µM YAT2150. To quantify Manders' overlap coefficient (63), images were analyzed using the Just Another Colocalization Plugin [JACoP (64)] in the Fiji software (65). Manders' coefficient ranges from 0 to 1 showing the pixel percentage that is overlapped, being 0 defined as no colocalization and 1 as total colocalization.

For the analysis of peptide targeting to promastigotes, 200 µL of the samples prepared as described above in the flow cytometry section was placed in an 8-well chamber slide and fluorescence microscopy was conducted in a Zeiss LSM 800 equipment (Zeiss, Oberkochen, Germany) with a 100×/1.4 oil DIC M27 objective. Hoechst 33342 was excited with a 405-nm diode laser, 5 mW, class 3B, and fluorescein with a 488-nm diode laser, 10 mW, class 3B; emission was collected in the 390–460- and 500–700-nm ranges, respectively. A Z-stack image of 30 layers of a promastigote incubated with the Flu-AISVFFLEP-amide peptide was acquired in a Leica TCS SP5 laser scanning confocal fluorescence microscope, where Hoechst 33342 and fluorescein were excited with 405- and 488-nm diode lasers and emission was collected in the 414–474- and 501–562-nm ranges, respectively.

For the targeting analysis in promastigotes of YAT2150 encapsulated in CF-PE-containing liposomes, 10^7 *L. infantum* promastigotes/mL were incubated in complete Schneider's medium for 1 h with 0.38 µM YAT2150 contained in the liposome suspension, during the last 30 min in the presence of 4 µg/mL Hoechst 33342. Cells were then washed three times with PBS, fixed with 3% paraformaldehyde for 20 min, washed again, and visualized with a Leica TCS SPE laser scanning confocal fluorescence microscope. Hoechst 33342, CF-PE, and YAT2150 were excited with 405-, 488-, and 532-nm solid-state lasers and the respective emissions were collected in the 408–521-, 491–564-, and 589–691-nm ranges.

For the analysis of macrophages treated with YAT2150-stained promastigotes, RAW 264.7 macrophages maintained in DMEMc at 37°C and in the presence of 5% CO_2 were seeded at 10^5 cells/mL in DMEMc in an 8-well chamber slide, placing 300 µL per well and allowing cells to adhere overnight. In parallel, 10^7 *L. infantum* stationary-phase promastigotes in 1 mL of DMEM 2% FBS were stained with 0.38 µM YAT2150 for 1 h at room temperature and thoroughly washed with DMEM 2% FBS (3×, 600 × *g*, 3 min). Then, RAW 264.7 cells were washed once with DMEM 2% FBS and 10^6 YAT2150-stained *L. infantum* promastigotes/mL were added to each well and incubated for 24 h. Afterwards, 2 µg/mL Hoechst 33342 and 5 µg/mL wheat germ agglutinin-Oregon Green 488 (Thermo Fisher Scientific Inc.) were added simultaneously and incubated for 10 min, and the samples were visualized with a Leica TCS SP5 laser scanning confocal fluorescence microscope. Hoechst 33342, Oregon Green 488, and YAT2150 were excited with 405-, 488-, and 532-nm solid-state lasers and their respective emissions were collected in the 408–521-, 491–537-, and 605–707-nm ranges. For the targeting analysis in RAW 264.7 macrophages exposed to *Leishmania* of YAT2150 encapsulated in CF-PE-containing liposomes, the cell samples were prepared as described above, except for the use of non-stained promastigotes. *Leishmania*-exposed macrophages were incubated in DMEM 2% FBS for 3 h with 0.38 µM YAT2150 contained in the liposome suspension, during the last 10 min in the presence of 2 µg/mL Hoechst 33342. Then the cells were washed and observed as described above for promastigote targeting analysis.

For the observation of intracellular amastigotes, 6×10^7 stationary-phase promastigotes were stained in 1 mL of cold PBS with 2.8 µg/mL of CFSE, incubated for 10 min (37°C, 5% CO_2), and washed with PBS (3×, 600 × *g*, 3 min). The final CFSE-stained promastigote pellet was taken up in DMEMc and added to 5×10^5 RAW 264.7 macrophages/mL that had been seeded in DMEMc and allowed to adhere overnight (10:1 promastigote:macrophage ratio). After 4 h of incubation, promastigotes were removed by washing five times with DMEM and cells were incubated for 10 min with 2 µg/mL of Hoechst 33342. Then, 0.38 µM YAT2150 was added, and after 6 h of incubation, the preparations were observed in an IX-51 Olympus (Tokyo, Japan) fluorescence microscope with a 100× objective. The fluorescence of Hoechst 33342, CFSE-stained parasites, and YAT2150 was detected with the fluorescence filter cubes U-MNU2, U-MWIBA3, and U-MWG2, which have excitation filters of 360–370, 460–495, and 534–588 nm and emission filters of 420, 510–550 and 609–683 nm, respectively.

For immunofluorescence microscopy analysis of the binding of anti-LPG monoclonal IgM antibody CA7AE to live promastigotes, the cells were treated as described above

for flow cytometry except for the fixation step, which was omitted, and the staining, after removal by washing in complete Schneider's medium of primary and secondary antibodies, with 4 µg/mL of the DNA dye Hoechst 33342 for 30 min. After three additional washes (600 × *g*, 3 min), 300 µL of a suspension of stained and washed promastigotes in complete Schneider's medium was visualized with an IX-51 Olympus microscope as described above, using for AF488 the CFSE settings. For anti-LPG targeting analysis to live *Leishmania*-exposed and control non-treated macrophages, 5×10^4 RAW 264.7 macrophages/mL were seeded in 300 µL/well of RPMI supplemented with 10% FBS and 1% penicillin-streptomycin in an 8-well chamber slide, and allowed to adhere for 24 h at 37°C in the presence of 5% CO_2. *Leishmania*-treated macrophages were infected by incubation for 24 h in the presence of 5×10^5 promastigotes of the *L. infantum* MHOM/ES/2016/CATB101 strain. After 3× PBS washes, the cells were prepared for immunocytochemistry analysis as described above for promastigotes, but using 2 µg/mL Hoechst 33342. Confocal fluorescence microscopy was conducted as described above for the analysis of fluorescein-tagged peptides.

Statistical analysis

Unless otherwise stated, experiments were performed in triplicate and the results are expressed as mean values ± standard error of the mean (SEM). The IC_{50} and CC_{50} were calculated through non-linear regression analysis using GraphPad Prism 8.4 (GraphPad software, La Jolla, CA, US). Differences between samples were analyzed by one-way analysis of variance using the same software, considering a significant *P* value ≤0.05. Mean values and SEM were calculated using Microsoft Office Excel version 2306.

ACKNOWLEDGMENTS

ISGlobal and IBEC are members of the CERCA Programme, *Generalitat de Catalunya*. We acknowledge support from the Spanish Ministry of Science, Innovation and Universities through the "*Centro de Excelencia Severo Ochoa* 2019–2023" Program (CEX2018-000806-S). This research is part of ISGlobal's Program on the Molecular Mechanisms of Malaria which is partially supported by the *Fundación Ramón Areces*.

We thank the Advanced Optical Microscopy Unit-Clinic Campus from the Scientific and Technological Centers at the University of Barcelona for their support and advice with confocal microscopy. V.I. was supported by the Spanish Ministry of Universities and the European Union-NextGenerationEU (ruling 02/07/2021, *Universitat Autònoma de Barcelon*a).

This work was supported by grants (i) *Fundació La Marató de TV3*, Ref. 201811 (X.F.-B.); (ii) PID2021-128325OB-I00 (X.F.-B.) and PID2020-118127RB-I00 (D.M.-T.), funded by *Ministerio de Ciencia e Innovación/Agencia Estatal de Investigación* (MCIN/AEI/10.13039/501100011033), which included ERDF funds; (iii) *II Premis Innovació Campus Clínic 2022*, *Hospital Clínic de Barcelona* (X.F.-B.); and (iv) *Generalitat de Catalunya*, Spain (http://agaur.gencat.cat/), grant numbers 2021-SGR-00635 (S.V.) and 2021-SGR-00357 (D.M.-T.). Work at Pompeu Fabra University was supported by "La Caixa" Banking Foundation (https://fundacionlacaixa.org/, grant HR17-00409) and by grant AGL2017-84097-C2-2-R and the "María de Maeztu" Program for Units of Excellence in R&D from the Spanish Ministry of Science, Innovation and Universities. Work at the *Centro de Investigaciones Biológicas* was supported by grants from MCIN *Subdirección General de Redes y Centros de Investigación Cooperativa*-FEDER RD16/0027/0010 and CSIC PIE 201620E038. The funders had no role in the study design, data collection and analysis, decision to publish, or preparation of the manuscript.

AUTHOR AFFILIATIONS

[1]Barcelona Institute for Global Health (ISGlobal), Hospital Clínic-Universitat de Barcelona, Barcelona, Spain

[2]Institute for Bioengineering of Catalonia (IBEC), The Barcelona Institute of Science and Technology, Barcelona, Spain
[3]Doctoral School of Biotechnology, Faculty of Pharmacy and Food Sciences, University of Barcelona, Barcelona, Spain
[4]Institut de Biotecnologia i de Biomedicina (IBB) and Departament de Bioquímica i Biologia Molecular, Universitat Autònoma de Barcelona, Bellaterra, Spain
[5]Centro de Investigaciones Biológicas Margarita Salas, Consejo Superior de Investigaciones Científicas (CSIC), Madrid, Spain
[6]Section of Parasitology Department of Biology, Health and Environment, Faculty of Pharmacy and Food Sciences, University of Barcelona, Barcelona, Spain
[7]Department of Medicine and Life Sciences, Barcelona Biomedical Research Park, Pompeu Fabra University, Barcelona, Spain
[8]Laboratory of Medicinal Chemistry (CSIC Associated Unit), Faculty of Pharmacy and Food Sciences, and Institute of Biomedicine (IBUB), University of Barcelona, Barcelona, Spain
[9]Nanoscience and Nanotechnology Institute (IN2UB), University of Barcelona, Barcelona, Spain

AUTHOR ORCIDs

Xavier Fernàndez-Busquets http://orcid.org/0000-0002-4622-9631

FUNDING

Funder	Grant(s)	Author(s)
Fundació la Marató de TV3 (Fundació la Marató)	Ref. 201811	Xavier Fernàndez-Busquets
Ministerio de Ciencia e Innovación (MCIN)	PID2021-128325OB-I00	Xavier Fernàndez-Busquets
Ministerio de Ciencia e Innovación (MCIN)	PID2020-118127RB-I00	Diego Muñoz-Torrero
Generalitat de Catalunya (Government of Catalonia)	2021-SGR-00635	Salvador Ventura
Generalitat de Catalunya (Government of Catalonia)	2021-SGR-00357	Diego Muñoz-Torrero
'la Caixa' Foundation ('la Caixa')	HR17-00409	David Andreu
Ministerio de Ciencia e Innovación (MCIN)	AGL2017-84097-C2-2-R	David Andreu
Ministerio de Ciencia e Innovación (MCIN)	RD16/0027/0010	Luis Rivas
MEC | Consejo Superior de Investigaciones Científicas (CSIC)	PIE 201620E038	Luis Rivas

AUTHOR CONTRIBUTIONS

Lucía Román-Álamo, Data curation, Formal analysis, Investigation, Writing – review and editing | Yunuen Avalos-Padilla, Data curation, Formal analysis, Investigation, Writing – review and editing | Inés Bouzón-Arnáiz, Formal analysis, Investigation, Writing – review and editing | Valentín Iglesias, Formal analysis, Writing – review and editing | Jorge Fernández-Lajo, Investigation, Writing – review and editing | Juan M. Monteiro, Investigation, Writing – review and editing | Luis Rivas, Data curation, Formal analysis, Funding acquisition, Investigation, Methodology, Resources, Supervision, Writing – review and editing | Roser Fisa, Formal analysis, Investigation, Writing – review and editing | Cristina Riera, Formal analysis, Investigation, Writing – review and editing | David Andreu, Formal analysis, Funding acquisition, Investigation, Methodology, Resources, Supervision, Writing – review and editing | Carlos Pintado-Grima, Investigation, Writing – review and editing | Salvador Ventura, Formal analysis, Funding

acquisition, Investigation, Methodology, Resources, Software, Supervision, Writing – review and editing | Elsa M. Arce, Investigation, Writing – review and editing | Diego Muñoz-Torrero, Data curation, Formal analysis, Funding acquisition, Investigation, Methodology, Resources, Supervision, Writing – review and editing | Xavier Fernàndez-Busquets, Conceptualization, Data curation, Formal analysis, Funding acquisition, Investigation, Methodology, Project administration, Resources, Supervision, Validation, Writing – original draft, Writing – review and editing

ADDITIONAL FILES

The following material is available online.

Supplemental Material

Figs. S1 to S7, Tables S1 to S3 (AAC01127-23-s0001.pdf). Supplemental figures and tables.

REFERENCES

1. Burza S, Croft SL, Boelaert M. 2018. Leishmaniasis. Lancet 392:951–970. https://doi.org/10.1016/S0140-6736(18)31204-2
2. World Health Organization. 2023. Leishmaniasis Factsheet. World Health Organization.
3. Ponte-Sucre A, Gamarro F, Dujardin JC, Barrett MP, López-Vélez R, García-Hernández R, Pountain AW, Mwenechanya R, Papadopoulou B. 2017. Drug resistance and treatment failure in leishmaniasis: a 21st century challenge. PLoS Negl Trop Dis 11:e0006052. https://doi.org/10.1371/journal.pntd.0006052
4. Sundar S, Singh B. 2018. Emerging therapeutic targets for treatment of leishmaniasis. Expert Opin Ther Targets 22:467–486. https://doi.org/10.1080/14728222.2018.1472241
5. Chiti F, Dobson CM. 2017. Protein misfolding, amyloid formation, and human disease: a summary of progress over the last decade. Annu Rev Biochem 86:27–68. https://doi.org/10.1146/annurev-biochem-061516-045115
6. Franzmann TM, Alberti S. 2019. Protein phase separation as a stress survival strategy. Cold Spring Harb Perspect Biol 11:a034058. https://doi.org/10.1101/cshperspect.a034058
7. Brown JCS, Lindquist S. 2009. A heritable switch in carbon source utilization driven by an unusual yeast prion. Genes Dev 23:2320–2332. https://doi.org/10.1101/gad.1839109
8. Maji SK, Perrin MH, Sawaya MR, Jessberger S, Vadodaria K, Rissman RA, Singru PS, Nilsson KPR, Simon R, Schubert D, Eisenberg D, Rivier J, Sawchenko P, Vale W, Riek R. 2009. Functional amyloids as natural storage of peptide hormones in pituitary secretory granules. Science 325:328–332. https://doi.org/10.1126/science.1173155
9. Si K, Kandel ER. 2016. The role of functional prion-like proteins in the persistence of memory. Cold Spring Harb Perspect Biol 8:a021774. https://doi.org/10.1101/cshperspect.a021774
10. Biosca A, Bouzón-Arnáiz I, Spanos L, Siden-Kiamos I, Iglesias V, Ventura S, Fernàndez-Busquets X. 2020. Detection of protein aggregation in live *Plasmodium* parasites. Antimicrob Agents Chemother 64:e02135-19. https://doi.org/10.1128/AAC.02135-19
11. Bouzón-Arnáiz I, Avalos-Padilla Y, Biosca A, Caño-Prades O, Román-Álamo L, Valle J, Andreu D, Moita D, Prudêncio M, Arce EM, Muñoz-Torrero D, Fernàndez-Busquets X. 2022. The protein aggregation inhibitor YAT2150 has potent antimalarial activity in *Plasmodium falciparum in vitro* cultures. BMC Biol 20:197. https://doi.org/10.1186/s12915-022-01374-4
12. eBioMedicine. 2023. Leishmania: an urgent need for new treatments. EBioMedicine 87:104440. https://doi.org/10.1016/j.ebiom.2023.104440
13. Ornellas-Garcia U, Cuervo P, Ribeiro-Gomes FL. 2023. Malaria and leishmaniasis: updates on co-infection. Front Immunol 14:1122411. https://doi.org/10.3389/fimmu.2023.1122411
14. Hamilton WL, Claessens A, Otto TD, Kekre M, Fairhurst RM, Rayner JC, Kwiatkowski D. 2017. Extreme mutation bias and high AT content in *Plasmodium falciparum*. Nucleic Acids Res 45:1889–1901. https://doi.org/10.1093/nar/gkw1259
15. Peacock CS, Seeger K, Harris D, Murphy L, Ruiz JC, Quail MA, Peters N, Adlem E, Tivey A, Aslett M, et al. 2007. Comparative genomic analysis of three *Leishmania* species that cause diverse human disease. Nat Genet 39:839–847. https://doi.org/10.1038/ng2053
16. Franssen SU, Durrant C, Stark O, Moser B, Downing T, Imamura H, Dujardin JC, Sanders MJ, Mauricio I, Miles MA, Schnur LF, Jaffe CL, Nasereddin A, Schallig H, Yeo M, Bhattacharyya T, Alam MZ, Berriman M, Wirth T, Schönian G, Cotton JA. 2020. Global genome diversity of the *Leishmania donovani* complex. Elife 9:e51243. https://doi.org/10.7554/eLife.51243
17. Battistuzzi FU, Schneider KA, Spencer MK, Fisher D, Chaudhry S, Escalante AA. 2016. Profiles of low complexity regions in Apicomplexa. BMC Evol Biol 16:47. https://doi.org/10.1186/s12862-016-0625-0
18. Lancaster AK, Nutter-Upham A, Lindquist S, King OD. 2014. PLAAC: a web and command-line application to identify proteins with prion-like amino acid composition. Bioinformatics 30:2501–2502. https://doi.org/10.1093/bioinformatics/btu310
19. Pallarès I, de Groot NS, Iglesias V, Sant'Anna R, Biosca A, Fernàndez-Busquets X, Ventura S. 2018. Discovering putative prion-like proteins in *Plasmodium falciparum*: a computational and experimental analysis. Front Microbiol 9:1737. https://doi.org/10.3389/fmicb.2018.01737
20. The UniProt Consortium. 2019. UniProt: a worldwide hub of protein knowledge. Nucleic Acids Res 47:D506–D515. https://doi.org/10.1093/nar/gky1049
21. Conchillo-Solé O, de Groot NS, Avilés FX, Vendrell J, Daura X, Ventura S. 2007. AGGRESCAN: a server for the prediction and evaluation of "hot spots" of aggregation in polypeptides. BMC Bioinformatics 8:65. https://doi.org/10.1186/1471-2105-8-65
22. Sherman BT, Hao M, Qiu J, Jiao X, Baseler MW, Lane HC, Imamichi T, Chang W. 2022. DAVID: a web server for functional enrichment analysis and functional annotation of gene lists. Nucleic Acids Res 50:W216–W221. https://doi.org/10.1093/nar/gkac194
23. Karamysheva ZN, Gutierrez Guarnizo SA, Karamyshev AL. 2020. Regulation of translation in the protozoan parasite *Leishmania*. Int J Mol Sci 21:2981. https://doi.org/10.3390/ijms21082981
24. Ciryam P, Kundra R, Morimoto RI, Dobson CM, Vendruscolo M. 2015. Supersaturation is a major driving force for protein aggregation in neurodegenerative diseases. Trends Pharmacol Sci 36:72–77. https://doi.org/10.1016/j.tips.2014.12.004
25. De Pablos LM, Ferreira TR, Walrad PB. 2016. Developmental differentiation in *Leishmania* lifecycle progression: post-transcriptional control conducts the orchestra. Curr Opin Microbiol 34:82–89. https://doi.org/10.1016/j.mib.2016.08.004
26. Törnquist M, Michaels TCT, Sanagavarapu K, Yang X, Meisl G, Cohen SIA, Knowles TPJ, Linse S. 2018. Secondary nucleation in amyloid formation. Chem Commun (Camb) 54:8667–8684. https://doi.org/10.1039/c8cc02204f

27. Betti C, Vanhoutte I, Coutuer S, De Rycke RM, Mishev K, Vuylsteke M, Aesaert S, Rombaut D, Gallardo R, De Smet F, Xu J, Van Lijsebettens M, Van Breusegem F, Inzé D, Rousseau F, Schymkowitz J, Russinova E. 2016. Sequence-specific protein aggregation generates defined protein knockdowns in plants. Plant Physiol 171:773–787. https://doi.org/10.1104/pp.16.00335
28. Jumper J, Evans R, Pritzel A, Green T, Figurnov M, Ronneberger O, Tunyasuvunakool K, Bates R, Žídek A, Potapenko A, et al. 2021. Highly accurate protein structure prediction with AlphaFold. Nature 596:583–589. https://doi.org/10.1038/s41586-021-03819-2
29. Maurer-Stroh S, Debulpaep M, Kuemmerer N, Lopez de la Paz M, Martins IC, Reumers J, Morris KL, Copland A, Serpell L, Serrano L, Schymkowitz JWH, Rousseau F. 2010. Exploring the sequence determinants of amyloid structure using position-specific scoring matrices. Nat Methods 7:237–242. https://doi.org/10.1038/nmeth.1432
30. Varadi M, Anyango S, Deshpande M, Nair S, Natassia C, Yordanova G, Yuan D, Stroe O, Wood G, Laydon A, et al. 2022. AlphaFold Protein Structure Database: massively expanding the structural coverage of protein-sequence space with high-accuracy models. Nucleic Acids Res 50:D439–D444. https://doi.org/10.1093/nar/gkab1061
31. Martins PM, Navarro S, Silva A, Pinto MF, Sárkány Z, Figueiredo F, Pereira PJB, Pinheiro F, Bednarikova Z, Burdukiewicz M, Galzitskaya OV, Gazova Z, Gomes CM, Pastore A, Serpell LC, Skrabana R, Smirnovas V, Ziaunys M, Otzen DE, Ventura S, Macedo-Ribeiro S. 2020. MIRRAGGE - Minimum Information Required for Reproducible AGGregation Experiments. Front Mol Neurosci 13:582488. https://doi.org/10.1016/j.foodres.2019.108872
32. Batlle C, de Groot NS, Iglesias V, Navarro S, Ventura S. 2017. Characterization of soft amyloid cores in human prion-like proteins. Sci Rep 7:12134. https://doi.org/10.1038/s41598-017-09714-z
33. Espargaró A, Pont C, Gamez P, Muñoz-Torrero D, Sabate R. 2019. Amyloid pan-inhibitors: one family of compounds to cope with all conformational diseases. ACS Chem Neurosci 10:1311–1317. https://doi.org/10.1021/acschemneuro.8b00398
34. Román-Álamo L, Allaw M, Avalos-Padilla Y, Manca ML, Manconi M, Fulgheri F, Fernández-Lajo J, Rivas L, Vázquez JA, Peris JE, Roca-Geronès X, Poonlaphdecha S, Alcover MM, Fisa R, Riera C, Fernàndez-Busquets X. 2023. *In vitro* evaluation of aerosol therapy with pentamidine-loaded liposomes coated with chondroitin sulfate or heparin for the treatment of *Leishmaniasis*. Pharmaceutics 15:1163. https://doi.org/10.3390/pharmaceutics15041163
35. Martínez-Orellana P, Baxarias M, Good L, Solano-Gallego L. 2020. The effects of polyhexamethylene biguanide (PHMB) and TLR agonists alone or as polyplex nanoparticles against *Leishmania infantum* promastigotes and amastigotes. Vet Sci 7:179. https://doi.org/10.3390/vetsci7040179
36. Hendrickx S, Van Bockstal L, Aslan H, Sadlova J, Maes L, Volf P, Caljon G. 2020. Transmission potential of paromomycin-resistant *Leishmania infantum* and *Leishmania donovani*. J Antimicrob Chemother 75:951–957. https://doi.org/10.1093/jac/dkz517
37. Ganguly S, Bandyopadhyay S, Sarkar A, Chatterjee M. 2006. Development of a semi-automated colorimetric assay for screening anti-leishmanial agents. J Microbiol Methods 66:79–86. https://doi.org/10.1016/j.mimet.2005.10.011
38. Amato VS, Rabello A, Rotondo-Silva A, Kono A, Maldonado TPH, Alves IC, Floeter-Winter LM, Neto VA, Shikanai-Yasuda MA. 2004. Successful treatment of cutaneous leishmaniasis with lipid formulations of amphotericin B in two immunocompromised patients. Acta Trop 92:127–132. https://doi.org/10.1016/j.actatropica.2004.06.006
39. Gomes CB, Souza-Silva F, Charret KDS, Pereira BAS, Finkelstein LC, Santos-de-Souza R, de Castro Côrtes LM, Pereira MCS, Rodrigues de Oliveira Jr FO, Alves CR. 2017. Increasing in cysteine proteinase B expression and enzymatic activity during *in vitro* differentiation of *Leishmania* (*Viannia*) *braziliensis*: first evidence of modulation during morphological transition. Biochimie 133:28–36. https://doi.org/10.1016/j.biochi.2016.11.015
40. Dias-Lopes G, Zabala-Peñafiel A, de Albuquerque-Melo BC, Souza-Silva F, Menaguali do Canto L, Cysne-Finkelstein L, Alves CR. 2021. Axenic amastigotes of *Leishmania* species as a suitable model for *in vitro* studies. Acta Trop 220:105956. https://doi.org/10.1016/j.actatropica.2021.105956
41. Graña-Montes R, Pujols-Pujol J, Gómez-Picanyol C, Ventura S. 2017. Prediction of protein aggregation and amyloid formation, p 205–263. In J.Rigden D (ed), From Protein Structure to Function with Bioinformatics. Springer, Dordrecht.
42. Wallace EWJ, Kear-Scott JL, Pilipenko EV, Schwartz MH, Laskowski PR, Rojek AE, Katanski CD, Riback JA, Dion MF, Franks AM, Airoldi EM, Pan T, Budnik BA, Drummond DA. 2015. Reversible, specific, active aggregates of endogenous proteins assemble upon heat stress. Cell 162:1286–1298. https://doi.org/10.1016/j.cell.2015.08.041
43. Lipinski CA, Lombardo F, Dominy BW, Feeney PJ. 2001. Experimental and computational approaches to estimate solubility and permeability in drug discovery and development settings. Adv Drug Deliv Rev 46:3–26. https://doi.org/10.1016/s0169-409x(00)00129-0
44. Słoczyńska K, Gunia-Krzyżak A, Koczurkiewicz P, Wójcik-Pszczoła K, Żelaszczyk D, Popiół J, Pękala E. 2019. Metabolic stability and its role in the discovery of new chemical entities. Acta Pharm 69:345–361. https://doi.org/10.2478/acph-2019-0024
45. Freitas-Junior LH, Chatelain E, Kim HA, Siqueira-Neto JL. 2012. Visceral leishmaniasis treatment: what do we have, what do we need and how to deliver it. Int J Parasitol Drugs Drug Resist 2:11–19. https://doi.org/10.1016/j.ijpddr.2012.01.003
46. Mowbray CE, Braillard S, Glossop PA, Whitlock GA, Jacobs RT, Speake J, Pandi B, Nare B, Maes L, Yardley V, Freund Y, Wall RJ, Carvalho S, Bello D, Van den Kerkhof M, Caljon G, Gilbert IH, Corpas-Lopez V, Lukac I, Patterson S, Zuccotto F, Wyllie S. 2021. DNDI-6148: a novel benzoxaborole preclinical candidate for the treatment of visceral leishmaniasis. J Med Chem 64:16159–16176. https://doi.org/10.1021/acs.jmedchem.1c01437
47. Martínez de Iturrate-Sanz P. 2021. Protein-kinase inhibitors as potential leishmanicidal drugs. Universidad Complutense de Madrid. https://docta.ucm.es/entities/publication/24549645-82d7-466e-b371-48784c38a434.
48. McConville MJ, Mullin KA, Ilgoutz SC, Teasdale RD. 2002. Secretory pathway of trypanosomatid parasites. Microbiol Mol Biol Rev 66:122–154; https://doi.org/10.1128/MMBR.66.1.122-154.2002
49. Moles E, Galiano S, Gomes A, Quiliano M, Teixeira C, Aldana I, Gomes P, Fernàndez-Busquets X. 2017. ImmunoPEGliposomes for the targeted delivery of novel lipophilic drugs to red blood cells in a falciparum malaria murine model. Biomaterials 145:178–191. https://doi.org/10.1016/j.biomaterials.2017.08.020
50. de Morais CGV, Castro Lima AK, Terra R, dos Santos RF, Da-Silva SAG, Dutra PML. 2015. The dialogue of the host-parasite relationship: *Leishmania* spp. and *Trypanosoma cruzi* infection. Biomed Res Int 2015:324915. https://doi.org/10.1155/2015/324915
51. Camps P, Formosa X, Galdeano C, Gómez T, Muñoz-Torrero D, Scarpellini M, Viayna E, Badia A, Clos MV, Camins A, Pallàs M, Bartolini M, Mancini F, Andrisano V, Estelrich J, Lizondo M, Bidon-Chanal A, Luque FJ. 2008. Novel donepezil-based inhibitors of acetyl- and butyrylcholinesterase and acetylcholinesterase-induced β-amyloid aggregation. J Med Chem 51:3588–3598. https://doi.org/10.1021/jm8001313
52. Galdeano C, Viayna E, Sola I, Formosa X, Camps P, Badia A, Clos MV, Relat J, Ratia M, Bartolini M, Mancini F, Andrisano V, Salmona M, Minguillón C, González-Muñoz GC, Rodríguez-Franco MI, Bidon-Chanal A, Luque FJ, Muñoz-Torrero D. 2012. Huprine-tacrine heterodimers as anti-amyloidogenic compounds of potential interest against Alzheimer's and prion diseases. J Med Chem 55:661–669. https://doi.org/10.1021/jm200840c
53. Sola I, Castellà S, Viayna E, Galdeano C, Taylor MC, Gbedema SY, Pérez B, Clos MV, Jones DC, Fairlamb AH, Wright CW, Kelly JM, Muñoz-Torrero D. 2015. Synthesis, biological profiling and mechanistic studies of 4-aminoquinoline-based heterodimeric compounds with dual trypanocidal-antiplasmodial activity. Bioorg Med Chem 23:5156–5167. https://doi.org/10.1016/j.bmc.2015.01.031
54. Hallgren J, Tsirigos KD, Pedersen MD, Almagro Armenteros JJ, Marcatili P, Nielsen H, Krogh A, Winther O. 2022. DeepTMHMM predicts alpha and beta transmembrane proteins using deep neural networks. BioRxiv. https://doi.org/10.1101/2022.04.08.487609
55. MacDonald RC, MacDonald RI, Menco BP, Takeshita K, Subbarao NK, Hu LR. 1991. Small-volume extrusion apparatus for preparation of large, unilamellar vesicles. Biochim Biophys Acta 1061:297–303. https://doi.org/10.1016/0005-2736(91)90295-j
56. Weinberger A, Tsai F-C, Koenderink GH, Schmidt TF, Itri R, Meier W, Schmatko T, Schröder A, Marques C. 2013. Gel-assisted formation of

giant unilamellar vesicles. Biophys J 105:154–164. https://doi.org/10.1016/j.bpj.2013.05.024
57. Callahan HL, Portal AC, Devereaux R, Grogl M. 1997. An axenic amastigote system for drug screening. Antimicrob Agents Chemother 41:818–822. https://doi.org/10.1128/AAC.41.4.818
58. Teixeira MCA, de Jesus Santos R, Sampaio RB, Pontes-de-Carvalho L, dos-Santos WLC. 2002. A simple and reproducible method to obtain large numbers of axenic amastigotes of different *Leishmania* species. Parasitol Res 88:963–968. https://doi.org/10.1007/s00436-002-0695-3
59. Gupta N, Goyal N, Rastogi AK. 2001. *In vitro* cultivation and characterization of axenic amastigotes of *Leishmania*. Trends Parasitol 17:150–153. https://doi.org/10.1016/s1471-4922(00)01811-0
60. Kryndushkin D, Pripuzova N, Burnett BG, Shewmaker F. 2013. Non-targeted identification of prions and amyloid-forming proteins from yeast and mammalian cells. J Biol Chem 288:27100–27111. https://doi.org/10.1074/jbc.M113.485359
61. Jain SK, Sahu R, Walker LA, Tekwani BL. 2012. A parasite rescue and transformation assay for antileishmanial screening against intracellular *Leishmania donovani* amastigotes in THP1 human acute monocytic leukemia cell line. J Vis Exp:4054. https://doi.org/10.3791/4054
62. Luque-Ortega JR, Saugar JM, Chiva C, Andreu D, Rivas L. 2003. Identification of new leishmanicidal peptide lead structures by automated real-time monitoring of changes in intracellular ATP. Biochem J 375:221–230. https://doi.org/10.1042/bj20030544
63. Manders EMM, Verbeek FJ, Aten JA. 1993. Measurement of co-localization of objects in dual-colour confocal images. J Microsc 169:375–382. https://doi.org/10.1111/j.1365-2818.1993.tb03313.x
64. Bolte S, Cordelières FP. 2006. A guided tour into subcellular colocalization analysis in light microscopy. J Microsc 224:213–232. https://doi.org/10.1111/j.1365-2818.2006.01706.x
65. Schindelin J, Arganda-Carreras I, Frise E, Kaynig V, Longair M, Pietzsch T, Preibisch S, Rueden C, Saalfeld S, Schmid B, Tinevez JY, White DJ, Hartenstein V, Eliceiri K, Tomancak P, Cardona A. 2012. Fiji: an open-source platform for biological-image analysis. Nat Methods 9:676–682. https://doi.org/10.1038/nmeth.2019

Effect of the aggregated protein dye YAT2150 on *Leishmania* parasite viability

Lucía Román-Álamo, Yunuen Avalos-Padilla, Inés Bouzón-Arnáiz, Valentín Iglesias, Jorge Fernández-Lajo, Juan M. Monteiro, Luis Rivas, Roser Fisa, Cristina Riera, David Andreu, Carlos Pintado-Grima, Salvador Ventura, Elsa M. Arce, Diego Muñoz-Torrero, Xavier Fernàndez-Busquets

Supplemental Material

Supplemental Figures and Tables

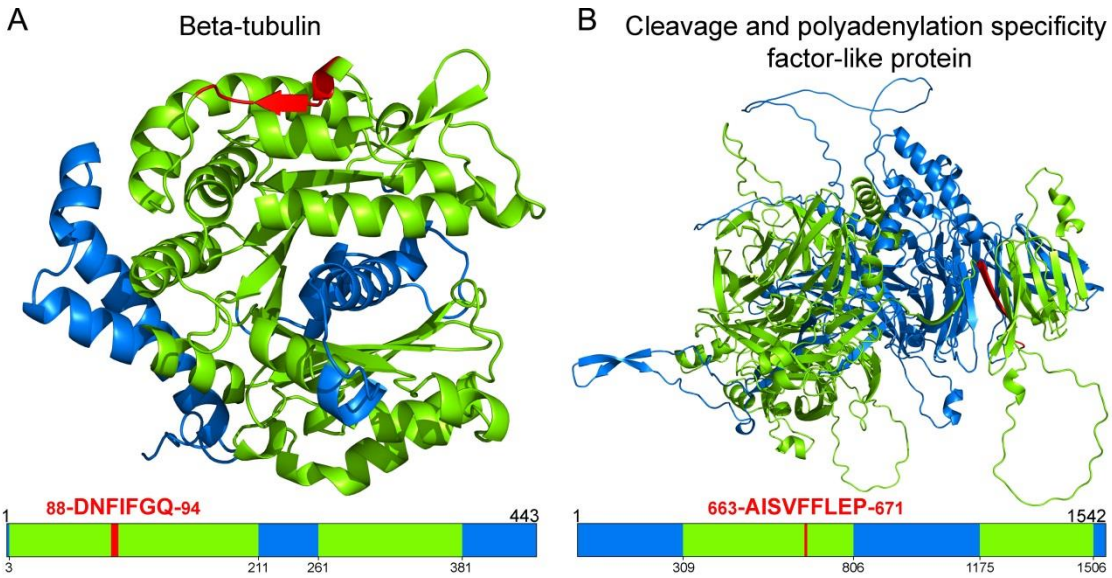

Fig. S1. Structural and sequential context of two amyloid peptides selected from the aggregation-prone *L. infantum* protein pool resisting dissolution in 0.1% SDS. Peptides from (A) β-tubulin and (B) cleavage and polyadenylation specificity factor-like protein (CPSF) (coloured red) are located inside "Tubulin" and "Mono-functional DNA-alkylating methyl methanesulfonate N-term" Pfam domains (coloured green). Non-identified globular domains are represented in blue. Protein models correspond to AlphaFold database version 3 (1).

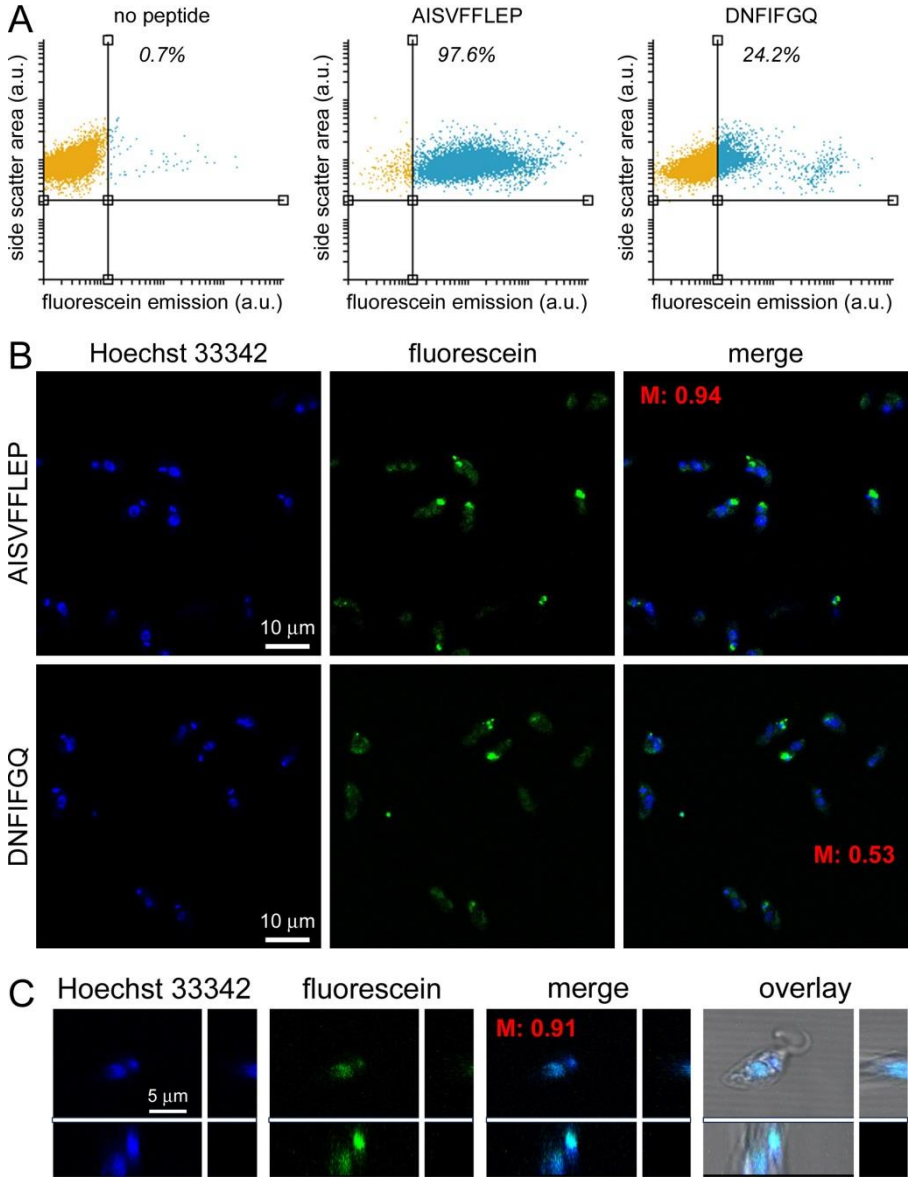

Fig. S2. Characterization of the interaction with *L. infantum* promastigotes of the fluorescein-labeled AISVFFLEP and DNFIFGQ peptides. (A) Flow cytometry analysis of promastigote targeting with 50 µM TFA-disaggregated fluorescein-labeled peptides after overnight coincubation. Percentages indicate the fraction of promastigotes with fluorescein signal above the set threshold. a.u.: arbitrary units. (B) Confocal fluorescence microscopy analysis of the intracellular location of 50 µM TFA-disaggregated fluorescein-labeled peptides after overnight coincubation with live promastigotes. (C) Z-stack image (30 layers) of AISVFFLEP viewed through orthogonal sections (XZ below and YZ on the right). M: Manders' correlation coefficients indicating the fraction of fluorescein-labeled peptide (green fluorescence) co-localized with Hoechst 33342 (blue fluorescence).

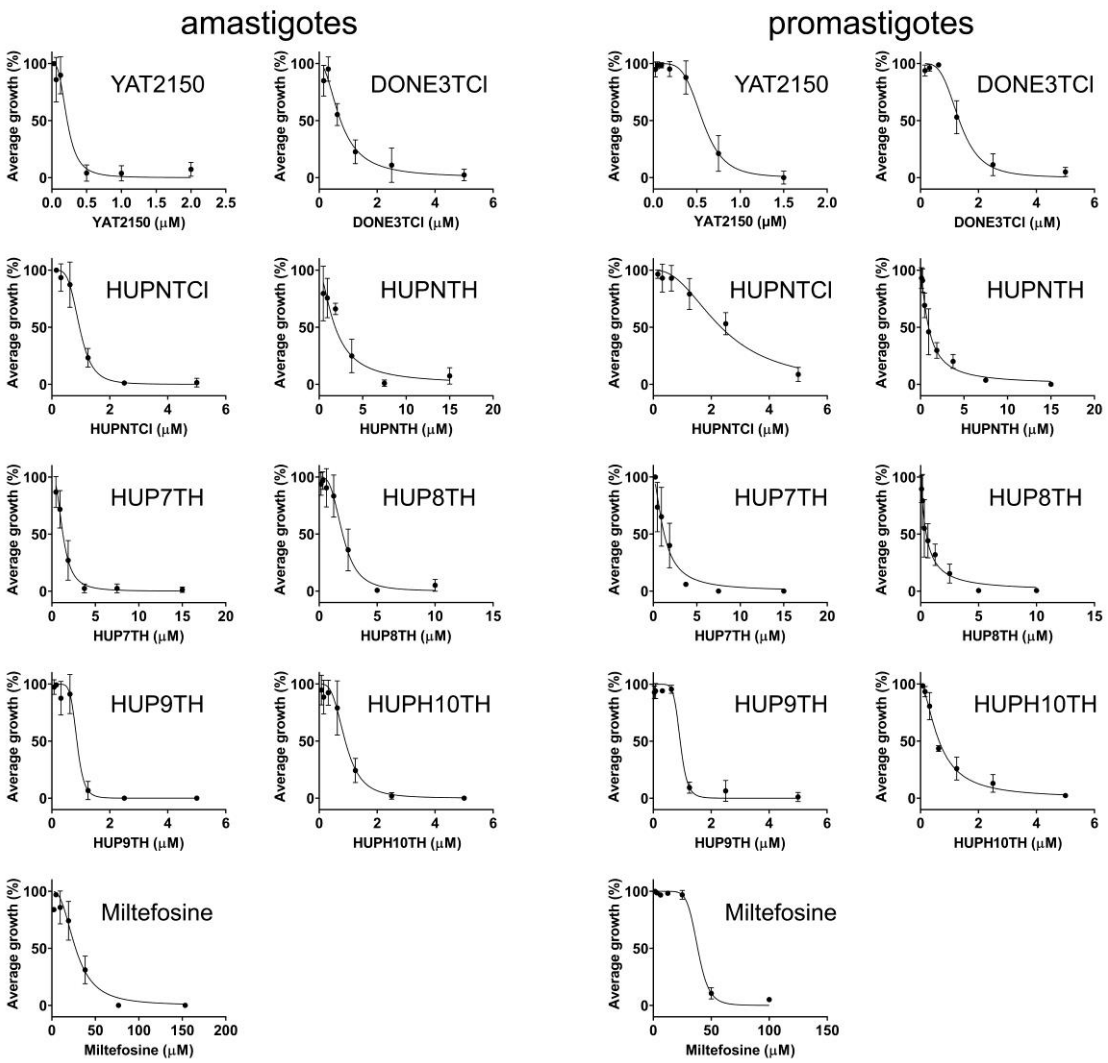

Fig. S3. Dose-response curves of the activity assays in *L. infantum* amastigotes and promastigotes for the compounds whose corresponding data are reported in Table 2.

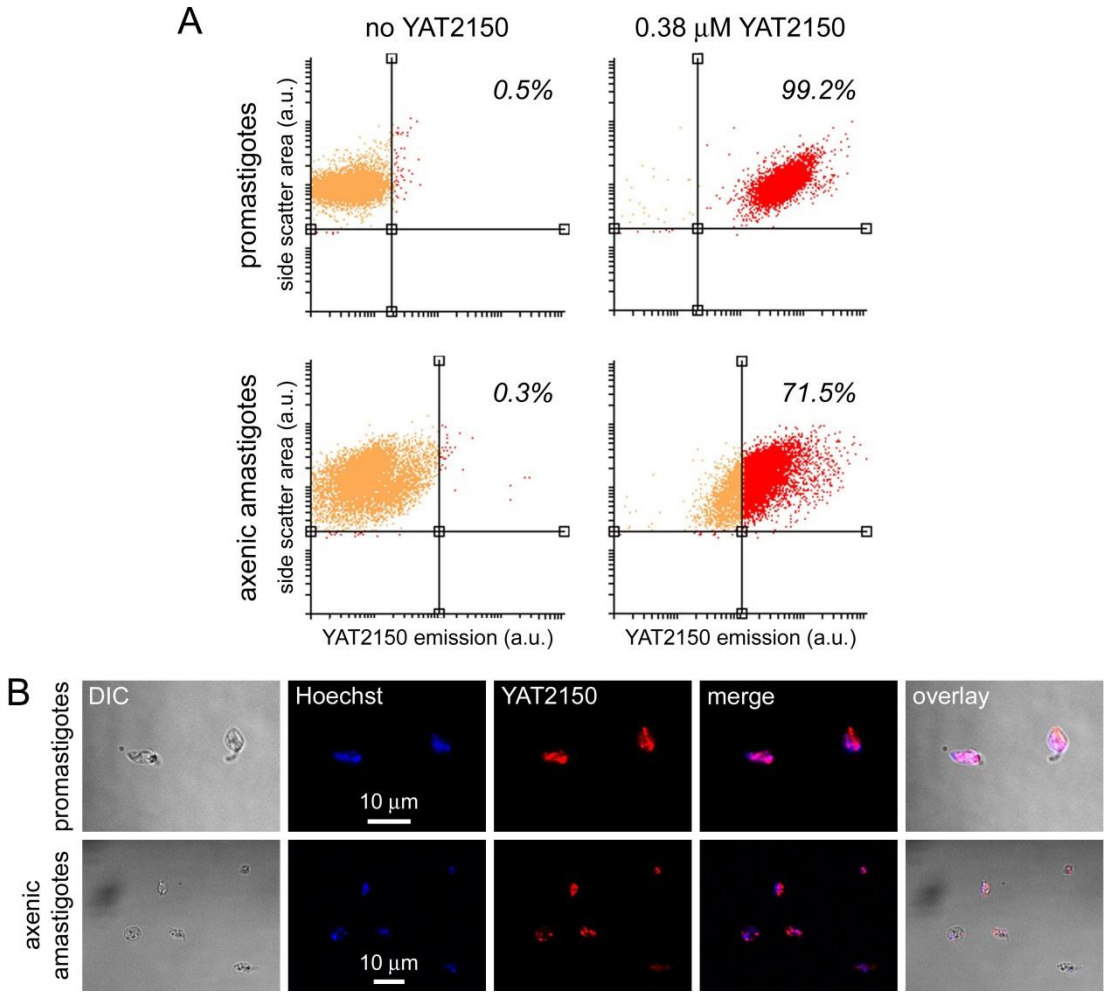

Fig. S4. Binding of YAT2150 to *L. infantum* promastigotes and axenic amastigotes. (A) Flow cytometry analysis of promastigotes and axenic amastigotes exposed for 30 min to 0.38 µM YAT2150. Percentages indicate the fraction of cells above the set YAT2150-positive threshold. a.u.: arbitrary units. (B) Detection by confocal fluorescence microscopy of intracellular protein aggregates in live promastigotes and axenic amastigotes following staining with 0.38 µM YAT2150 for 15 min. DIC: differential interference contrast image.

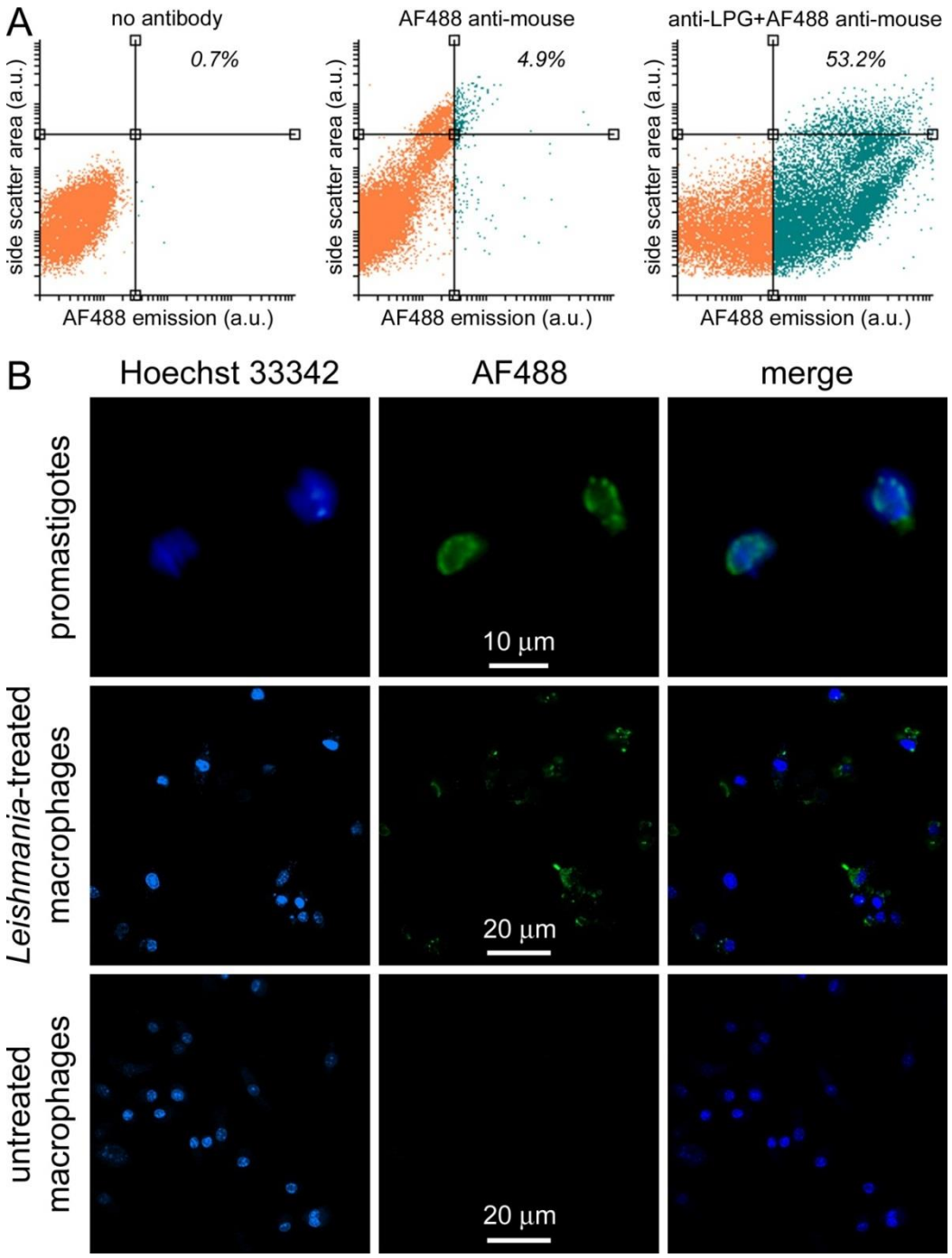

Fig. S5. Detection of *L. infantum* by the commercial anti-LPG monoclonal IgM antibody CA7AE. (A) Flow cytometry analysis of fixed promastigote targeting. Controls include an antibody-free promastigote preparation and a promastigote sample where the primary anti-LPG antibody had been omitted. Percentages indicate the fraction of promastigotes above the set LPG-positive threshold. a.u.: arbitrary units. (B) Fluorescence microscopy analysis of live promastigote and amastigote-infected macrophage targeting, including a control of macrophages not exposed to *Leishmania* and incubated with the anti-LPG antibody (untreated macrophages).

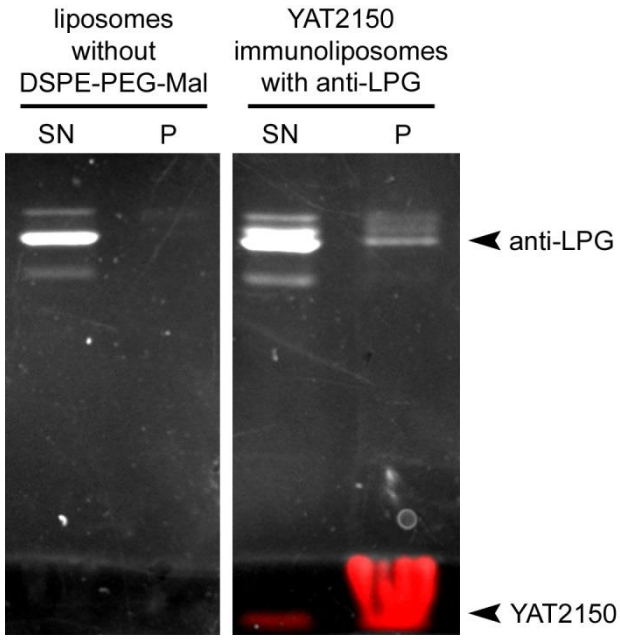

Fig. S6. Immunoliposome characterization. SDS-PAGE analysis of YAT2150-containing immunoliposomes functionalized with anti-LPG monoclonal antibody, compared to control liposomes lacking DSPE-PEG-Mal and subjected to the same experimental procedure. SN: supernatant after ultracentrifugation, P: pellet after ultracentrifugation, taken up in the same volume as the supernatant of PBS containing 10 mM EDTA.

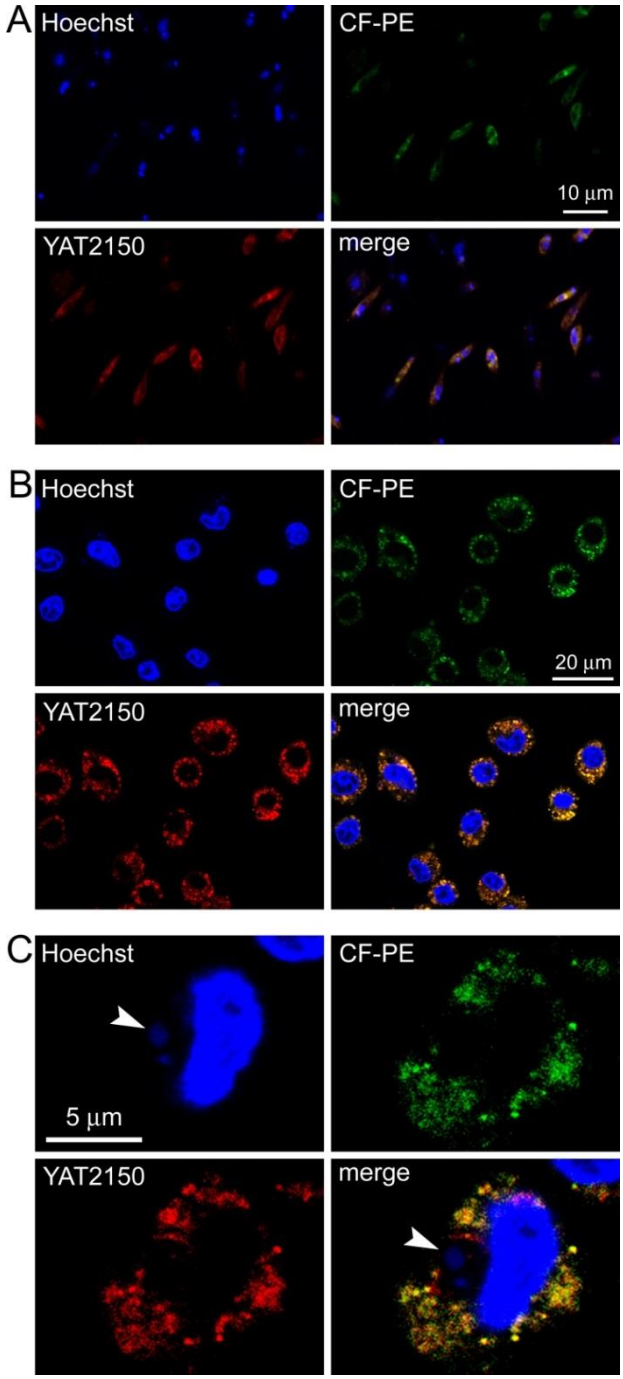

Fig. S7. Confocal fluorescence microscopy analysis of the cell targeting of 0.38 µM YAT2150 encapsulated in fluorescein-labeled liposomes. (A) Live *L. infantum* promastigotes were incubated for 1 h with liposomes, stained with Hoechst 33342, and fixed. (B,C) RAW 264.7 macrophages that had been exposed to *L. infantum* promastigotes were incubated for 3 h with liposomes, stained with Hoechst 33342, and fixed. The green fluorescence corresponds to CF-PE incorporated in the liposome formulation. The arrowhead indicates a *Leishmania* amastigote inside its phagolysosome.

Supplementary Table S1. *L. infantum* proteins insoluble in 0.1% SDS. Membrane proteins are shadowed in grey.

Accession	UniProtKB protein name	Score	Coverage	# Proteins	# Unique Peptides	# Peptides	# PSMs	# AAs	MW (kDa)	pI
A4I4B4	ATP-binding cassette protein subfamily A, member 10	293.68	31.99	1	62	62	128	1866	206.8	6.90
A0A381MFJ0	Plasma membrane ATPase	156.39	30.49	2	29	29	70	974	107.3	5.63
A0A381MS01	Tubulin β chain	128.56	44.47	2	18	18	50	443	49.7	4.82
A4I0B5	Hypothetical protein - conserved	127.54	35.43	1	21	21	52	556	62.5	6.99
A4HY43	ADP,ATP carrier protein 1, mitochondrial	116.48	48.58	1	15	15	51	317	35.1	9.70
A4HUE7	Putative folate / biopterin transporter	113.29	17.29	1	13	13	46	700	76.2	6.67
A4I6P8	H(+)-exporting diphosphatase	103.11	31.21	1	19	19	45	801	83.2	5.25
A0A6L0X265	Tb-292 membrane associated protein-like protein	85.01	46.77	2	23	23	38	2739	304.0	5.19
A4I1M5	Enoyl-CoA reductase, putative	84.65	36.27	1	15	15	36	306	34.1	9.51
A4IBA6	Calcium motif p-type ATPase, putative	80.06	25.70	1	20	20	33	1109	121.8	5.69
A4HRH5	Long-chain-fatty-acid-CoA ligase, putative	73.52	22.10	1	13	13	30	715	77.7	6.57
A4HW91	Hypothetical protein - conserved	71.39	18.99	1	15	15	28	1006	111.5	4.42
A4HSP6	Guanine nucleotide-binding protein subunit β-like protein	69.62	34.07	1	17	17	31	675	75.4	6.80
A0A381MCS3	Tubulin α chain	66.72	45.90	3	18	18	30	451	49.7	5.02
A4IAK2	Coatomer subunit α	65.15	18.98	1	20	20	27	1196	132.6	7.52
A4HW58	Putative kinesin K39	60.33	44.57	2	7	7	22	2926	326.2	4.48
A0A6L0XIU2	Nodulin-like, putative	52.37	19.79	2	9	9	22	672	73.7	7.61
A4I8D8	Putative ribosomal protein L3	50.56	26.97	1	10	10	21	419	47.5	11.05
A4IC24	TPR repeat / tetratricopeptide repeat / uncharacterized protein family (UPF0121)	49.96	31.41	1	10	10	20	382	42.7	9.19
E9AG72	Pteridine transporter (truncated), putative	49.91	20.83	1	10	10	21	653	71.0	7.99
E9AHC1	Putative cysteine peptidase, Clan CA, family C2	40.29	3.43	1	10	11	21	4343	489.5	5.66
A4I9R3	ATP-binding cassette protein subfamily B - member 2, putative	38.83	13.05	1	14	14	17	1341	146.5	6.28
A4HW10	Elongation of fatty acids protein	38.38	13.27	1	3	3	17	294	32.8	8.84
Q9NJS2	Reticulon-like protein	37.67	26.40	1	7	7	17	197	22.1	8.97
A4HWJ3	40S ribosomal protein S3, putative	36.36	42.01	1	8	8	19	219	24.5	9.79
A4HW09	Elongation of fatty acids protein	36.00	18.31	1	4	4	13	284	32.3	9.41
A4I9N9	Uncharacterized protein (fragment)	35.08	14.30	1	7	7	11	1322	144.4	4.70
A0A6L0WSB2	ATP-binding cassette protein subfamily G - member 1, putative	31.52	19.18	3	10	10	12	657	73.2	9.00
A4HW14	Elongation of fatty acids protein	30.91	31.27	1	8	9	15	323	37.2	9.07
A4IB09	Dolichyl-diphosphooligosaccharide-protein glycotransferase	29.83	11.61	4	2	9	13	784	86.9	9.00
A4I059	ATP-binding cassette protein subfamily C, member 1	28.55	8.03	1	2	9	11	1570	173.1	6.71
A4IC65	SPRY domain / HECT-domain (ubiquitin transferase)	28.33	2.22	1	12	12	13	6624	732.7	6.44
A0A6L0X791	Elongation factor 1-α	27.75	29.62	4	9	9	16	449	49.0	8.98
E9AHU4	Dolichyl-diphosphooligosaccharide-protein glycotransferase	26.34	11.60	1	2	9	12	836	92.2	8.59
A4I060	ATP-binding cassette protein subfamily C, member 2	25.49	8.90	1	2	9	11	1562	172.1	7.40
E9AHD7	Amino acid transporter aATP11, putative	22.70	10.60	1	5	5	9	500	55.4	6.54
A0A6L0XP99	Hypothetical protein - conserved	20.88	20.01	1	6	6	8	2804	317.0	4.79
A4I6E4	Cytoskeleton-associated protein CAP5.5, putative	20.27	12.43	1	8	8	9	724	79.9	5.68
A4HWK2	Tryparedoxin peroxidase	19.98	33.67	1	7	7	9	199	22.2	7.15
A4IDZ5	Mkiaa0324 protein-like protein	19.55	14.00	1	7	7	13	500	56.4	12.34
A4I9G8	Delta-12 fatty acid desaturase	19.04	12.94	1	4	4	9	394	45.4	8.03
A4HY18	NADH:ubiquinone oxidoreductase 78 kDa subunit-like protein	18.35	27.91	2	4	4	7	258	28.6	5.01
A4I9L8	Calcium channel protein, putative	18.29	3.01	1	6	6	8	2556	291.2	8.47
A4I8T4	Putative sterol C-24 reductase	18.20	13.10	1	5	5	10	496	58.1	9.14
A4HUD2	Amastin surface glycoprotein, putative	18.10	6.53	1	3	3	8	490	54.3	8.69
A0A6L0Y277	Polyubiquitin, putative	17.97	44.74	5	3	3	8	3040	341.0	7.77

E9AH65	UBA / TS-N domain containing protein, putative	17.76	14.14	1	4	4	6	396	42.9	10.35
A4HW18	Elongation of fatty acids protein	17.53	15.51	1	4	4	8	303	34.4	8.46
A4IAD3	Transmembrane 9 superfamily member	17.10	10.52	1	5	5	7	637	70.7	8.85
E9AGL0	Elongation of fatty acids protein	17.05	15.38	2	3	4	7	299	34.7	8.21
A4HVZ0	Amastin surface glycoprotein, putative	15.42	9.12	2	3	3	7	274	30.3	9.50
A4HWX5	N-terminal region of chorein - a TM vesicle-mediated sorter, putative	15.10	1.31	1	5	5	9	5661	605.6	8.18
A4I9G2	Coatomer subunit β	14.73	6.79	1	6	6	6	884	97.6	5.19
A4IBY3	Mitochondrial phosphate transporter, putative	14.53	24.92	1	7	7	8	317	34.6	9.16
A4I1J0	Protein of unknown function (DUF1295) / phospholipid methyltransferase, putative	14.38	8.56	1	3	3	7	257	28.8	9.86
A4HZQ0	Amino acid permease, putative	14.33	10.72	1	4	4	7	485	53.9	8.00
E9AHT2	Amastin-like protein	14.21	10.43	1	2	2	6	211	23.9	4.54
A4IB10	Dolichyl-diphosphooligosaccharide-protein glycotransferase	13.38	7.43	1	2	5	6	794	88.7	7.28
A0A381MN47	Histone H2A	13.18	25.76	3	3	3	5	132	13.9	10.96
E9AHB8	CDP-diacylglycerol-inositol 3-phosphatidyltransferase	13.04	32.16	1	5	5	7	227	25.3	7.83
A4HSI0	Hypothetical protein - conserved	12.77	6.68	1	3	3	4	779	86.4	7.64
A4I186	Guanine nucleotide-binding protein subunit β-like protein	12.70	6.00	1	4	4	4	1017	109.6	6.79
E9AHM8	Heat shock protein 83-1	12.68	7.43	2	4	4	5	686	78.7	5.21
A4I132	Hypothetical predicted multi-pass transmembrane protein	12.27	12.57	1	2	2	5	175	20.0	9.06
A4HTD0	Cation-transporting ATPase	12.24	8.12	1	7	7	9	1244	139.4	7.28
A4HSE7	Very-long-chain (3R)-3-hydroxyacyl-CoA dehydratase	12.20	22.77	1	4	4	5	224	25.0	9.63
A4I7B9	Phosphatidylethanolamine N-methyltransferase-like protein	11.75	4.81	1	3	3	6	582	66.7	7.94
A4HTE1	N-terminal region of chorein - a TM vesicle-mediated sorter, putative	11.30	2.64	1	5	5	5	2542	276.2	6.37
A4IA88	Lipophosphoglycan biosynthetic protein (Lpg2)	11.14	6.45	1	2	2	4	341	37.2	9.28
A4HW98	Histone H4	11.05	18.00	2	2	2	4	100	11.4	10.55
A4I7K4	ATP-dependent RNA helicase, putative	11.03	6.35	1	3	3	4	614	66.8	8.88
A0A381N054	Glucose transporter, lmGT2	10.68	5.11	1	2	2	4	567	61.2	6.25
A4IAI4	ER membrane protein complex subunit 1	10.42	6.01	1	3	3	6	815	87.0	6.38
E9AGW6	Intraflagellar transport protein 172, putative	10.18	4.83	1	5	5	6	1800	199.8	6.61
A4HYL7	Midasin	10.09	0.91	1	4	4	4	4825	534.6	5.31
A4HWJ9	NAD-specific glutamate dehydrogenase	9.94	6.47	1	5	5	5	1020	115.2	7.77
A4I020	Hypothetical protein - conserved	9.45	4.93	1	3	3	4	730	76.9	8.41
A4HX43	Putative kinesin	9.44	62.26	1	3	3	3	2811	304.9	4.21
A4I3I9	Amastin surface glycoprotein, putative	9.22	7.51	1	3	3	4	519	57.8	9.44
A4HYZ5	40S ribosomal protein S11, putative	9.11	15.60	1	2	2	5	141	16.3	10.89
A4HSH2	ATP synthase F1 - α subunit, putative	8.92	7.67	1	4	4	4	574	62.5	9.72
A4I7T3	Elongation of fatty acids protein	8.36	5.77	1	2	2	3	381	43.1	9.64
A4HWS5	Ankyrin repeats / α/β hydrolase family, putative	8.10	6.87	1	3	3	3	495	56.1	8.40
A0A381MCU2	40S ribosomal protein S4	8.07	7.33	2	2	2	3	273	30.6	10.29
A4I2N6	Calpain-like cysteine peptidase, putative	8.02	1.44	1	5	6	6	6168	701.1	5.33
A4HV14	Pretranslocation protein - α subunit, putative	7.88	12.35	1	4	4	4	486	53.9	8.87
A4IDG6	Inosine-guanosine transporter	7.81	7.41	1	3	3	3	499	54.0	6.89
Q9BHZ6	Elongation factor-1 gamma	7.74	5.45	3	2	2	3	404	46.2	5.49
A4HW07	Elongation of fatty acids protein	7.50	12.14	1	2	2	4	280	31.7	9.03
A4I6K0	Amino acid transporter aATP11, putative	7.31	4.50	1	2	2	3	511	55.9	7.88
A4I194	ABC transporter - mitochondrial, putative	7.23	5.95	1	3	3	4	656	71.6	8.82
A4I115	Transketolase	7.20	4.17	1	2	2	3	671	71.8	6.64

A4I7B1	Iron / zinc transporter protein-like protein	7.04	15.28	1	5	5	6	432	45.4	6.07
A4HTF0	Putative vacuolar-type Ca^{2+}-ATPase (fragment)	7.03	4.41	3	3	3	3	929	101.7	6.38
A4I4G7	Putative ribosomal protein L1a	7.03	7.51	2	3	3	3	373	41.1	11.60
A4HUB4	Putative ribosomal protein l35a	7.01	22.92	1	3	3	3	144	16.4	11.77
A0A499SND2	Amastin (fragment)	6.82	16.39	3	2	2	4	183	19.6	8.69
A4IBZ5	Hypothetical protein - conserved	6.77	2.03	1	3	3	3	1479	161.2	6.54
A0A6L0WK02	Microtubule-associated protein, putative	6.74	46.77	2	2	2	3	1732	195.4	4.78
A4I7V5	Cleavage and polyadenylation specificity factor-like protein	6.49	2.79	1	3	3	3	1542	167.3	6.62
A0A381MVV1	D-isomer specific 2-hydroxyacid dehydrogenase-like protein	6.43	7.16	1	2	2	2	335	36.8	5.63
A4HUB6	Dehydrogenase-like protein	6.31	5.83	1	2	2	2	412	44.9	8.46
A4HW08	Elongation of fatty acids protein	5.74	10.88	1	3	3	4	285	32.3	8.68
A4IE10	Hypothetical protein - conserved	5.73	4.01	1	2	2	2	623	70.2	8.43
A4HY08	Putative pyruvate dehydrogenase E1 component α subunit	5.67	6.08	1	2	2	2	378	42.7	8.18
A4ICH2	Dihydrolipoamide acetyltransferase component of pyruvate dehydrogenase complex	5.49	7.34	1	2	2	2	463	48.6	7.42
A4I4W0	60S ribosomal protein L13, putative	5.37	13.18	1	2	2	2	220	24.7	10.89
A4I4A1	Hypothetical protein - conserved	5.31	6.04	1	2	2	2	364	42.1	9.38
A0A6L0WLW0	Pteridine transporter (truncated), putative	5.31	3.46	1	2	2	2	722	78.9	5.49
A4I1D9	Dynein heavy chain, putative	5.19	1.06	1	3	3	3	4702	536.4	6.55
A4IAM6	Hypothetical protein - conserved	5.17	19.23	1	2	2	2	156	17.1	10.13
A4I5R7	Hypothetical protein - conserved	5.11	0.69	1	2	2	2	3790	408.7	6.39
A4I401	Cytochrome oxidase assembly protein-like protein	5.09	5.54	1	2	2	2	415	46.3	10.18
A4I4W5	ATP-dependent 6-phosphofructokinase	4.81	3.91	1	2	2	2	486	54.0	9.06
A4I0V7	Inhibitor of apoptosis-promoting Bax1, putative	4.78	10.54	1	2	2	3	313	33.1	9.83
A4I5B9	Amastin-like surface protein-like protein	4.49	9.46	1	2	2	2	222	24.5	6.89
A4I1H9	Hypothetical protein - conserved	4.39	0.77	1	2	2	2	2596	277.6	6.74
A4IAU0	40S ribosomal protein S3a-1	4.35	8.71	2	2	2	2	264	30.0	10.29
A4HT92	40S ribosomal protein S9, putative	4.00	8.95	1	2	2	2	190	22.1	10.65
A0A6L0XS88	Calpain-like cysteine peptidase, putative	3.91	16.66	3	2	2	5	4681	539.7	5.12
A4IBE6	*Chlamydia* CHLPS protein (DUF818) / α/β hydrolase family, putative	3.69	10.25	1	3	3	3	400	44.3	8.21
A0A381MBS1	Amino acid permease 24, putative	3.54	4.30	2	2	2	2	488	53.9	6.42
A4I948	ATP-binding cassette protein subfamily D, member 3	2.95	3.28	1	2	2	2	640	71.1	8.98
A4I116	40S ribosomal protein S8	2.90	10.91	1	2	2	2	220	24.9	11.33
A4HW62	Phosphopyruvate hydratase	2.77	6.99	1	2	2	2	429	46.0	5.45
A0A6L0XPU2	Short chain dehydrogenase, putative	2.69	7.69	2	2	2	2	273	29.9	9.06
A4I8A1	Hypothetical protein - conserved	2.57	1.62	1	2	2	2	1361	148.3	7.75
A4HVJ3	Palmitoyltransferase	2.44	4.28	1	2	2	2	607	65.8	5.31
A4HWI7	ATP-binding cassette protein subfamily G, member 4	2.38	4.72	1	2	2	4	741	83.0	6.61
A4I3D7	ER lumen protein-retaining receptor	2.23	15.98	1	2	2	3	219	26.0	9.39
A4HU00	Hypothetical protein - conserved	2.04	3.45	1	2	2	3	1247	132.8	7.59
A4I1Y3	GPN-loop GTPase 2	0.00	14.72	1	2	2	2	326	36.5	4.98

Accession: UniProtKB protein accession number.
Score: Sum of the scores of the individual peptides.
Coverage: Percentage of amino acids found in the analyzed peptides compared to the total number of amino acids in the entire sequence of the protein.
Proteins: The number of identified proteins in a protein group (all proteins that are identified by the same set of peptides).
Unique peptides: The number of peptide sequences unique to a protein group.
Peptides: The number of distinct peptide sequences in the protein group.
PSMs: The total number of identified peptide sequences for the protein.
AAs: The total number of amino acids of the entire sequence of the protein.
MW (kDa): The molecular weight of the protein calculated as the sum of the molecular weight of each amino acid without considering post-translational modifications.
pI: Protein isoelectric point.

Supplementary Table S2. GO enrichment analysis for the dataset of *L. infantum* proteins found in 0.1% SDS-resistant aggregates.

Category	Term	Count	%	*p*-value	Genes	List total	Pop hits	Pop total	Fold enrichment	Bonferroni	Benjamini	FDR
Biological process	Translation	18	19.35	5.19^{-10}	A4HT92, A4HWJ3, A4HYZ5, A4I4G7, A0A381MCU2, A4I116, A4HUB4, A4I4W0, A4IAU0, A4I8D8	34	170	1804	5.62	7.27^{-9}	7.27^{-9}	7.27^{-9}
Cell component	Nucleosome	6	6.45	2.60^{-4}	A4HW98	68	23	2531	9.71	0.004	0.004	0.004
	Ribosome	15	16.13	1.46^{-3}	A4I186, A4HYZ5, A4I4G7, A0A381MCU2, A4I116, A4HUB4, A4HSP6, A4I4W0, A4I8D8		221	2531	2.53	0.025	0.012	0.012
	Small ribosomal subunit	4	4.30	4.19^{-3}	A4HT92, A4HWJ3		13	2531	11.45	0.069	0.024	0.024
Molecular function	Structural constituent of ribosome	18	19.35	2.07^{-8}	A4HT92, A4HWJ3, A4HYZ5, A4I4G7, A0A381MCU2, A4I116, A4HUB4, A4I4W0, A4IAU0, A4I8D8	64	176	3190	5.10	8.5^{-7}	8.5^{-7}	8.5^{-7}
	Protein heterodimerization activity	6	6.45	1.00^{-4}	A4HW98		25	3190	11.96	4.1^{-3}	2.1^{-3}	2.1^{-3}
	ATPase activity, coupled to transmembrane movement of substances	4	4.30	4.60^{-2}	A4I4B4, A4I9R3, A4I948, A4I194		41	3190	4.86	8.5^{-1}	5.3^{-1}	5.3^{-1}
	rRNA binding	3	3.23	5.29^{-2}	A4HT92, A0A381MCU2		19	3190	7.87	8.9^{-1}	5.3^{-1}	5.3^{-1}
	Calcium-dependent cysteine-type endopeptidase activity	3	3.23	7.45^{-2}	A4I6E4, E9AHC1, A4I2N6		23	3190	6.50	9.6^{-1}	5.3^{-1}	5.3^{-1}
	Hydrolase activity	7	7.53	7.72^{-2}	A4HTD0, A4I7K4, A4IBE6, A4IBA6, A4I1Y3, A4I9R3, A4HWS5		152	3190	2.30	9.6^{-1}	5.3^{-1}	5.3^{-1}

Count: Number of gene names involved in a specific annotation term.
%: Genes belonging to an annotation term/total genes in the table.
p-value (probability value): Probability that a null hypothesis happens.
Genes: UniProt accession codes of the "count" belonging to an annotation term.
List total: Number of total genes detected by DAVID for a specific category.
Pop hits (population hits): Genes involved in a specific term from the whole *L. infantum* genome detected by DAVID.
Pop total (population total): The *L. infantum* genome background detected by DAVID in each category.
Fold enrichment: Percentage of genes within the total list annotated for a specific term divided by the percentage of genes annotated for the same term in the background (count/list total)/(pop hits/pop total).
Bonferroni: Bonferroni Šidák *p*-value (2).
Benjamini: Use of the linear step-up method of Benjamini and Hochberg to calculate the adjusted *p*-values (3).
FDR (false discovery rate): Expected proportion of false positives.

Supplementary Table S3. *L. infantum* proteins containing the peptides DNFIFGQ and AISVFFLEP or a part of them, with a minimum threshold of 5 continuous amino acids. Data obtained using the Basic Local Alignment Search Tool from the National Center for Biotechnology Information (https://blast.ncbi.nlm.nih.gov/Blast.cgi) and TriTrypDB (htpps://tritrypdb.org).

Peptide	Part of the peptide	Protein and gene name	Molecular function	Biological process	Cellular component
DNFIFGQ	DNFIFGQ	Beta tubulin (LINF_330015200)	GTPase activity, GTPase binding, structural constituent of cytoskeleton	Microtubule-based process	Microtubule
	FIFGQ	Oligosaccharyl transferase-like protein (LINF_350016300)	Oligosaccharyl transferase activity	Protein glycosylation	Nuclear envelope, ER, membrane
AISVFFLEP	AISVFFLEP	CPSF-like protein (LINF_320019100)	Nucleic acid binding, protein binding	N/A	Nucleus
	SVFFLE	Multi drug resistance protein-like (LINF_240020050)	ATP binding, ATPase-coupled transmembrane activity	Transmembrane transport	Integral component of membrane
	VFFLEP	Permease-like protein (LINF_230009700)	N/A	N/A	Membrane
	FFLEP	Conserved hypothetical protein (LINF_350051200)	Protein binding	N/A	N/A
	VFFLE	Neutral sphingomyelinase activation associated factor-like protein (LINF_230026400)	Protein binding	N/A	N/A
	VFFLE	BRE1 E3 ubiquitin ligase – putative (LINF_330012700)	N/A	Axoneme assembly	N/A
	VFFLE	Phosphate-repressible phosphate permease-like protein (LINF_030009800)	Inorganic phosphate transmembrane transporter activity	Phosphate ion transport	Membrane
	VFFLE	Conserved hypothetical protein (LINF_160008800)	N/A	N/A	N/A
	ISVFF	Conserved hypothetical protein (LINF_060007500)	N/A	N/A	Axoneme
	SVFFL	Dynein heavy chain – putative (LINF_340049400)	ATP binding, minus-end-directed microtubule motor activity	Microtubule-based movement, mitotic spindle organization, chromosome segregation, minus-end-directed vesicle transport along microtubule	Axoneme, dynein complex
	SVFFL	Hypothetical protein – conserved (LINF_300020000)	N/A	N/A	N/A
	SVFFL	Putative phosphatidylinositol 3-kinase 2 (LINF_140005100)	Kinase activity	Phosphatidylinositol phosphate biosynthetic process	N/A
	AISVF	HECT-domain (ubiquitin-transferase) – putative (LINF_340041000)	Ubiquitin-protein transferase activity	N/A	N/A
	AISVF	Enriched in surface-labeled proteome protein 11 – putative (LINF_340018700)	N/A	N/A	Ciliary pocket

N/A: not annotated data.

References

1. Varadi M, Anyango S, Deshpande M, Nair S, Natassia C, Yordanova G, Yuan D, Stroe O, Wood G, Laydon A, Žídek A, Green T, Tunyasuvunakool K, Petersen S, Jumper J, Clancy E, Green R, Vora A, Lutfi M, Figurnov M, Cowie A, Hobbs N, Kohli P, Kleywegt G, Birney E, Hassabis D, Velankar S 2022. AlphaFold Protein Structure Database: massively expanding the structural coverage of protein-sequence space with high-accuracy models. Nucleic Acids Res 50:D439-D444.
2. Šidák Z 1967. Rectangular confidence regions for the means of multivariate normal distributions. J Am Stat Assoc 62:626-633.
3. Benjamini Y, Hochberg Y 1995. Controlling the false discovery rate: a practical and powerful approach to multiple testing. J Roy Statist Soc Ser 57:289-300.

Article 3: Development of DNA aptamers against *L. infantum* GP63 protein

Authors: Lucía Román-Álamo, Daniela Currea-Ayala, Gabriel S. Oliveira, Timen Mooren, Yunuen Avalos-Padilla, Xavier Fernàndez-Busquets

Unpublised

General summary: The study titled "Development of DNA aptamers against *L. infantum* GP63 protein", unpublished yet, investigates the development of ligands that specifically recognize the *Leishmania* parasite, aiming to improve drug delivery systems and diagnostic tools. Aptamers were identified as a cost-effective and stable alternative to antibodies for diagnosing tropical parasitic diseases, including leishmaniasis. DNA aptamers were developed against the major surface protein GP63 of *Leishmania* promastigotes using the SELEX method. After seven SELEX cycles, five aptamer sequences were selected for their high specificity and affinity to the target protein, confirmed through dot blot and flow cytometry analyses. These aptamers demonstrated a strong binding affinity to the endogenous GP63 within promastigote lysates. The findings suggest that these aptamers are promising candidates for developing diagnostic tools and functionalizing drug delivery systems to improve treatments for leishmaniasis.

Development of DNA aptamers against the *L. infantum* GP63 protein

Lucía Román-Álamo [1,2,3], Daniela Currea-Ayala[1,2], Gabriel S. Oliveira[4,5], Timen Mooren[6], Yunuen Avalos-Padilla[1,2], Xavier Fernàndez-Busquets [1,2,7]

[1]Barcelona Institute for Global Health (ISGlobal), Hospital Clínic-Universitat de Barcelona, Barcelona, Spain

[2]Institute for Bioengineering of Catalonia (IBEC), The Barcelona Institute of Science and Technology, Barcelona, Spain

[3]Doctoral School of Biotechnology, Faculty of Pharmacy and Food Sciences, University of Barcelona, Barcelona, Spain

[4]i3S – Institute for Research and Innovation in Health, University of Porto, Porto, Portugal

[5]ICBAS/UP - Institute for the Biomedical Sciences Abel Salazar, University of Porto, Porto, Portugal

[6]Biomedical MRI (BMRI), KU Leuven, Herestraat 49, Leuven, Belgium

[7]Nanoscience and Nanotechnology Institute (IN2UB), University of Barcelona, Barcelona, Spain

Abstract

Leishmaniasis is a disease affecting millions of people around the world produced by a parasite of the genus *Leishmania*. *L. infantum* GP63 (*Li*GP63) protein is one of the main virulence factors of *Leishmania infantum* playing a role in the adhesion of the parasite to the macrophage and survival of the amastigotes. Also is a major surface protein present in *Leishmania* promastigotes. Due to the importance of this protein, DNA aptamers were developed against a *L. infantum* mature form of GP63 (*Li*GP63m) using the systematic evolution of ligands by exponential enrichment (SELEX) method. After 7 cycles, the single stranded DNA sequences were able to target fixed promastigotes, so those sequences were subcloned and 20 were selected. Those 20 aptamers were tested in fluorescence confocal and flow cytometry analysis showing targeting for more than 70% of the fixed promastigotes with 14 aptamers. Following this, dot blot analyses were conducted, leading to the selection of only five aptamers for further characterization through an aptamer-linked immobilized sorbent assay (ALISA) to detect the interaction with the endogenous *Li*GP63. These selected aptamers showed an ability to recognize the isolated protein with a binding affinity in the µM range. Our results suggest that these chosen aptamers have high affinity for *Li*GP63m and can detect the endogenous protein within *L. infantum* promastigotes lysates. Aptamers are cheaper and more stable than antibodies, what make them optimal molecules for places where leishmaniasis is endemic. Those aptamers may have a potential role in diagnostics and as a molecule to functionalize nanoparticles for targeted drug delivery to the parasite.

1. Introduction

Over 20 species of *Leishmania* can infect humans, leading to various clinical manifestations of leishmaniasis. These range from self-healing skin lesions to potentially fatal visceral forms, with disease severity depending on the specific *Leishmania* species and the host immune response. With over 12 million people infected worldwide and an annual incidence of 50,000 to 90,000 new cases of visceral leishmaniasis (VL) and 600,000 to 1 million of cutaneous leishmaniasis (CL), it is still considered a neglected tropical disease [1]. The *Leishmania* life cycle involves two main morphological forms: promastigotes and amastigotes. The flagellated

and mobile promastigote resides within the midgut of certain sandfly species and is transmitted to the vertebrate host through a bite. Inside macrophages and other mononuclear phagocytic cells, the parasite transforms into the non-motile amastigote stage, whose location within phagolysosomes compromises the accession of antileishmanial drugs, requiring long and painful treatment regimens [2]. To overcome this problem, targeted delivery has been reported to ameliorate drug bioavailability, reduce cytotoxicity, expand release kinetics, and improve cellular uptake [3,4]. The functionalization of liposomes with aptamers has been proved to increase targeting to specific cells, ameliorating the efficacy of encapsulated drugs, such as cisplatin [5] or 5-fluorouracil [6]. Single-stranded oligonucleotide DNA aptamers fold into three-dimensional structures capable of binding target molecules or cells with high affinity and specificity [7-9]. Aptamers offer several advantages over antibodies, including smaller size for enhanced tissue penetration, stability at room temperature, non-immunogenicity, and animal-free production, which makes them more cost-effective, scalable, and ethically superior to antibodies. In addition, aptamers can be easily modified to confer them higher resistance to nucleases, extended circulation times, or the potential for incorporating a range of chemical functionalizations for diagnostic [10] and therapeutic uses [11].

The usual diagnosis technique for leishmaniasis is the detection of amastigotes by microscopic examination. For CL this is done in ulcer biopsies, aspirates from the active lesion border, and dermal scrapings, whereas for VL invasive splenic aspirates are required [12]. *Leishmania* antigen detection in serological tests (ELISA, immunofluorescence, Western blot or agglutination analysis) cannot reliably differentiate active from quiescent infection. These tests have low sensitivity and encounter difficulties for their application in most endemic areas, and the humoral response in CL is poor [13]. Antigen detection tests applied to non-invasively obtained fluids are easier to use and cost-efficient. For instance, an agglutination test was able to detect a *Leishmania* carbohydrate antigen in urine [14], and ELISA detection of antibodies against the rK28 antigen for VL diagnosis had a sensitivity similar to the same assay done in serum [15]. The leishmanin skin test is based on a T cell inflammatory reaction when the leishmanin antigen is injected intradermally in the forearm of individuals. It has been widely used in epidemiological studies to detect exposure and immunity to *Leishmania*, and as complementary diagnostic tool for CL in endemic regions of South America. However, it is no longer used nowadays due to the unavailability of leishmanin obtained under good manufacturing practice conditions [16]. Rapid diagnostic tests (RDTs) for leishmaniasis offer varying sensitivity and can be used to complement clinical identification [13]. A RDT, approved by the U.S. Food and Drug Administration, is based on the detection of peroxidoxin, an antigen expressed in both promastigotes and amastigotes, although one study reported that its sensitivity for detecting CL caused by *Leishmania donovani* was only 36% that of PCR [17]. Molecular techniques like PCR are sensitive, but they are not routinely used in the field. To overcome this limitation, a reverse transcriptase loop-mediated isothermal amplification assay has been developed as a point-of-care diagnostic tool able to detect all *Leishmania* species in one test using basic equipment [18].

Several aptamers targeting *Leishmania* proteins have been reported for diagnostic applications. Aptamers binding the *Leishmania infantum* kinetoplastid membrane protein 11 (*Li*KMP-11) [19], involved in parasite mobility, were incorporated into an aptasensor able to detect 2.27 µM *Li*KMP-11 [20]. The *L. infantum*

histones H2A (*Li*H2A) and H3 (*Li*H3) were used to develop specific aptamers against them, which showed a K_D in the nM range [21], although the limits of detection (7,500 parasites for *Li*H2A [22] and 6,000 for *Li*H3 [23]) were too high for diagnostic applications. Aptamers selected against *Leishmania major* promastigotes were employed to assemble a fluorescent enzyme-linked aptamer-magnetic bead sandwich assay, which offered rapid and sensitive detection of promastigote protein extracts in sandfly homogenates [24]. Aptamers developed against the *L. infantum* poly (A)-binding protein, which plays a crucial role in translation, disrupted its interaction with poly(A) tails, representing one of the few examples of the therapeutic potential of aptamers for parasitic diseases [25].

The metalloprotease GP63 is the most abundant protein on the surface of *Leishmania* promastigotes and it is one of the main virulence factors in *L. infantum*, playing a key role in both adhesion of the parasite to the macrophage and survival of the amastigote once internalized [26] (Figure 1). GP63 interacts with fibronectin receptors present on the surface of the host macrophage, which facilitates the adhesion of the parasites and allows for a rapid and efficient internalization [27]. In this work, DNA aptamers against *L. infantum* GP63 have been generated and evaluated for their potential in diagnostic and prophylactic applications.

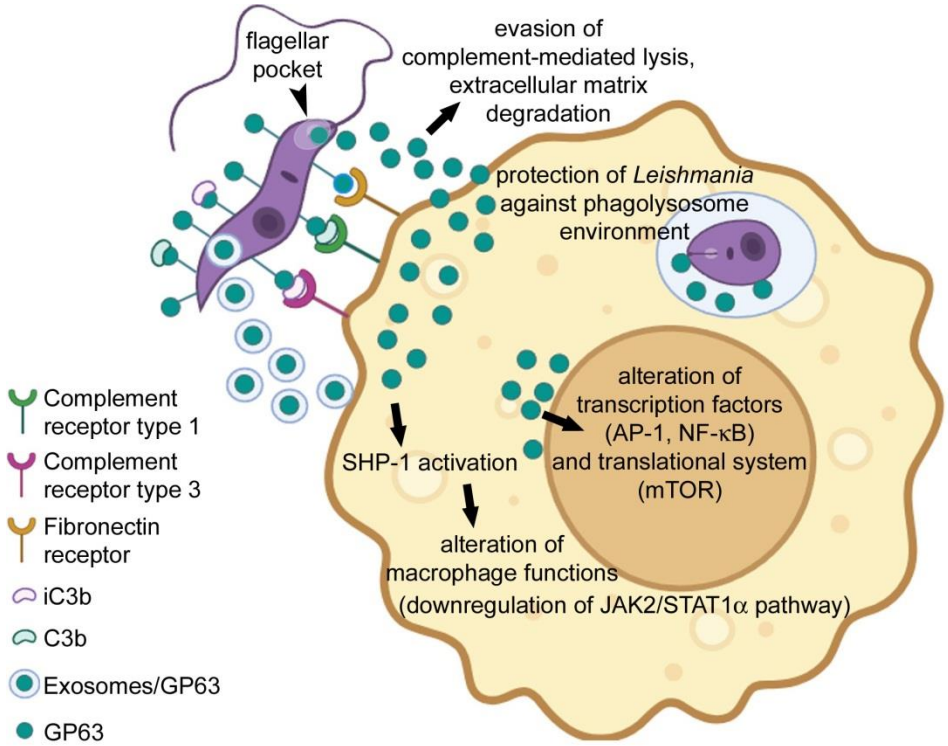

Figure 1. Schematic diagram of GP63 functions. GP63 appears to facilitate the migration of the parasite through the extracellular matrix by degrading its components. It also protects the parasite from complement-mediated lysis by cleaving C3b into iC3b, which can bind to complement receptor type 1 and 3. Additionally, GP63 can bind to macrophage fibronectin receptors, playing a key role in the adhesion of promastigotes to macrophages. GP63 is also secreted from the promastigote either via the classical pathway through the flagellar pocket or via exosomes. It is believed that GP63 enters the macrophage cytoplasm through lipid rafts, where it cleaves and activates some tyrosine phosphatases, such as SHP-1. This activation downregulates some signalling pathways, including JAK2/STAT1α, leading to an alteration in macrophage function. GP63 also affects the transcriptional system (inhibition of the mTOR pathway) and reaches the perinuclear region to alter

transcription factors, such as AP-1 or NF-κB. In the amastigote stage, GP63 is thought to protect the parasite from the harsh phagolysosomal environment. All these functions ultimately aim to protect and promote the survival of the parasite within the host [28,29]. Created with BioRender (https://app.biorender.com/).

2. Results and discussion

2.1 Aptamer Selection against L. infantum GP63

GP63 is encoded by eight genes in *L. infantum* [26], being GP63-2 (LINF_100010200) the isoform used here for aptamer selection. The mature form of *L. infantum* GP63 (*Li*GP63m), spanning from Val97 to Asn574 and lacking the N-terminal propeptide that maintains the enzyme inactive during translation (Figure 2A), was cloned into the pGEX-5X vector and expressed in C41 *Escherichia coli* with a glutathione-S-transferase (GST) tag to facilitate protein purification (Figure S1). GST-*Li*GP63m bound to Sepharose-glutathione beads was used as a target for a bead-based systematic evolution of ligands by exponential enrichment (SELEX) process (Figure 2B). Specific DNA aptamers targeting *Li*GP63m were selected from an initial ssDNA library after several SELEX rounds. The forward primer used for PCR amplification was labelled with 6-carboxyfluorescein (6-FAM), allowing the binding of the aptamer pools to fixed *L. infantum* promastigotes to be tracked by flow cytometry (Figure 2C). The 6-FAM-ssDNA pool from cycle 7 targeted a significantly higher proportion of the promastigote population (65%) than the cycle 2 pool (5%) or the negative control aptamer Apt700 (5%), indicating a significant enrichment in oligonucleotide sequences binding *Li*GP63m in the target cells.

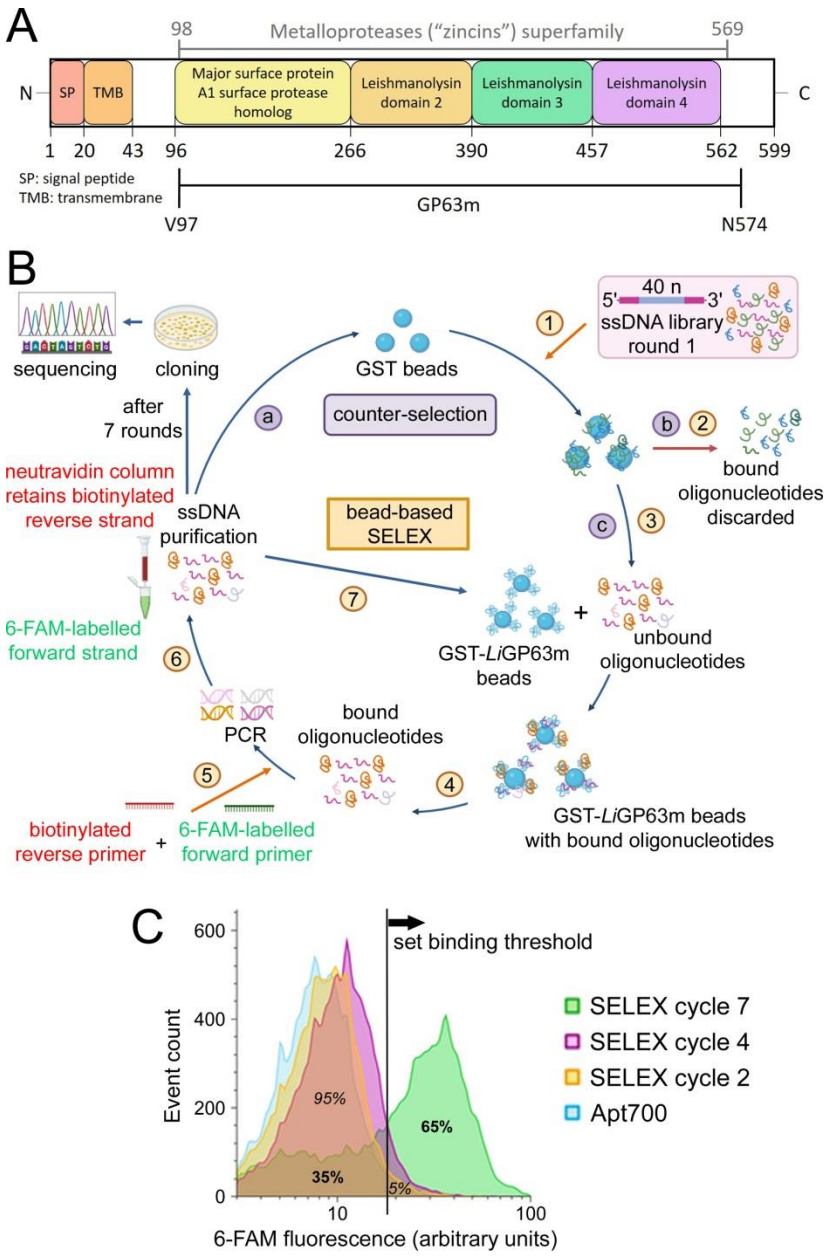

Figure 2. Strategy followed for the selection of aptamers against *L. infantum* GP63. (A) Domain scheme of *L. infantum* GP63-2 indicating the *Li*GP63m region used for aptamer selection. (B) Diagram of the bead-based SELEX process used to obtain aptamers against GST-*Li*GP63m. The methodology involves iterative cycles of: (1) incubation of GST-beads with the initial ssDNA library, (2) removal of the oligonucleotides bound to GST-beads, (3) incubation of GST-beads-unbound oligonucleotides with GST-*Li*GP63m beads, (4) extraction of the oligonucleotides bound to target beads, (5) amplification of the bound oligonucleotides by PCR with reverse and forward primers labelled on their 5' ends with biotin and 6-FAM respectively, (6) purification of the 6-FAM-labelled DNA strand upon retention of the biotinylated strand in a neutravidin column, and (7) incubation of the 6-FAM-labelled ssDNA pool resulting from each SELEX cycle with GST-*Li*GP63m beads, to start a new cycle. Counter-selection (performed every three cycles) is indicated with purple boxes, where (a) the ssDNA purified from one cycle is incubated with GST-beads, (b) ssDNA sequences bound to GST beads are removed, and (c) the unbound sequences are incubated with GST-*Li*GP63m beads to start a new cycle. After 7 cycles, the aptamer pool was cloned and sequenced. Created with BioRender

(https://app.biorender.com/). (C) Flow cytometry analysis of the binding of 6-FAM-labelled aptamer pools from cycles 2, 4 and 7 to *L. infantum* promastigotes. The randomly selected unspecific Apt700 sequence [7] was included as negative control.

2.2. Isolation and Characterization of Individual LiGP63m-Specific Aptamers

After confirming its specificity for the target cells, the enriched oligonucleotide pool from cycle 7 was cloned into the pJET1.2/*blunt* plasmid and used to transform *E. coli* DH5α cells. Twenty colonies were isolated, and their plasmid inserts sequenced (Table 1); the resulting aptamers will be henceforth named *Li*GP63Apt-N, N corresponding to the respective original colonies. To confirm that the aptamers specifically recognised the target protein and not the GST tag, *Li*GP63m was cloned into the pCold™ TF plasmid and expressed in C43 *E. coli* as a 6×histidine-tagged protein fused to trigger factor to increase solubility (henceforth referred to as His-TF-*Li*GP63m). The purified protein was then used in dot blot assays probed with the 20 aptamer sequences synthesized carrying a 6-FAM group in their 5' end (Figure S2A). Different degrees of aptamer specificity were observed according to densitometry analysis (Figure S2B), being *Li*GP63Apt-23, -27 and -28 the sequences with highest recognition efficiency (more than 80%). Afterwards, the aptamer binding affinities for fixed *L. infantum* promastigotes were estimated by fluorescence confocal microscopy (Figure S3) and flow cytometry (Figure S4). All individual aptamers showed targeting to fixed *L. infantum* promastigotes, with binding percentages ranging from 94% to 60% based on quantitative data obtained from flow cytometry analysis. The aptamer ranking, from the highest to the lowest degree of targeting was as follows: *Li*GP63Apt-27>-10>-4>-16>-7>-22>-1>-28>-30>-20>-19>-23>-29>-24>-15>-2>-3>-25>-9>-13). Of the 20 selected aptamers, 14 had a strong likelihood to form G-quadruplexes (G-4), with a G-score [30] ≥38. G-4 are planar arrays of four guanines, each one of them pairing with two neighbour guanines through Hoogsteen bonds, which results in stable secondary structures [31].

Table 1. Twenty aptamers sequenced from the pool obtained after 7 SELEX cycles. In bold font are indicated the PCR primer binding sites. The sequence of the unspecific aptamer Apt700 [7] is included.

Aptamer	Aptamer sequence	G-score
*Li*GP63Apt-1	**ATACCAGCTTATTCAATT**ATCGGGGGTGGCCAGGTGGGAGGGTGGGCGGGTGCTGGTA**AGATAGTAAGTGCAATCT**	42
*Li*GP63Apt-2	T**TACCAGCTTATTCAATT**GCACATAGGGGGATGGGTGGGTGGGGCTATGTGGTTAGGC**AGATAGTAAGTGCAATCT**	41
*Li*GP63Apt-3	**ATACCAGCTTATTCAATT**ACGACCTGACCCAACATCCCGTGCCCCCGTTTAGTAACCG**AGATAGTAAGTGCAATCT**	-
*Li*GP63Apt-4	T**TACCAGCTTATTCAATT**CGTCGGTGGGTGGGTCGGGTGGGGACGAAGTGACGTTTCA**AGATAGTAAGTGCAATAT**	41
*Li*GP63Apt-7	**ATACCAGCTTATTCAATT**ACGGGGACCGTGGGTGGGTGGGGGGGAGGTCCATGGCTTA**AGATAGTAAGTGCAATCT**	42
*Li*GP63Apt-9	**ATACCAGCTTATTCAATT**GCCAGCATATAATAACCGGGCCATACCGCTAACGTCTACC**AGATAGTAAGTGCAATCT**	-
*Li*GP63Apt-10	T**TACCAGCTTATTCAATT**CCATCGGGCGGGGGGGTGGGTAGCATGGAATCAGAGTCGT**AGATAGTAAGTGCAATAT**	42
*Li*GP63Apt-13	**ATACCAGCTTATTCAATT**ATCACAGGCAACACACGCCCGCGGGCTCGCGACGGTAGTGTTG**AGATAGTAAGTGCAATCT**	-
*Li*GP63Apt-15	**ATACCAGCTTATTCAATT**GGGGCGGGCGGGATACGACCTTATTTACCTGCTACTC**AGATAGTAAGTGCAATC**	19
*Li*GP63Apt-16	**ATACCAGCTTATTCAATT**CGGGATGGGTGGGCGGGGGTGGCGGTTCGGTATGGGGCTT**AGATAGTAAGTGCAAATC**	41
*Li*GP63Apt-19	**ATACCAGCTTATTCAATT**CGTGCGGGAGGGTGGTACGGGGTGGGAGGCGGGCTGCTGG**AGATAGTAAGTGCAATCT**	38
*Li*GP63Apt-20	**ATACCAGCTTATTCAATT**ACGGGCGGGGGCGGGCGGGTGGGGTGCGGCAATTCTCTGG**AGATAGTAAGTGCAATCT**	42
*Li*GP63Apt-22	**ATACCAGCTTATTCAATT**ACCGAGGGTGGGGCGGGGGGGCGGGGGAGGAGGAGGTCAGTGCCTCA**AGATAGTAAGTGCAATC**	42
*Li*GP63Apt-23	**ATACCAGCTTATTCAATT**CTGGTGGGGGGGGCAGGGCGGGTCATACTGCATTACTTGG**AGATAGTAAGTGCAATCT**	41
*Li*GP63Apt-24	**ATACCAGCTTATTCAATT**ACCGGGGGGGGAGGGTGGGTCCTGGCGGAAAATGGCGCGG**AGATAGTAAGTGCAATCT**	17
*Li*GP63Apt-25	**ATACCAGCTTATTCAATT**GCTAGGTCACGCACTGGGGTGGGTTGGGTGGGAGTTTACC**AGATAGTAAGTGCAATCT**	-
*Li*GP63Apt-27	T**TACCAGCTTATTCAATT**GCGGGGGGGGGGGGGGGGTGGAGGGGGTTGTAACTGTGAG**AGATAGTAAGTGCAATCT**	80
*Li*GP63Apt-28	**ATACCAGCTTATTCAATT**GTACGCGTGTGGGGGTGGGGGGGCGGGTTCATACGGTGA**AGATAGTAAGTGCAATCT**	42
*Li*GP63Apt-29	T**TACCAGCTTATTCAATT**GACGAGAATCGGGGCGGGCGGGGGGGGTAAGCATGATCGG**AGATAGTAAGTGCAATCT**	42
*Li*GP63Apt-30	**ATACCAGCTTATTCAATT**GTGCAGGGGTGTGGGTGGGTGGGCGGGTACGGCTAAGGGT**AGATAGTAAGTGCAATCT**	42
Apt700	**ATACCAGCTTATTCAATT**AGTTGTGGTTGCAACTTTTTATTATTTGTTCGTATCTTTA**AGATAGTAAGTGCAATCT**	

Among the 20 aptamers from Table 1, five (*Li*GP63Apt-4, -10, -23, -27 and -28) were selected for further analysis those with highest binding affinity to the purified His-TF-*Li*GP63m according to dot blot assays (*Li*GP63Apt-23, -27 and -28), and to *L. infantum* promastigotes according to flow cytometry (*Li*GP63Apt-4, -10 and -27). In dot blot assays (Figure 3), all 5 aptamers detected *Li*GP63 in whole *L. infantum* promastigote lysates and in Triton X-100 extracts, which contain the membrane-associated proteins, in agreement with the expected location of GP63 in the plasma membrane. Accordingly, *Li*GP63 was not detected by any aptamer in RIPA extracts containing cytoskeletal and nuclear proteins. The negative control aptamer Apt700 gave only a weak signal in the whole cell lysate and the Triton X-100 extract, possibly reflecting unspecific interactions with nuclear histones.

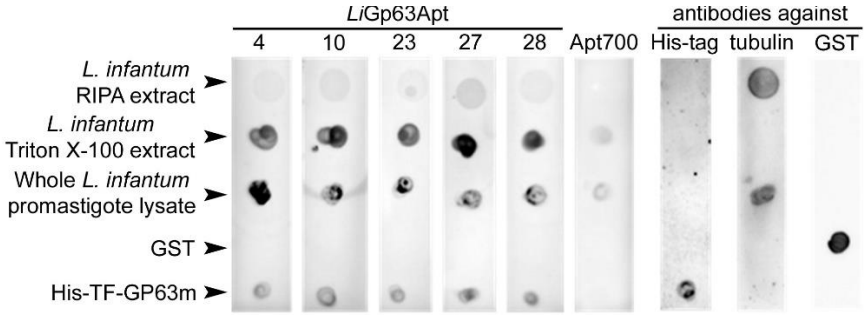

Figure 3. Dot-blot assay to determine the specificity of the selected aptamers towards *Li*GP63. His-TF-*Li*GP63m, GST, *L. infantum* promastigote lysate and TritonX-100 and RIPA extracts were dotted on a nitrocellulose membrane (1.25 µg of protein in 2.5 µL) and incubated with 600 nM of 6-FAM-labelled aptamers or antibodies, whose binding was detected as indicated in the Methods. Apt700 was used as an unspecific aptamer control. Anti-tubulin confirmed the presence of cytoskeleton components in *L. infantum* total lysate and in RIPA extract.

Flow cytometry targeting analysis of the five selected aptamers (Figure 4), showing the specificity of binding to *L. infantum* promastigotes (>75%), correlated well with fluorescence microscopy images (Figure 4) where the negative control Apt700 (1.1% targeting according to cytometry data) did not exhibit any detectable signal, whereas the GP63-specific aptamers offered a strong 6-FAM fluorescence. Remarkably, exposure to different aptamers resulted in different subcellular fluorescence patterns, ranging from a generalized cytoplasmic distribution (*Li*GP63Apt-10 and -27) or a significant membrane association (*Li*GP63Apt-4 and -28) to localization in small perinuclear regions (*Li*GP63Apt-23). This result likely reflected the binding of each individual aptamer sequence to a particular region in *Li*GP63, which might be differently exposed throughout the cell. Although most of GP63 is located on the parasite surface (ca. 75%), a small proportion of it (ca. 1.5%) remains in the endoplasmic reticulum, and the rest is membrane cleaved or exported through vesicles to the extracellular space [26].

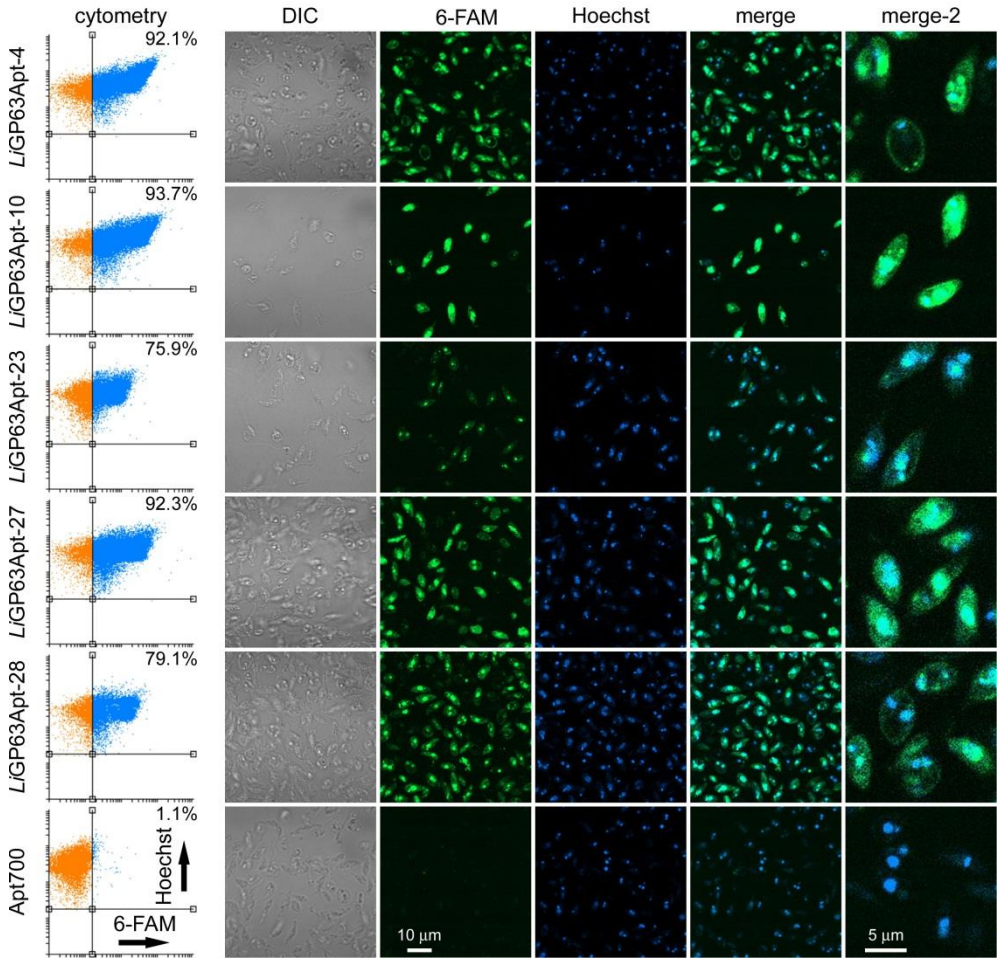

Figure 4. Flow cytometry (first column) and confocal fluorescence microscopy targeting analysis to fixed *L. infantum* promastigotes of the five 6-FAM-labelled selected aptamers. Cytometry panels show arbitrary fluorescence units. Percentages indicate the fraction of promastigotes positive for 6-FAM (upper right quadrant in each panel). DIC: differential interference contrast. Merge refers to Hoechst 33342 and 6-FAM channels only; merge-2 panels are blow-ups of the corresponding merge panels. Scale bar is 10 µm for all microscopy panels, except for those in the last column where it is 5 µm.

2.3. Aptamer Binding Affinity Characterization

The apparent B_{max} and K_D and the binding affinity for *Li*GP63m of the selected aptamers was assessed through the incubation of different concentrations of the 6-FAM-labelled aptamers with a fixed amount of His-TF-*Li*GP63m protein (2.5 µg) bound to latex beads (Figure S5 and Table 2). The aptamer with the highest B_{max} was *Li*GP63Apt-28, indicating that it was able to bind more sites within the protein than the other aptamers, whereas the lowest value for the apparent K_D (i.e., highest affinity) corresponded to *Li*GP63Apt-27, although all five aptamers had K_D values in the one-digit µM range. The aptamer with highest binding affinity (B_{max}/K_D) was also *Li*GP63Apt-27. The K_D value for the unspecific Apt700 is a negative value because of an incorrect fitting of the binding curve data (Figure S5) due to the lack of binding affinity for the His-TF-*Li*Gp63m.

Table 2. Apparent K_D, B_{max} and binding potential (B_{max}/K_D) for the selected aptamers, determined from the data obtained in the experiment reported in Figure S5.

Aptamer	Apparent K_D (µM)	Apparent B_{max} (a.u.)	B_{max}/K_D
*Li*GP63Apt-4	0.65	3187	4903
*Li*GP63Apt-10	0.59	8753	14836
*Li*GP63Apt-23	0.69	14097	20430
*Li*GP63Apt-27	0.27	8399	31107
*Li*GP63Apt-28	2.10	24242	11544
Apt700	–0.03	434	–14467

The limit of detection of the aptamers for their target protein was determined in an aptamer-linked immobilized sorbent assay (ALISA, [32]) through the incubation of a fixed concentration of the selected 6-FAM-labelled aptamers (600 nM) with serial dilutions of His-TF-*Li*GP63m (from 1.8 to 0.11 µg). *Li*GP63Apt-4, -23, -27 and -28 were able to detect down to 0.45 µg of protein (Figure 5A).

As a proof of concept to explore the potential use of the selected aptamers as diagnostic tools, an ALISA was performed with a whole parasite lysate, where the amount of protein was used to determine the corresponding number of promastigotes [22]. Aptamers *Li*GP63Apt-4, -23, -27 and -28 could detect down to 7,500 promastigotes (Figure 5A). In the assayed conditions, the limit of detection of *Li*GP63Apt-10 was 15,000 promastigotes.

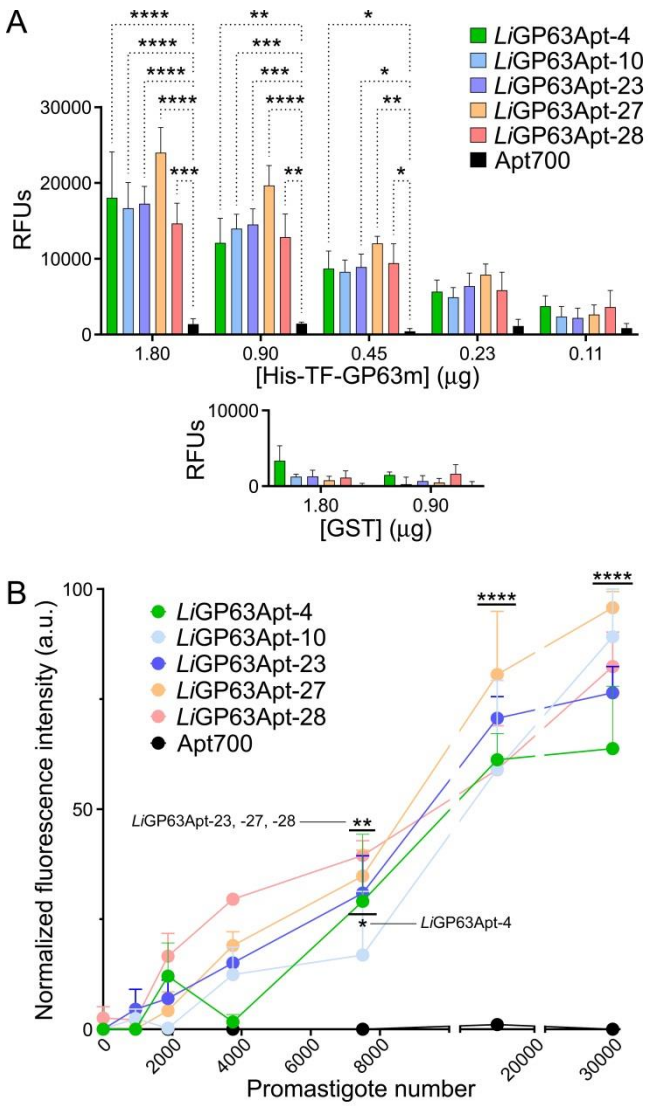

Figure 5. Analysis of the limit of detection of the selected aptamers for *Li*GP63. (A) Sensitivity of the aptamers for the detection of His-TF-*Li*GP63m. The immobilized protein amount varied between 1.8 to 0.11 µg, while the concentration of aptamer was fixed at 600 nM. GST was incubated at the two highest protein concentrations used (1.8 and 0.9 µg) as a negative binding control. RFUs: relative fluorescence units. Average ± SEM of three different experiments is shown. For each His-TF-*Li*GP63m amount, the statistical significance between each aptamer and the unspecific Apt700 was calculated. (B) Sensitivity of the selected aptamers for the detection of *L. infantum* promastigotes. ALISA assays were done with total lysate from *L. infantum* promastigotes that corresponds to a number of parasites ranging from 938 to 30,000. Average ± SEM of three different experiments is shown. Statistical significance was calculated between each aptamer and the unspecific Apt700 (*, p<0.05; **, p<0.01; ***, p < 0.001; ****, p<0.0001).

2.4. Assessment of Aptamers as Targeting Moieties of Liposomes

The aptamers *Li*GP63Apt-4 and -28, which bound *L. infantum* promastigote plasma membranes according to fluorescence microscopy images (Figure 4), were selected to test their potential as targeting elements on liposomes for the improved delivery of encapsulated drugs. Aptamers functionalized in their 5' end with a thiol group were covalently conjugated onto maleimide-containing liposomes. Aptamer binding was assessed

by measurement of the change in zeta potential of liposomes to a more negative value, and by the corresponding detection of DNA bound to them [33] (Table 3). Physicochemical characteristics like size and polydispersity index were maintained, indicating that liposome stability was not affected by the conjugation of aptamers.

Table 3. Determination of size, polydispersity index, zeta potential and DNA concentration of liposome suspensions, containing 5 mM lipid, with and without aptamer functionalization. The values are expressed as the mean ± SD from three different measurements. LP: liposomes.

	Size (nm)	PDI	Zeta potential (mV)	[ssDNA] (ng/µL)
LP	154.70 ± 4.10	0.12 ± 0.01	-7.55 ± 0.26	0.00 ± 0.00
LP- *Li*GP63Apt-4	141.10 ± 1.20	0.13 ± 0.03	-9.90 ± 0.98	41.50 ± 6.50
LP- *Li*GP63Apt-28	114.00 ± 0.60	0.13 ± 0.03	-9.14 ± 1.97	68.50 ± 6.61

3. Conclusions

In this work, we selected five aptamers (Apt4, Apt10, Apt23, Apt27 and Apt28) from the ssDNA sequences pool from cycle 7 of SELEX. These five aptamers had a K_D in the µM range for the protein-aptamer interaction. Furthermore, four of these aptamers could detect endogenous GP63 in whole parasite lysates containing down to 7,500 promastigotes. *Li*GP63Apt-4 and -28 were successfully conjugated with the Maleimide-liposome, what would allow a target delivery of an encapsulated drug in the liposome.

Aptamers represent an attractive tool in biomedical research for diagnostic and therapeutic applications [34]. GP63 has an important role in amastigote survival modulating the response of the host cell [35], and in promastigotes it is the most abundant surface protein [36]. Among its multiple functions in the parasite are participating in the adhesion to macrophages [27], the creation of a favourable environment for *Leishmania* by cleaving numerous host proteins and protecting the pathogen from antimicrobial peptides [37], and the suppression of an efficient immune response [29].

Although no GP63 inhibitors have reached preclinical studies, some of them have shown significant activity, such as Glycoside-2 (IC_{50} of 1.13 µM in *L. donovani* promastigotes [38]), benzimidazole compounds (IC_{50} of 0.62 to 0.92 µg/mL on *L. major* promastigotes [39]), and the 7-hydroxycoumarin derivative L1 compound (IC_{50} of 1.24 µM on *Leishmania amazonensis* promastigotes [40]). By exploiting the proteolytic activity of GP63 for diagnostic approaches, casein was conjugated to gold nanoparticles, which, upon interaction with GP63, enabled the detection of 0.55 *Leishmania* parasites/mL [41]. However, because casein can interact with multiple molecules, developing specific aptamers against GP63 could provide the basis for improved diagnosis of leishmaniasis.

In this context, an interesting option could be an aptasensor wherein an aptamer selectively binds to a *Leishmania*-specific protein, similar to the aptasensor designed for detecting *Plasmodium* lactate

dehydrogenase [42]. In addition, aptamers against GP63 could have a therapeutic application by blocking the interaction between macrophage receptors and promastigote GP63, reducing the internalization of the parasite into the macrophage.

4. Materials and Methods

3.1. Protein Expression and Purification

The region encoding the mature form of *L. infantum* GP63-2 (*Li*GP63m, LINF_100010200), spanning from residue Val97 to Asn574 of the full-length protein, was PCR-amplified from genomic DNA extracted from a *L. infantum* culture with the DNeasy® Blood & Tissue kit (Qiagen, Venlo, The Netherlands), according to the manufacturer's protocol. The selected primers (forward: 5'GAAGGTCGTGGGATCGTCGTGCGCGCCGCGAACTGG3', reverse: 5'GGCCGCTCGAGTCGAGTTGCCGCCGTCCTTGGC3') allowed the cloning of the gene into the *Bam*HI and *Sal*I p*GEX-5X* plasmid using the InFusion cloning system (Clontech, Japan), following the manufacturer's instructions. For GST purification, the empty p*GEX-5X* plasmid was used. After confirming by Sanger sequencing the insertion of the *Li*GP63m gene (1433 bp), C41 *Escherichia coli* competent cells were transformed with either p*GEX-5X* or p*GEX-5X*/*Li*GP63m constructs. The protein expression of GST and GST-*Li*GP63m was induced by adding 0.1 mM isopropyl β-D-thiogalactoside (IPTG) to a transformed C41 *E. coli* culture during the logarithmic growth phase. Following this, the culture was incubated for 16 h at 20 °C in Terrific Broth medium (TB: 24 g/L yeast extract, 20 g/L tryptone, 4 mL/L glycerol, 10% potassium phosphate (0.17 M monobasic, 0.72 M dibasic), 1% glucose) supplemented with 0.1 mg/mL ampicillin. To prepare the cell lysate, bacteria were subjected to sonication in lysis buffer (50 mM tris-HCl, pH 8.0, 300 mM NaCl, 1 mM ethylenediaminetetraacetic acid (EDTA), 1 mM PEFABLOC SC (Roche, Basel, Switzerland), and 2 mg/mL lysozyme), and centrifuged at 16,000× g for 90 min at 4°C to separate the insoluble from the soluble fraction. In the case of GST-*Li*GP63m, as it remained in the insoluble fraction, the protein was extracted from inclusion bodies using two rounds of solubilisation buffer. First, the cell pellet was suspended in buffer 1 (2 M urea, 500 mM NaCl, 2% Triton X-100, 1 mM EDTA, 20 mM tris-HCl, pH 8.0), sonicated (8 min, 30 s on, 30 s off, amplification 80) with a Sonics Materials VCX-130PB Ultrasonic Processor (Thermo Fisher Scientific, Waltham, MA, US) and centrifuged as above. The new resulting pellet was then resuspended in buffer 2 (4 M urea, 500 mM NaCl, 2% Triton X-100, 1 mM EDTA, 20 mM tris-HCl, pH 8.0), sonicated and centrifuged again with the same settings as before. The solubilized protein fraction was dialyzed using Pur-A-Lyzer™ Mega Dialysis Kit (Sigma-Aldrich, St. Louis, MO, US) against decreasing concentrations of urea to allow refolding of the protein. GST and refolded GST-*Li*GP63m were then purified by affinity chromatography using Glutathione Sepharose® 4B beads (Cytiva, Marlborough, MA, US), according to the manufacturer's protocol. Briefly, 500 µL of a 50% washed bead slurry was incubated overnight at 4 °C under gentle stirring with each of the proteins. After this time, beads carrying GST and GST-*Li*GP63m were washed and aliquoted (at, respectively, 2×10^5 and 1×10^5 beads/vial, which bound ca. 21 and 15 µg of protein), and frozen at –20 °C until their use. To confirm the presence and integrity of GST and GST-*Li*GP63m, 10 µL of protein-carrying beads was incubated for 5 min at 95 °C, diluted in Laemmli solution (0.14 M sodium dodecyl sulfate (SDS),

20% glycerol, 10% 2-mercaptoethanol, 3 mM bromophenol blue, 0.125 M tris-HCl, pH 6.8) and resolved in a 10% SDS-polyacrylamide gel electrophoresis (SDS-PAGE; Mini Protean II System, Bio-Rad) stained with Coomassie Blue.

To obtain larger protein amounts for binding affinity characterization, and to have *Li*GP63m with a tag different from GST in order to confirm aptamer specificity, the gene encoding *Li*GP63m was cloned into the pCold™ TF DNA plasmid (Takara Bio, Kusatsu, Shiga, Japan), using the InFusion cloning system, to obtain a 6×histidine-tagged protein (forward and reverse primers used were 5'TACCCTCGAGGGATCCGTCGTGCGCGCCGCGAACTGG3' and 5'TAGACTGCAGGTCGACGTTGCCGCCGTCCTTGGC3', respectively). After confirming the insertion of the gene by Sanger sequencing, C43 *E. coli* competent cells were transformed with the pColdTF-*Li*GP63m construct, and the expression of the protein (His-TF-*Li*GP63m) was induced by the addition of 1 mM IPTG to bacteria cultured in TB medium supplemented with 0.1 mg/mL ampicillin, followed by incubation for 24 h at 15 °C. Cells were lysed by sonication in lysis buffer (500 mM NaCl, 20 mM imidazole, 1 mM PEFABLOC SC, 2 mg/mL lysozyme, 20 µg/mL DNAse I, 1 mM $MgCl_2$, 20 mM sodium phosphate, pH 7.4), and centrifuged (16,000× g, 1 h, 4 °C) to separate the insoluble from the soluble fraction. The His-tagged protein was subsequently purified from the soluble fraction using a HisTrap HP His tag protein purification column (Cytiva) connected to an ÄKTA pure chromatography system (Cytiva). The purified protein was eluted with increasing concentrations of imidazole (up to 500 mM) and positive fractions were buffer exchanged with phosphate buffered saline, pH 7.4 (PBS) using PD-10 desalting columns (GE Healthcare, Chicago, IL, US), and concentrated with an Amicon® Ultra-4, NMWL 10 kDa (Merck, Darmstadt, Germany). Protein aliquots were quantified as described above and maintained at –20 °C until use. The successful expression and purification of the His-TF-*Li*GP63m was corroborated in an SDS-PAGE analysis performed as detailed above.

3.2. Generation of DNA Aptamers against LiGP63m

DNA aptamers against recombinant *Li*GP63m were obtained using the systematic evolution of ligands by exponential enrichment (SELEX) method [43,44], starting from a ssDNA random library pool (DNA Technology A/S, Denmark). Each ssDNA sequence in the pool was 76 bases long (ATACCAGCTTATTCAATTNNNNNNNNNNNNNNNNNNNNNNNNNNNNNNNNNNNNNAGA TAGTAAGTGCAATCT), of which the central 40 were randomised, and the two 18-base ends were complementary to the forward and reverse primers used for PCR amplification, which were tagged at their 5' ends with 6-FAM and dual biotin, respectively. In the first cycle, 10 nmol of DNA library in 1 mL of binding buffer (PBS containing 1 mg/mL of bovine serum albumin (BSA)) were mixed and heated to 95 °C for 5 min and then cooled in ice for 10 min to allow ssDNA folding. The oligonucleotides were then incubated with 2×10^5 protein-free GST-Sepharose beads for 1 h under stirring at room temperature (counter selection). Non-binding sequences were then incubated with 2×10^5 GST-*Li*GP63m-beads in the same conditions. In this case, the non-binding ssDNA present in the supernatant after a centrifugation (500× g, 5 min) were removed. The resulting bead pellet was taken up in 300 µL of binding buffer and incubated at 95 °C for 10 min to release the bound oligonucleotides, which were separated from the beads by centrifugation as above. To regenerate a

sufficient amount of ssDNA for the next SELEX cycle, PCR amplification was performed after each selection using the 2X PCR Master Mix (Thermo Fisher Scientific). The amplified DNA was precipitated by the addition of 0.1 vol of 3 M sodium acetate and 2.5 vol of cold absolute ethanol. After thoroughly mixing, the tubes were stored at –20°C for at least 30 min and centrifuged (20,100× g, 40 min, 4 °C). The resulting pellet was washed with 70% ethanol, centrifuged as before, and the solvent was evaporated with a SpeedVac concentrator (SPD 1010, Savant) for 35 min. The dsDNA was taken up in PBS and quantified in a Nanodrop 2000 (Thermo Fisher Scientific), and the forward single strand was purified in Micro Bio-Spin chromatography columns (Bio-Rad) loaded with High Capacity NeutrAvidin™ Agarose (Thermo Fisher Scientific), which bound the dual-biotin tag in the reverse chain. Following the manufacturer´s instructions, 6-FAM-ssDNA was eluted with 500 µL of 0.1 M NaOH. To neutralize the base, 50 µL of 1 M HCl were added to each elution. The resulting ssDNA was precipitated as above, taken up in 200 µL of binding buffer, and incubated again with 2×10^5 GST-*Li*GP63m-beads to start the next round of selection. The number of GST-*Li*GP63m-beads used from cycle 1 to 3 was 2×10^5, whereas from cycle 4 onwards, a concentration of 1×10^5 beads was used to increase the stringency of the selection. Seven SELEX cycles were performed and a counter-selection with 1×10^5 protein-free GST-Sepharose beads was done every three cycles to remove unspecific binding sequences.

3.3. Selection of Individual Aptamer Sequences

The ssDNA in the oligonucleotide pool obtained after the 7 SELEX cycles was PCR-amplified with unlabelled forward and reverse primers using a high-fidelity *Pfu* DNA polymerase (BioTools, South San Francisco, CA, US). The resulting dsDNA was cloned into the pJET1.2/blunt plasmid according to the manufacturer´s instructions, and transformed into competent *E. coli* DH5α cells (Thermo Fisher Scientific), which were seeded in Luria Broth (LB) containing 100 µg/mL ampicillin agar plates and incubated overnight at 37 °C. Thirty colonies were selected for plasmid extraction and purification using the GeneJET mini-prep kit (Thermo Fisher Scientific), following the manufacturer protocol. The inserts were sequenced by GENEWIZ (Azenta Life Sciences) and the resulting aptamer sequences were analysed with the QGRS Mapper software (https://bioinformatics.ramapo.edu/QGRS/index.php) to predict the presence of G-quadruplexes.

3.4. Confocal Fluorescence Microscopy and Flow Cytometry Analysis

L. infantum promastigotes were fixed with 4% paraformaldehyde (PFA) for 10 min and subsequently washed three times with PBS. Then, 2×10^7 promastigotes were incubated overnight in binding buffer at 4 °C with previously folded 1 µM individual aptamers or 0.2 µM aptamer pools from cycles 2 and 7. To allow a correct pre-folding, aptamers had been incubated in binding buffer as follows: 10 min at 90 °C, 15 min at 5 °C, 8 min at 37 °C and left at 4°C until use. Promastigotes were then washed with PBS, and nuclei were counterstained for 30 min with 4 µg/µL Hoechst 33342 and rinsed with PBS. For confocal fluorescence analysis, samples were placed in 8-well chamber slides (ibidi GmbH, Gräfelfing, Germany), and observed in a Zeiss LSM 800 confocal microscope (Zeiss, Oberkochen, Germany) with a 100×/1.4 oil DIC M27 objective. Hoechst 33342 was excited with a 405 nm diode laser, and 6-FAM with a 488 nm diode laser; emission was collected in the 390-460 and 500-700 nm ranges, respectively. For flow cytometry analysis, samples were diluted 1:25 with PBS, and targeting was analysed in a five-laser LSRFortessa flow cytometer (BD Biosciences, San Jose, CA,

US) in the 20-parameter standard configuration. 50,000 events were recorded, and the promastigote population was selected on a forward-side scattering dot plot. The lasers used to excite Hoechst 33342 and 6-FAM were, respectively, 350 and 488 nm, and the corresponding emissions were collected with 450/50 BP and 525/50 BP nm bandpass filters. An unspecific 6-FAM-labelled aptamer (Apt700, [7]) and parasites stained only with Hoechst 33342 were used as negative controls.

3.5. Dot Blots and Western Blots

L. infantum cultures containing 1.5×10^7 promastigotes/mL in the stationary phase were pelleted by centrifugation (600× g, 3 min), and washed three times in PBS supplemented with 1× cOmplete™ protease inhibitor cocktail (Roche). Promastigote suspensions were diluted 1:100 in 4% PFA and counted in a Neubauer chamber. To obtain a whole parasite lysate, promastigotes were frozen at –80 °C for 24 h and then thawed. In parallel, 200 µL of 1% Triton X-100 in PBS supplemented with 1× cOmplete™ was added to a different promastigote pellet and incubated for 30 min at 4 °C. Then, the samples were centrifuged (20,000× g, 30 min, 4 °C) and the supernatant was recovered (Triton X-100 extract). The resulting pellet was further washed two times with PBS supplemented with 1× cOmplete™ and suspended in 300 µL of RIPA buffer (150 mM NaCl, 1% Triton X-100, 0.1% SDS, 2 mM EDTA, 5% glycerol, 50 mM tris-HCl, pH 9.4) supplemented with 1× cOmplete™. After 15 min of incubation at 4 °C, the sample was centrifuged (20,000× g, 5 min, 4 °C) and the resulting supernatant constituted the RIPA extract. The protein concentration of all the samples was determined with the Pierce BCA Protein Assay Kit. For dot blots, 1.25 or 2.4 µg of protein sample in 2.5 or 5 µL of PBS was deposited onto an Amersham Hybond ECL nitrocellulose membrane (GE Healthcare), and dots were air-dried. The membrane was then blocked overnight with tris-buffered saline containing 0.1% Tween® 20 (TBSt) supplemented with 3% (w/v) skim milk, washed with TBSt, and incubated with 600 nM 6-FAM-labelled pre-folded aptamers for 1 h at room temperature, with gentle stirring. Control membranes were probed with monoclonal mouse anti-His tag (Ref. MAB050, R&D Systems, Minneapolis, MN, US; 1:2,500 dilution in TBSt), monoclonal mouse anti-tubulin (Ref. T9026, Sigma-Aldrich; 1:1,000 dilution in TBSt containing 3% skim milk), and polyclonal goat anti-GST (Ref. GE27-4577-01, Sigma-Aldrich; 1:10,000 dilution in TBSt containing 3% skim milk) antibodies for 1 h at 37 °C. After this time, membranes were washed 3× with TBSt, incubated for 1 h at room temperature with anti-mouse or anti-goat horseradish peroxidase-conjugated secondary antibodies (Sigma-Aldrich Refs. 12-349 and A8919, respectively; both at a1:10,000 dilution in TBSt), and developed with the ECL Prime Western Blotting Detection Reagent (GE Healthcare). The fluorescence of 6-FAM-labelled aptamers and the peroxidase chemiluminescent signal were detected with an ImageQuant™ LAS 4000 image reader (GE Healthcare), using the SYBR green fluorescence filter and the chemiluminescent method, respectively. When required, the density of the dots was quantified using ImageJ software (https://doi.org/10.1038/nmeth.2089). Data was normalized using as reference the intensity obtained with the antibody anti-His tag, which was established as 100% of signal.

For Western blot analysis, 1 and 5 µg, of the purified recombinant GST-*Li*GP63m and His-TF-*Li*GP63m proteins, respectively, were separated in a 10% SDS-PAGE, transferred to a nitrocellulose membrane and

blocked with 5% skim milk dissolved in TBS containing 0.5% Tween 20. Membranes were probed with either anti-GST or anti-His tag, as for dot blot assays.

3.6. Determination of Apparent K_D and Apparent B_{max}

Fifty µg/mL of purified His-TF-*Li*GP63m and GST, in PBS volumes of 4 and 1 mL, respectively, were combined with aldehyde/sulfate latex beads, 4 µm, 4% w/v (Thermo Fisher Scientific) at a concentration of 0.052% (v/v). Following an overnight incubation at 4°C with gentle stirring, beads were pelleted (3× PBS washes, 3000× g, 15 min, 4 °C) and taken up in the original PBS volumes. Subsequently, 50 µL of His-TF-*Li*GP63m-beads (containing 50 µg/mL protein) were incubated with 50 µL of 6-FAM-labelled pre-folded aptamers (seven different dilutions ranging from 2000 to 62.5 nM) overnight at 4 °C with gentle stirring. After one PBS wash, cells were diluted 1:5 in PBS immediately before analysis using a five-laser LSRFortessa flow cytometer, as described above for 6-FAM. Control aldehyde/sulfate latex beads carrying GST were incubated only with the two highest aptamer concentrations, and Apt700 served as an additional negative control. Mean fluorescence intensity was determined using FACSDiva Version 6.1.3 software (BD Biosciences, San Jose, CA, US). The ligand maximum number of binding sites (B_{max}), the concentration that binds to half the receptor sites at equilibrium (K_D), and the ratio between them (binding potential) for the protein-aptamer interactions was obtained by fitting the intensity of specific binding to the aptamer concentration using the equation $Y = B_{max}\,X/(K_D + X)$. GraphPad Prism 9 (GraphPad Software, San Diego, CA, US) was used to generate the saturation curve, with non-linear regression fit for binding analysis, selecting a one-site binding equation.

3.7. Binding Affinity Assays

The aptamer-linked immobilized sorbent assay (ALISA, [32]) was used to determine the limit of detection of the aptamers for the recombinant His-TF-*Li*GP63m and for *Li*GP63 in a whole parasite lysate. His-TF-*Li*GP63m and GST were diluted at 3.6 µg/100 µL carbonate-bicarbonate buffer (pH 9.6), and seven 1:2 serial dilutions were deposited for overnight immobilization at 4 °C in 96-well immunoassay plates with transparent flat bottom (Thermo Fisher Scientific). The volume added per well was 50 µL, and therefore the highest amount of protein in the assay was 1.8 µg. Then, samples were washed three times with PBS containing 0.05% Tween® 20 (PBSt) and subsequently blocked for 1 h at 37 °C with 100 µL/well of PBS containing 3% BSA. In parallel, 6-FAM-labelled aptamers (15 µM) were pre-folded as described above, diluted in PBSt to a concentration of 600 nM, and 50 µL/well were added after removing the blocking solution. After an overnight incubation at 4 °C and two washes with PBSt, the fluorescence emission of 6-FAM was collected at 530 nm using an excitation wavelength of 488 nm (Infinite Nano+ multimode microplate reader; Tecan Trading AG, Männedorf, Switzerland). Binding affinity to whole parasite lysates was done as for His-TF-*Li*GP63m except for the incubation with the aptamers (1 h at room temperature), the number of PBSt washes (3) before fluorescence reading, and the amount of total protein/well (0.11 µg to 3.5 ng, corresponding to ca. 30,000 and 938 *L. infantum* promastigotes, respectively).

3.8. Preparation of Maleimide-Functionalized Liposomes

Liposomes were prepared with the thin lipid film hydration method [45]. Briefly, the lipids (all from Avanti Polar Lipids Inc., Alabaster, AL, US) 1,2-dioleoyl-*sn*-glycero-3-phosphocholine (DOPC), 1,2-distearoyl-*sn*-glycero-3-phosphoethanolamine-*N*-(maleimide(polyethylene glycol)-2000) (DSPE-PEG-Mal), cholesterol, and carboxyfluorescein-phosphatidylethanolamine (CF-PE) (74.5:5:20:0.5 molar ratio), were mixed in chloroform in a glass vial. The thin film obtained following evaporation of chloroform with a nitrogen stream was hydrated in the PBS volume necessary to obtain a final lipid concentration of 10 mM, followed by three rounds of constant vortexing for 2 min, and bath sonication at 35 °C for 3 min. Then, liposomes were extruded through 200 nm polycarbonate membranes with a mini extruder device (Avanti Polar Lipids Inc.) and stored at 4 °C until used. The conjugation of aptamers to liposomes was performed using the thiol-maleimide cross-linking reaction between the maleimide group in DSPE-PEG-Mal and the C6-thiol-modified aptamers (Integrated DNA Technologies, Coralville, IA, US). Prior to conjugation with liposomes, aptamers were subjected to a chemical reduction where 100 µM aptamer was treated with 10 mM dithiothreitol (DTT) for 1 h at room temperature. Then, the solution was passed through a Zeba™ Spin Desalting Column (Thermo Fisher Scientific) to remove unreacted DTT. The purified aptamers (12.5 µM) were pre-folded as described above and conjugated to maleimide-containing liposomes (1:40 aptamer:DSPE-PEG-Mal ratio) by incubation overnight at 4 °C, followed by ultracentrifugation to remove free aptamers from the liposome suspension. The size, polydispersity index and zeta potential of liposomes (diluted 1:100 in PBS) were measured in a Zetasizer NanoZS90 (Malvern Ltd., Malvern, UK). The amount of DNA in aptamer-functionalized liposomes was calculated using a Nanodrop 2000 (Thermo Fisher Scientific), following measurements of 260/280 and 260/230 ratios. Data was normalized using the values obtained for plain liposomes.

5. Reference List

1. World Health Organization. World Health Organization Leishmaniasis Factsheet. https://www.who.int/news-room/fact-sheets/detail/leishmaniasis . 2023. Ref Type: Electronic Citation
2. Bates, P.A.; Rogers, M.E. New insights into the developmental biology and transmission mechanisms of *Leishmania*. *Curr. Mol. Med.* **2004**, *4* (6), 601-609.
3. de Almeida, L.; Terumi Fujimura, A.; Del Cistia, M.L.; Fonseca-Santos, B.; Braga Imamura, K.; Michels, P.A.M.; Chorilli, M.; Graminha, M.A.S. Nanotechnological strategies for treatment of leishmaniasis--a review. *J. Biomed. Nanotechnol.* **2017**, *13* (2), 117-133.
4. Sun, Y.; Chen, D.; Pan, Y.; Qu, W.; Hao, H.; Wang, X.; Liu, Z.; Xie, S. Nanoparticles for antiparasitic drug delivery. *Drug Deliv.* **2019**, *26* (1), 1206-1221.
5. Cao, Z.; Tong, R.; Mishra, A.; Xu, W.; Wong, G.C.; Cheng, J.; Lu, Y. Reversible cell-specific drug delivery with aptamer-functionalized liposomes. *Angew. Chem. Int. Ed. Engl.* **2009**, *48* (35), 6494-6498.
6. Cadinoiu, A.N.; Rata, D.M.; Atanase, L.I.; Daraba, O.M.; Gherghel, D.; Vochita, G.; Popa, M. Aptamer-functionalized liposomes as a potential treatment for basal cell carcinoma. *Polymers (Basel)* **2019**, *11* (9).

7. Lantero, E.; Belavilas-Trovas, A.; Biosca, A.; Recolons, P.; Moles, E.; Sulleiro, E.; Zarzuela, F.; Avalos-Padilla, Y.; Ramírez, M.; Fernàndez-Busquets, X. Development of DNA aptamers against *Plasmodium falciparum* blood stages using cell-systematic evolution of ligands by exponential enrichment. *J. Biomed. Nanotechnol.* **2020**, *16* (3), 315-334.

8. Roca, C.; Avalos-Padilla, Y.; Prieto-Simon, B.; Iglesias, V.; Ramírez, M.; Imperial, S.; Fernàndez-Busquets, X. Selection of an aptamer against the enzyme 1-deoxy-D-xylulose-5-phosphate reductoisomerase from *Plasmodium falciparum*. *Pharmaceutics* **2022**, *14* (11).

9. Ospina-Villa, J.D.; López-Camarillo, C.; Castañón-Sánchez, C.A.; Soto-Sánchez, J.; Ramírez-Moreno, E.; Marchat, L.A. Advances on aptamers against protozoan parasites. *Genes* **2018**, *9* (12), 584.

10. Futane, A.; Narayanamurthy, V.; Jadhav, P.; Srinivasan, A. Aptamer-based rapid diagnosis for point-of-care application. *Microfluid. Nanofluidics* **2023**, *27* (2), 15.

11. Zhou, J.; Rossi, J. Aptamers as targeted therapeutics: current potential and challenges. *Nat. Rev. Drug Discov.* **2017**, *16* (3), 181-202.

12. WHO Expert Committee on the Control of the Leishmaniases & World Health Organization. Control of the leishmaniases: report of a meeting of the WHO Expert Commitee on the Control of Leishmaniases. World Health Organization. 2010. Geneva, World Health Organization. Ref Type: Online Source

13. Burza, S.; Croft, S.L.; Boelaert, M. Leishmaniasis. *Lancet* **2018**, *392* (10151), 951-970.

14. Attar, Z.J.; Chance, M.L.; el-Safi, S.; Carney, J.; Azazy, A.; El-Hadi, M.; Dourado, C.; Hommel, M. Latex agglutination test for the detection of urinary antigens in visceral leishmaniasis. *Acta Trop.* **2001**, *78* (1), 11-16.

15. Ghosh, P.; Bhaskar, K.R.; Hossain, F.; Khan, M.A.; Vallur, A.C.; Duthie, M.S.; Hamano, S.; Salam, M.A.; Huda, M.M.; Khan, M.G.; Coler, R.N.; Reed, S.G.; Mondal, D. Evaluation of diagnostic performance of rK28 ELISA using urine for diagnosis of visceral leishmaniasis. *Parasit. Vectors* **2016**, *9* (1), 383.

16. Carstens-Kass, J.; Paulini, K.; Lypaczewski, P.; Matlashewski, G. A review of the leishmanin skin test: a neglected test for a neglected disease. *PLoS Negl. Trop. Dis.* **2021**, *15* (7), e0009531.

17. De Silva, G.; Somaratne, V.; Senaratne, S.; Vipuladasa, M.; Wickremasinghe, R.; Wickremasinghe, R.; Ranasinghe, S. Efficacy of a new rapid diagnostic test kit to diagnose Sri Lankan cutaneous leishmaniasis caused by *Leishmania donovani*. *PLoS ONE* **2017**, *12* (11), e0187024.

18. Adams, E.R.; Schoone, G.J.; Ageed, A.F.; Safi, S.E.; Schallig, H.D. Development of a reverse transcriptase loop-mediated isothermal amplification (LAMP) assay for the sensitive detection of *Leishmania* parasites in clinical samples. *Am. J. Trop. Med. Hyg.* **2010**, *82* (4), 591-596.

19. Moreno, M.; Rincón, E.; Piñeiro, D.; Fernández, G.; Domingo, A.; Jiménez-Ruíz, A.; Salinas, M.; González, V.M. Selection of aptamers against KMP-11 using colloidal gold during the SELEX process. *Biochem. Biophys. Res. Commun.* **2003**, *308* (2), 214-218.

20. Moreno, M.; González, V.M.; Rincón, E.; Domingo, A.; Domínguez, E. Aptasensor based on the selective electrodeposition of protein-linked gold nanoparticles on screen-printed electrodes. *Analyst* **2011**, *136* (9), 1810-1815.

21. Iborra, S.; Soto, M.; Carrión, J.; Alonso, C.; Requena, J.M. Vaccination with a plasmid DNA cocktail encoding the nucleosomal histones of *Leishmania* confers protection against murine cutaneous leishmaniosis. *Vaccine* **2004**, *22* (29-30), 3865-3876.

22. Martín, M.E.; García-Hernández, M.; García-Recio, E.M.; Gómez-Chacón, G.F.; Sánchez-López, M.; González, V.M. DNA aptamers selectively target *Leishmania infantum* H2A protein. *PLoS ONE* **2013**, *8* (10), e78886.

23. Frezza, V.; Pinto-Díez, C.; Fernández, G.; Soto, M.; Martín, M.E.; García-Sacristán, A.; González, V.M. DNA aptamers targeting *Leishmania infantum* H3 protein as potential diagnostic tools. *Anal. Chim. Acta* **2020**, *1107*, 155-163.

24. Bruno, J.G.; Richarte, A.M.; Phillips, T.; Savage, A.A.; Sivils, J.C.; Greis, A.; Mayo, M.W. Development of a fluorescent enzyme-linked DNA aptamer-magnetic bead sandwich assay and portable fluorometer for sensitive and rapid leishmania detection in sandflies. *J. Fluoresc.* **2014**, *24* (1), 267-277.

25. Guerra-Pérez, N.; Ramos, E.; García-Hernández, M.; Pinto, C.; Soto, M.; Martín, M.E.; González, V.M. Molecular and functional characterization of ssDNA aptamers that specifically bind *Leishmania infantum* PABP. *PLoS ONE* **2015**, *10* (10), e0140048.

26. Isnard, A.; Shio, M.T.; Olivier, M. Impact of *Leishmania* metalloprotease GP63 on macrophage signaling. *Front. Cell. Infect. Microbiol.* **2012**, *2*, 72.

27. Brittingham, A.; Chen, G.; McGwire, B.S.; Chang, K.P.; Mosser, D.M. Interaction of *Leishmania* gp63 with cellular receptors for fibronectin. *Infect. Immun.* **1999**, *67* (9), 4477-4484.

28. Olivier, M.; Atayde, V.D.; Isnard, A.; Hassani, K.; Shio, M.T. *Leishmania* virulence factors: focus on the metalloprotease GP63. *Microbes Infect.* **2012**, *14* (15), 1377-1389.

29. Devsani, N.; Vemula, D.; Bhandari, V. The glycoprotein gp63- a potential pan drug target for developing new antileishmanial agents. *Biochimie* **2023**, *207*, 75-82.

30. Kikin, O.; D'Antonio, L.; Bagga, P.S. QGRS Mapper: a web-based server for predicting G-quadruplexes in nucleotide sequences. *Nucleic Acids Res.* **2006**, *34* (Web Server issue), W676-W682.

31. Gatto, B.; Palumbo, M.; Sissi, C. Nucleic acid aptamers based on the G-quadruplex structure: therapeutic and diagnostic potential. *Curr. Med. Chem.* **2009**, *16* (10), 1248-1265.

32. Taneja, V.; Goel, M.; Shankar, U.; Kumar, A.; Khilnani, G.C.; Prasad, H.K.; Prasad, G.B.K.S.; Gupta, U.D.; Sharma, T.K. An aptamer linked immobilized sorbent assay (ALISA) to detect circulatory IFN-α, an inflammatory protein among tuberculosis patients. *ACS Comb. Sci.* **2020**, *22* (11), 656-666.

33. Alshaer, W.; Hillaireau, H.; Vergnaud, J.; Ismail, S.; Fattal, E. Functionalizing liposomes with anti-CD44 aptamer for selective targeting of cancer cells. *Bioconjug. Chem.* **2015**, *26* (7), 1307-1313.

34. Li, L.; Xu, S.; Yan, H.; Li, X.; Yazd, H.S.; Li, X.; Huang, T.; Cui, C.; Jiang, J.; Tan, W. Nucleic acid aptamers for molecular diagnostics and therapeutics: advances and perspectives. *Angew. Chem. Int. Ed. Engl.* **2021**, *60* (5), 2221-2231.

35. Olivier, M.; Gregory, D.J.; Forget, G. Subversion mechanisms by which *Leishmania* parasites can escape the host immune response: a signaling point of view. *Clin. Microbiol. Rev.* **2005**, *18* (2), 293-305.

36. Schlagenhauf, E.; Etges, R.; Metcalf, P. The crystal structure of the *Leishmania major* surface proteinase leishmanolysin (gp63). *Structure* **1998**, *6* (8), 1035-1046.

37. Gurjar, D.; Kumar, P.S.; Bodhale, N.; Lenka, N.; Saha, B. *Leishmania* intercepts IFN-γR signaling at multiple levels in macrophages. *Cytokine* **2022**, *157*, 155956.

38. Chakrabarti, A.; Narayana, C.; Joshi, N.; Garg, S.; Garg, L.C.; Ranganathan, A.; Sagar, R.; Pati, S.; Singh, S. Metalloprotease Gp63-targeting novel glycoside exhibits potential antileishmanial activity. *Front. Cell. Infect. Microbiol.* **2022**, *12*, 803048.

39. Shaukat, A.; Mirza, H.M.; Ansari, A.H.; Yasinzai, M.; Zaidi, S.Z.; Dilshad, S.; Ansari, F.L. Benzimidazole derivatives: synthesis, leishmanicidal effectiveness, and molecular docking studies. *Med. Chem. Res.* **2013**, *22*, 3606-3620.

40. Moreno, C.J.G.; Farias, H.M.; Medeiros, R.; Brito, T.; Oliveira, J.; de Sousa, F.L.J.; de Medeiros, M.J.C.; Amorim, B.; Santos-Gomes, G.; Pontes, D.; Rocha, H.A.O.; Frazao, N.F.; Silva, M.S. Quantum biochemistry screening and *in vitro* evaluation of *Leishmania* metalloproteinase inhibitors. *Int. J. Mol. Sci.* **2022**, *23* (15).

41. Diouani, M.F.; Ouerghi, O.; Belgacem, K.; Sayhi, M.; Ionescu, R.; Laouini, D. Casein-conjugated gold nanoparticles for amperometric detection of *Leishmania infantum*. *Biosensors (Basel)* **2019**, *9* (2).

42. Lee, S.; Song, K.M.; Jeon, W.; Jo, H.; Shim, Y.B.; Ban, C. A highly sensitive aptasensor towards *Plasmodium* lactate dehydrogenase for the diagnosis of malaria. *Biosens. Bioelectron.* **2012**, *35* (1), 291-296.

43. Sefah, K.; Shangguan, D.; Xiong, X.; O'Donoghue, M.B.; Tan, W. Development of DNA aptamers using cell-SELEX. *Nat. Protoc.* **2010**, *5*, 1169.

44. Wu, J.; Wang, C.; Li, X.; Song, Y.; Wang, W.; Li, C.; Hu, J.; Zhu, Z.; Li, J.; Zhang, W.; Lu, Z.; Yang, C.J. Identification, characterization and application of a G-quadruplex structured DNA aptamer against cancer biomarker protein anterior gradient homolog 2. *PLoS ONE* **2012**, *7* (9), e46393.

45. MacDonald, R.C.; MacDonald, R.I.; Menco, B.P.; Takeshita, K.; Subbarao, N.K.; Hu, L.R. Small-volume extrusion apparatus for preparation of large, unilamellar vesicles. *Biochim. Biophys. Acta* **1991**, *1061* (2), 297-303.

.

6. Supplementary material

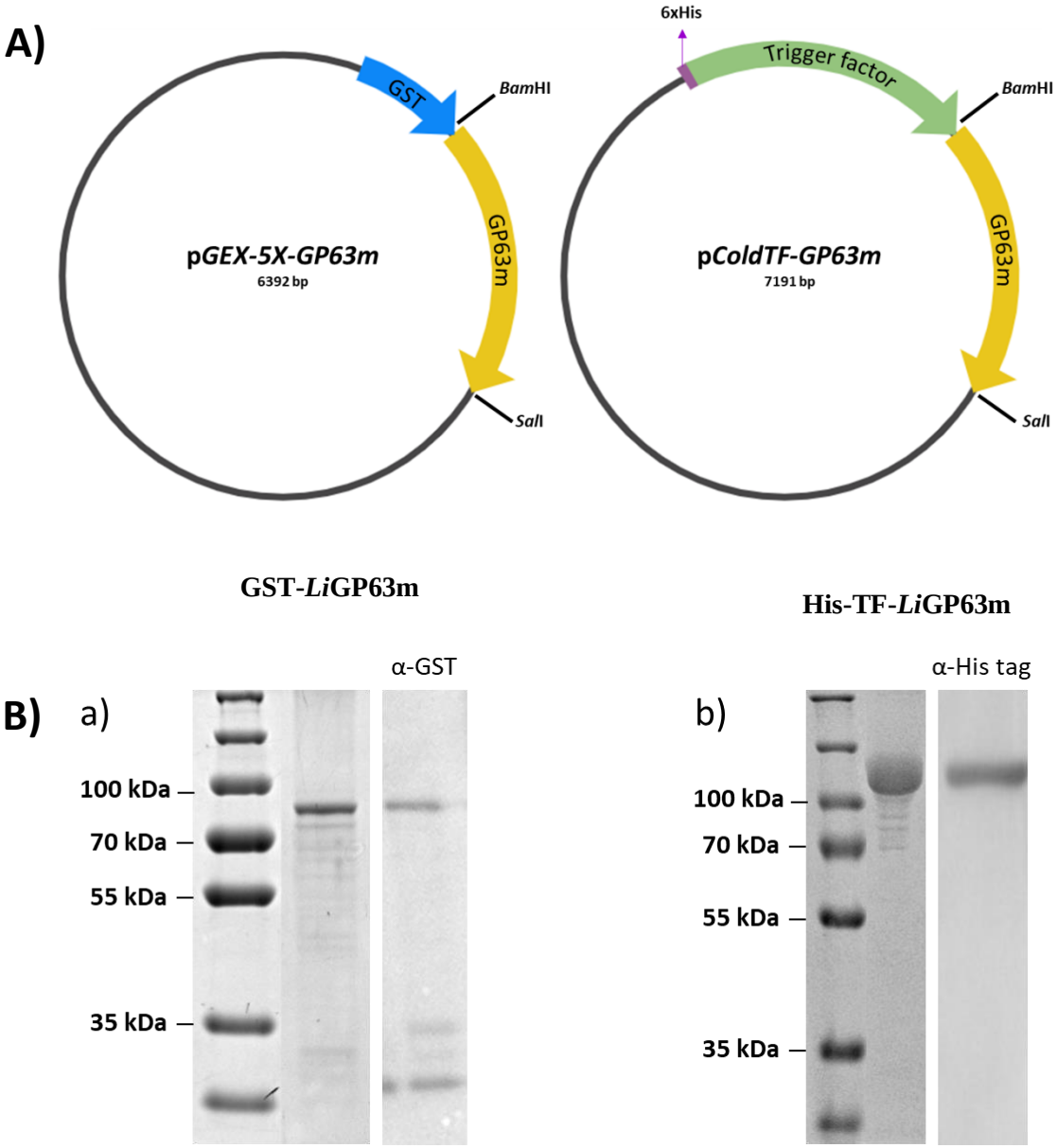

Figure S1. Expression of *Li*GP63m protein. A) Scheme of p*GEX-5X* and p*ColdTF-GP63m* plasmids containing the *GP63m* gene. Created with BioRender (https://app.biorender.com/). B) Expression and purification of *Li*GP63m and Western blot validation. Left panels: SDS-PAGE gels stained with Coomassie showing purified fractions of GST-*Li*GP63m bound to Sepharose glutathione-beads after its induction in C41 *E. coli* transformed with p*GEX-5X* containing the *Li*Gp63m gene; and His-TF-*Li*GP63m after its expression in C43 *E. coli* transformed with the pColdTF-*Li*GP63m construct and its purification with AKTA pure chromatography system. The right panels show Western blot assays using the antibodies α-GST and α-His tag. The molecular weight of GST-*Li*GP63m is 77 kDa (51 kDa from GP63m and 26 kDa from the GST-tag) and the TF-*Li*Gp63m, 103 kDa (51 kDa from GP63m and 52 kDa from the His-TF-tag).

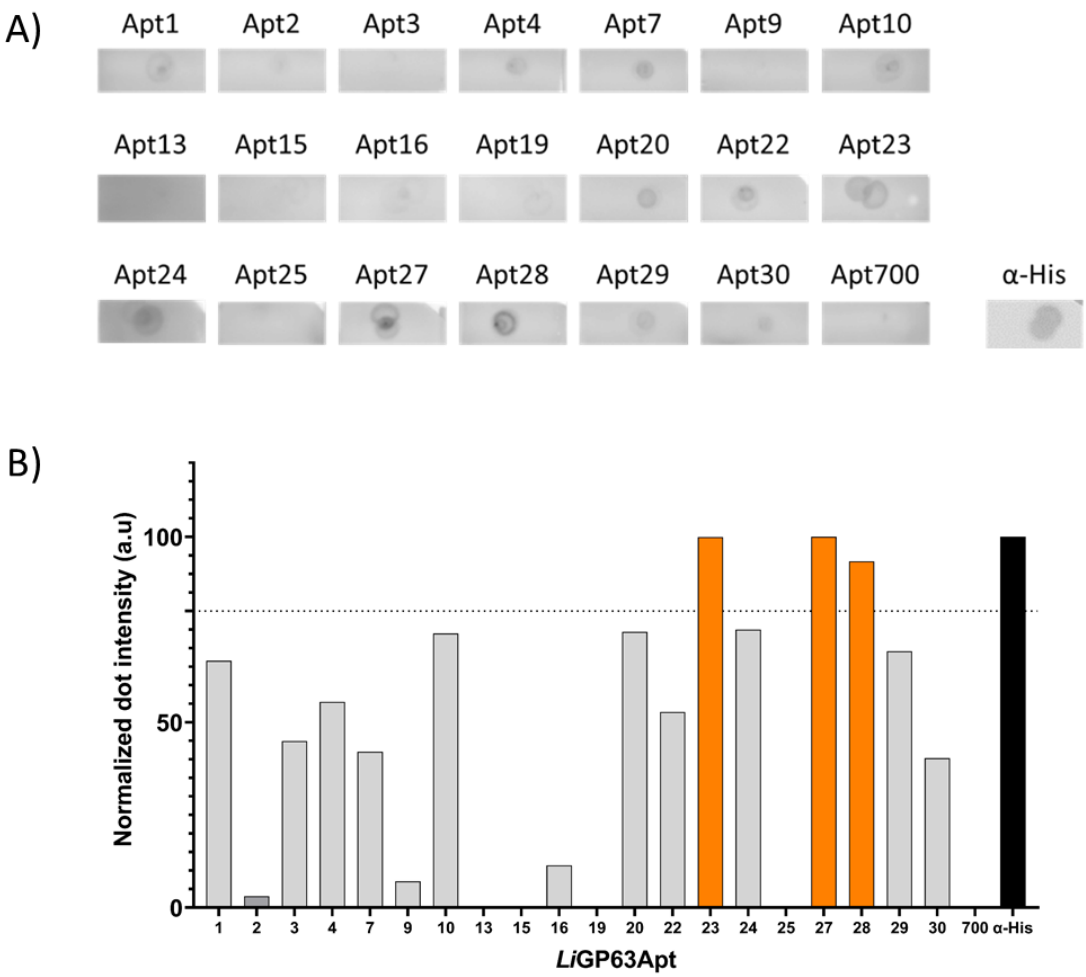

Figure S2. Binding affinity of the individual aptamer sequences for His-TF-*Li*Gp63m by dot blot analysis. A) Dot blot test. 5 µL containing 2.4 µg of His-TF-*Li*Gp63m were dotted on a nitrocellulose membrane, subsequently blotted with 600 nM of each 6-FAM labelled aptamer or with a dilution (1:2500) of an antibody α-His tag overnight. B) The results were quantified with ImageJ (https://doi.org/10.1038/nmeth.2089) by measuring each dot intensity and normalize the data establishing the dot intensity from α-His tag as 100%.

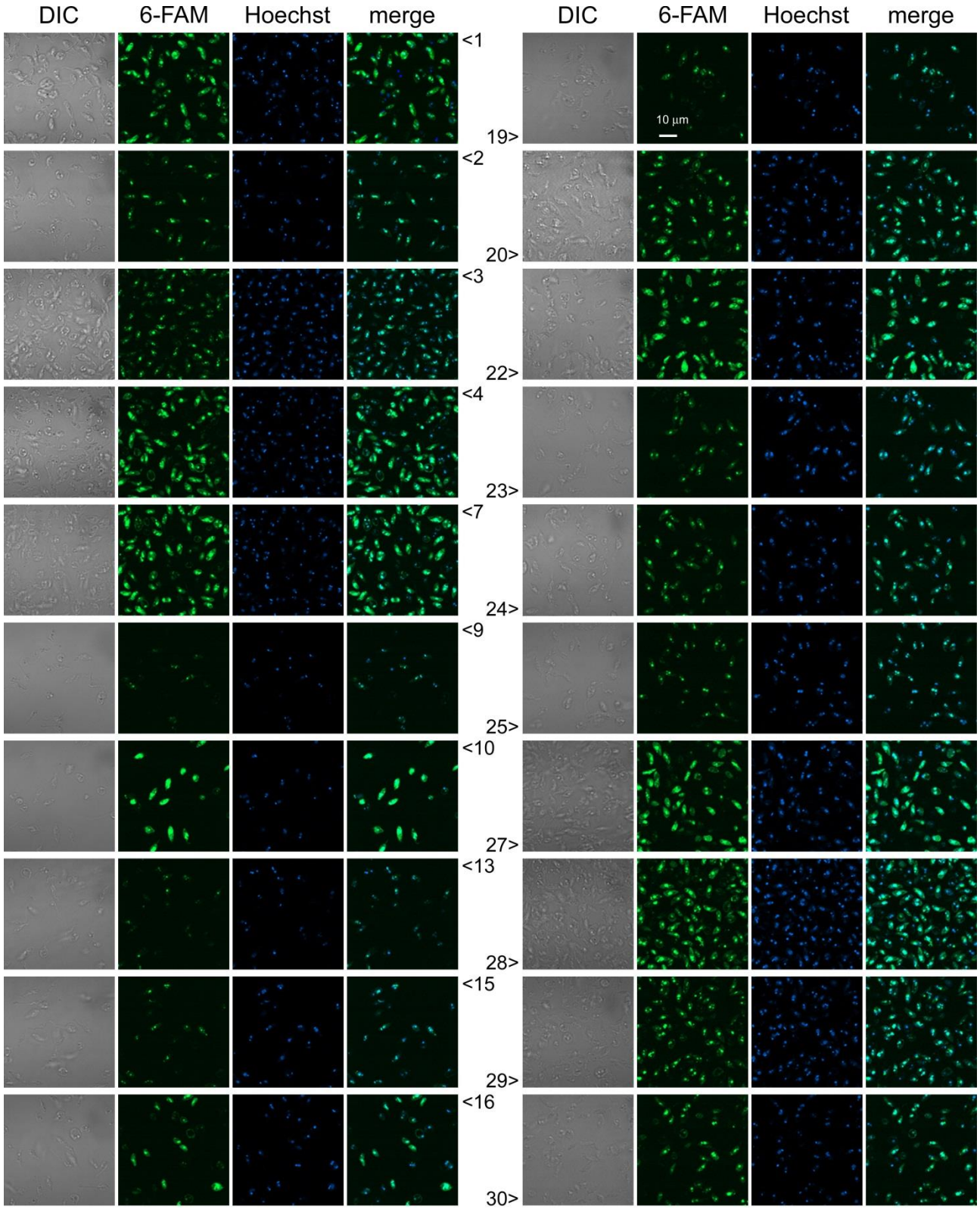

Figure S3. *L. infantum* promastigotes fixed and stained with a 6-FAM-labelled aptamers. Promastigote nuclei was stained with Hoechst 33342 (blue). Merge refers to aptamers-fluorescein and nuclei signals, while Overlay refers to the superimposition of merge on the DIC image. Scale bar: 10 µm. DIC: differential interference contrast image.

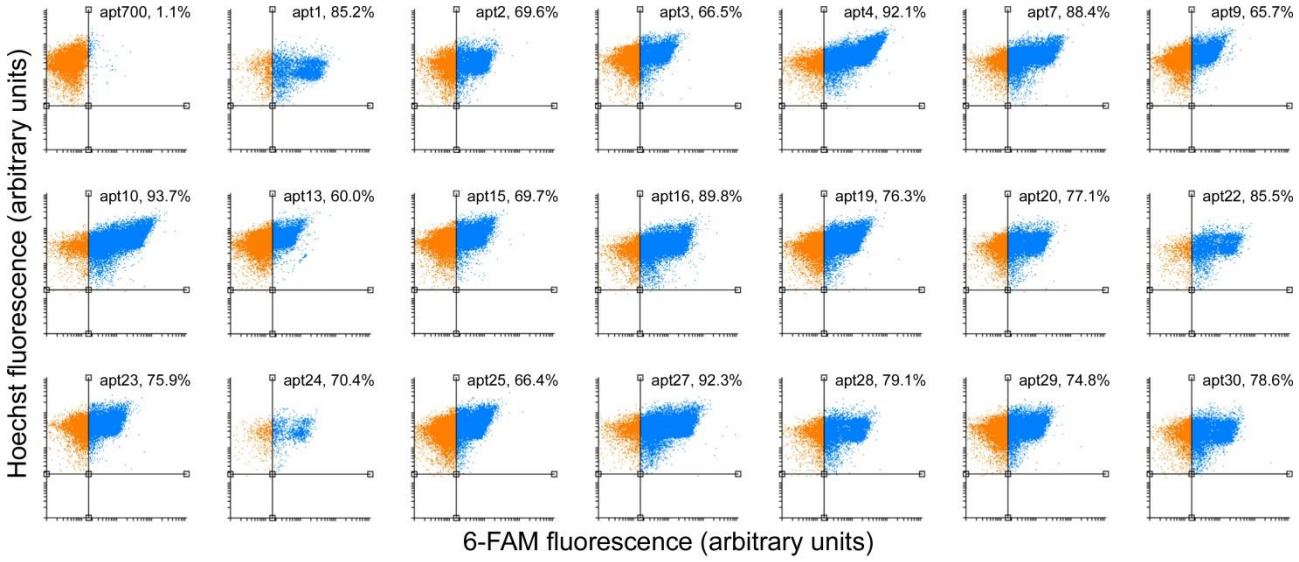

Figure S4. Flow cytometry analysis to quantify aptamers targeting to *L. infantum* fixed promastigotes during an overnight incubation. Apt: aptamer.

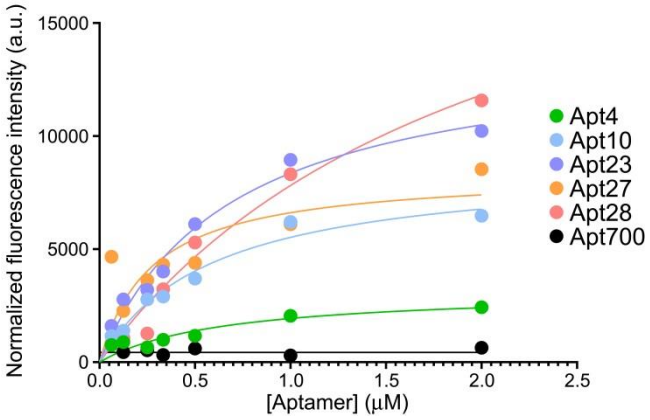

Figure S5. Aptamer binding affinity characterization. The His-TF-*Li*Gp63m protein amount was fixed at 2.5 µg, while the concentration of the aptamer varied between 2.0 and 0.06 µM.

Discussion

This work has been motivated by the urgent need of developing improved drug alternatives for the treatment of leishmaniasis, addressing these challenges (Ghorbani & Farhoudi, 2017; Sundar & Singh, 2018b):

- Drug resistance
- Nonspecific toxicity and side effects
- Concerns associated with parenteral administration
- Limited drug availability and high costs of specific formulations

Three approaches were taken to tackle these issues: (1) optimizing existing drug formulations, (2) developing novel therapeutic options and (3) developing ligands for functionalization of drug delivery systems or for potential early diagnosis.

Optimizing existing drug formulations: In vitro evaluation of aerosol therapy with pentamidine loaded liposomes coated with chondroitin sulfate or heparin for the treatment of leishmaniasis

The first strategy consisting of optimizing existing drug formulations was implemented through the utilization of nanotechnology, which enables the design of drug delivery systems for targeting to *Leishmania* parasites (Sundar & Singh, 2018b). Specifically, in the first article **"*In vitro* evaluation of aerosol therapy with pentamidine loaded liposomes coated with chondroitin sulfate or heparin for the treatment of leishmaniasis"** (PMID: 37111648), we encapsulated pentamidine into liposomes, a nano-drug delivery system. It has been previously observed that nano-drug delivery systems enhance the pharmacokinetic properties, efficacy, bioavailability, and tolerability of potent antileishmanial agents. Simultaneously, they can reduce toxicity and release drugs in a controlled way (Akbari et al., 2017). The final application of liposomes would depend on their composition, determined by factors such as the type and proportion of phospholipid utilized, liposome size, surface charge, and the incorporation of specific ligands to enhance targeting (Nsairat et al., 2022). To increase liposome targeting, pentamidine-loaded liposomes were coated with chondroitin sulfate or heparin, two glycosaminoglycans known to interact with molecules from the midgut of the sand fly vector (Martins et al., 2018) and/or the host macrophages (F. Wu et al., 2018).

The key points of the paper are:

a) Liposomes coated with heparin or chondroitin sulfate showed a significant reduction in the IC_{50} against *L. infantum* and *L. pifanoi* promastigotes. On the other hand, the capacity of liposomes to accumulate in the mononuclear phagocyte system represents an interesting property for passively targeting the infected macrophages, where *Leishmania* amastigotes reside within the phagolysosome (A. K. Agrawal & Gupta, 2000). After three hours of incubation, pentamidine-loaded liposomes targeted approximately 40% of macrophages. However, when coated with heparin or chondroitin sulfate, the targeting fraction increased to ca. 85% and 90%, respectively, as determined by flow cytometry. This improved targeting did not translate in a lower *in vitro* IC_{50} in *L. infantum* amastigotes when pentamidine was encapsulated. This observation could be due to difficulties for the drug in entering the phagolysosome once inside the macrophage. An important point to highlight is the fact that although a targeting molecule might enhance macrophage uptake, naked liposomes were efficiently internalized by macrophages, a finding confirmed by flow cytometry and confocal microscopy. This finding is relevant, because it illustrates that macrophages engulf liposomes, regardless of whether there is a specific receptor involved. This feature will likely makes challenging for the parasite to evolve resistance against liposomes, making them promising drug delivery systems (Unciti-Broceta et al., 2015). To tackle drug resistance challenges, nanoparticle usage proves highly effective, as it requires less drug dosage to achieve the same effect than with the free drug.

b) Liposomes are known for reducing the toxicity profile of the encapsulated drug (Date et al., 2007). In our case, trying to design the more biocompatible option, we focused on two points: (1) the chosen phospholipid to form liposomes was the Phospholipon® 90G (P90G), which is a natural phospholipid from soybean; (2) the liposome solution was prepared using a green and scalable methodology, avoiding the use of organic solvents, such as chloroform, so that avoiding the potential toxicity that these solvents could have if they are not correctly removed. The reduction of unspecific toxicity when pentamidine was encapsulated into liposomes was confirmed in human umbilical vein endothelial cells.

c) With the exception of miltefosine, the only oral FDA-approved drug against *Leishmania* (Aronson et al., 2017), the administration of antileishmanial drugs

typically occurs intramuscularly or intravenously in repetitive doses. This administration route is painful and the drug regimens are long, ranging from days to weeks (WHO Regional Office for Europe, 2017). Trying to deliver the pentamidine-liposomes in a more patient-friendly way, the nebulization of these formulations was explored using a Next Generation Impactor, a model that mimics the human airways. The nebulization of pentamidine-liposomes resulted in a higher percentage of pentamidine recovered from the lower stages of the impactor with mass median aerodynamic diameter <5 mm (68%), compared to the free drug (53%). Moreover, the mass median aerodynamic diameter decreased from 2.8 µm to ca. 1.6 µm when pentamidine was encapsulated, which may be translated into a better ability to potentially reach the lung alveoli. This represented a promising advancement in the development of formulations for the optimized administration of antileishmanial drugs. Regarding pentamidine, it is important to note that this drug is used to treat pneumonia caused by *Pneumocystis carinii* and *Pneumocystis jiroveci* under the brand name Nebupent, when delivered as an oral inhalation solution. Considering the success of this commercial formulation administered via inhalation using a nebulizer, there's promise in adapting pentamidine-loaded liposomes into an aerosolized solution because the small size of the liposomes designed (below 100 nm) would facilitate the uptake by macrophages, amplifying the pentamidine therapeutic impact (Ahsan et al., 2002). Moreover, the designed liposomes are composed of soybean phosphatidylcholine (P90G), while the main component of the lung surfactant is dipalmitoylphosphatidylcholine, appearing to be an optimal option for lung delivery, since they will be well-tolerated and well-absorbed by the lung tissue, as observed in previous studies with soya phosphatidylcholine liposomes (Taylor & Newton, 1992). Furthermore, the deposition of the largest droplets in the upper and central airways could effectively target and eliminate *Leishmania* in cases of MCL infection, where the parasites are located in the mucosa of the upper respiratory tract. This innovative approach presents an alternative solution for managing this challenging manifestation of the disease. Although some rare cases of mucosal leishmaniasis caused by *L. infantum* have been reported (WHO, 2010), further experiments are needed to test the efficacy of pentamidine-loaded liposomes

on the *Leishmania* species that commonly cause MCL, such as *L. braziliensis* and *L. panamensis*.

d) The best example of a liposomal drug for treating leishmaniasis is Ambisome®, commercialized by Gilead (FDA, 2008). However, in some endemic countries, Ambisome® is employed as the first-line treatment for VL only in specific cases, such as pregnancy, due to its expensive cost and the requirement for a cold chain, which represents a challenge (Somali Federal Government Ministry of Health and WHO, 2012). We utilized P90G, a natural and cost-effective lipid, instead of other pure lipids such as DOPC or DSPC, which are approximately 600 times more expensive. Thus, the formulations presented in this work could constitute a good alternative to address the high costs attributed to liposomes. The evaluation of the physicochemical properties of pentamidine-loaded liposomes showed a small size below 100 nm, as observed through cryo-TEM analysis, a polydispersity index below 0.3, which indicates a uniform liposome population (Zhang & Wang, 2023), and a zeta potential above 30 mV. High zeta potential values will translate into an electric repulsion, which may prevent particle aggregation, thereby leading to a stable liposome dispersion (Jain & Thareja, 2019). The formulations remained stable for at least two months when stored at 4°C in solution, a prolonged period for a solution-based formulation.

The encapsulation of pentamidine into the proposed liposomes is a promising antileishmanial formulation for an aerosol administration. However, for further *in vivo* experiments, it would be interesting to consider the lyophilization of the formulations to enhance their stability even further. Although the physicochemical characteristics of pentamidine-encapsulating liposomes are good, they can change depending on the medium (e.g., the zeta potential may vary depending on the ion concentration in the medium or the pH). This should be taken into account when designing future eventual *in vivo* tests.

Developing novel therapeutic options: Effect of the aggregated protein dye YAT2150 on *Leishmania* parasite viability

The second strategy explored in this Thesis to improve the current chemotherapy to treat leishmaniasis is developing novel therapeutic options. In the second article **"Effect of the aggregated protein dye YAT2150 on *Leishmania* parasite viability"** (PMID: 38349159) we built on a previously published work from

our group where a compound belonging to a novel class of antiplasmodials inhibited the growth of the malaria parasite with an IC_{50} of 90 nM (Bouzón-Arnáiz et al., 2022).

The key points of this second paper are:

a) YAT2150, the main component of the commercial aggregated protein dye ProteoStat, was initially employed to identify intracellular protein aggregates in *L. infantum*. YAT2150 stained the promastigote and amastigote stages of the parasite, which suggested the presence of abundant aggregated proteins in *L. infantum.* Then, we isolated *L. infantum* proteins insoluble in 0.1% SDS, which are mostly aggregation-prone. After gene ontology (GO) analysis, one of the most enriched categories in the molecular function section was RNA-binding proteins (ca. 20% of the *L. infantum* proteins insoluble in 0.1% SDS). This fact aligns with the findings found in other organisms (Van Der Lee et al., 2014), such as *P. falciparum* (Pallarès et al., 2018). Among the 0.1% SDS-insoluble *L. infantum* proteins, two endogenous peptides with a high propensity for amyloidogenicity were selected based on the WALTZ amyloid prediction method and their exposure to solvent according to the AlphaFold structural model. These two peptides were DNFIFGQ and AISVFFLEP from the β chain of tubulin and from the cleavage and polyadenylation specificity factor (CPSF)-like protein, respectively, and formed amyloid fibrils *in vitro*, as evidenced by TEM visualization and Thioflavin T fluorescence analysis. Once this was confirmed, the two peptides were incubated with the parasite with the aim of associating with the endogenous peptides within the parasite and reaching a sufficient seed concentration to induce amyloid formation and, eventually have a visible aggregation-associated phenotype. Although, in fluorescence confocal analysis it was observed that the peptides were inside the parasite, they did not have any effect on the parasite viability. Therefore, we conclude that this strategy was not valid as a potential treatment. However, it would be interesting to explore alternative approaches to induce protein aggregation in the parasite, such as the overexpression of aggregation-prone peptides, which has been shown to be effective in plants, where a visible phenotype was observed when aggregated-prone regions were overexpressed (Betti et al., 2016).

b) Following the alternative strategy of inhibiting protein aggregation, YAT2150 demonstrated its capability to inhibit the *L. infantum* growth with a lower IC_{50}

(ca. 0.5 µM for promastigotes and amastigotes) than most currently used antileishmanial drugs (Román-Álamo et al., 2023). This fact, presents an opportunity for the treatment of co-infections involving malaria and leishmaniasis, a public health problem since at least 38 countries are at risk of co-infection (Ornellas-Garcia et al., 2023). To prove if YAT2150 would be a suitable option for the treatment of a leishmaniasis and malaria co-infection, further experiments using a co-infection murine model of *Plasmodium* and *Leishmania* like the proposed in the Pinna R.A. et al study (Pinna et al., 2016) will be required.

c) In the Roadmap for Neglected Tropical Diseases 2021-2030 designed by the WHO, it is emphasized that, among the necessary actions, there is a critical need to monitor resistance and increase the treatment options to address resistance more effectively (WHO, 2020). The emergence of antimony resistance is particularly pronounced in the Indian subcontinent, where treatment failure rates exceeding 60% have been observed in VL caused by *L. donovani*. Additionally, second-line options such as amphotericin B are currently facing resistance, or are expected to face it, as laboratory studies have shown that *Leishmania* can develop resistance against them (Capela et al., 2019; Ponte-Sucre et al., 2017). Aligned with the WHO recommendations, YAT2150 represents a compound from a novel chemical family for which no other antileishmanial drugs have been identified thus far. Its presumed mode of action, inhibiting protein aggregation in the parasite, has been validated in *P. falciparum* (Bouzón-Arnáiz et al., 2022) and *L. infantum*, potentially targeting multiple proteins. Furthermore, beyond this mechanism, in *Leishmania major,* YAT2150 rapidly decreased ATP levels, indicating either an alternative antileishmanial mechanism or a consequence of the previously described inhibition of protein aggregation. These characteristics (especially the presumed targeting of multiple proteins) suggest that developing resistance against this compound might be challenging for the *Leishmania* parasite. Further experiments testing the efficacy of the compound against different *Leishmania* species and drug-resistant strains are required to gauge the potential contribution of YAT2150 to the control and elimination of leishmaniasis.

   With the aim of reducing the eventual development of resistance and shortening the treatment duration for VL, different clinical trials on combination therapies

by different sponsors such as WHO, DNDi or Doctors Without Borders Spain have been carried out, mostly in India and East-Africa. In some of the studies, the multidrug therapies have been effective, leading to changes in the antileishmanial regimen recommendations, such as the combination of pentavalent antimonials and paromomycin in east Africa (van Griensven et al., 2024). However, there is a need to incorporate new chemical compounds for novel combinations. The encapsulation of YAT2150 into liposomes and immunoliposomes functionalized with an antibody against LPG, significantly improved its selectivity index to above 100. Liposomes are suitable nanocarriers for drug delivery since they are able to encapsulate hydrophilic and hydrophobic compounds in the aqueous lumen and in the lipophilic membrane, respectively (Nsairat et al., 2022). This allows the use of a fixed-dose combination (FDC) therapy product, where two or more drugs are co-formulated into a single dosage form. This approach improves treatment adherence and reduces the likelihood of misusing one of the drugs, contributing to reduce the evolution of resistance. In this context, YAT2150, a lipophilic compound with a clogP of 3.37, can be combined with another hydrophilic drug within the same liposome. YAT2150 would be encapsulated in the liposomal membrane, as demonstrated by fluorescence microscopy, which showed YAT2150 located in the membrane of giant unilamellar vesicles, while hydrophilic drugs would be encapsulated into the aqueous lumen. This FDC would allow the controlled co-delivery of two antileishmanial drugs, reducing the likelihood of drug resistance emergence. In addition, as it was shown in the three papers published in this thesis, liposomes can be easily conjugated to different molecules such as glycosaminoglycans, antibodies or aptamers to increase their targeting.

d) All the antileishmanial drugs present side effects related to their nonspecific toxicity, as exemplified by the antimonial drugs that have been for a long time the reference treatment for leishmaniasis (Sundar & Singh, 2018a). Moreover, the therapeutic window of antimonials is very narrow (Ponte-Sucre et al., 2017). As another example, miltefosine was initially used as an antitumoral drug, but it was later discarded for this purpose due to safety concerns, including its teratogenic effect and renal and gastrointestinal impact. Nevertheless, miltefosine is still being used for leishmaniasis (Pijpers et al., 2019). Our compound, YAT2150, has a low IC_{50} for *L. infantum* promastigotes and

amastigotes, but it also presents unspecific cytotoxicity, which leads to a selectivity index of 6.6. Using the same strategy as before for pentamidine to reduce the unspecific toxicity, YAT2150 was encapsulated into liposomes. As expected, the toxicity in HUVECs of liposomes loaded with YAT2150 was reduced, which was translated into a selectivity index with values higher than 100. Therefore, liposomes loaded with YAT2150 accomplished the criteria for antileishmanial compounds to treat VL, i.e., a SI>100 and an IC_{50} <10 µM (Katsuno et al., 2015), demonstrating their therapeutic potential for this disease. Furthermore, YAT2150 has been tested in promastigotes and amastigotes derived from two clinical isolates revealing an IC_{50} between 0.5 to 1.5 µM (data not shown). These results are highly promising compared to the existing antileishmanial drug.

e) YAT2150 synthesis is easy, rapid and inexpensive. Furthermore, it can be stored at room temperature during long periods, maintaining its stability (Bouzón-Arnáiz et al., 2022). These characteristics make YAT2150 very attractive for the regions where leishmaniasis is endemic, which includes areas with challenging socioeconomic contexts, including weak health systems, limited access to hospitals, and a lack of affordable treatments and storage facilities with cold chain maintenance.

Although YAT2150 is a promising antileishmanial candidate with a good DMPK profile, it has some drawbacks that need to be addressed: (1) YAT2150 has a relatively high unspecific toxicity. We have proposed to address this issue by encapsulating the drug into liposomes, which has already proved to be effective. However, we are also developing less toxic structural analogues; (2) the mode of action of the compound remains to be characterized. Knowing the specific target(s) of the drug, would allow us to perform further experiments, such as a silencing of the target gene(s) to help identifying its antileishmanial mechanism.

Developing ligands for functionalization of drug delivery systems or potential early diagnosis: Development of DNA aptamers against the *L. infantum* GP63 protein

The third strategy to overcome the challenges associated with the current drawbacks in leishmaniasis treatment is developing ligands for the functionalization of drug delivery systems or for a potential early diagnosis. In the third article "**Development of DNA aptamers against the *L. infantum* GP63 protein**", we

developed DNA aptamers against the mature form of the *L. infantum* protein GP63 (*Li*GP63m). This protein is one of the main virulence factors of the parasite, being the major surface promastigote protein and a key factor for amastigote survival within the macrophage (Olivier et al., 2005). The methodology selected to generate the aptamers was bead-based SELEX (J. Wu et al., 2012), which provided an aptamer pool enriched in oligonucleotides binding *L. infantum* promastigotes. Selected individual aptamers were tested in confocal fluorescence microscopy and flow cytometry analyses, showing targeting to more than 59% of promastigotes.

The key points of the third paper are:

a) The five aptamers characterized were highly specific as demonstrated by their ability to bind the purified TF-*Li*GP63m in the µM range, whereas no recognition of a control protein, GST, was observed. Four of the selected aptamers also recognised the endogenous GP63 in *L. infantum* promastigote lysates down to 7,500 parasites in an Aptamer Linked Immobilized Sorbent Assay (ALISA) format (Taneja et al., 2020). This ALISA represents the first prototype of a potential aptasensor (an aptamer-based biosensor) capable of detecting an antigen from the parasite. Aptamers are comparable to antibodies regarding their binding specificity and affinity; in fact, they are sometimes called synthetic antibodies. Moreover, as commented previously in the introduction section, they present some advantages over antibodies, such as stability at room temperature and a faster, easier, cheaper, and ethically acceptable production (Li, L., et al., 2021). An aptasensor stands out as one of the most promising options for transitioning from the bench to a commercially viable point-of-care testing device (Futane et al., 2023). The current diagnosis strategies for leishmaniasis consist either in the direct microscopic detection of the parasite or in molecular assays, which require specialized personnel and/or expensive equipment, not available in most leishmaniasis endemic regions. Serological tests are also useful, but only as a complementary method, since they cannot distinguish between current or past infections (WHO, 2010). The next step in the path to developing an aptasensor with the selected aptamers will be the detection of promastigotes in homogenized infected sandflies as the group of Bruno, J.G. et al. previously tested (Bruno et al., 2014).

b) The functionalization of liposomes with different molecules can improve targeted drug delivery. As it was shown for pentamidine-loaded liposomes, the conjugation of the glycosaminoglycans heparin and chondroitin sulfate on

liposomes increased macrophage uptake when compared to plain liposomes. Besides these naturally occurring ligands targeting infected macrophages or the free parasite, in this thesis, we had the aim of generating a new ligand that could specifically detect *L. infantum*. The C6-thiol-modified *Li*GP63Apt4 was successfully bound to maleimide-containing liposomes through a thiol-maleimide cross-linking reaction, as confirmed by a decrease in the zeta potential value, due to the negative charge of the aptamer sequence. Further experiments need to be done to determine whether the functionalization with specific aptamers improves liposome targeting relative to plain liposomes.

Targeting molecules can be used for different purposes within the leishmaniasis elimination framework. They can be employed as ligands to functionalize nanocarriers for targeted drug delivery, as diagnostic tools for detecting specific antigens, to study molecular interactions between the parasite and host cells, or as therapeutic agents operating through different mechanisms, such as inhibiting essential protein activities or blocking interactions between molecules. With the selected aptamers we also propose a potential prophylactic application.

It is known that GP63 is involved in the invasion process through the interaction with different macrophage receptors. Therefore, the binding of the aptamers to the endogenous GP63 in promastigotes may block the interaction between macrophage receptors and *Leishmania*, reducing the internalization of the parasite into the macrophage.

The complement subunit 3b (C3b) participates in the phagocytosis of *Leishmania* by macrophages through its interaction with the complement receptors CR3 or CR1, besides the interaction between GP63 and fibronectin receptors (Brittingham et al., 1999; De Morais et al., 2015; Filho et al., 2021; Soulat & Bogdan, 2017). Because GP63 converts C3b into the inactive complement fragment iC3b, the aptamer interaction with GP63 in promastigotes might inactivate it, eventually increasing the susceptibility of *Leishmania* to complement by inhibiting the conversion of C3b into iC3b.

GP63 is also essential in amastigotes, although it is less expressed there than in promastigotes, as it protects the amastigote from the harsh environment of the phagolysosome, facilitating its survival. Moreover, GP63 has been detected in the

amastigote form of all the *Leishmania* species studied (Olivier et al., 2012). This fact is relevant because it confirms that anti-*Li*GP63m aptamers, when conjugated to liposomes or used as a diagnostic tool, would potentially recognize the amastigote form in addition to the promastigote stage. Furthermore, from a therapeutic perspective, the binding of the aptamers to GP63 in amastigotes might inhibit the protective role of the protein, potentially leading to a higher death rate of the parasites. This hypothesis is based on studies previously conducted by Chaudhuri *et al*. (Chaudhuri et al., 1989) or Seay *et al.* (Seay et al., 1996), but further experiments are needed to confirm it.

As mentioned above, aptamers have some relevant advantages like stability at room temperature and a fast, easy and cheap production. However, they also present some disadvantages. For instance, DNA aptamers are prone to nuclease degradation, which reduces their usefulness. Nevertheless, they are easy to modify, by chemically changing or adding non-natural analogues of the nucleotides (Li, L., et al., 2021). Additionally, they can be conjugated with a nanocarrier, which could provide two benefits. On one hand, the nanocarrier might increase the stability of the aptamer. On the other hand, the aptamer can act as a ligand molecule to target the drug delivery system to the desired site.

Future perspectives

After confirming the *in vitro* effectiveness of liposomes loaded with pentamidine, from the first publication, we aim to assess their efficacy in an experimental mouse model of leishmaniasis using the inhalation administration route.

The compound from the second publication, YAT2150, may not be the most suitable candidate for further *in vivo* studies. Despite its promising characteristics as a potential antileishmanial drug, it exhibits drawbacks such as a relatively high nonspecific toxicity. While encapsulating YAT2150 into liposomes addressed this issue, we are also planning to modify its chemical structure. This involves developing YAT2150 analogues with the aim of achieving reduced nonspecific toxicity. If any of these analogues demonstrate an improved selectivity index compared to YAT2150, they will be considered as candidates for further *in vivo* studies. Additionally, YAT2150-containing liposomes could serve as promising candidates for *in vivo*

testing and it would be very interesting to co-encapsulate some currently used antileishmanial drugs along with YAT2150 in the same liposomes to generate a FDC therapy product. As mentioned above, since YAT2150 inhibited both *L. infantum* and *P. falciparum* growth, it would be important to carry out *in vivo* experiments using a murine model of *Plasmodium* and *Leishmania* co-infection.

The conjugation of the selected aptamers to YAT2150-containing liposomes could increase targeted drug delivery, enhancing the antileishmanial activity of the compound.

Conclusions

1. Liposomes loaded with pentamidine, which remained stable for at least two months at 4°C in solution, targeted 40% of macrophages and when functionalized with CS of heparin, this percentage increased by ca. two-fold.
2. Pentamidine-loaded liposomes significantly increased the efficacy against *L. infantum* promastigotes. However, in *L. pifanoi* promastigotes, only chondroitin sulfate- or heparin-coated liposomes decreased the IC_{50} significantly.
3. Pentamidine-loaded liposomes significantly reduced the drug cytotoxicity in human umbilical vein endothelial cells.
4. Liposomes encapsulated with pentamidine provided higher deposition of the nebulized liposomal preparations in the deeper stages of a human lung airway simulator when compared to free pentamidine, suggesting their potential for aerosol administration.
5. YAT2150 had a better *in vitro* activity against *L. infantum* (IC_{50} of ca. 0.5 µM) than most drugs currently used for the clinical treatment of leishmaniasis.
6. YAT2150 encapsulation into liposomes significantly reduced its *in vitro* cytotoxicity by 10 fold relative to the free drug, which led to a SI > 100.
7. The mechanism of action of YAT2150 seems to be multiple, reducing the overall protein aggregation in *L. infantum* promastigote cultures according to ThT analysis and the reduction of ATP levels in *L. major* promastigotes.
8. YAT2150 constitutes an excellent drug candidate against *Plasmodium* and *Leishmania* and holds promise for its use in the treatment of co-infections for both pathogens.
9. Aptamers against *Li*GP63m have been selected, targeting ≥75% of fixed *L. infantum* promastigotes. These five aptamers have a K_d in the µM range for the recombinant *Li*GP63m protein-aptamer interaction.
10. Four of these aptamers were capable of detecting the endogenous GP63 protein in whole-parasite lysates containing down to 7,500 promastigotes in an ALISA format.
11. Thiolated *Li*GP63Apt4 was successfully conjugated with maleimide-liposomes, which may allow a target delivery of an encapsulated drug into the liposome.

Liposomes encapsulating YAT2150 and functionalized with aptamers developed against *Li*GP63m*,* would enable an efficient targeted drug delivery, thereby enhancing the antileishmanial activity of the compound. Ideally, these liposomes would be administered through an aerosol, representing an innovative alternative treatment and a step forward in the pathway towards the control and elimination of leishmaniasis.

References

Abu Ammar, A., Nasereddin, A., Ereqat, S., Dan-Goor, M., Jaffe, C. L., Zussman, E., & Abdeen, Z. (2019). Amphotericin B-loaded nanoparticles for local treatment of cutaneous leishmaniasis. *Drug Delivery and Translational Research*, *9*(1), 76–84. https://doi.org/10.1007/S13346-018-00603-0/FIGURES/5

Adams, E. R., Schoone, G. J., Ageed, A. F., El Safi, S., & Schallig, H. D. F. H. (2010). Development of a reverse transcriptase Loop-Mediated Isothermal Amplification (LAMP) assay for the sensitive detection of Leishmania parasites in clinical samples. *The American Journal of Tropical Medicine and Hygiene*, *82*(4), 591–596. https://doi.org/10.4269/AJTMH.2010.09-0369

Afrasiabi, S., Pourhajibagher, M., Raoofian, R., Tabarzad, M., & Bahador, A. (2020). Therapeutic applications of nucleic acid aptamers in microbial infections. *Journal of Biomedical Science*, *27*(1), 1–13. https://doi.org/10.1186/S12929-019-0611-0/FIGURES/5

Agrawal, A. K., & Gupta, C. M. (2000). Tuftsin-bearing liposomes in treatment of macrophage-based infections. *Advanced Drug Delivery Reviews*, *41*(2), 135–146. https://doi.org/10.1016/S0169-409X(99)00061-7

Agrawal, S., Kuo, P. H., Chu, L. Y., Golzarroshan, B., Jain, M., & Yuan, H. S. (2019). RNA recognition motifs of disease-linked RNA-binding proteins contribute to amyloid formation. *Scientific Reports 2019 9:1*, *9*(1), 1–12. https://doi.org/10.1038/s41598-019-42367-8

Ahsan, F., Rivas, I. P., Khan, M. A., & Torres Suárez, A. I. (2002). Targeting to macrophages: Role of physicochemical properties of particulate carriers - Liposomes and microspheres - On the phagocytosis by macrophages. *Journal of Controlled Release*, *79*(1–3), 29–40. https://doi.org/10.1016/S0168-3659(01)00549-1

Akbari, M., Oryan, A., & Hatam, G. (2017). Application of nanotechnology in treatment of leishmaniasis: A Review. *Acta Tropica*, *172*, 86–90. https://doi.org/10.1016/J.ACTATROPICA.2017.04.029

Alhalili, Z. (2023). Metal oxides nanoparticles: general structural description, chemical, physical, and biological synthesis methods, role in pesticides and heavy metal removal through wastewater treatment. *Molecules (Basel, Switzerland)*, *28*(7). https://doi.org/10.3390/MOLECULES28073086

Allahverdiyev, A. M., Abamor, E. S., Bagirova, M., Baydar, S. Y., Ates, S. C., Kaya, F., Kaya, C., & Rafailovich, M. (2013). Investigation of antileishmanial activities of Tio2@Ag nanoparticles on biological properties of L. tropica and L. infantum parasites, in vitro.

Experimental Parasitology, *135*(1), 55–63. https://doi.org/10.1016/J.EXPPARA.2013.06.001

Allahverdiyev, A. M., Abamor, E. S., Bagirova, M., Ustundag, C. B., Kaya, C., Kaya, F., & Rafailovich, M. (2011). Antileishmanial effect of silver nanoparticles and their enhanced antiparasitic activity under ultraviolet light. *International Journal of Nanomedicine*, *6*, 2705–2714. https://doi.org/10.2147/IJN.S23883

Alshaer, W., Hillaireau, H., Vergnaud, J., Ismail, S., & Fattal, E. (2015). Functionalizing liposomes with anti-CD44 aptamer for selective targeting of cancer cells. *Bioconjugate Chemistry*, *26*(7), 1307–1313. https://doi.org/10.1021/BC5004313/SUPPL_FILE/BC5004313_SI_001.PDF

Alves, F., Bilbe, G., Blesson, S., Goyal, V., Monnerat, S., Mowbray, C., Ouattara, G. M., Pécoul, B., Rijal, S., Rode, J., Solomos, A., Strub-Wourgaft, N., Wasunna, M., Wells, S., Zijlstra, E. E., Arana, B., & Alvar, J. (2018). Recent development of visceral leishmaniasis treatments: successes, pitfalls, and perspectives. *Clinical Microbiology Reviews*, *31*(4), 1–30. https://doi.org/10.1128/CMR.00048-18

Arenas, R., Torres-Guerrero, E., Quintanilla-Cedillo, M. R., & Ruiz-Esmenjaud, J. (2017). Leishmaniasis: A review. *F1000Research*, *6*, 750. https://doi.org/10.12688/F1000RESEARCH.11120.1/DOI

Aronson, N., Herwaldt, B. L., Libman, M., Pearson, R., Lopez-Velez, R., Weina, P., Carvalho, E., Ephros, M., Jeronimo, S., & Magill, A. (2017). Diagnosis and treatment of leishmaniasis: Clinical practice guidelines by the infectious diseases society of America (IDSA) and the American Society of tropical medicine and hygiene (ASTMH). In *American Journal of Tropical Medicine and Hygiene* (Vol. 96, Issue 1, pp. 24–45). American Society of Tropical Medicine and Hygiene. https://doi.org/10.4269/ajtmh.16-84256

Attar, Z. J., Chance, M. L., El-Safi, S., Carney, J., Azazy, A., El-Hadi, M., Dourado, C., & Hommel, M. (2001). Latex agglutination test for the detection of urinary antigens in visceral leishmaniasis. *Acta Tropica*, *78*(1), 11–16. https://doi.org/10.1016/S0001-706X(00)00155-8

Azevedo, E. G., Ribeiro, R. R., Da Silva, S. M., Ferreira, C. S., De Souza, L. E., Ferreira, A. A. F., De Oliveira E Castro, R. A., Demicheli, C., Rezende, S. A., & Frézard, F. (2014). Mixed formulation of conventional and pegylated liposomes as a novel drug delivery strategy for improved treatment of visceral leishmaniasis. *Expert Opinion on Drug Delivery*, *11*(10), 1551–1560. https://doi.org/10.1517/17425247.2014.932347

Azevedo-Pereira, R. L., Pereira, M. C. S., Oliveria-Junior, F. O. R., Brazil, R. P., Côrtes, L. M. C., Madeira, M. F., Santos, A. L. S., Toma, L., & Alves, C. R. (2007). Heparin binding proteins from Leishmania (Viannia) braziliensis promastigotes. *Veterinary Parasitology*, *145*(3–4), 234–239. https://doi.org/10.1016/J.VETPAR.2006.12.019

Azzouz, S., & Lawton, P. (2017). In vitro effects of purine and pyrimidine analogues on Leishmania donovani and Leishmania infantum promastigotes and intracellular amastigotes. *Acta Parasitologica*, *62*(3), 582–588. https://doi.org/10.1515/AP-2017-0070/MACHINEREADABLECITATION/RIS

Banerjee, G., Nandi, G., Mahato, S. B., Pakrashi, A., & Basu, M. K. (1996a). Drug delivery system: targeting of pentamidines to specific sites using sugar grafted liposomes. *The Journal of Antimicrobial Chemotherapy*, *38*(1), 145–150. https://doi.org/10.1093/JAC/38.1.145

Banerjee, G., Nandi, G., Mahato, S. B., Pakrashi, A., & Basu, M. K. (1996b). Drug delivery system: Targeting of pentamidines to specific sites using sugar grafted liposomes. *Journal of Antimicrobial Chemotherapy*, *38*(1), 145–150. https://doi.org/10.1093/JAC/38.1.145

Bangham, A. D., & Horne, R. W. (1964). Negative staining of phospholipids and their structural modification by surface-active agents as observed in the electron microscope. *Journal of Molecular Biology*, *8*(5), 660-IN10. https://doi.org/10.1016/S0022-2836(64)80115-7

Bates, P. A. (2007). Transmission of Leishmania metacyclic promastigotes by phlebotomine sand flies. *International Journal for Parasitology*, *37*(10), 1097–1106. https://doi.org/10.1016/J.IJPARA.2007.04.003

Bates, P. A. (2018). Revising Leishmania's life cycle. *Nature Microbiology*, *3*(5), 529–530. https://doi.org/10.1038/S41564-018-0154-2

Bates, P., & Rogers, M. (2004). New insights into the developmental biology and transmission mechanisms of Leishmania. *Current Molecular Medicine*, *4*(6), 601–609. https://doi.org/10.2174/1566524043360285

Batlle, C., De Groot, N. S., Iglesias, V., Navarro, S., & Ventura, S. (2017). Characterization of soft amyloid cores in human prion-like proteins. *Scientific Reports 2017 7:1*, *7*(1), 1–16. https://doi.org/10.1038/S41598-017-09714-Z

Batlle, C., Yang, P., Coughlin, M., Messing, J., Pesarrodona, M., Szulc, E., Salvatella, X., Kim, H. J., Taylor, J. P., & Ventura, S. (2020). hnRNPDL phase separation is regulated by alternative splicing and disease-causing mutations accelerate its aggregation. *Cell Reports*, *30*(4), 1117-1128.e5. https://doi.org/10.1016/J.CELREP.2019.12.080

Beheshti, N., Soflaei, S., Shakibaie, M., Yazdi, M. H., Ghaffarifar, F., Dalimi, A., & Shahverdi, A. R. (2013). Efficacy of biogenic selenium nanoparticles against Leishmania major: In vitro and in vivo studies. *Journal of Trace Elements in Medicine and Biology*, *27*(3), 203–207. https://doi.org/10.1016/J.JTEMB.2012.11.002

Betti, C., Vanhoutte, I., Coutuer, S., De Rycke, R., Mishev, K., Vuylsteke, M., Aesaert, S., Rombaut, D., Gallardo, R., De Smet, F., Xu, J., Van Lijsebettens, M., Van Breusegem, F., Inzé, D., Rousseau, F., Schymkowitz, J., & Russinova, E. (2016). Sequence-specific protein aggregation generates defined protein knockdowns in plants. *Plant Physiology*, *171*(2), 773–787. https://doi.org/10.1104/PP.16.00335

Biosca, A., Bouzón-Arnáiz, I., Spanos, L., Siden-Kiamos, I., Iglesias, V., Ventura, S., & Fernàndez-Busquets, X. (2020). Detection of protein aggregation in live Plasmodium parasites. *Antimicrobial Agents and Chemotherapy*, *64*(6). https://doi.org/10.1128/AAC.02135-19

Biosca, A., Dirscherl, L., Moles, E., Imperial, S., & Fernàndez-Busquets, X. (2019). An ImmunoPEGliposome for Targeted Antimalarial Combination Therapy at the Nanoscale. *Pharmaceutics*, *11*(7). https://doi.org/10.3390/PHARMACEUTICS11070341

Bogdan, C., Donhauser, N., Döring, R., Röllinghoff, M., Diefenbach, A., & Rittig, M. G. (2000). Fibroblasts as host cells in latent leishmaniosis. *The Journal of Experimental Medicine*, *191*(12), 2121–2129. https://doi.org/10.1084/JEM.191.12.2121

Bouzón-Arnáiz, I., Avalos-Padilla, Y., Biosca, A., Caño-Prades, O., Román-Álamo, L., Valle, J., Andreu, D., Moita, D., Prudêncio, M., Arce, E. M., Muñoz-Torrero, D., & Fernàndez-Busquets, X. (2022). The protein aggregation inhibitor YAT2150 has potent antimalarial activity in Plasmodium falciparum in vitro cultures. *BMC Biology*, *20*(1). https://doi.org/10.1186/S12915-022-01374-4

Braillard, S., Keenan, M., Breese, K. J., Heppell, J., Abbott, M., Lslam, R., Shackleford, D. M., Katneni, K., Crighton, E., Chen, G., Patil, R., Lee, G., White, K. L., Carvalho, S., Wall, R. J., Chemi, G., Zuccotto, F., González, S., Marco, M., … Chatelain, E. (2023). DNDI-6174 is a preclinical candidate for visceral leishmaniasis that targets the cytochrome bc1. *Science Translational Medicine*, *15*(726). https://doi.org/10.1126/SCITRANSLMED.ADH9902

Brindha, J., Balamurali, M. M., & Chanda, K. (2021). An overview on the therapeutics of neglected infectious diseases-leishmaniasis and Chagas diseases. *Frontiers in Chemistry*, *9*(622286). https://doi.org/10.3389/FCHEM.2021.622286

Brittingham, A., Chen, G., Mcgwire, B. S., Chang, K. P., & Mosser, D. M. (1999). Interaction of Leishmania gp63 with cellular receptors for fibronectin. *Infection and Immunity*, *67*(9), 4477–4484. https://doi.org/10.1128/IAI.67.9.4477-4484.1999/ASSET/BAAA47AB-41D9-4F1A-B071-267C5B08EDF6/ASSETS/GRAPHIC/II0991512006.JPEG

Brittingham, A., Morrison, C. J., McMaster, W. R., McGwire, B. S., Chang, K. P., & Mosser, D. M. (1995). Role of the Leishmania surface protease gp63 in complement fixation, cell adhesion, and resistance to complement-mediated lysis. *The Journal of Immunology*, *155*(6), 3102–3111. https://doi.org/10.4049/JIMMUNOL.155.6.3102

Broni, E., Kwofie, S. K., Asiedu, S. O., Miller, W. A., & Wilson, M. D. (2021). A molecular modeling approach to identify potential antileishmanial compounds against the Cell Division Cycle (cdc)-2-Related Kinase 12 (CRK12) Receptor of Leishmania donovani. *Biomolecules 2021, Vol. 11, Page 458*, *11*(3), 458. https://doi.org/10.3390/BIOM11030458

Bruno, J. G., Richarte, A. M., Phillips, T., Savage, A. A., Sivils, J. C., Greis, A., & Mayo, M. W. (2014). Development of a fluorescent enzyme-linked DNA aptamer-magnetic bead sandwich assay and portable fluorometer for sensitive and rapid leishmania detection in sandflies. *Journal of Fluorescence*, *24*(1), 267–277. https://doi.org/10.1007/S10895-013-1315-6/FIGURES/8

Burza, S., Croft, S. L., & Boelaert, M. (2018). Leishmaniasis. *Lancet (London, England)*, *392*(10151), 951–970. https://doi.org/10.1016/S0140-6736(18)31204-2

Butcher, B. A., Sklar,', L. A., Seamer,' And, L. C., & Glew3', R. H. (1992). Heparin enhances the interaction of infective Leishmania donovani promastigotes with mouse peritoneal macrophages. A fluorescence flow cytometric analysis. *The Journal of Immunology*, *148*(9), 2879–2886. https://doi.org/10.4049/JIMMUNOL.148.9.2879

Cao, Z., Tong, R., Mishra, A., Xu, W., Wong, G. C. L., Cheng, J., & Lu, Y. (2009). Reversible cell-specific drug delivery with aptamer-functionalized liposomes. *Angewandte Chemie International Edition*, *48*(35), 6494–6498. https://doi.org/10.1002/ANIE.200901452

Capela, R., Moreira, R., & Lopes, F. (2019). An overview of drug resistance in protozoal diseases. *International Journal of Molecular Sciences 2019, Vol. 20, Page 5748*, *20*(22), 5748. https://doi.org/10.3390/IJMS20225748

Carnielli, J. B. T., Dave, A., Romano, A., Forrester, S., de Faria, P. R., Monti-Rocha, R., Costa, C. H. N., Dietze, R., Graham, I. A., & Mottram, J. C. (2022). 3'Nucleotidase/nuclease is required for Leishmania infantum clinical isolate susceptibility to miltefosine. *EBioMedicine*, *86*, 104378. https://doi.org/10.1016/J.EBIOM.2022.104378

Carstens-Kass, J., Paulini, K., Lypaczewski, P., & Matlashewski, G. (2021). A review of the leishmanin skin test: A neglected test for a neglected disease. *PLOS Neglected Tropical Diseases*, *15*(7), e0009531. https://doi.org/10.1371/JOURNAL.PNTD.0009531

Casale, J., & Crane, J. S. (2023). Biochemistry, Glycosaminoglycans. *StatPearls*. https://www.ncbi.nlm.nih.gov/books/NBK544295/

CDC. (2017, December 14). *Leishmaniasis*. https://www.cdc.gov/dpdx/leishmaniasis/index.html

Chakrabarti, A., Narayana, C., Joshi, N., Garg, S., Garg, L. C., Ranganathan, A., Sagar, R., Pati, S., & Singh, S. (2022). Metalloprotease Gp63-targeting novel glycoside exhibits potential antileishmanial activity. *Frontiers in Cellular and Infection Microbiology*, *12*, 803048. https://doi.org/10.3389/FCIMB.2022.803048/BIBTEX

Chaudhuri, G., Chaudhuri, M., Pan, A., & Chang, K. P. (1989). Surface acid proteinase (gp63) of Leishmania mexicana: A metalloenzyme capable of protecting liposome-encapsulated proteins from phagolysosomal degradation by macrophages. *Journal of Biological Chemistry*, *264*(13), 7483–7489. https://doi.org/10.1016/S0021-9258(18)83260-4

Chiti, F., & Dobson, C. M. (2006). Protein misfolding, functional amyloid, and human disease. *Annual Review of Biochemistry*, *75*(Volume 75, 2006), 333–366. https://doi.org/10.1146/ANNUREV.BIOCHEM.75.101304.123901/CITE/REFWORKS

Chiti, F., & Dobson, C. M. (2009). Amyloid formation by globular proteins under native conditions. *Nature Chemical Biology*, *5*(1), 15–22. https://doi.org/10.1038/NCHEMBIO.131

Chiti, F., & Dobson, C. M. (2017). Protein misfolding, amyloid formation, and human disease: A summary of progress over the last decade. *Annual Review of Biochemistry*, *86*(Volume 86, 2017), 27–68. https://doi.org/10.1146/ANNUREV-BIOCHEM-061516-045115/1

Conchillo-Solé, O., de Groot, N. S., Avilés, F. X., Vendrell, J., Daura, X., & Ventura, S. (2007). AGGRESCAN: A server for the prediction and evaluation of "hot spots" of aggregation in polypeptides. *BMC Bioinformatics*, *8*(1), 1–17. https://doi.org/10.1186/1471-2105-8-65/FIGURES/1

Culley, F. J., Harris, R. A., Kaye, P. M., M ~ A D A R N , ~, K. P. W. J., & Raynes, J. G. (1996). C-reactive protein binds to a novel ligand on Leishmania donovani and increases uptake into human macrophages. *The Journal of Immunology*, *156*(12), 4691–4696. https://doi.org/10.4049/JIMMUNOL.156.12.4691

Cummings, R. D. (2022). The mannose receptor ligands and the macrophage glycome. *Current Opinion in Structural Biology*, *75*. https://doi.org/10.1016/J.SBI.2022.102394

Cyrus Levinthal. (1696). *How to fold graciously*. https://faculty.cc.gatech.edu/~turk/bio_sim/articles/proteins_levinthal_1969.pdf

Date, A. A., Joshi, M. D., & Patravale, V. B. (2007). Parasitic diseases: Liposomes and polymeric nanoparticles versus lipid nanoparticles. *Advanced Drug Delivery Reviews*, *59*(6), 505–521. https://doi.org/10.1016/J.ADDR.2007.04.009

De Almeida, L., Fujimura, A. T., Del Cistia, M. L., Fonseca-Santos, B., Imamura, K. B., Michels, P. A. M., Chorilli, M., & Graminha, M. A. S. (2017). Nanotechnological strategies for treatment of leishmaniasis-a review. *Journal of Biomedical Nanotechnology*, *13*(2), 117–133. https://doi.org/10.1166/JBN.2017.2349

De Castro Côrtes, L. M., De Souza Pereira, M. C., De Oliveira, F. O. R., Corte-Real, S., Da Silva, F. S., Pereira, B. A. S., De Fátima Madeira, M., De Moraes, M. T. B., Brazil, R. P., & Alves, C. R. (2012). Leishmania (Viannia) braziliensis: insights on subcellular distribution and biochemical properties of heparin-binding proteins. *Parasitology*, *139*(2), 200–207. https://doi.org/10.1017/S0031182011001910

Delavari, M., Dalimi, A., Ghaffarifar, F., & Sadraei, J. (2014). In Vitro Study on Cytotoxic Effects of ZnO Nanoparticles on Promastigote and Amastigote Forms of Leishmania major (MRHO/IR/75/ER). *Iranian Journal of Parasitology*, *9*(1), 6–13. https://pubmed.ncbi.nlm.nih.gov/25642254/

De Menezes, J. P., Saraiva, E. M., & Da Rocha-Azevedo, B. (2016). The site of the bite: Leishmania interaction with macrophages, neutrophils and the extracellular matrix in the dermis. *Parasites and Vectors*, *9*(264). https://doi.org/10.1186/S13071-016-1540-3/METRICS

De Morais, C. G. V., Castro Lima, A. K., Terra, R., Dos Santos, R. F., Da-Silva, S. A. G., & Dutra, P. M. L. (2015). The Dialogue of the Host-Parasite Relationship: Leishmania spp. and Trypanosoma cruzi Infection. *BioMed Research International*, *2015*. https://doi.org/10.1155/2015/324915

De Pablos, L. M., Ferreira, T. R., & Walrad, P. B. (2016). Developmental differentiation in Leishmania lifecycle progression: post-transcriptional control conducts the orchestra. *Current Opinion in Microbiology*, *34*, 82–89. https://doi.org/10.1016/J.MIB.2016.08.004

Descoteaux, A., & Turco, S. J. (1999). Glycoconjugates in Leishmania infectivity. *Biochimica et Biophysica Acta (BBA) - Molecular Basis of Disease*, *1455*(2–3), 341–352. https://doi.org/10.1016/S0925-4439(99)00065-4

De Silva, G., Somaratne, V., Senaratne, S., Vipuladasa, M., Wickremasinghe, R., Wickremasinghe, R., & Ranasinghe, S. (2017). Efficacy of a new rapid diagnostic test kit to diagnose Sri Lankan cutaneous leishmaniasis caused by Leishmania donovani. *PLoS ONE*, *12*(11), e0187024. https://doi.org/10.1371/JOURNAL.PONE.0187024

de Souza, A., Marins, D. S. S., Mathias, S. L., Monteiro, L. M., Yukuyama, M. N., Scarim, C. B., Löbenberg, R., & Bou-Chacra, N. A. (2018). Promising nanotherapy in treating leishmaniasis. *International Journal of Pharmaceutics*, *547*(1–2), 421–431. https://doi.org/10.1016/J.IJPHARM.2018.06.018

de Vries, H. J. C., Reedijk, S. H., & Schallig, H. D. F. H. (2015). Cutaneous leishmaniasis: Recent developments in diagnosis and management. *American Journal of Clinical Dermatology*, *16*(2), 99–109. https://doi.org/10.1007/S40257-015-0114-Z

Devsani, N., Vemula, D., & Bhandari, V. (2023). The glycoprotein gp63– a potential pan drug target for developing new antileishmanial agents. *Biochimie*, *207*, 75–82. https://doi.org/10.1016/J.BIOCHI.2022.11.015

Dey, R., Meneses, C., Salotra, P., Kamhawi, S., Nakhasi, H. L., & Duncan, R. (2010). Characterization of a Leishmania stage-specific mitochondrial membrane protein that enhances the activity of cytochrome c oxidase and its role in virulence. *Molecular Microbiology*, *77*(2), 399–414. https://doi.org/10.1111/J.1365-2958.2010.07214.X

Diouani, M. F., Ouerghi, O., Belgacem, K., Sayhi, M., Ionescu, R., & Laouini, D. (2019). Casein-conjugated gold nanoparticles for amperometric detection of Leishmania infantum. *Biosensors*, *9*(2). https://doi.org/10.3390/BIOS9020068

DNDi. (2011). *Sodium Stibogluconate & Paromomycin (SSG&PM) combination treatment*.

DNDi. (2018). *Clinical trial protocol synopsis. A Phase 1, blinded, randomized, single centre, parallel-group, single-dose, dose-escalation, placebo-controlled study of the safety, tolerability, and pharmacokinetics of DNDI-6148 after oral dosing in healthy male subjects*.

DNDi. (2020). *Annual report 2019: advancing the best science for the most neglected*.

DNDi. (2021a). *Study protocol synopsis: A Phase I, double-blind, randomised, single centre, parallel-group, multiple-dose, dose-escalation, placebo controlled study of the safety, tolerability and pharmacokinetics of DNDI-0690 after oral dosing in healthy subjects*.

DNDi. (2021b). *Study protocol synopsis:A phase I, double-blind, randomised, single centre, parallel-group, single ascending cose, placebo-controlled study of the safety, tolerability, pharmacokinetics, and pharmacodynamics of CpG ODN D35 after subcutaneous administration in healthy male subjects*.

DNDi. (2022). *Clinical trial protocol synopsis. A randomized, open-label, phase II, single-centre study to evaluate the efficacy, safety and pharmacokinetics of LXE408 in patients with primary visceral leishmaniasis in Ethiopia*.

DNDi. (2024, March). *DNDI-6174 | DNDi*. https://dndi.org/research-development/portfolio/dndi-6174/

Dobson, C. M. (2003). Protein folding and misfolding. *Nature 2003 426:6968*, *426*(6968), 884–890. https://doi.org/10.1038/nature02261

Dunker, A. K., Babu, M. M., Barbar, E., Blackledge, M., Bondos, S. E., Dosztányi, Z., Dyson, H. J., Forman-Kay, J., Fuxreiter, M., Gsponer, J., Han, K.-H., Jones, D. T., Longhi, S., Metallo, S. J., Nishikawa, K., Nussinov, R., Obradovic, Z., Pappu, R. V., Rost, B., … Uversky, V. N. (2013). What's in a name? Why these proteins are intrinsically disordered: Why these proteins are intrinsically disordered. *Intrinsically Disordered Proteins*, *1*(1), e24157. https://doi.org/10.4161/IDP.24157

eBioMedicine. (2023a). Leishmania: an urgent need for new treatments. *EBioMedicine*, *87*, 104440. https://doi.org/10.1016/J.EBIOM.2023.104440

eBioMedicine. (2023b). Leishmania: an urgent need for new treatments. *EBioMedicine*, *87*, 104440. https://doi.org/10.1016/j.ebiom.2023.104440

Ellington, A. D., & Szostak, J. W. (1990). In vitro selection of RNA molecules that bind specific ligands. *Nature 1990 346:6287*, *346*(6287), 818–822. https://doi.org/10.1038/346818a0

FDA. (1997). *Drug approval package: Ambisome (Amphotericin B) NDA# 050740*. https://www.accessdata.fda.gov/drugsatfda_docs/nda/97/050740_ambisome_toc.cfm

FDA. (2001, January 16). *Pentam® 300 (pentamidine isethionate for injection)*. https://dailymed.nlm.nih.gov/dailymed/fda/fdaDrugXsl.cfm?setid=cc2b635e-4840-4dc3-a177-5484371680e8&type=display

FDA. (2004, December 17). *Drug approval package: Macugen (Pegaptanib sodium) NDA #021756*. https://www.accessdata.fda.gov/drugsatfda_docs/nda/2004/21-756_Macugen.cfm

FDA. (2008). *AmBisome® (amphotericin B) liposome for injection*.

FDA. (2010). *NebuPent*. https://www.fda.gov/drugsatfda

FDA. (2014). *IMPAVIDO (miltefosine) capsules, for oral use*. www.fda.gov/medwatch

FDA. (2019). *Pentamidine isethionate for injection*. https://www.accessdata.fda.gov/spl/data/589fcce2-fa9a-4dc0-a79b-ae87cd024365/589fcce2-fa9a-4dc0-a79b-ae87cd024365.xml

Fernández Cotrina, J., Iniesta, V., Monroy, I., Baz, V., Hugnet, C., Marañon, F., Fabra, M., Gómez-Nieto, L. C., & Alonso, C. (2018). A large-scale field randomized trial demonstrates safety and efficacy of the vaccine LetiFend® against canine leishmaniosis. *Vaccine*, *36*(15), 1972–1982. https://doi.org/10.1016/J.VACCINE.2018.02.111

Fernández Martínez, B. (2023). Situación de leishmaniasis en España. Años 2019, 2020 y 2021. *Boletín Epidemiológico Semanal ISCIII: Vigilancia Epidemiológica, ISSN 1135-6286,* , *31*(2), 83–92. https://dialnet.unirioja.es/servlet/articulo?codigo=9018211&info=resumen&idioma=ENG

Fidalgo, L. M., & Gille, L. (2011). Mitochondria and trypanosomatids: Targets and drugs. *Pharmaceutical Research*, *28*(11), 2758–2770. https://doi.org/10.1007/S11095-011-0586-3/TABLES/1

Filho, A. A. P., Nascimento, A. A. de S., Saab, N. A. A., Fugiwara, R. T., D'Ávila Pessoa, G. C., Koerich, L. B., Pereira, M. H., Araújo, R. N., Sant'Anna, M. R. V., & Gontijo, N. F. (2021). Evasion of the complement system by Leishmania through the uptake of factor H, a complement regulatory protein. *Acta Tropica*, *224*, 106152. https://doi.org/10.1016/J.ACTATROPICA.2021.106152

Floudas, C. A., Fung, H. K., McAllister, S. R., Mönnigmann, M., & Rajgaria, R. (2006). Advances in protein structure prediction and de novo protein design: A review. *Chemical Engineering Science*, *61*(3), 966–988. https://doi.org/10.1016/J.CES.2005.04.009

Forman-Kay, J. D., & Mittag, T. (2013). From sequence and forces to structure, function, and evolution of intrinsically disordered proteins. *Structure*, *21*(9), 1492–1499. https://doi.org/10.1016/J.STR.2013.08.001

Frezza, V., Pinto-Díez, C., Fernández, G., Soto, M., Martín, M. E., García-Sacristán, A., & González, V. M. (2020). DNA aptamers targeting Leishmania infantum H3 protein as potential diagnostic tools. *Analytica Chimica Acta*, *1107*, 155–163. https://doi.org/10.1016/J.ACA.2020.02.012

Futane, A., Narayanamurthy, V., Jadhav, P., & Srinivasan, A. (2023). Aptamer-based rapid diagnosis for point-of-care application. *Microfluidics and Nanofluidics*, *27*(2). https://doi.org/10.1007/S10404-022-02622-3

Gaspar, R., Opperdoes, F. R., Preat, V., & Roland, M. (1992). Drug targeting with polyalkylcyanoacrylate nanoparticles: in vitro activity of primaquine-loaded nanoparticles against intracellular Leishmania donovani. *Annals of Tropical Medicine & Parasitology*, *86*(1), 41–49. https://doi.org/10.1080/00034983.1992.11812629

Ghorbani, M., & Farhoudi, R. (2017). Leishmaniasis in humans: drug or vaccine therapy? *Drug Design, Development and Therapy*, *12*, 25–40. https://doi.org/10.2147/DDDT.S146521

Ghosh, P., Bhaskar, K. R. H., Hossain, F., Khan, M. A. A., Vallur, A. C., Duthie, M. S., Hamano, S., Salam, M. A., Huda, M. M., Khan, M. G. M., Coler, R. N., Reed, S. G., & Mondal, D. (2016). Evaluation of diagnostic performance of rK28 ELISA using urine for diagnosis of visceral leishmaniasis. *Parasites and Vectors*, *9*(1), 383. https://doi.org/10.1186/S13071-016-1667-2/FIGURES/2

Gil-Prieto, R., Walter, S., Alvar, J., & De Miguel, A. G. (2011). Epidemiology of leishmaniasis in Spain based on hospitalization records (1997-2008). *The American Journal of Tropical Medicine and Hygiene*, *85*(5), 820–825. https://doi.org/10.4269/AJTMH.2011.11-0310

Gow, I., Smith, N. C., Stark, D., & Ellis, J. (2022). Laboratory diagnostics for human Leishmania infections: a polymerase chain reaction-focussed review of detection and identification methods. *Parasites & Vectors*, *15*(1), 412. https://doi.org/10.1186/S13071-022-05524-Z

Guerra-Pérez, N., Ramos, E., García-Hernández, M., Pinto, C., Soto, M., Martín, M. E., & González, V. M. (2015). Molecular and functional characterization of ssDNA aptamers that specifically bind Leishmania infantum PABP. *PLOS ONE*, *10*(10), e0140048. https://doi.org/10.1371/JOURNAL.PONE.0140048

Gurjar, D., Kumar Patra, S., Bodhale, N., Lenka, N., & Saha, B. (2022). Leishmania intercepts IFN-γR signaling at multiple levels in macrophages. *Cytokine*, *157*, 155956. https://doi.org/10.1016/J.CYTO.2022.155956

Haldar, A. K., Sen, P., & Roy, S. (2011). Use of antimony in the treatment of leishmaniasis: current status and future directions. *Molecular Biology International*, *2011*, 1–23. https://doi.org/10.4061/2011/571242

Hartl, F. U., Bracher, A., & Hayer-Hartl, M. (2011). Molecular chaperones in protein folding and proteostasis. *Nature 2011 475:7356*, *475*(7356), 324–332. https://doi.org/10.1038/nature10317

Heath, T. D., Macher, B. A., & Papahadjopoulos, D. (1981). Covalent attachment of immunoglobulins to liposomes via glycosphingolipids. *Biochimica et Biophysica Acta*

(BBA) - Biomembranes, *640*(1), 66–81. https://doi.org/10.1016/0005-2736(81)90532-0

Heidari-Kharaji, M., Taheri, T., Doroud, D., Habibzadeh, S., Badirzadeh, A., & Rafati, S. (2016). Enhanced paromomycin efficacy by solid lipid nanoparticle formulation against Leishmania in mice model. *Parasite Immunology*, *38*(10), 599–608. https://doi.org/10.1111/PIM.12340

Hussain, Z., Khan, S., Imran, M., Sohail, M., Shah, S. W. A., & de Matas, M. (2019). PEGylation: a promising strategy to overcome challenges to cancer-targeted nanomedicines: a review of challenges to clinical transition and promising resolution. *Drug Delivery and Translational Research*, *9*(3). https://doi.org/10.1007/S13346-019-00631-4

Iborra, S., Soto, M., Carrión, J., Alonso, C., & Requena, J. M. (2004). Vaccination with a plasmid DNA cocktail encoding the nucleosomal histones of Leishmania confers protection against murine cutaneous leishmaniosis. *Vaccine*, *22*(29–30), 3865–3876. https://doi.org/10.1016/J.VACCINE.2004.04.015

Iglesias, V., de Groot, N. S., & Ventura, S. (2015). Computational analysis of candidate prion-like proteins in bacteria and their role. *Frontiers in Microbiology*, *6*(OCT), 162802. https://doi.org/10.3389/FMICB.2015.01123/BIBTEX

Isnard, A., Shio, M. T., & Olivier, M. (2012). Impact of Leishmania metalloprotease GP63 on macrophage signaling. *Frontiers in Cellular and Infection Microbiology*, *2*, 72. https://doi.org/10.3389/FCIMB.2012.00072/BIBTEX

Jaafari, M. R., Bavarsad, N., Bazzaz, B. S. F., Samiei, A., Soroush, D., Ghorbani, S., Heravi, M. M. L., & Khamesipour, A. (2009). Effect of topical liposomes containing paromomycin sulfate in the course of Leishmania major infection in susceptible BALB/c mice. *Antimicrobial Agents and Chemotherapy*, *53*(6), 2259–2265. https://doi.org/10.1128/AAC.01319-08

Jain, A. K., & Thareja, S. (2019). In vitro and in vivo characterization of pharmaceutical nanocarriers used for drug delivery. *Artificial Cells, Nanomedicine, and Biotechnology*, *47*(1), 524–539. https://doi.org/10.1080/21691401.2018.1561457

Karamysheva, Z. N., Guarnizo, S. A. G., & Karamyshev, A. L. (2020). Regulation of translation in the protozoan parasite Leishmania. *International Journal of Molecular Sciences*, *21*(8). https://doi.org/10.3390/IJMS21082981

Katsuno, K., Burrows, J. N., Duncan, K., Van Huijsduijnen, R. H., Kaneko, T., Kita, K., Mowbray, C. E., Schmatz, D., Warner, P., & Slingsby, B. T. (2015). Hit and lead criteria

in drug discovery for infectious diseases of the developing world. *Nature Reviews Drug Discovery 2015 14:11*, *14*(11), 751–758. https://doi.org/10.1038/nrd4683

Kavian, Z., Alavizadeh, S. H., Golmohamadzadeh, S., Badiee, A., Khamesipour, A., & Jaafari, M. R. (2019). Development of topical liposomes containing miltefosine for the treatment of Leishmania major infection in susceptible BALB/c mice. *Acta Tropica*, *196*, 142–149. https://doi.org/10.1016/J.ACTATROPICA.2019.05.018

Kelly, P. H., Bahr, S. M., Serafim, T. D., Ajami, N. J., Petrosino, J. F., Meneses, C., Kirby, J. R., Valenzuela, J. G., Kamhawi, S., & Wilson, M. E. (2017). The gut microbiome of the vector Lutzomyia longipalpis is essential for survival of Leishmania infantum. *MBio*, *8*(1), e01121-16. https://doi.org/10.1128/MBIO.01121-16

Khare, S., Nagle, A. S., Biggart, A., Lai, Y. H., Liang, F., Davis, L. C., Barnes, S. W., Mathison, C. J. N., Myburgh, E., Gao, M. Y., Gillespie, J. R., Liu, X., Tan, J. L., Stinson, M., Rivera, I. C., Ballard, J., Yeh, V., Groessl, T., Federe, G., … Supek, F. (2016). Proteasome inhibition for treatment of leishmaniasis, Chagas disease and sleeping sickness. *Nature*, *537*(7619), 229–233. https://doi.org/10.1038/NATURE19339

Kima, P. E. (2007). The amastigote forms of Leishmania are experts at exploiting host cell processes to establish infection and persist. *International Journal for Parasitology*, *37*(10), 1087–1096. https://doi.org/10.1016/J.IJPARA.2007.04.007

Kim, Y. E., Hipp, M. S., Bracher, A., Hayer-Hartl, M., & Ulrich Hartl, F. (2013). Molecular chaperone functions in protein folding and proteostasis. *Annual Review of Biochemistry*, *82*(Volume 82, 2013), 323–355. https://doi.org/10.1146/ANNUREV-BIOCHEM-060208-092442/CITE/REFWORKS

Koutsoni, O. S., Karampetsou, K., & Dotsika, E. (2019). In vitro screening of antileishmanial activity of natural product compounds: determination of IC50, CC50 and SI values. *Bio-Protocol*, *9*(21). https://doi.org/10.21769/BIOPROTOC.3410

Kraus, A., Groveman, B. R., & Caughey, B. (2013). Prions and the potential transmissibility of protein misfolding diseases. *Annual Review of Microbiology*, *67*, 543–564. https://doi.org/10.1146/ANNUREV-MICRO-092412-155735

Kumar, R., Sahoo, G. C., Pandey, K., Das, V., & Das, P. (2015). Study the effects of PLGA-PEG encapsulated Amphotericin B nanoparticle drug delivery system against Leishmania donovani. *Drug Delivery*, *22*(3), 383–388. https://doi.org/10.3109/10717544.2014.891271

Kyu, H. H., Abate, D., Abate, K. H., Abay, S. M., Abbafati, C., Abbasi, N., Abbastabar, H., Abd-Allah, F., Abdela, J., Abdelalim, A., Abdollahpour, I., Abdulkader, R. S., Abebe, M., Abebe, Z., Abil, O. Z., Aboyans, V., Abrham, A. R., Abu-Raddad, L. J., Abu-Rmeileh, N.

M. E., … Murray, C. J. L. (2018). Global, regional, and national disability-adjusted life-years (DALYs) for 359 diseases and injuries and healthy life expectancy (HALE) for 195 countries and territories, 1990–2017: a systematic analysis for the Global Burden of Disease Study 2017. *The Lancet*, *392*(10159), 1859–1922. https://doi.org/10.1016/S0140-6736(18)32335-3

Lagasse, E., & Weissman, I. L. (1994). bcl-2 inhibits apoptosis of neutrophils but not their engulfment by macrophages. *The Journal of Experimental Medicine*, *179*(3), 1047–1052. https://doi.org/10.1084/JEM.179.3.1047

Lakhin, A. V., Tarantul, V. Z., Lakhin, A. V. , T. V. Z. , & G. L. V., & Gening, L. V. (2013). Aptamers: Problems, solutions and prospects. *Acta Naturae*, *5*(4), 34–43. https://doi.org/10.32607/20758251-2013-5-4-34-43

Lancaster, A. K., Nutter-Upham, A., Lindquist, S., & King, O. D. (2014). PLAAC: a web and command-line application to identify proteins with prion-like amino acid composition. *Bioinformatics (Oxford, England)*, *30*(17), 2501–2502. https://doi.org/10.1093/BIOINFORMATICS/BTU310

Lantero, E., Aláez-Versón, C. R., Romero, P., Sierra, T., & Fernàndez-Busquets, X. (2020). Repurposing heparin as antimalarial: Evaluation of multiple modifications toward in vivo application. *Pharmaceutics 2020, Vol. 12, Page 825*, *12*(9), 825. https://doi.org/10.3390/PHARMACEUTICS12090825

Lantero, E., Belavilas-Trovas, A., Biosca, A., Recolons, P., Moles, E., Sulleiro, E., Zarzuela, F., Ávalos-Padilla, Y., Ramírez, M., & Fernàndez-Busquets, X. (2020). Development of DNA aptamers against Plasmodium falciparum blood stages using cell-Systematic Evolution of Ligands by EXponential Enrichment. *Journal of Biomedical Nanotechnology*, *16*(3), 315–334. https://doi.org/10.1166/JBN.2020.2901

Lasic, D. D. (1998). Novel applications of liposomes. *Trends in Biotechnology*, *16*(7), 307–321. https://doi.org/10.1016/S0167-7799(98)01220-7

Laskay, T., Van Zandbergen, G., & Solbach, W. (2003). Neutrophil granulocytes – Trojan horses for Leishmania major and other intracellular microbes? *Trends in Microbiology*, *11*(5), 210–214. https://doi.org/10.1016/S0966-842X(03)00075-1

Laskowski, R. A., & Thornton, J. M. (2008). Understanding the molecular machinery of genetics through 3D structures. *Nature Reviews Genetics 2008 9:2*, *9*(2), 141–151. https://doi.org/10.1038/nrg2273

LeishVet. (2024). *Vaccines*. https://www.leishvet.org/fact-sheet/vaccines/

Li, L., Xu, S., Yan, H., Li, X., Yazd, H. S., Li, X., Huang, T., Cui, C., Jiang, J., & Tan, W. (2021). Nucleic acid aptamers for molecular diagnostics and therapeutics: Advances and perspectives. *Angewandte Chemie*, *133*(5), 2249–2259. https://doi.org/10.1002/ANGE.202003563

Li, L., Xu, S., Yan, H., Li, X., Yazd, H. S., Li, X., Huang, T., Heng Cui, C., Jiang, J., & Tan, W. (2021). Nucleic acid aptamers for molecular diagnostics and therapeutics: advances and perspectives. *Angewandte Chemie*, *133*(5), 2249–2259. https://doi.org/10.1002/ANGE.202003563

Maji, S. K., Perrin, M. H., Sawaya, M. R., Jessberger, S., Vadodaria, K., Rissman, R. A., Singru, P. S., Nilsson, K. P. R., Simon, R., Schubert, D., Eisenberg, D., Rivier, J., Sawchenko, P., Vale, W., & Riek, R. (2009). Functional amyloids as natural storage of peptide hormones in pituitary secretory granules. *Science (New York, N.Y.)*, *325*(5938), 328–332. https://doi.org/10.1126/SCIENCE.1173155

March, Z. M., King, O. D., & Shorter, J. (2016). Prion-like domains as epigenetic regulators, scaffolds for subcellular organization, and drivers of neurodegenerative disease. *Brain Research*, *1647*, 9–18. https://doi.org/10.1016/J.BRAINRES.2016.02.037

Martín, M. E., García-Hernández, M., García-Recio, E. M., Gómez-Chacón, G. F., Sánchez-López, M., & González, V. M. (2013). DNA aptamers selectively target Leishmania infantum H2A protein. *PLOS ONE*, *8*(10), e78886. https://doi.org/10.1371/JOURNAL.PONE.0078886

Martins, T. V. F., De Carvalho, T. V., De Oliveira, C. V. M., De Paula, S. O., Cardoso, S. A., De Oliveira, L. L., & Marques-Da-Silva, E. D. A. (2015). Leishmania chagasi heparin-binding protein: Cell localization and participation in L. chagasi infection. *Molecular and Biochemical Parasitology*, *204*(1), 34–43. https://doi.org/10.1016/J.MOLBIOPARA.2015.12.005

Martins, T. V. F., Zeraik, A. E., Alves, N. O., de Oliveira, L. L., Mendes, T. A. de O., Demarco, R., & Marques-Da-Silva, E. de A. (2018). Lipophosphoglycan 3 from Leishmania infantum chagasi binds heparin with micromolar affinity. *Bioinformatics and Biology Insights*, *12*. https://doi.org/10.1177/1177932218763363

Maurer-Stroh, S., Debulpaep, M., Kuemmerer, N., De La Paz, M. L., Martins, I. C., Reumers, J., Morris, K. L., Copland, A., Serpell, L., Serrano, L., Schymkowitz, J. W. H., & Rousseau, F. (2010). Exploring the sequence determinants of amyloid structure using position-specific scoring matrices. *Nature Methods 2010 7:3*, *7*(3), 237–242. https://doi.org/10.1038/nmeth.1432

Maza Vega, D., Di Meglio, M., Alonso, S. del V., Alvira, F., & Montanari, J. (2023). Nanomaterials for diagnosis, treatment, and prevention of human cutaneous leishmaniasis: A review. *OpenNano*, *12*, 100158. https://doi.org/10.1016/J.ONANO.2023.100158

McConville, M. J., de Souza, D., Saunders, E., Likic, V. A., & Naderer, T. (2007). Living in a phagolysosome; metabolism of Leishmania amastigotes. *Trends in Parasitology*, *23*(8), 368–375. https://doi.org/10.1016/J.PT.2007.06.009

Merida-De-Barros, D. A., Chaves, S. P., Belmiro, C. L. R., & Wanderley, J. L. M. (2018). Leishmaniasis and glycosaminoglycans: a future therapeutic strategy? *Parasites & Vectors 2018 11:1*, *11*(1), 1–12. https://doi.org/10.1186/S13071-018-2953-Y

Moles, E., Urbán, P., Jiménez-Díaz, M. B., Viera-Morilla, S., Angulo-Barturen, I., Busquets, M. A., & Fernàndez-Busquets, X. (2015). Immunoliposome-mediated drug delivery to Plasmodium-infected and non-infected red blood cells as a dual therapeutic/prophylactic antimalarial strategy. *Journal of Controlled Release : Official Journal of the Controlled Release Society*, *210*, 217–229. https://doi.org/10.1016/J.JCONREL.2015.05.284

Monsellier, E., & Chiti, F. (2007). Prevention of amyloid-like aggregation as a driving force of protein evolution. *EMBO Reports*, *8*(8), 737–742. https://doi.org/10.1038/SJ.EMBOR.7401034

Montoya, A., Gálvez, R., Checa, R., Sarquis, J., Plaza, A., Barrera, J. P., Marino, V., & Miró, G. (2020). Latest trends in L. infantum infection in dogs in Spain, Part II: Current clinical management and control according to a national survey of veterinary practitioners. *Parasites and Vectors*, *13*(1), 205. https://doi.org/10.1186/S13071-020-04080-8/TABLES/2

Moreno, C. J. G., Farias, H. M., de Lima Medeiros, R., de Brito Pinto, T. K., de Freitas Oliveira, J. W., de Sousa, F. L., de Medeiros, M. J. C., Amorim-Carmo, B., Santos-Gomes, G., de Lima Pontes, D., Rocha, H. A. O., Frazão, N. F., & Silva, M. S. (2022). Quantum biochemistry screening and in vitro evaluation of Leishmania metalloproteinase Inhibitors. *International Journal of Molecular Sciences*, *23*(15), 8553. https://doi.org/10.3390/IJMS23158553/S1

Moreno, M., González, V. M., Rincón, E., Domingo, A., & Domínguez, E. (2011). Aptasensor based on the selective electrodeposition of protein-linked gold nanoparticles on screen-printed electrodes. *Analyst*, *136*(9), 1810–1815. https://doi.org/10.1039/C1AN15070G

Moreno, M., Rincón, E., Piñeiro, D., Fernández, G., Domingo, A., Jiménez-Ruíz, A., Salinas, M., & González, V. M. (2003). Selection of aptamers against KMP-11 using colloidal gold during the SELEX process. *Biochemical and Biophysical Research Communications*, *308*(2), 214–218. https://doi.org/10.1016/S0006-291X(03)01352-4

Mowbray, C. E., Braillard, S., Glossop, P. A., Whitlock, G. A., Jacobs, R. T., Speake, J., Pandi, B., Nare, B., Maes, L., Yardley, V., Freund, Y., Wall, R. J., Carvalho, S., Bello, D., Van Den Kerkhof, M., Caljon, G., Gilbert, I. H., Corpas-Lopez, V., Lukac, I., … Wyllie, S. (2021). DNDI-6148: A novel benzoxaborole preclinical candidate for the treatment of visceral leishmaniasis. *Journal of Medicinal Chemistry*, *64*(21), 16159–16176. https://doi.org/10.1021/ACS.JMEDCHEM.1C01437

Musa, A. M., Mbui, J., Mohammed, R., Olobo, J., Ritmeijer, K., Alcoba, G., Muthoni Ouattara, G., Egondi, T., Nakanwagi, P., Omollo, T., Wasunna, M., Verrest, L., Dorlo, T. P. C., Musa Younis, B., Nour, A., Taha Ahmed Elmukashfi, E., Ismail Omer Haroun, A., Khalil, E. A. G., Njenga, S., … Alves, F. (2023). Paromomycin and miltefosine combination as an alternative to treat patients with visceral leishmaniasis in Eastern Africa: A randomized, controlled, multicountry trial. *Clinical Infectious Diseases*, *76*(3), e1177–e1185. https://doi.org/10.1093/CID/CIAC643

Nafari, A., Cheraghipour, K., Sepahvand, M., Shahrokhi, G., Gabal, E., & Mahmoudvand, H. (2020). Nanoparticles: New agents toward treatment of leishmaniasis. *Parasite Epidemiology and Control*, *10*. https://doi.org/10.1016/j.parepi.2020.e00156

Nagar, D. N., Yathirajarao, T., Kumar, P., Kushwaha, P., & Suman, P. (2021). Bead-based SELEX for aptamers selection and their application in detection of diverse antigens. *Immunodiagnostic Technologies from Laboratory to Point-Of-Care Testing*, 125–139. https://doi.org/10.1007/978-981-15-5823-8_7

Nagle, A., Biggart, A., Be, C., Srinivas, H., Hein, A., Caridha, D., Sciotti, R. J., Pybus, B., Kreishman-Deitrick, M., Bursulaya, B., Lai, Y. H., Gao, M. Y., Liang, F., Mathison, C. J. N., Liu, X., Yeh, V., Smith, J., Lerario, I., Xie, Y., … Molteni, V. (2020). Discovery and characterization of clinical candidate LXE408 as a kinetoplastid-selective proteasome inhibitor for the treatment of leishmaniases. *Journal of Medicinal Chemistry*, *63*(19), 10773–10781. https://doi.org/10.1021/ACS.JMEDCHEM.0C00499/SUPPL_FILE/JM0C00499_SI_001.CSV

Navarro, M., Gabbiani, C., Messori, L., & Gambino, D. (2010). Metal-based drugs for malaria, trypanosomiasis and leishmaniasis: recent achievements and perspectives. *Drug Discovery Today*, *15*(23–24), 1070–1078. https://doi.org/10.1016/J.DRUDIS.2010.10.005

NCBI. (n.d.). *GP63 and Leishmania infantum - Gene - NCBI*. Retrieved June 18, 2024, from https://www.ncbi.nlm.nih.gov/gene/?term=GP63+and+LEISHMANIA+INFANTUM

Nobel Prize Outreach. (2024). *Ronald Ross – Facts* . https://www.nobelprize.org/prizes/medicine/1902/ross/facts/

Nsairat, H., Khater, D., Sayed, U., Odeh, F., Al Bawab, A., & Alshaer, W. (2022). Liposomes: structure, composition, types, and clinical applications. *Heliyon*, *8*(5), e09394. https://doi.org/10.1016/J.HELIYON.2022.E09394

Olías-molero, A. I., de la Fuente, C., Cuquerella, M., Torrado, J. J., & Alunda, J. M. (2021). Antileishmanial drug discovery and development: time to reset the model? *Microorganisms*, *9*(12), 2500. https://doi.org/10.3390/MICROORGANISMS9122500

Olivier, M., Atayde, V. D., Isnard, A., Hassani, K., & Shio, M. T. (2012). Leishmania virulence factors: focus on the metalloprotease GP63. *Microbes and Infection*, *14*(15), 1377–1389. https://doi.org/10.1016/J.MICINF.2012.05.014

Olivier, M., Gregory, D. J., & Forget, G. (2005). Subversion mechanisms by which Leishmania parasites can escape the host immune response: a signaling point of view. *Clinical Microbiology Reviews*, *18*(2), 293–305. https://doi.org/10.1128/CMR.18.2.293-305.2005

Ornellas-Garcia, U., Cuervo, P., & Ribeiro-Gomes, F. L. (2023). Malaria and leishmaniasis: Updates on co-infection. *Frontiers in Immunology*, *14*. https://doi.org/10.3389/FIMMU.2023.1122411

Ortiz, D., Forquer, I., Boitz, J., Soysa, R., Elya, C., Fulwiler, A., Nilsen, A., Polley, T., Riscoe, M. K., Ullman, B., & Landfear, S. M. (2016). Targeting the cytochrome bc1 complex of Leishmania parasites for discovery of novel drugs. *Antimicrobial Agents and Chemotherapy*, *60*(8), 4972–4982. https://doi.org/10.1128/AAC.00850-16/ASSET/C9208D63-912A-4A3A-A08F-0C7432AC02F9/ASSETS/GRAPHIC/ZAC0081654350005.JPEG

Ospina-Villa, J. D., López-Camarillo, C., Castañón-Sánchez, C. A., Soto-Sánchez, J., Ramírez-Moreno, E., & Marchat, L. A. (2018). Advances on aptamers against protozoan parasites. *Genes 2018, Vol. 9, Page 584*, *9*(12), 584. https://doi.org/10.3390/GENES9120584

PAHO. (2018). *Leishmaniasis in the Americas: treatment recommendations.* https://www.paho.org/en/documents/leishmaniasis-americas-recommendations-treatment-2018

Pallarès, I., de Groot, N. S., Iglesias, V., Sant'Anna, R., Biosca, A., Fernàndez-Busquets, X., & Ventura, S. (2018). Discovering putative prion-like proteins in Plasmodium falciparum: A computational and experimental analysis. *Frontiers in Microbiology*, *9*(AUG), 381158. https://doi.org/10.3389/FMICB.2018.01737/BIBTEX

Pan American Health Organization (PAHO). (2022). *Guideline for the treatment of leishmaniasis in the Americas*.

Peacock, C. S., Seeger, K., Harris, D., Murphy, L., Ruiz, J. C., Quail, M. A., Peters, N., Adlem, E., Tivey, A., Aslett, M., Kerhornou, A., Ivens, A., Fraser, A., Rajandream, M. A., Carver, T., Norbertczak, H., Chillingworth, T., Hance, Z., Jagels, K., … Berriman, M. (2007). Comparative genomic analysis of three Leishmania species that cause diverse human disease. *Nature Genetics*, *39*(7), 839–847. https://doi.org/10.1038/NG2053

Perry, D., Dixon, K., Garlapati, R., Gendernalik, A., Poché, D., & Poché, R. (2013). Visceral leishmaniasis prevalence and associated risk factors in the saran district of Bihar, India, from 2009 to July of 2011. *The American Journal of Tropical Medicine and Hygiene*, *88*(4), 778–784. https://doi.org/10.4269/AJTMH.12-0442

Piccica, M., Lagi, F., Bartoloni, A., & Zammarchi, L. (2021). Efficacy and safety of pentamidine isethionate for tegumentary and visceral human leishmaniasis: a systematic review. *Journal of Travel Medicine*, *28*(6), 1–13. https://doi.org/10.1093/JTM/TAAB065

Pijpers, J., Den Boer, M. L., Essink, D. R., & Ritmeijer, K. (2019). The safety and efficacy of miltefosine in the long-term treatment of post-kala-azar dermal leishmaniasis in South Asia – A review and meta-analysis. *PLOS Neglected Tropical Diseases*, *13*(2), e0007173. https://doi.org/10.1371/JOURNAL.PNTD.0007173

Pinheiro, A. C., & de Souza, M. V. N. (2022). Current leishmaniasis drug discovery. *RSC Medicinal Chemistry*, *13*(9), 1029–1043. https://doi.org/10.1039/D1MD00362C

Pinna, R. A., Silva-dos-Santos, D., Perce-da-Silva, D. S., Oliveira-Ferreira, J., Villa-Verde, D. M. S., De Luca, P. M., & Banic, D. M. (2016). Malaria-Cutaneous Leishmaniasis co-infection: Influence on disease outcomes and immune response. *Frontiers in Microbiology*, *7*(JUN), 198794. https://doi.org/10.3389/FMICB.2016.00982/BIBTEX

Ponte-Sucre, A., Gamarro, F., Dujardin, J. C., Barrett, M. P., López-Vélez, R., García-Hernández, R., Pountain, A. W., Mwenechanya, R., & Papadopoulou, B. (2017). Drug resistance and treatment failure in leishmaniasis: A 21st century challenge. *PLOS Neglected Tropical Diseases*, *11*(12), e0006052. https://doi.org/10.1371/JOURNAL.PNTD.0006052

Rajendran, M., & Ellington, A. D. (2008). Selection of fluorescent aptamer beacons that light up in the presence of zinc. *Analytical and Bioanalytical Chemistry*, *390*(4), 1067–1075. https://doi.org/10.1007/S00216-007-1735-8/FIGURES/5

Ramos, E., Moreno, M., Martín, M. E., Soto, M., & Gonzalez, V. M. (2010). In vitro selection of Leishmania infantum H3-binding ssDNA aptamers. *Oligonucleotides*, *20*(4), 207–213. https://doi.org/10.1089/OLI.2010.0240/ASSET/IMAGES/LARGE/FIGURE3.JPEG

Ramos, E., Pĩeiro, D., Soto, M., Abanades, D. R., Martín, M. E., Salinas, M., & González, V. M. (2007). A DNA aptamer population specifically detects Leishmania infantum H2A antigen. *Laboratory Investigation; a Journal of Technical Methods and Pathology*, *87*(5), 409–416. https://doi.org/10.1038/LABINVEST.3700535

Raskatov, J. A., & Teplow, D. B. (2017). Using chirality to probe the conformational dynamics and assembly of intrinsically disordered amyloid proteins. *Scientific Reports 2017 7:1*, *7*(1), 1–7. https://doi.org/10.1038/s41598-017-10525-5

Rathore, A., Jain, A., Gulbake, A., Shilpi, S., Khare, P., Jain, A., & Jain, S. K. (2011). Mannosylated liposomes bearing Amphotericin B for effective management of visceral Leishmaniasis. *Journal of Liposome Research*, *21*(4), 333–340. https://doi.org/10.3109/08982104.2011.575381

Real, F., Vidal, R. O., Carazzolle, M. F., Mondego, J. M. C., Costa, G. G. L., Herai, R. H., Würtele, M., De Carvalho, L. M., E Ferreira, R. C., Mortara, R. A., Barbiéri, C. L., Mieczkowski, P., Da Silveira, J. F., Briones, M. R. D. S., Pereira, G. A. G., & Bahia, D. (2013). The genome sequence of Leishmania (Leishmania) amazonensis: functional annotation and extended analysis of gene models. *DNA Research: An International Journal for Rapid Publication of Reports on Genes and Genomes*, *20*(6), 567–581. https://doi.org/10.1093/DNARES/DST031

Riaz, M. K., Riaz, M. A., Zhang, X., Lin, C., Wong, K. H., Chen, X., Zhang, G., Lu, A., & Yang, Z. (2018). Surface functionalization and targeting strategies of liposomes in solid tumor therapy: A review. *International Journal of Molecular Sciences 2018, Vol. 19, Page 195*, *19*(1), 195. https://doi.org/10.3390/IJMS19010195

Roca, C., Avalos-Padilla, Y., Prieto-Simón, B., Iglesias, V., Ramírez, M., Imperial, S., & Fernàndez-Busquets, X. (2022). Selection of an aptamer against the enzyme 1-deoxy-D-xylulose-5-phosphate reductoisomerase from Plasmodium falciparum. *Pharmaceutics*, *14*(11). https://doi.org/10.3390/PHARMACEUTICS14112515

Román-Álamo, L., Allaw, M., Avalos-Padilla, Y., Manca, M. L., Manconi, M., Fulgheri, F., Fernández-Lajo, J., Rivas, L., Vázquez, J. A., Peris, J. E., Roca-Geronès, X., Poonlaphdecha, S., Alcover, M. M., Fisa, R., Riera, C., & Fernàndez-Busquets, X. (2023).

In vitro evaluation of aerosol therapy with pentamidine-loaded liposomes coated with chondroitin sulfate or heparin for the treatment of leishmaniasis. *Pharmaceutics*, *15*(4). https://doi.org/10.3390/PHARMACEUTICS15041163

Roquero, I., Cantizani, J., Cotillo, I., Manzano, M. P., Kessler, A., Martín, J. J., & McNamara, C. W. (2019). Novel chemical starting points for drug discovery in leishmaniasis and Chagas disease. *International Journal for Parasitology. Drugs and Drug Resistance*, *10*, 58–68. https://doi.org/10.1016/J.IJPDDR.2019.05.002

Ross, M. R. (1903). Further notes on leishman's bodies. *British Medical Journal*, *2*(2239), 1401. https://doi.org/10.1136/BMJ.2.2239.1401

Ruy, P. de C., Torrieri, R., Toledo, J. S., Alves, V. de S., Cruz, A. K., & Ruiz, J. C. (2014). Intrinsically disordered proteins (IDPs) in trypanosomatids. *BMC Genomics*, *15*(1), 1–15. https://doi.org/10.1186/1471-2164-15-1100/FIGURES/7

Salvatella, X. (2013). Structural aspects of amyloid formation. *Progress in Molecular Biology and Translational Science*, *117*, 73–101. https://doi.org/10.1016/B978-0-12-386931-9.00004-0

Santos, J., Pujols, J., Pallarès, I., Iglesias, V., & Ventura, S. (2020). Computational prediction of protein aggregation: Advances in proteomics, conformation-specific algorithms and biotechnological applications. *Computational and Structural Biotechnology Journal*, *18*, 1403–1413. https://doi.org/10.1016/J.CSBJ.2020.05.026

Sanvictores, T., & Farci, F. (2022). Biochemistry, primary protein structure. *StatPearls*. https://www.ncbi.nlm.nih.gov/books/NBK564343/

Satyanarayana, A., & Kaldis, P. (2009). Mammalian cell-cycle regulation: several Cdks, numerous cyclins and diverse compensatory mechanisms. *Oncogene 2009 28:33*, *28*(33), 2925–2939. https://doi.org/10.1038/onc.2009.170

Schlagenhauf, E., Etges, R., & Metcalf, P. (1998). The crystal structure of the Leishmania major surface proteinase leishmanolysin (gp63). *Structure*, *6*(8), 1035–1046. https://doi.org/10.1016/S0969-2126(98)00104-X

Seay, M. B., Heard, P. L., & Chaudhuri, G. (1996). Surface Zn-proteinase as a molecule for defense of Leishmania mexicana amazonensis promastigotes against cytolysis inside macrophage phagolysosomes. *Infection and Immunity*, *64*(12), 5129–5137. https://doi.org/10.1128/IAI.64.12.5129-5137.1996

Sefah, K., Shangguan, D., Xiong, X., O'Donoghue, M. B., & Tan, W. (2010). Development of DNA aptamers using cell-selex. *Nature Protocols*, *5*(6), 1169–1185. https://doi.org/10.1038/nprot.2010.66

Serafim, T. D., Coutinho-Abreu, I. V., Dey, R., Kissinger, R., Valenzuela, J. G., Oliveira, F., & Kamhawi, S. (2021). Leishmaniasis: the act of transmission. *Trends in Parasitology*, *37*(11), 976–987. https://doi.org/10.1016/J.PT.2021.07.003

Serafim, T. D., Coutinho-Abreu, I. V., Oliveira, F., Meneses, C., Kamhawi, S., & Valenzuela, J. G. (2018). Sequential blood meals promote Leishmania replication and reverse metacyclogenesis augmenting vector infectivity. *Nature Microbiology* , *3*(5), 548–555. https://doi.org/10.1038/S41564-018-0125-7

Shaukat, A., Mirza, H. M., Ansari, A. H., Yasinzai, M., Zaidi, S. Z., Dilshad, S., & Ansari, F. L. (2013). Benzimidazole derivatives: Synthesis, leishmanicidal effectiveness, and molecular docking studies. *Medicinal Chemistry Research*, *22*(8), 3606–3620. https://doi.org/10.1007/S00044-012-0375-5/TABLES/2

Sinha, N., & Nussinov, R. (2001). Point mutations and sequence variability in proteins: redistributions of preexisting populations. *Proceedings of the National Academy of Sciences of the United States of America*, *98*(6), 3139–3144. https://doi.org/10.1073/PNAS.051399098

Somali Federal Government Ministry of Health and WHO. (2012). *Guidelines for diagnosis, treatment and prevention of visceral leishmaniasis in Somalia*. https://www.who.int/leishmaniasis/burden/Guidelines_for_diagnosis_treatment_and_prevention_of_VL_in_Somalia.pdf

Soulat, D., & Bogdan, C. (2017). Function of macrophage and parasite phosphatases in leishmaniasis. *Frontiers in Immunology*, *8*(DEC), 311253. https://doi.org/10.3389/FIMMU.2017.01838/BIBTEX

Steverding, D. (2017). The history of leishmaniasis. *Parasites & Vectors*, *10*(1), 82. https://doi.org/10.1186/S13071-017-2028-5

Stoltenburg, R., Reinemann, C., & Strehlitz, B. (2007). SELEX—A (r)evolutionary method to generate high-affinity nucleic acid ligands. *Biomolecular Engineering*, *24*(4), 381–403. https://doi.org/10.1016/J.BIOENG.2007.06.001

Strebhardt, K., & Ullrich, A. (2008). Paul Ehrlich's magic bullet concept: 100 years of progress. *Nature Reviews Cancer 2008 8:6*, *8*(6), 473–480. https://doi.org/10.1038/nrc2394

Sundar, S., & Chakravarty, J. (2008). Paromomycin in the treatment of leishmaniasis. *Expert Opinion on Investigational Drugs*, *17*(5), 787–794. https://doi.org/10.1517/13543784.17.5.787

Sundar, S., & Singh, A. (2018a). Chemotherapeutics of visceral leishmaniasis: present and future developments. *Parasitology*, *145*(4), 481–489. https://doi.org/10.1017/S0031182017002116

Sundar, S., & Singh, B. (2018b). Emerging therapeutic targets for treatment of leishmaniasis. *Expert Opinion on Therapeutic Targets*, *22*(6), 467–486. https://doi.org/10.1080/14728222.2018.1472241

Sunter, J., & Gull, K. (2017). Shape, form, function and Leishmania pathogenicity: from textbook descriptions to biological understanding. *Open Biology*, *7*(9), 170165. https://doi.org/10.1098/RSOB.170165

Taneja, V., Goel, M., Shankar, U., Kumar, A., Khilnani, G. C., Prasad, H. K., Prasad, G. B. K. S., Gupta, U. D., & Sharma, T. K. (2020). An Aptamer Linked Immobilized Sorbent Assay (ALISA) to detect circulatory IFN-α, an inflammatory protein among tuberculosis patients. *ACS Combinatorial Science*, *22*(11), 656–666. https://doi.org/10.1021/ACSCOMBSCI.0C00108/ASSET/IMAGES/LARGE/CO0C00108_0005.JPEG

Tartaglia, G. G., Cavalli, A., Pellarin, R., & Caflisch, A. (2005). Prediction of aggregation rate and aggregation-prone segments in polypeptide sequences. *Protein Science*, *14*(10), 2723–2734. https://doi.org/10.1110/PS.051471205

Taylor, K. M. G., & Newton, J. M. (1992). Liposomes for controlled delivery of drugs to the lung. *Thorax*, *47*(4), 257. https://doi.org/10.1136/THX.47.4.257

Torchilin, V. P. (2005). Recent advances with liposomes as pharmaceutical carriers. *Nature Reviews Drug Discovery 2005 4:2*, *4*(2), 145–160. https://doi.org/10.1038/nrd1632

Treiger Borborema, S. E., Schwendener, R. A., Osso Junior, J. A., De Andrade Junior, H. F., & Do Nascimento, N. (2011). Uptake and antileishmanial activity of meglumine antimoniate-containing liposomes in Leishmania (Leishmania) major-infected macrophages. *International Journal of Antimicrobial Agents*, *38*(4), 341–347. https://doi.org/10.1016/J.IJANTIMICAG.2011.05.012

Unciti-Broceta, J. D., Arias, J. L., Maceira, J., Soriano, M., Ortiz-González, M., Hernández-Quero, J., Muñóz-Torres, M., de Koning, H. P., Magez, S., & Garcia-Salcedo, J. A. (2015). Specific Cell Targeting Therapy Bypasses Drug Resistance Mechanisms in African Trypanosomiasis. *PLOS Pathogens*, *11*(6), e1004942. https://doi.org/10.1371/JOURNAL.PPAT.1004942

Vaish, M., Singh, O. P., Chakravarty, J., & Sundar, S. (2012). rK39 Antigen for the Diagnosis of Visceral Leishmaniasis by Using Human Saliva. *The American Journal of Tropical Medicine and Hygiene*, *86*(4), 598–600. https://doi.org/10.4269/AJTMH.2012.11-0127

Van Bocxlaer, K., McArthur, K. N., Harris, A., Alavijeh, M., Braillard, S., Mowbray, C. E., & Croft, S. L. (2021). Film-forming systems for the delivery of DNDI-0690 to treat cutaneous leishmaniasis. *Pharmaceutics 2021, Vol. 13, Page 516*, *13*(4), 516. https://doi.org/10.3390/PHARMACEUTICS13040516

Van Der Lee, R., Buljan, M., Lang, B., Weatheritt, R. J., Daughdrill, G. W., Dunker, A. K., Fuxreiter, M., Gough, J., Gsponer, J., Jones, D. T., Kim, P. M., Kriwacki, R. W., Oldfield, C. J., Pappu, R. V., Tompa, P., Uversky, V. N., Wright, P. E., & Babu, M. M. (2014). Classification of intrinsically disordered regions and proteins. *Chemical Reviews*, *114*(13), 6589–6631. https://doi.org/10.1021/CR400525M/ASSET/IMAGES/LARGE/CR-2013-00525M_0006.JPEG

Van De Ven, H., Paulussen, C., Feijens, P. B., Matheeussen, A., Rombaut, P., Kayaert, P., Van Den Mooter, G., Weyenberg, W., Cos, P., Maes, L., & Ludwig, A. (2012). PLGA nanoparticles and nanosuspensions with amphotericin B: Potent in vitro and in vivo alternatives to Fungizone and AmBisome. *Journal of Controlled Release*, *161*(3), 795–803. https://doi.org/10.1016/J.JCONREL.2012.05.037

van Griensven, J., & Diro, E. (2019). Visceral leishmaniasis: recent advances in diagnostics and treatment regimens. *Infectious Disease Clinics of North America*, *33*(1), 79–99. https://doi.org/10.1016/J.IDC.2018.10.005

van Griensven, J., Dorlo, T. P., Diro, E., Costa, C., & Burza, S. (2024). The status of combination therapy for visceral leishmaniasis: an updated review. *The Lancet Infectious Diseases*, *24*(1), e36–e46. https://doi.org/10.1016/S1473-3099(23)00353-5

van Zandbergen, G., Klinger, M., Mueller, A., Dannenberg, S., Gebert, A., Solbach, W., & Laskay, T. (2004). Cutting edge: neutrophil granulocyte serves as a vector for Leishmania entry into macrophages. *The Journal of Immunology*, *173*(11), 6521–6525. https://doi.org/10.4049/JIMMUNOL.173.11.6521

Ventura, S., Zurdo, J., Narayanan, S., Parreño, M., Mangues, R., Reif, B., Chiti, F., Giannoni, E., Dobson, C. M., Aviles, F. X., & Serrano, L. (2004). Short amino acid stretches can mediate amyloid formation in globular proteins: The Src homology 3 (SH3) case. *Proceedings of the National Academy of Sciences of the United States of America*, *101*(19), 7258–7263. https://doi.org/10.1073/PNAS.0308249101/SUPPL_FILE/08249SUPPTEXT.HTML

Wagner, V., Dullaart, A., Bock, A. K., & Zweck, A. (2006). The emerging nanomedicine landscape. *Nature Biotechnology 2006 24:10*, *24*(10), 1211–1217. https://doi.org/10.1038/nbt1006-1211

Wall, R. J., Carvalho, S., Milne, R., Bueren-Calabuig, J. A., Moniz, S., Cantizani-Perez, J., MacLean, L., Kessler, A., Cotillo, I., Sastry, L., Manthri, S., Patterson, S., Zuccotto, F., Thompson, S., Martin, J., Marco, M., Miles, T. J., De Rycker, M., Thomas, M. G., … Wyllie, S. (2020). The Qi site of cytochrome b is a promiscuous drug target in Trypanosoma cruzi and Leishmania donovani. *ACS Infectious Diseases*, *6*(3), 515–528. https://doi.org/10.1021/ACSINFECDIS.9B00426/ASSET/IMAGES/MEDIUM/ID9B00426_M004.GIF

Wang, Y., Qin, B., Xia, G., & Choi, S. H. (2021). FDA's Poly (Lactic-Co-Glycolic Acid) research program and regulatory outcomes. *AAPS Journal*, *23*(4), 1–7. https://doi.org/10.1208/S12248-021-00611-Y/TABLES/1

WHO. (2010). Control of the leishmaniases: report of a meeting of the WHO Expert Commitee on the Control of Leishmaniases, Geneva, 22-26 March 2010. *WHO Technical Report Series*, *949*. https://iris.who.int/handle/10665/44412

WHO. (2012). Post Kala-Azar Dermal Leishmaniasis: a manual for case management and control. *Report of a WHO Consultative Meeting, Kolkata, India.* . www.who.int

WHO. (2020). *Ending the neglect to attain the Sustainable Development Goals: A road map for neglected tropical diseases 2021–2030*. Geneva. https://www.who.int/publications/i/item/9789240010352

WHO. (2023a). Global leishmaniasis surveillance, 2022: assessing trends over the past 10 years. *WHO Weekly Epidemiological Record*, *40*, 471–488. https://www.who.int/publications/i/item/who-wer9840-471-487

WHO. (2023b, January 12). *Leishmaniasis*. https://www.who.int/news-room/fact-sheets/detail/leishmaniasis

WHO. (2024). *The global health observatory-Leishmaniasis*. https://www.who.int/data/gho/data/themes/topics/gho-ntd-leishmaniasis

WHO Regional Office for Europe. (2017). *Manual on case management and surveillance of the leishmaniases in the WHO European region*. http://www.euro.who.int/pubrequest

WHO, R. O. for S.-E. A. (2022). *Regional strategic framework for accelerating and sustaining elimination of kala-azar in the South-East Asia region*. http://apps.who.int/bookorders.

Wijnant, G. J., Van Bocxlaer, K., Yardley, V., Harris, A., Alavijeh, M., Silva-Pedrosa, R., Antunes, S., Mauricio, I., Murdan, S., & Croft, S. L. (2018). Comparative efficacy, toxicity and biodistribution of the liposomal amphotericin B formulations Fungisome® and AmBisome® in murine cutaneous leishmaniasis. *International Journal for*

Parasitology: Drugs and Drug Resistance, *8*(2), 223. https://doi.org/10.1016/J.IJPDDR.2018.04.001

World Health Organization. (2010). Control of the leishmaniases. In *World Health Organization technical report series* (WHO techni, Issue 949).

Wu, F., Zhou, C., Zhou, D., Ou, S., Liu, Z., & Huang, H. (2018). Immune-enhancing activities of chondroitin sulfate in murine macrophage RAW 264.7 cells. *Carbohydrate Polymers*, *198*, 611–619. https://doi.org/10.1016/J.CARBPOL.2018.06.071

Wu, J., Wang, C., Li, X., Song, Y., Wang, W., Li, C., Hu, J., Zhu, Z., Li, J., Zhang, W., Lu, Z., & Yang, C. J. (2012). Identification, characterization and application of a G-quadruplex structured DNA aptamer against cancer biomarker protein anterior gradient homolog 2. *PLoS ONE*, *7*(9). https://doi.org/10.1371/JOURNAL.PONE.0046393

Wyllie, S., Brand, S., Thomas, M., De Rycker, M., Chung, C. wa, Pena, I., Bingham, R. P., Bueren-Calabuig, J. A., Cantizani, J., Cebrian, D., Craggs, P. D., Ferguson, L., Goswami, P., Hobrath, J., Howe, J., Jeacock, L., Ko, E. J., Korczynska, J., MacLean, L., … Wyatt, P. G. (2019). Preclinical candidate for the treatment of visceral leishmaniasis that acts through proteasome inhibition. *Proceedings of the National Academy of Sciences of the United States of America*, *116*(19), 9318–9323. https://doi.org/10.1073/PNAS.1820175116/SUPPL_FILE/PNAS.1820175116.SAPP.PDF

Wyllie, S., Thomas, M., Patterson, S., Crouch, S., De Rycker, M., Lowe, R., Gresham, S., Urbaniak, M. D., Otto, T. D., Stojanovski, L., Simeons, F. R. C., Manthri, S., MacLean, L. M., Zuccotto, F., Homeyer, N., Pflaumer, H., Boesche, M., Sastry, L., Connolly, P., … Gilbert, I. H. (2018). Cyclin-dependent kinase 12 is a drug target for visceral leishmaniasis. *Nature 2018 560:7717*, *560*(7717), 192–197. https://doi.org/10.1038/s41586-018-0356-z

Zambrano, R., Conchillo-Sole, O., Iglesias, V., Illa, R., Rousseau, F., Schymkowitz, J., Sabate, R., Daura, X., & Ventura, S. (2015). PrionW: a server to identify proteins containing glutamine/asparagine rich prion-like domains and their amyloid cores. *Nucleic Acids Research*, *43*(W1), W331–W337. https://doi.org/10.1093/NAR/GKV490

Zhang, S., & Wang, C. (2023). Effect of stirring speed on particle dispersion in silica synthesis. *Nano-Structures & Nano-Objects*, *35*, 100994. https://doi.org/10.1016/J.NANOSO.2023.100994

Zielinska, A., Carreiró, F., Oliveira, A. M., Neves, A., Pires, B., Nagasamy Venkatesh, D., Durazzo, A., Lucarini, M., Eder, P., Silva, A. M., Santini, A., & Souto, E. B. (2020). Polymeric nanoparticles: Production, characterization, toxicology and ecotoxicology.

Molecules 2020, Vol. 25, Page 3731, *25*(16), 3731. https://doi.org/10.3390/MOLECULES25163731

Zink, A. R., Spigelman, M., Schraut, B., Greenblatt, C. L., Nerlich, A. G., & Donoghue, H. D. (2006). Leishmaniasis in ancient Egypt and Upper nubia. *Emerging Infectious Diseases*, *12*(10), 1616–1617. https://doi.org/10.3201/EID1210.060169